TECHNISCHE UNIVERSITÄT DRESDEN

Doctoral Thesis

Microscopic Modeling of Human and Automated Driving: Towards Traffic-Adaptive Cruise Control

Dipl.-Phys. Arne Kesting

Faculty of Traffic Sciences „Friedrich List"

Technische Universität Dresden (Germany)

Dresden, February 2008

Von der Fakultät Verkehrswissenschaften „Friedrich List" an der Technischen Universität Dresden zur Erlangung des akademischen Grades eines Doktors der Ingenieurwissenschaften genehmigte Dissertation.

Vorgelegt von Dipl.-Phys. Arne Kesting.
Tag des Rigorosums: 9. Januar 2008, Tag der Disputation: 22. Januar 2008.

Deutsche Übersetzung des Titels: "Mikroskopische Verkehrsmodellierung menschlichen und automatisierten Fahrverhaltens: Verkehrsadaptive Strategie für Geschwindigkeitsregler"

Thesis Committee:

Prof. Dr. phil. habil. Bernhard Schlag (Chairman)
Chair for Traffic and Transportation Psychology
Technische Universität Dresden

Prof. Dr. rer. nat. habil. Dirk Helbing (Supervisor)
Chair for Sociology, in particular of Modeling and Simulation
Swiss Federal Institute of Technology Zürich

Prof. Dr. rer. nat. habil. Karl Nachtigall
Chair for Traffic Flow Science
Technische Universität Dresden

Prof. Dr.-Ing. Bernhard Bäker
Chair for Vehicle Mechatronics
Technische Universität Dresden

PD Dr.-Ing. habil. Christian Schiller
Theoretical Transportation Planning
Technische Universität Dresden

Dr.-Ing. Hans-Jürgen Stauss
Group Research Mobility
Volkswagen AG, Wolfsburg

Email: mail@akesting.de
Institute for Transport & Economics
Andreas-Schubert-Straße 23
Department of Transport and Traffic Sciences
Technische Universität Dresden
D-01062 Dresden (Germany)
Homepage: http://www.akesting.de
URL: http://nbn-resolving.de/urn:nbn:de:bsz:14-ds-1204804167720-57734

Abstract[1]

Efficient transportation systems are essential to the functioning and prosperity of modern, industrialized societies. Mobility is also an integral part of our quality of life, sense of self-fulfillment and personal freedom. Our traffic demands of today are predominantly served by individual motor vehicle travel which is the primary means of transportation. However, the limited road capacity and thus traffic congestion has become a severe problem in many countries. On the one hand, traffic demand can only be affected indirectly by means of policy measures. On the other hand, an extension of transport infrastructure is no longer an appropriate or desirable option in densely populated areas. Moreover, construction requires high investments and maintenance is costly in the long run. Therefore, engineers are now seeking solutions to the questions of how the capacity of the road network could be used more efficiently and how operations can be improved by way of intelligent transportation systems (ITS).

Achieving this efficiency through automated vehicle control is the long-standing vision in transport telematics. With the recent advent of advanced driver assistance systems, at least partly automated driving is already available for basic driving tasks such as accelerating and braking by means of *adaptive cruise control* (ACC) systems. An ACC system extends earlier cruise control to situations with significant traffic in which driving at constant speed is not possible. The driver cannot only adjust the desired velocity but also set a certain safety time gap determining the distance to the leading car when following slower vehicles. The task of the ACC system is to calculate the appropriate acceleration or deceleration as a function of the input quantities and the driver's settings. Therefore, the actual distance and speed difference to the vehicle ahead is measured by means of a long-range radar sensor.

The thesis is composed of two main parts. The first part deals with a microscopic traffic flow theory. Models describing the individual acceleration, deceleration and lane-changing behavior are formulated and the emerging collective traffic dynamics are investigated by means of numerical simulations. The models and simulation tools presented provide the methodical prerequisites for the second part of the thesis in which a novel concept of a traffic-adaptive control strategy for ACC systems is presented. The impact of such systems on the traffic dynamics can solely be investigated and assessed by traffic simulations.

[1]For a summary in German, we refer to Page 187.

Microscopic Model Calibration and Validation

The Intelligent Driver Model (IDM)[2], a microscopic car-following model, is the starting point of the thesis. It is well-known from the literature that the IDM is able to reproduce all essential traffic dynamic phenomena observed on freeways. Furthermore, the IDM features a small number of parameters which are easy to interpret and therefore allow for a intuitive characterization of different driver-vehicle classes (e.g., cars and trucks) but also heterogeneous driving behavior. A basic understanding of the properties of the IDM is obtained by the in-depth investigation of the single-vehicle dynamics, the equilibrium characteristics and the emergence of collective instabilities.

In the literature, the IDM has been calibrated using macroscopic quantities derived from empirical speed and flow data. In the thesis, a microscopic calibration and validation framework for car-following models is presented which aims to minimize deviations between the observed driving dynamics and the simulated trajectory when following the same leading vehicle. For the numerical solution of this nonlinear optimization problem, a genetic algorithm has been developed. Three different objective functions were formulated to assess the reliability and robustness of the calibration results. The IDM was able to reproduce the driving behavior reflected in the empirical trajectories. The calibrated model parameters are in the expected range whilst the errors obtained are between 10% and 30% which is consistent with errors typically found in previous studies for other models. The results indicate that dynamic adaption processes of the drivers (*intra-driver variability*) rather than varying driving characteristics of different drivers (*inter-driver variability*) account for a large part of the calibration errors.

Model for the Human Driving Behavior

As shown in the calibration study, the Intelligent Driver Model is able to describe the human driving behavior on a microscopic level to a satisfactory extent. With respect to obvious operational differences between a human driver and a simplistic car-following model which simply reacts instantaneously to the immediate vehicle ahead, it is important to ask for a theoretical justification. This is not only of fundamental scientific interest but also relevant to the underlying modeling assumptions in the second part of the thesis.

A complex microscopic traffic model is formulated which comprises essential aspects of human driver behavior not captured by simple car-following models. In the first place, there is a finite reaction time, the mathematical formulation of which leads to delay-differential equations. It is known from the literature that human reaction times are of the order of one second leading to very unstable modeled driving behavior. Stability

[2] M. Treiber, A. Hennecke, D. Helbing, *Congested traffic states in empirical observations and microscopic simulations*, Physical Review E 62, 1805 -1824 (2000).

is further reduced by limited human perception and estimation capabilities which are treated by Wiener processes leading to stochastic model elements. For a stabilization of the microscopic driving behavior, two anticipation mechanisms are considered: First, the modeled driver reacts not only to the immediate leader but also (with decreasing weights) to the vehicles further ahead ("spatial" or multi-anticipation). In this respect, the proposed model goes well beyond the usual car-following approximation. As the driver knows about his or her reaction time while perceiving the vehicles in front we moreover assume a heuristic that extrapolates the actual traffic situation on the scale of the reaction time ("temporal" anticipation).

The three characteristic time constants that influence the collective dynamics and stability of traffic flow are: (i) The delay caused by the finite reaction time of the drivers, (ii) the time lag due to a finite velocity adaptation time needed to accelerate to a new desired velocity, and (iii) the numerical update time[3]. In the proposed model, these effects are incorporated by independent parameters. By means of numerical simulations, we investigate how these times are interrelated and act to influence the local and collective mechanisms for instability in a platoon of vehicles. The long-wavelength string instability is mainly driven by the velocity adaptation time (due to the vehicles' limited acceleration capabilities) whilst short-wavelength local instabilities arise by sufficiently high reaction and/or update times. Furthermore, we investigate the relationship between large update time steps and finite reaction times, both of which introduce delays in the reaction to the traffic situation. Remarkably, the numerical update time is dynamically equivalent to about half the reaction time which clarifies the meaning of the time step in models formulated as iterated maps such as the Newell and the Gipps models. With respect to stability, we found an *optimal* adaptation time (corresponding to moderate vehicle accelerations) as a function of the reaction time.

Furthermore, we simulate the emerging macroscopic traffic dynamics in the presence of finite reaction times and driver anticipation in a complex scenario with a flow-conserving bottleneck (e.g., a lane closure or roadworks) in the open system with a time-dependent inflow as upstream boundary condition. It is shown that various spatiotemporal patterns of congested traffic can be reproduced by varying intrinsic model parameters such as reaction times and multi-anticipation. Moreover, we show that the destabilizing effects of reaction times and estimation errors can essentially be compensated for by spatial and temporal anticipation. Remarkably, the anticipation allows accident-free smooth driving

[3] As well as the numerical necessity for a finite time discretization to solve differential equations by means of numerical integration, the update time can be interpreted as representing *finite attention to the traffic*: Only at times that are a multiple of the update step do drivers look at the traffic situation and instantaneously adapt their acceleration to the new situation. Because of the intuitive meaning of this update procedure in the context of traffic, the explicit integration scheme is sometimes considered as an explicit model parameter rather than as a numerical approximation. Popular examples of such *coupled maps* include the models by Newell and Gipps.

in complex traffic situations even if reaction times exceed typical safety time gaps. Within the proposed modeling framework, these findings are able to explain why the simplified car-following models are capable of quantitatively describing the empirically observed traffic phenomena.

Modeling Lane-Changing Decisions

In addition to the acceleration and deceleration behavior of the drivers in the lane, a fully multi-lane simulation framework is needed for a realistic microscopic description of freeway traffic as only the possibility of passing slower vehicles allows for a consideration of effects that are caused by heterogeneous driver types and different vehicle classes. In addition, realistic on-ramp bottlenecks require the explicit modeling of the merging decision to the main road.

The general model MOBIL ("Minimizing Overall Braking Induced by Lane Change") is proposed to derive lane-changing rules for discretionary and mandatory lane changes for a wide class of car-following models. Both the utility of a given lane and the risk associated with lane changes are determined in terms of longitudinal accelerations calculated with microscopic traffic models. This determination in terms of a "meta model" allows for the formulation of compact and general safety and incentive criteria for both symmetric and asymmetric passing rules. Moreover, anticipative elements and the crucial influence of velocity differences of these car-following models are automatically transferred to the lane-changing rules. Although the safety criterion prevents critical lane changes and collisions, the incentive criterion takes into account the respective advantages and disadvantages of all drivers via a "politeness factor" which rise out of a lane change. This novel feature allows one to vary the motivation for changing lane from purely egoistic to more cooperative driving behavior. Firstly, the politeness parameter prevents lane changes for a marginal advantage if other drivers are obstructed. Secondly, it induces a lane change by a slower driver ahead if an aggressive driver in the same lane is approaching quickly. The latter phenomenon is common for asymmetric passing rules with a dedicated lane for passing. Simulations of an open system result in realistic lane-changing rates as a function of traffic density.

Traffic-adaptive Driving Strategy extending ACC Systems

In the second part of the thesis, the focus is on future adaptive cruise control (ACC) systems and their potential applications in the context of vehicle-based intelligent transportation systems. Present implementations of ACC systems are exclusively designed to increase driving comfort and the influence on the surrounding traffic is neither considered

nor optimized. This is justified as long as the number of ACC-equipped vehicles is negligible but the growing market penetration of these devices makes the question of their impact on traffic flow more pressing. Therefore, it is important to understand the effects of ACC systems on the capacity and stability of traffic flow at an early stage so that their design can be adjusted before adverse traffic effects can widely manifest themselves.

In order to ensure that ACC systems are implemented in ways that improve rather than degrade traffic conditions, the thesis proposes an extension of ACC systems towards *traffic-adaptive cruise control* by means of implementing an actively jam-avoiding driving strategy.

The newly developed *traffic assistance system* introduces a *driving strategy layer* which modifies the driver's individual settings of the ACC driving parameters depending on the local traffic situation. Whilst the conventional operational control layer of an ACC system calculates the response to the input sensor data in terms of accelerations and decelerations on a short time scale, the automated adaptation of the ACC driving parameters happens on a somewhat longer time scale of, typically, minutes. By changing only temporarily the comfortable parameter settings of the ACC system in specific traffic situations, the driving strategy is capable of improving the traffic flow efficiency whilst retaining the comfort for the driver. The traffic-adaptive modifications are specified relative to the driver settings in order to maintain the individual preferences.

The proposed system consists of three components: (i) the ACC system itself, (ii) an algorithm for the automatic real-time detection of the traffic situation based on local information, and (iii) a "strategy matrix" that associates the autonomously detected traffic situation with different parameter settings of the underlying ACC system, that is, it implements different driving characteristics. In order to do this, a finite set of five "traffic situations" is considered, each of which is associated with a specific set of ACC driving parameters:

- Moving in *free traffic* is the default situation. The ACC settings are determined solely with regard to the individual driving comfort. Since each driver adjusts his or her ACC parameter settings individually, this may lead to different settings for each ACC system.
- When *entering a traffic jam* (approaching an upstream congestion front) the driving strategy aims at reducing velocity gradients in order to reduce the risk of rear-end collisions, thus increasing collective safety. Compared to the default situation, this implies earlier braking when approaching slow vehicles which also increases the driving comfort. Note that the operational layer of the ACC system always assures a safe individual approaching process independent of the detected traffic state.

- Since drivers *moving in congested traffic* cannot influence the development of traffic congestion in the bulk of a traffic jam, the ACC settings revert to the individual parameter values of the driver again.
- Once traffic flow has broken down, the dynamics of the evolving congestion is determined first by the inflow (the externally given traffic demand) and second by the outflow from the traffic jam at the downstream congestion front. When *passing the downstream congestion front*, accelerations are therefore increased and time gaps temporarily decreased in order to raise that dynamic capacity.
- It is known that most traffic breakdowns are initiated at some sort of road inhomogeneities or infrastructure-based bottlenecks such as on-ramps, off-ramps or sections of roadworks. When passing these infrastructural *bottleneck sections*, the objective is to locally increase the capacity, that is, to *dynamically "fill" the capacity gap*. This requires a temporary modest reduction of the parameter value for the time gap.

Note that drivers typically experience the full sequence of these five traffic states when traveling through congested traffic. In free flow conditions, only the default and the bottleneck state are relevant. Therefore, the cumulative time period during which the ACC settings deviate from the default state is usually only a few percent.

The proposed system requires an autonomous real-time detection of the five traffic states by each ACC-equipped vehicle. The formulated algorithm is based on the evaluation of the locally available data such as the vehicle's velocity time series and its geo-referenced position (GPS) in conjunction with a digital map. It is assumed that the digital map is complemented by information about stationary bottlenecks as most of the observed traffic flow breakdowns occur at these fixed locations. By means of a heuristic, the algorithm determines which of the five traffic states mentioned above applies best to the actual traffic situation. Optionally, inter-vehicle and infrastructure-to-car communication technologies can be used to further improve the accuracy of determining the respective traffic state by providing non-local information.

Evaluation by means of Microscopic Traffic Simulations

The effects of upcoming driver assistance systems on the collective traffic dynamics can only be evaluated by means of traffic simulations. In order to study the proposed traffic-assistance system we have implemented the proposed components within a microscopic multi-lane traffic simulator which considers both "human drivers" as well as which fraction of vehicles are equipped with the traffic-adaptive cruise control system. As the autonomous traffic state detection requires real-time traffic data, the simulations first serve as "proof of concept" of the system components. Depending on the detected local traffic situation,

the corresponding driving strategy is realized by the underlying ACC system. From a formal point of view, this corresponds to a car-following model with an automatic, event-driven choice of parameters which therefore become time-dependent. Furthermore, we simulated a road section with an on-ramp bottleneck using empirical loop-detector data for an afternoon rush-hour as inflow at the upstream boundary.

By means of simulation, we found that the automatic traffic-adaptive driving strategy improves traffic stability and increases the effective road capacity. Depending on the fraction of ACC vehicles, the driving strategy "passing a bottleneck" effects a reduction of the bottleneck strength and therefore delays (or even prevents) the breakdown of traffic flow. Changing to the driving mode "leaving the traffic jam" increases the outflow from congestion resulting in reduced queue lengths in congested traffic and, consequently, a faster recovery to free flow conditions. The current travel time (as most important criterion for road users) and the cumulated travel time (as an indicator of the system performance) are used to evaluate the impact on the quality of service. While traffic congestion in the reference scenario was completely eliminated when simulating a proportion of 25% ACC vehicles, travel times were significantly reduced even with much lower penetration rates. Moreover, the cumulated travel times decreased consistently with the increase in the proportion of ACC vehicles.

For a systematic analysis of the impact of a given proportion of ACC vehicles on capacity, we varied external parameters such as the proportions of trucks and ACC-equipped vehicles and also the parameterization of the proposed driving strategy. First, we considered the maximum capacity in free flow determining the maximum throughput up to the breakdown of traffic flow. As a dynamic quantity depending on collective stability properties, the maximum capacity has to be distinguished from the static road capacity. For the purpose of clarification, the stochastic nature of a traffic flow breakdown has been demonstrated by considering multiple simulation runs. The variance of the maximum free capacity (treated as a random variable) depends on the heterogeneity of the driver-vehicle composition. Furthermore, it has been shown that the consideration of different vehicle classes has a stronger impact on the arithmetic mean than the consideration of statistically distributed model parameters within a driver-vehicle class.

Finally, the simulations allow the identification of limitations to the autonomous traffic-state detection. In particular, the adaptation when approaching a dynamically propagating front (e.g., a stop wave) requires knowledge of the jam front position at an early stage in order to be able to switch to the new driving strategy in time. It has been shown that propagating jam fronts cannot be detected reliably enough on the basis of the vehicle's local information. In order to improve the accuracy of determining the traffic states the detection algorithm is extended by adding non-local information that can be provided by inter-vehicle or infrastructure-to-car communication. As concerns inter-vehicle communi-

cation, a simulation study has demonstrated the whole cycle of information generation, propagation, reception, processing and autonomous on-board estimation of the upcoming traffic situation. The simulations demonstrate that the “store and forward” strategy (that is, vehicles in the opposite driving direction serving as intermediate stations keeping information and sending messages at a later point in time to other equipped vehicles in the considered driving direction) allows for a sufficient connectivity resulting in the effectual propagation of information even in the case of a limited broadcast range and a low percentage of equipped vehicles.

The efficiency of the proposed driving strategy even with a low market penetration is a promising result for the successful application of future driver assistance systems. In addition to the application for traffic-adaptive cruise control, the detection, interpretation and prediction of local traffic situations in combination with future communications technologies can be used for the development of future driver information systems.

Preface

> *The volume of vehicular traffic in the past several years has rapidly out-stripped the capacities of the nation's highways. It has become increasingly necessary to understand the dynamics of traffic flow and obtain a mathematical description of the process.*
>
> Harold Greenberg (1959)

Starting from this quotation by H. Greenberg, the present doctoral thesis intends to approach these essential and still relevant problems for an efficient transportation system from two perspectives. To begin with, the fundamental issue of a quantitative and microscopic modeling of the human driving behavior and the emerging collective traffic dynamics are addressed. Furthermore, an automated driving strategy for future advanced driver assistance systems is proposed and the impact on the capacity and, thus, for a more efficient road usage is investigated. I hope that this work will contribute to a better understanding of the fascinating dynamics of vehicular traffic and to the development of future applications of not only autonomous but also cooperative vehicles on our roads.

This work has been conducted at the Chair of Traffic Modelling and Econometrics at the Technische Universität Dresden. First and foremost, I would like to express my gratitude to Prof. Dr. Dirk Helbing for having supervised this work and for providing perfect working conditions and a stimulating environment. It has been an exciting and challenging time to work in his international research group. Parts of the work were carried out within the framework of the German research project INVENT. I would like to thank Dr. H.-J. Stauss for the excellent collaboration and the Volkswagen AG for financial support.

I would also like to express my gratitude to my dear colleague Dr. Martin Treiber for the innumerable inspiring discussions over the years. He introduced me to his exciting work in the field of traffic dynamics. I greatly appreciate his extraordinary generosity in sharing his knowledge and his ability for teamwork. I also thank Alison C. Wade and Christian Thiemann for carefully reading the manuscript. Furthermore, I thank Martin Schönhof for the never-ending discussions and the shared experiences as office mates, physicists and doctoral candidates. I also would like to thank all my colleagues for our time together.

Last but not least, I would like to express my gratitude to my parents Ingrid and Bernd and my sister Dörte for their support and confidence in me. And, albeit impossible to express in one sentence, I deeply thank Claudia for all her love and understanding over the years. When looking at our daughter, all words are dispensable anyway.

Arne Kesting, February 2008.

Contents

List of Figures

List of Tables

1 Introduction

An efficient transportation system is essential for the functioning and prosperity of modern, industrialized societies. Mobility is also an integral part of our quality of life, self-fulfillment, and personal freedom. Improving traffic safety and keep traffic flowing in the face of growing demands on the road networks is one of the greatest challenges. Nowadays, we additionally have to balance the human desire for personal mobility with the societal concerns about its environmental impact and energy consumption.

Today's traffic demand is predominantly served by individual motor vehicle travel which is the primary means of transportation. In Germany, for example, motorized vehicles constitute 77 % of the individual transport (measured in terms of passenger-kilometers) and 70% of the total freight traffic (measured in tonne-km) [153]. Therefore, the capacity of the national freeway networks is of prime importance. While the German *autobahn* system only represents 4% (i.e., 12 000 km) of the total road network, it accounts for about 25% of the total motorized traffic performance while providing a higher traffic safety compared to the total road network by a factor of two [153].[1]

However, as the volume of transport has continuously grown faster than the construction of transportation infrastructure over the last decades, traffic congestion has become a severe problem in many countries. It is expected that the traffic volume will further rise in most major urban areas worldwide. According to a study of the European Commission, the external costs of congestion already amount to 0.5% of the gross national product (GNP) in the European Union and will increase up to 1% by the year 2010 [148].[2] In Germany alone, the financial damage due to congested traffic is estimated at € 20 billion each year. Similar proportions are determined for the USA with total costs of about € 55 billion due to congestion in 2005, which corresponds to 0.7% of the GNP [105].

A sound approach to reducing congestion will require a mix of policies affecting *demand* as well as *capacity*. On the one hand, travel demand might be reduced (or shifted in time thereby levelling out peaks) by raising tolls or other taxes or by promoting public transport

[1] Fortunately, much progress has been made in reducing the number of transportation-related fatalities since the 1970s. It is the ambition of the European Union to continue this progress with the goal of halving the number of traffic fatalities by 2010 [149].

[2] The cost components associated with congestion are delay costs and fuel costs, whereas it is typically assumed that the time loss is the predominant influencing factor. Nevertheless, the economic loss of traffic accidents and the environmental impact due to traffic congestion are not considered in this estimate.

or greater vehicle occupancy (e.g, car-pooling). In any case, this involves the enforcement by public authorities. On the other hand, an extension of transport infrastructure is no longer an appropriate or desirable option in densely populated areas. Moreover, the planning can take ten or more years, the construction requires high investments, and the maintenance is costly in the long run.

Hence, engineers are seeking solutions how the capacity of the road network could be used more efficiently and how operations can be improved by using new technologies. In order to reach a more efficient road usage and to relieve traffic congestion, considerable research is performed in the area of *Intelligent Transportation Systems* (ITS). The term ITS is used to describe a collection of concepts and services to improve the safety, mobility, efficiency, and environmental impact of vehicle and, particularly, freeway systems, while the main focus is on the integration of information and communication technologies (ICT) with transport infrastructure, vehicles, and users [97]. *Road-based* ITS strategies are, e.g., advanced traffic control systems such as variable message signs, adaptive speed limits, dynamic route guidance, incident management, and entrance ramp metering. In the 1990s, *automated highway systems* (AHS) based on automated road vehicles have been proposed as a visionary application of *vehicle-based* ITS [50, 130, 117, 42]. The concept of fully automated vehicle control allows for very small time headways and platoon driving, which is obviously a key to greater capacity. Nevertheless, such systems need special infrastructure and dedicated lanes which can only be justified if the percentage of automated vehicles is sufficiently high. These constraints seem to make this scenario unlikely for the foreseeable future [99].

However, with the recent advent of advanced driver assistance systems, at least partly automated driving is already available for basic driving tasks such as accelerating and braking by means of adaptive cruise control systems. These systems are already available on the market and they are expected to spread in the future. So far, ACC systems have been considered exclusively as convenience systems. Nevertheless, a growing market penetration makes the question of their impact on traffic flow more pressing. The challenging question is whether it is possible to design vehicle-based control strategies aimed at improving the capacity and stability of traffic flow. This thesis will propose an extension of today's ACC systems by considering an adaptive driving strategy which contains several driving modes depending on the traffic conditions. The effects of those upcoming driver assistance systems on the collective freeway traffic dynamics will be addressed by means of microscopic traffic simulations.

This provides the starting point for the remainder of the Introduction. In the following Sec. 1.1, an overview of actual advanced driver assistance systems will be provided. In particular, the focus will be on adaptive cruise control systems which are the first driver assistance systems with the potential to influence traffic flow characteristics. In Sec. 1.2,

mathematical approaches for describing the driving behavior and the traffic flow dynamics will be reviewed. This introductory chapter will be completed by giving an outline of the thesis structure and an overview of the remaining chapters (Sec. 1.3).

1.1 Driver Assistance and Adaptive Cruise Control Systems

Technology is rapidly increasing the capabilities of modern vehicles. Continuous advances in solid-state electronics, sensors, computer technology and control systems are pushing this trend. During the last decades, a variety of driver assistance systems have been deployed by automotive manufacturers to improve longitudinal and lateral vehicle control, to automate driving operations, and to reduce the driver burden. Prominent and well-established examples are *anti-lock braking systems*, preventing the wheels from locking during braking maneuvers, and the *electronic stability control*, preventing vehicles from spinning and drifting out.

In the future, this trend will most likely be continued by the emergence and advancement of *Advanced Driver Assistance Systems* (ADAS). These involve sensor-based systems which continuously evaluate the surroundings of the vehicle, display relevant information to the driver and even take control of the vehicle. In cooperation with upcoming information and communication technologies, ADAS hold great promise in increasing the safety, convenience and efficiency of driving. Functionality that is already available, either commercially or as a prototype, include the following:

- In-vehicle navigation systems using up-to-date traffic information.
- Lane departure warning and lane-keeping assistance systems.
- Collision warning systems and active pre-crash assistance.
- Intelligent speed adaptation using extended digital maps.
- Infrared technology for enhanced vision during the night and automated marking of pedestrians.
- Driver condition/drowsiness monitoring systems.
- Automatic parking and 'steer-by-wire' technologies.

Adaptive cruise control (ACC) systems[3] have been available on the market since the late 1990s. These systems enable the automation of basic driving tasks such as accelerating and

[3]The terminology is not fixed until now. In the literature, the abbreviation ACC refers to *adaptive*, *automatic* or *advanced* cruise control systems. Sometimes, these systems are also called *intelligent cruise control* (ICC) or *intelligent adaptive cruise control* (IACC) systems. However, all these terms are typically used synonymously.

braking thereby extending earlier cruise control systems which were designed to reach and maintain a certain speed preset by the driver. The ACC system extends this functionality to situations with significant traffic in which driving at constant speed is not possible. The driver cannot only adjust the desired velocity but also set a certain safety time gap (typically in the range between 1 and 2.5 s) determining the distance to the leading car when following slower vehicles. The task of the ACC system is to calculate the appropriate acceleration or deceleration as a function of the input quantities and the driver's settings. Therefore, the actual distance and speed difference to the vehicle ahead is measured by means of a long-range radar sensor which is able to detect and to track vehicles at a distance of up to 200 m. Figure 1.1 shows the components of an ACC system.

The development and use of new driver support systems naturally raises questions about the driver activity and behavioral adaptation aspects which are addressed in the literature as well [127, 45, 111]. Concerning ACC systems, the study 'The Assisted Driver' as part of the Dutch innovation program Roads to the future [147] observed the individual use of ACC and lane departure warning (LDW) systems. After three months of driving with both systems, the participants were more satisfied with the ACC than with the LDW system. They stated that they had more confidence in the ACC system and thought it had a greater effect on traffic safety. It was observed that participants were able to concentrate better, anticipate better and be more vigilant. However, the participants were also more inclined to perform secondary tasks. Furthermore, it had been stated that the ACC system reacted too slowly in terms of acceleration when overtaking.

Hence, present ACC systems offer a gain in comfort in most driving situations on freeways and they are expected to spread in the future. Nevertheless, it should be emphasized that today's ACC systems only operate above a certain velocity threshold (typically 30 km/h) and are limited in their acceleration and braking range, typically to magnitudes below $3\,\mathrm{m/s^2}$. However, the next generation of ACC will be designed to operate in all speed ranges and in most traffic situations on freeways including stop-and-go traffic by offering a 'follow-to-stop' functionality. In addition, future ACC systems will also have the potential to actively prevent a rear-end collision and thus to achieve a gain in safety. Note, however, that ACC systems only control the longitudinal driving task. In contrast, merging, lane changing or creating gaps for other vehicles still need the intervention of the driver. So, as the driver still stays fully responsible, he or she can override the system at any time.

However, today's implementations of ACC systems are exclusively designed to increase the individual driving comfort, while the influence of ACC systems on the surrounding traffic is not yet considered or optimized. Nowadays, expecting a growing market penetration of these devices, this is no longer justified and the question of their impact on traffic flow becomes more pressing. For example, the German research initiative Invent focused on the development and deployment of innovative vehicle technologies and ad-

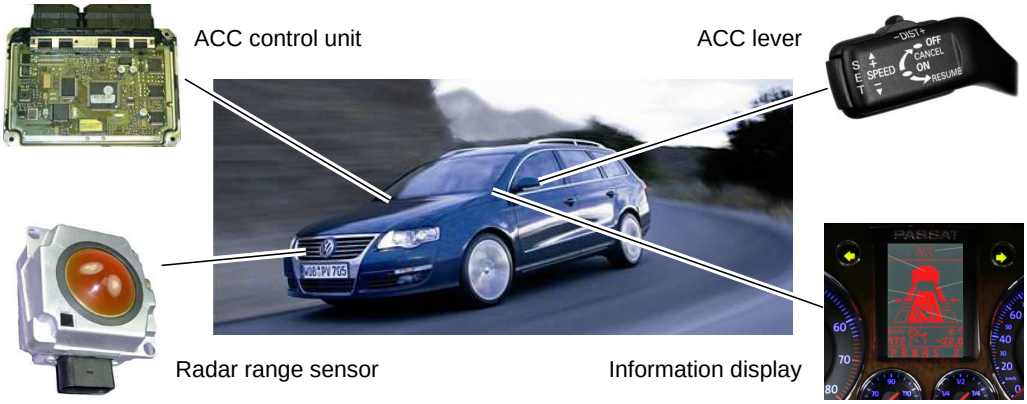

Figure 1.1: Components of an adaptive cruise control (ACC) system as presented in Ref. [66]. The key component of an ACC system is a (typically 77 GHz) *radar sensor* which is able to detect vehicles ahead at a distance of up to 200 m. The required acceleration is calculated from the distance and the velocity data by a *control unit*. The driver presets a desired speed and a preferred safety time gap via a *lever* near the steering wheel. The actual coverage of the radar sensor and the tracking status is displayed in the vehicle's instrument panel.

vanced driver assistance systems for safer and more efficient future traffic systems[4]. In particular, Volkswagen presented an ACC system that has been able to operate in all speed regimes including stop-and-go conditions and follow-to-stop behavior [67, 66].

In order to ensure that ACC systems will be developed and implemented in ways that improve, rather than degrade, traffic conditions, the impact of these systems on the traffic dynamics has to be taken into account. The challenging question is whether it is possible to design *vehicle-based control strategies aimed at improving the capacity and stability of traffic flow*. This thesis will provide a simulation framework for considering collective aspects emerging from individual driving characteristics. In particular, an extension of ACC towards *traffic-adaptive cruise control* systems will be proposed by introducing an automated driving strategy that depends on the local traffic situation.

1.2 Modeling of Driver Behavior and Traffic Dynamics

As mentioned, ACC systems are the first driver assistance systems with the potential to influence traffic flow characteristics. For a quantitative description and assessment of the *collective traffic dynamics of mixed traffic flows* emerging from the *driving behavior of individuals*, one has to start with traffic models which capture the 'nature' of automated and manual driving to a realistic degree.

Remarkably, the mathematical description of the dynamics of traffic flow has a long history

[4]See Appendix B on page 169 for a more detailed overview.

already. The scientific activity had its beginnings in the 1930s with the pioneering studies on the fundamental relations of traffic flow, velocity and density conducted by Greenshields [30]. By the 1950s, scientists had started to describe the physical propagation of traffic flows by means of dynamic macroscopic and microscopic models. During the 1990s, the number of scientists engaged in traffic modeling grew rapidly because of the availability of better traffic data and higher computational power for numerical analysis.

Traffic models have been successful in reproducing the observed collective, self-organized traffic dynamics including phenomena such as breakdowns of traffic flow, the propagation of stop-and-go waves (with a characteristic propagation velocity), the capacity drop, and different spatiotemporal patterns of congested traffic due to instabilities and nonlinear interactions [33, 59, 55, 14, 19].[5] For an overview of experimental studies and the development of miscellaneous traffic models, please consult the recently published extensive review literature [33, 15, 83, 76, 47, 71].

Before going into detail about the possible mathematical models, it is worth mentioning differences between modeling traffic flow and the approach used for transportation planning. While dynamic flow models explicitly describe the *physical propagation of traffic flows* of a given traffic volume in a road network, transportation planning models deal with the calculation of the traffic demand by considering the *decisions of travellers* to participate in economical, social and cultural activities. The need for transportation arises because these activities are spatially separated. The classical approach in trip-based transportation models is based on a four-step methodology of *trip generation*, *trip distribution*, *mode split* and *traffic assignment* [90, 101, 17, 77]. In the fourth step, the origin-destination matrix of trips with a typical minimum disaggregation of time slices of one hour is assigned to routes in the actual (or prospective) transportation network while taking into account the limited capacity of the road infrastructure by means of simplified effective models.

In general, there are two major approaches to describe the spatiotemporal propagation of traffic flows. *Macroscopic traffic flow models* make use of the picture of traffic flow as a physical flow of some fluid. They describe the traffic dynamics in terms of aggregated macroscopic quantities like the traffic density, traffic flow or the average velocity as a function of space and time corresponding to partial differential equations (cf. Fig. 1.2). The underlying assumption of all macroscopic models is the conservation of vehicles (expressed by the continuity equation) which was initially considered by Lighthill, Whitham and Richard [72, 100]. More advanced, so-called 'second-order' models additionally treat the

[5] At first glance, it may be surprising that simple (and deterministic) mathematical models aimed at describing the complexity of and variations in the human behavior, individual skills and driving attitudes would lead to reasonable results. However, a traffic flow can (in a good approximation) be considered as a one-dimensional system (with reduced degrees of freedom). Furthermore, traffic models typically assume rational and safe driving behavior as a reaction to the surrounding traffic while taking into account the fundamental laws of kinematics.

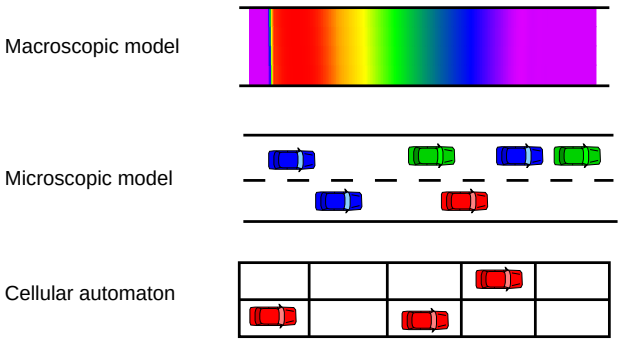

Figure 1.2: Illustration of different traffic modeling approaches: A snapshot of a road section at time t_0 is either characterized by *macroscopic traffic quantities* like traffic density $\rho(x, t_0)$, flow $Q(x, t_0)$ or average velocity $V(x, t_0)$, or, *microscopically*, by the positions $x_\alpha(t_0)$ of single driver-vehicle units α. For cellular automata (CA), the road is divided into cells which can be either occupied by a vehicle or empty.

macroscopic velocity as a dynamic variable in order to also consider the finite acceleration capability of vehicles [54, 123].

By way of contrast, *microscopic traffic models* describe the motion of each individual vehicle, i.e., they model the action (such as accelerations, decelerations and lane changes) of each driver as a response to the surrounding traffic. Microscopic traffic models are especially suited to the study of heterogeneous traffic streams consisting of different and individual types of driver-vehicle units.[6] The result is the individual trajectories of all vehicles and, consequently, any macroscopic information by appropriate aggregation (cf. Fig. 1.2).

In order to describe the complete task of car driving, microscopic models generally comprise an *acceleration strategy* towards a desired velocity in the free-flow regime, a *braking strategy* for approaching other vehicles or obstacles, and a *car-driving strategy* for maintaining a safe distance when driving behind another vehicle. Microscopic traffic models typically assume that human drivers react to the stimulus from neighboring vehicles with the dominant influence originating from the directly leading vehicle.[7] In addition, the individual driver's behavior is characterized in terms of *model parameters* such as a desired velocity, a preferred gap to the vehicle ahead while following, a limited acceleration, a comfortable deceleration, a reaction time, etc. Furthermore, human drivers often exhibit more complex driving patterns such as different kinds of anticipation, limited attention spans

[6] The term *driver-vehicle unit* refers to the concept that an atomic entity includes characteristics of the human driver (e.g., driving 'conservatively' or 'aggressively') as well as features of the vehicle (such as its length, motorization, etc.).

[7] Note that the restriction to interactions regarding only the leader is the basic approximation of so-called 'follow-the-leader' or car-following models.

and miscellaneous adaptation processes that might be taken into account as well. Finally, the individual driving style is often influenced and restricted by the environment (e.g., rain and limited visibility), traffic legislation (e.g., speed limits) or physical limitations (e.g., uphill gradients, motorization of the vehicle, its braking capabilities).

Specifically, one can distinguish the following major subclasses of microscopic traffic models (cf. Fig. 1.2):

- *Time-continuous models* are formulated as ordinary- or delay-differential equations and, consequently, space and time are treated as continuous variables. *Car-following models* are the most prominent examples of this approach [3, 124, 51, 113]. In general, these models are deterministic but stochasticity can be added in a natural way [126]. For example, a modified version of the Wiedemann model [133] is used in the commercial traffic simulation software PTV-VISSIM™ [145].

- *Cellular automata* (CA) use integer variables to describe the dynamic state of the system. The time is discretized and the road is divided into cells which can be either occupied by a vehicle or empty (cf. Fig. 1.2). Besides rules for accelerating and braking, most CA models require additional stochasticity. The first CA for describing traffic has been proposed by Nagel and Schreckenberg [84]. Although CA lack the accuracy of time-continuous models, they are able to reproduce some traffic phenomena [69, 39, 63]. Due to their simplicity, they can be implemented very efficiently and are suited to simulating large road networks [152].

- *Iterated coupled maps* are between CA and time-continuous models. In this model class, the update time is considered as an explicit model parameter rather than an auxiliary parameter needed for numerical integration. Consequently, the time is discretized while the spatial coordinate is still continuous. Popular examples are the Gipps model [26] and the Newell model [88]. However, these models are typically associated with car-following models as well.

In assessing the effects of upcoming driver assistance systems (such as ACC systems) on the collective traffic dynamics (in particular, on the capacity and stability of traffic flow), the microscopic modeling approach is the most appropriate because it allows for a natural representation of heterogeneous driver-vehicle units and for a detailed specification of the parameters and proportions of ACC vehicles and manually driven vehicles. Therefore, the effects of ACC systems on traffic flow have usually been addressed in the literature by simulations [128, 129, 62, 48, 81, 22, 112]. However, up to now, there is not even clarity about the sign of these effects. Some investigations predict a positive effect [120, 22] while others are more pessimistic [59, 79]. Nevertheless, in realistically assessing the impact of ACC on the capacity and traffic stability, the modeling approaches have to capture

the driving dynamics of ACC and manually driven vehicles and the relevant interactions between them. Consequently, the findings depend on the model fidelity, the modeling assumptions and, in particular, on the settings for the time gaps [128, 130].

This is the starting point for this thesis, in which the question of the impact of individual (and automated) driving behavior on the collective traffic dynamics will be assessed. Before this, the methodological fundamentals will be dealt with. Time-continuous microscopic models will be presented and the evolving system dynamics studied numerically. For these purposes, traffic simulation software has been developed which will be described particularly with regard to the traffic simulations of mixed traffic flows consisting of driver-vehicle units characterizing ACC systems and 'human drivers'.

1.3 Thesis Overview and Outline

The thesis consists of two major parts. The focus will be on future ACC systems and their potentials for applications in the context of vehicle-based intelligent transportation systems (Part II). This relates to the *collective characteristics of traffic flow* which can solely be answered by means of computer simulations and requires an integrated microscopic simulation approach. In Part I, the methodological fundamentals will be developed which will deal with microscopic models for both the longitudinal vehicle control and the lane-changing behavior. The outline of the thesis is illustrated in Fig. 1.3.

Chapter 2 will introduce the **Intelligent Driver Model (IDM)** which has been published by M. Treiber *et al.* in 2000 [124]. The IDM will be used as the basic car-following model throughout the thesis because it realistically reproduces the observed phenomena of freeway traffic. Moreover, the model parameters are all meaningful and therefore allow for an intuitive description of different driving styles which will be needed in Part II. The model's acceleration function and its model parameters will be carefully investigated. The properties of equilibrium traffic and collective instabilities will also be discussed.

In **Chapter 3**, a **methodology to calibrate and validate** a car-following model with respect to empirical microscopic (floating car) data will be presented. By means of a nonlinear optimization procedure based on a genetic algorithm, the IDM parameters will be calibrated by minimizing the deviations between the observed driving dynamics and the simulated trajectory with respect to the same leading vehicle. The calibration study will show to what degree the IDM is able to reproduce human driving behavior and will provide further insights into the model's parameter space.

In **Chapter 4**, the **Human Driver Model (HDM)** will be presented as a general framework for extending car-following models towards especially human characteristics such as reaction time, perception errors, limited attention spans and different kinds of

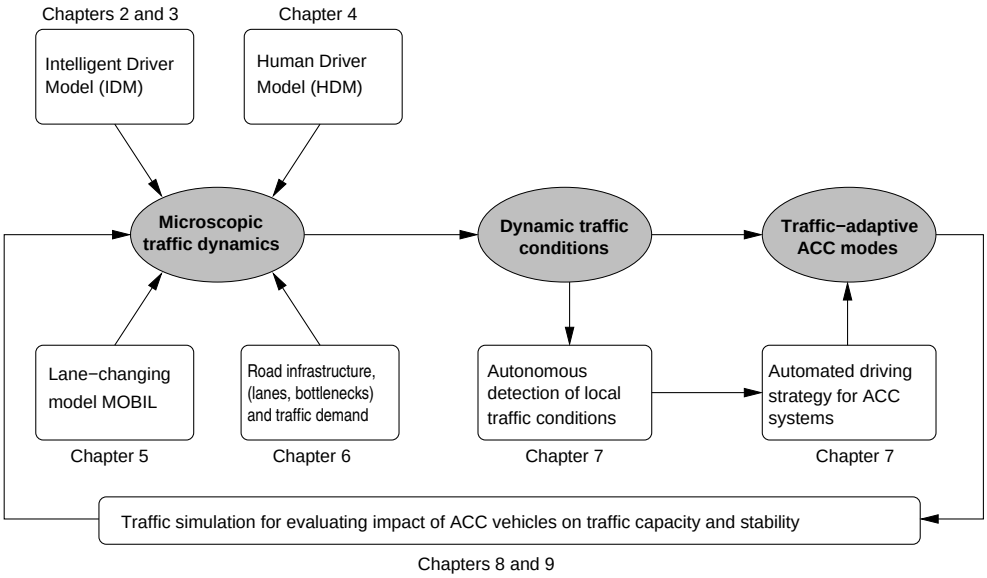

Figure 1.3: Illustration of the thesis structure. In Part I, the components needed for the development of a microscopic multi-lane freeway simulator are introduced. Part II presents a concept for extending ACC systems towards a strategy layer that adapts the ACC driving characteristics to the local traffic situation which has to be detected autonomously by a detection model. The impact of a given proportion of ACC-equipped vehicles on the traffic dynamics will directly be evaluated ('in-the-loop') within the traffic simulation software.

human anticipation. Applying the concept to the IDM allows us to carefully distinguish between reaction time, adaptation time and update time. By means of simulation, the role of each of these times will be investigated with respect to instabilities of traffic flow. The analysis of the model enables us to understand and to assess the impact of generically *human factors* on the driving behavior. This research question will also be relevant against the background of the operational differences between human drivers and automatically controlled vehicles by means of ACC.

In addition to the task of longitudinal vehicle control, **lane-changing behavior** is an important component of microscopic traffic simulators (**Chapter 5**). **MOBIL**[8] will be presented as a general decision model for lane changes. Apart from using accelerations as utility measures for the attractiveness of a prospective lane change, the main novel feature of the proposed lane-changing model lies in the taking into account of the (dis-)advantage of the followers via a 'politeness parameter'.

In **Chapter 6**, the developed software framework that integrates these model components into a **microscopic multi-lane simulator** for freeway traffic will be summarized. The simulator will be needed for the evaluation of the impact of ACC-equipped vehicles on the resulting traffic dynamics in Part II (cf. Fig. 1.3).

[8] An acronym meaning 'Minimizing Overall Braking Induced by Lane Changes'.

In order to ensure that adaptive cruise control (ACC) systems (cf. Sec. 1.1) are implemented in ways that improve, rather than degrade, traffic conditions, the thesis proposes an extension of ACC towards *traffic-adaptive cruise control* with an actively jam-avoiding driving strategy (**Chapter 7**). The novel concept of a **traffic-adaptive cruise control system** will be introduced and the system components presented in detail. The three components of the model are (i) the ACC itself, (ii) an algorithm for the automatic real-time detection of the traffic situation based on local information, and (iii) a 'strategy matrix' that associates the autonomously detected traffic situation with different parameters of the ACC, i.e., implements different driving characteristics. Optionally, inter-vehicle and infrastructure-to-car communication can be used to improve the accuracy of determining the traffic states.

The autonomous traffic-state detection requires surrounding traffic as input while the ACC-equipped vehicles respond to the overall traffic dynamics. Consequently, the impact of a given ACC proportion on the resulting traffic dynamics can only be studied by means of microscopic traffic simulations. In **Chapter 8**, the **impact of the proposed ACC extension on the traffic dynamics** will be investigated by means of simulations of a freeway with different bottlenecks (more specifically, an on-ramp and an uphill gradient) and different kinds of driver-vehicle units (such as cars and trucks). The simulations serve as 'proof of concept' and give quantitative estimates for the effectiveness of the proposed driving strategy on the relevant capacities. In particular, the question of how a variable percentage of ACC-equipped vehicles influences the stability and capacity of traffic flow is assessed.

In **Chapter 9**, the proportion of ACC-equipped vehicles will be systematically varied. The relevant capacities of the system dynamics under free and congested traffic, namely, the **maximum free flow until the traffic flow breaks down** (i.e., the maximum throughput) and the **dynamic capacity** (i.e., the downstream outflow from traffic congestion) will be evaluated. A summary of the findings and a discussion of potential applications for future driver assistance systems will conclude the thesis (**Chapter 10**).

Part I

Microscopic Modeling of Human and Automated Driving

2 The Intelligent Driver Model

In this chapter, the Intelligent Driver Model (IDM) will be described which has been published by Treiber, Hennecke and Helbing in 2000 [124, 154]. The IDM belongs to the class of deterministic follow-the-leader models which are a subset of microscopic traffic flow models as presented in Sec. 1.2 of the Introduction.

2.1 Acceleration Equation

A microscopic traffic flow model describes the motion of each individual vehicle. Car-following models such as the IDM assume that the dominant influence on driving behavior comes from the vehicle ahead, called the leading vehicle, cf. Fig. 2.1.

The IDM acceleration function $\dot{v}_\alpha(t) := \frac{\mathrm{d}v}{\mathrm{d}t}$ of each vehicle α is a continuous function of the actual velocity $v_\alpha(t)$, the net distance gap $s_\alpha(t) = x_{\alpha-1}(t) - x_\alpha(t) - l_{\alpha-1}$ and the velocity difference $\Delta v_\alpha(t)$ to the leading vehicle of length $l_{\alpha-1}$:

$$\dot{v}_\alpha(s_\alpha, v_\alpha, \Delta v_\alpha) = a \left[1 - \left(\frac{v_\alpha}{v_0} \right)^\delta - \left(\frac{s^*(v_\alpha, \Delta v_\alpha)}{s_\alpha} \right)^2 \right]. \tag{2.1}$$

This expression is a superposition of the acceleration $\dot{v}_{\mathrm{free}}(v) = a[1-(v/v_0)^\delta]$ on a free road and the braking deceleration $-\dot{v}_{\mathrm{int}}(s, v, \Delta v) = a(s^*/s)^2$ reflecting a repulsive interaction, when vehicle α comes too close to the vehicle ahead. The deceleration term depends on the ratio between the effective 'desired minimum gap'

$$s^*(v, \Delta v) = s_0 + vT + \frac{v\Delta v}{2\sqrt{ab}} \tag{2.2}$$

and the actual gap s_α. Here and throughout this thesis, we assume that the vehicle indices α are ordered such that $(\alpha - 1)$ denotes the preceding vehicle. Notice that the velocity difference is defined as approaching rate, $\Delta v_\alpha := v_\alpha - v_{\alpha-1}$.

The minimum distance s_0 in congested traffic is significant for low velocities only. The main contribution in stationary traffic is the term vT which corresponds to following the leading vehicle with a constant 'safety time gap' T.[1] The last term is only active in non-stationary

[1] In the original definition of the IDM in Ref. [124], the Eq. (2.2) for s^* contains an additional term

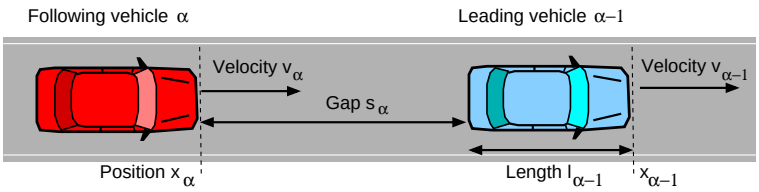

Figure 2.1: Illustration of the input quantities of a car-following model: The bumper-to-bumper distance s for a vehicle α with respect to the vehicle $(\alpha - 1)$ (the 'leader') in front is given by $s_\alpha = x_{\alpha-1} - x_\alpha - l_{\alpha-1}$, where l_α is the vehicle length and x the position on the considered road stretch. The approaching rate (relative velocity) is defined by $\Delta v_\alpha := v_a - v_{\alpha-1}$. Notice that the vehicle indices α are ordered such that $(\alpha - 1)$ denotes the preceding vehicle.

traffic with $\Delta v \neq 0$ and implements an 'intelligent' driving behavior including a braking strategy that, in nearly all situations, limits braking decelerations to the 'comfortable deceleration' b. Moreover, the IDM braking strategy guarantees collision-free driving. For a detailed discussion, we refer to the following Sec. 2.2.

The IDM as defined in Eq. (2.1) has six parameters. For the sake of simplicity, we set the acceleration exponent constant to $\delta = 4$ throughout this thesis because this setting corresponds to the most realistic acceleration behavior (see Sec. 2.2). The remaining five IDM parameters, with typical values for freeway traffic together with their reasonable ranges, are listed in Table 2.1. An important feature of the IDM are its few parameters which additionally have an intuitive meaning. All parameters are measurable, and the best values are in a realistic range.[2] In Sec. 2.3 we will show that the *fundamental relations* of homogeneous traffic are calibrated by adaptation of the desired velocity v_0 (at low densities), the safety time gap T (at high density) and the jam distance s_0 (for jammed traffic). In contrast to the stationary behavior, the *stability properties* of the IDM are mainly determined by the maximum acceleration a, the desired deceleration b and by T. Since the accelerations a and b do not influence the fundamental diagram, the IDM can be calibrated essentially independently with respect to the behavior in stationary situations and with respect to the stability of traffic flow.

If the distance to the leading vehicle s_α is large, the interaction term $\dot{v}_{\text{int}}$ is negligible and the IDM equation reduces to the free-road acceleration $\dot{v}_{\text{free}}(v)$ which is a decreasing function of the velocity with the maximum value $\dot{v}(0) = a$. The minimum value is $\dot{v}(v_0) = 0$. Figure 2.2 shows the IDM acceleration function (2.1) as a smooth function of the input quantities s, v and Δv. The model parameters are taken from Table 2.1. Since Eq. (2.1) does not limit the IDM braking deceleration, we also incorporate a maximum physical

with a second 'jam distance' parameter s_1, namely $s_1\sqrt{v/v_0}$. We ignore this term by setting $s_1 = 0$ throughout this thesis. Note that a nonzero s_1 would be necessary for features requiring an inflection point in the fundamental diagram, cf. Sec. 2.3 below.

[2] For matters of illustration, we refer to Chap. 3, in which the IDM parameters are automatically calibrated and validated with respect to microscopic floating car data.

IDM Parameter	Typical value	Reasonable range
Desired velocity v_0 [km/h]	120	50 – 200
Safety time gap T [s]	1.5	0.9 – 3
Jam distance s_0 [m]	2.0	1 – 5
Maximum acceleration a [m/s^2]	1.4	0.3 – 3
Desired deceleration b [m/s^2]	2.0	0.5 – 3

Table 2.1: Model parameters of the Intelligent Driver Model (IDM) together with typical settings and reasonable parameter ranges for different kinds of driver-vehicle units and driving situations. The acceleration parameter is set to $\delta = 4$. Notice that the absolute value of braking decelerations is usually larger than that of accelerations which is limited by the maximum motorization and the desired and comfortable acceleration of the the individual driver.

deceleration of $b_{\max} = 9\,\mathrm{m/s^2}$ corresponding to blocking wheels on dry roads, i.e., we limit $\dot{v}_\alpha$ from below to the value $-b_{\max}$, see Fig. 2.2. Notice that this limit typically is not reached in single-lane simulations, but sometimes in multi-lane traffic simulations where the input quantities s and Δv might change abruptly due to lane changes.

We consider another refinement of the IDM for the case when the actual velocity is larger than the desired velocity, $v > v_0$. For example, an excess of $v = 2v_0$ would lead to an unrealistic braking of $-15a$ for $\delta = 4$. This situation may occur when simulating, e.g., a speed limit on a road segment that reduces the desired velocity locally. Therefore, we replace the free acceleration for the case $v > v_0$ by

$$\dot{v}_{\mathrm{free}}(v) = -b\left[1 - \left(\frac{v_0}{v}\right)^{\delta}\right], \tag{2.3}$$

i.e., the IDM vehicle brakes with the comfortable deceleration b in the limit $v \gg v_0$.

2.2 Dynamic Single-Vehicle Properties

The IDM acceleration function (2.1) is a continuous function of the input quantities s, v and Δv. Let us now discuss the dynamic properties of a single IDM driver-vehicle unit by considering the following limiting cases:

(1) Acceleration to the desired velocity: If the distance s is large (corresponding to the situation of a nearly empty road), the interaction $\dot{v}_{\mathrm{int}}$ is negligible and the IDM equation reduces to the free-road acceleration $\dot{v}_{\mathrm{free}}(v) = a\left[1 - (v/v_0)^{\delta}\right]$. The driver accelerates to

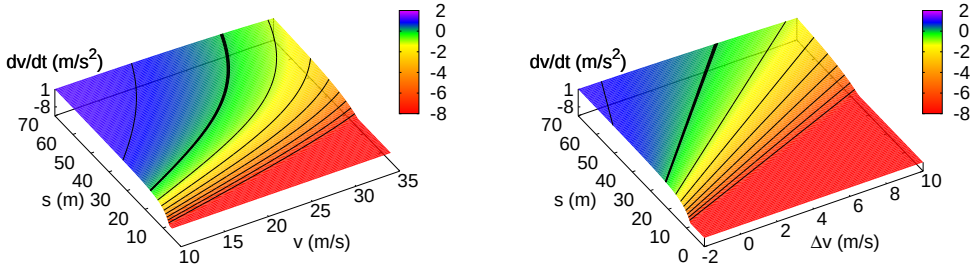

Figure 2.2: Acceleration function (2.1) of the Intelligent Driver Model (IDM) as a function of the net distance to the leading vehicle, s and the actual velocity v while keeping $\Delta v = 0$ constant (left diagram), and as a function of s and the velocity difference Δv at a constant speed of $v = 20\,\mathrm{m/s} = 72\,\mathrm{km/h}$ (right diagram). The contour lines indicate changes in the acceleration of $1\,\mathrm{m/s^2}$. The constant velocity state $\dot{v} = 0$ is marked by a thicker contour line. The IDM parameters are taken from the Table 2.1. The maximum deceleration is limited to $9\,\mathrm{m/s^2}$.

his or her desired velocity v_0 with the maximum acceleration $\dot{v}(0) = a$. The acceleration exponent δ specifies how the acceleration decreases when approaching the desired velocity. The limiting case $\delta \to \infty$ corresponds to approaching v_0 with a constant acceleration a while $\delta = 1$ corresponds to an exponential relaxation to the desired velocity with the relaxation time $\tau = v_0/a$. In the latter case, the free-traffic acceleration is equivalent to that of the optimal velocity model [3]. However, the most realistic behavior is expected in between the two limiting cases of exponential acceleration (for $\delta = 1$) and constant acceleration (for $\delta \to \infty$). Therefore, we set the acceleration exponent constant to $\delta = 4$ throughout this thesis.

In Fig. 2.3, acceleration periods from a standstill to the desired velocity $v_0 = 120\,\mathrm{km/h}$ are simulated for two different settings of the maximum acceleration (the other model parameters are listed in Table 2.1): For $a = 1.4\,\mathrm{m/s^2}$, the acceleration phase takes approximately 40 s while an increased maximum acceleration of $a = 3\,\mathrm{m/s^2}$ reduces the acceleration period to $\sim 15\,\mathrm{s}$. Notice that the acceleration parameter a of $1.4\,\mathrm{m/s^2}$ ($3\,\mathrm{m/s^2}$) corresponds to a free-road acceleration from $v = 0$ to $v = 100\,\mathrm{km/h}$ within 23 s (10.5 s).

(2) Equilibrium traffic: In dense equilibrium traffic corresponding to stationary conditions with $\dot{v} = 0$ and $v \lesssim v_0/2$, drivers follow each other at a constant distance $s_e(v) \approx s^*(v, 0) = s_0 + vT$. This distance is equal to a small contribution s_0 denoting a minimum bumper-to-bumper distance kept in standing traffic, plus a velocity-dependent contribution vT corresponding to a safety time gap T. The equilibrium properties of the IDM are discussed in more detail in Sec. 2.3 below.

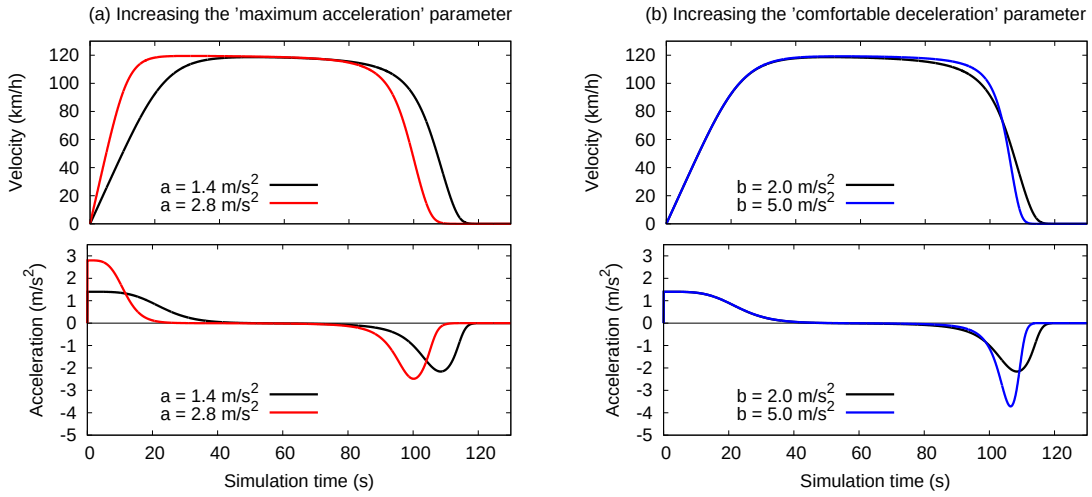

Figure 2.3: Simulation of a single IDM vehicle: The diagrams show the acceleration to the desired velocity $v_0 = 120\,\mathrm{km/h}$ followed by braking as reaction to a standing obstacle located 3000 m ahead for several combinations of the IDM acceleration parameters a [in diagram (a)] and b [in (b)]. The remaining parameters are listed in Table 2.1 on page 17.

(3) Braking as reaction to high approach rates: When approaching slower or standing vehicles with sufficiently high approaching rates ($\Delta v > 0$), the equilibrium part $s_0 + vT$ of the dynamical desired distance s^*, Eq. (2.2), can be neglected with respect to the non-equilibrium part which is proportional to $v\Delta v$. Notice that the restriction to the interaction term with neglecting vT and s_0 corresponds to a *worst-case scenario*. Then, the interaction part $-\dot{v}_{\mathrm{int}} = a(s^*/s)^2$ of the acceleration equation (2.1) is given by

$$\dot{v}_{\mathrm{int}}(s, v, \Delta v) \approx \frac{(v\Delta v)^2}{4bs^2}. \tag{2.4}$$

When assuming a constant deceleration during the whole approaching process towards a standing obstacle ($\Delta v = v$), a minimum kinematic deceleration $b_{\mathrm{kin}} = v^2/(2s)$ would be necessary to avoid a collision, leading to

$$\dot{v}_{\mathrm{int}}(s, v, \Delta v = v) \approx \frac{b_{\mathrm{kin}}^2}{b}. \tag{2.5}$$

The situation is assumed to be 'under control', if b_{kin} is smaller than the 'comfortable' deceleration given by the model parameter b, i.e., $\beta := b_{\mathrm{kin}}/b \leq 1$. With this definition, Eq. (2.5) results in $\dot{v}_{\mathrm{int}} = \beta b_{\mathrm{kin}} < b_{\mathrm{kin}}$. The IDM brakes less than b_{kin} and therefore in an *anticipative* way. With increasing β, the IDM deceleration approaches b_{kin}. Figure 2.3 demonstrates this behavior by means of a simulation: The IDM vehicles with two different settings for b approach a standing obstacle located 3000 m ahead and brakes for $t > 70\,\mathrm{s}$. As expected, the maximum decelerations are lower than, but of the same order as, the

comfortable deceleration b.

(4) Braking in emergency situations: In contrast to the situation (3), an emergency situation is characterized by $b_{\text{kin}} > b$ or $\beta > 1$, leading to $\dot{v}_{\text{int}} > b_{\text{kin}}$. Under the deceleration law (2.5), we get for the considered situation of approaching a standing obstacle

$$\ddot{v}_{\text{int}} = \frac{\mathrm{d}}{\mathrm{d}t}\left[\frac{v^4}{4bs^2}\right] = \frac{v^5}{2b^2s^3}\left(b_{\text{kin}} - b\right). \tag{2.6}$$

Thus, the IDM deceleration *increases* in an emergency case in order to get the situation under control again. Notice that, for $s \to 0$, the braking interaction grows even stronger because of $\ddot{v}_{\text{int}} \to \infty$. Furthermore, Eq. (2.6) shows that the acceleration approaches $\dot{v} = -b$ in both cases of $\beta > 1$ and $\beta < 1$. This driving strategy of the IDM can be characterized as an *'intelligent'* braking behavior which makes the model *collision-free*.

(5) Braking in response to small gaps: This driving mode is active when the gap is much smaller than the 'desired gap' s^*, but there are no large velocity differences. Then, the equilibrium part of s^*, $s_0 + vT$, dominates the dynamic contribution proportional to Δv. Neglecting the free-road acceleration, the IDM acceleration (2.1) reduces to $\dot{v} \approx -a(s_0 + vT)^2/s^2$, corresponding to a Coulomb-like repulsion.

Figure 2.4 shows the car-following dynamics in this regime. For the standard parameters listed in Table 2.1, one clearly sees a *non-oscillatory* relaxation to the equilibrium distance while for very high values of b (e.g., $b = 10\,\mathrm{m/s^2}$), the approach to the equilibrium distance would occur with damped oscillations. Notice that, for the latter parameter set, the *collective* traffic dynamics would already be extremely unstable, cf. Sec. 2.4.

2.3 Equilibrium Traffic and Fundamental Diagram

Equilibrium traffic is defined by vanishing velocity differences and accelerations of the driver-vehicle units α, i.e.,

$$\Delta v_\alpha = 0, \tag{2.7}$$

$$\frac{\mathrm{d}v_\alpha}{\mathrm{d}t} = 0, \tag{2.8}$$

$$\text{and} \quad \frac{\mathrm{d}v_{\alpha-1}}{\mathrm{d}t} = 0. \tag{2.9}$$

Under these stationary traffic conditions, drivers tend to keep a velocity-dependent *equilibrium gap* $s_e(v_\alpha)$ to the leading vehicle. In the following, we consider a homogeneous

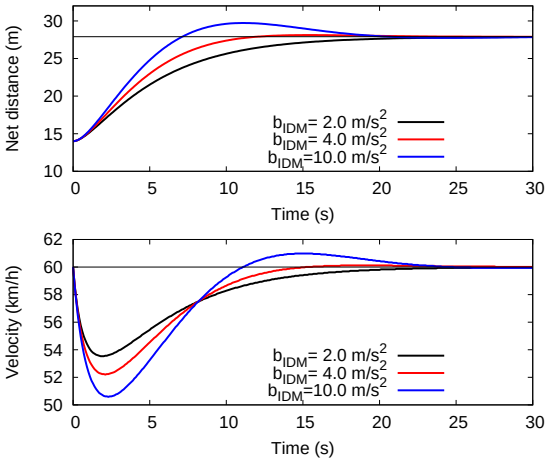

Figure 2.4: Velocity reduction and following adaptation of an IDM vehicle in response to a gap that is initially too small. The upper diagram shows the time series of the gap $s(t)$ and the lower diagram shows the velocity $v(t)$ of a single vehicle following a vehicle that drives at a constant speed of 60 km/h corresponding to an equilibrium distance of $s_e = 28\,\text{m}$ (displayed as a thin straight line). The initial conditions at $t = 0\,\text{s}$ are $v(0) = 60\,\text{km/h}$ and $s(0) = s_e/2 = 14\,\text{m}$. The three curves demonstrate the effect of different settings for the comfortable deceleration parameter b: For $b \leq 4\,\text{m/s}^2$, the braking reaction leads to a non-oscillatory relaxation to the equilibrium distance while for the (unrealistically) high value $b = 10\,\text{m/s}^2$, the approach to s_e occurs with damped oscillations. The other parameters used in the simulation are listed in Table 2.1.

ensemble of identical driver-vehicle units corresponding to identical parameter settings. Then, the IDM acceleration equation (2.1) with the constant setting $\delta = 4$ simplifies to

$$s_e(v) = \frac{s_0 + vT}{\sqrt{1 - \left(\frac{v}{v_0}\right)^4}}. \tag{2.10}$$

The equilibrium distance only depends on the minimum jam distance s_0, the safety time gap T and the desired velocity v_0. The diagrams (a) and (b) in Figure 2.5 show the equilibrium distance as a function of the velocity, $s_e(v)$, for different v_0 and T parameter settings while keeping the minimum distance constant to $s_0 = 2\,\text{m}$. In particular, the equilibrium gap of homogeneous *congested* traffic (with $v \ll v_0$) is essentially equal to the desired gap, $s_e(v) \approx s^*(v, 0) = s_0 + vT$, i.e., it is composed of the minimum bumper-to-bumper distance s_0 kept in standing traffic and an additional velocity-dependent contribution vT corresponding to a constant safety time gap T as shown in the diagrams by straight lines. For $v \to 0$, the equilibrium distance approaches the minimum distance s_0. If the velocity is close to the desired velocity, $v \approx v_0$, the equilibrium distance s_e is clearly larger than the distance vT according to the safety time gap parameter. For $v \to v_0$, the equilibrium distance diverges due to the vanishing denominator in Eq. (2.10). That is, the free speed

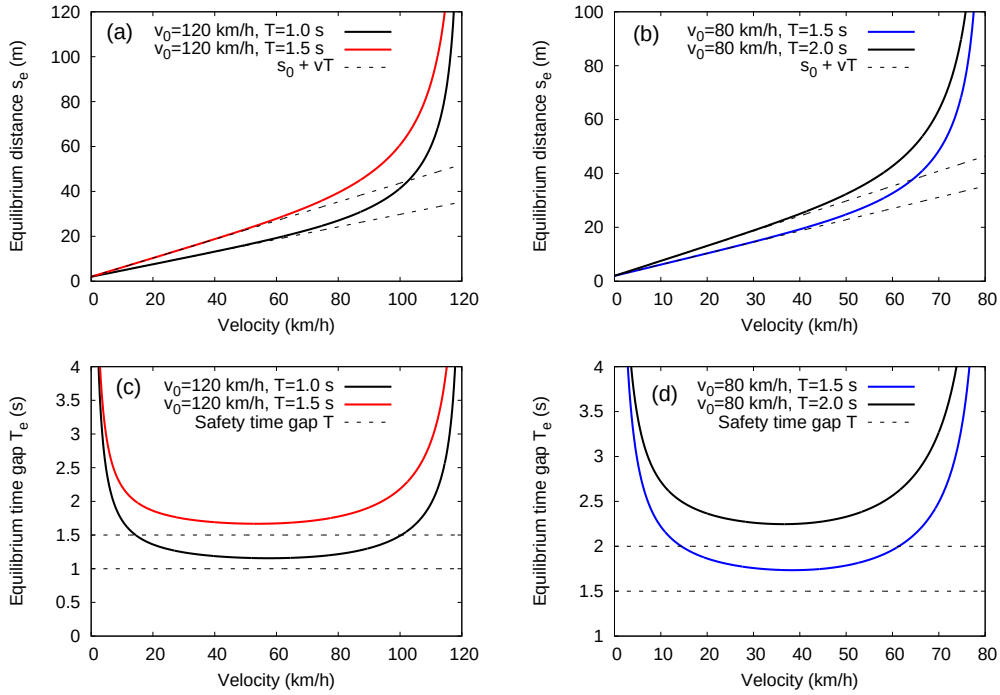

Figure 2.5: Equilibrium distance $s_e(v)$ according to Eq. (2.10) (top), and equilibrium time gap $T_e(v)$ (bottom) according to Eq. (2.11) as functions of the velocity for different settings of the desired velocity v_0 and the safety time gap T. The deviations from the dashed lines are discussed in the main text. The other parameters are those displayed in Table 2.1. Notice that the curve $s_e(v)$ corresponds directly to the contour line for zero acceleration in Fig. 2.2 (i.e., $\dot{v} = 0$).

is reached *exactly* only on a free road.

Additionally, for the interpretation of the safety time gap T, we consider the *equilibrium time gap*,

$$T_e(v) = \frac{s_e(v)}{v}, \tag{2.11}$$

displayed in the diagrams (c) and (d) of Fig. 2.5. Obviously, the actually observed time gap is always larger than the value of the IDM parameter, $T_e > T$. For comparison, notice that T is displayed as a straight line in the plots. For low velocities, we have $T_e \simeq T + s_0/v$, i.e., the *effective* time gap is mainly determined by s_0. For higher velocities, the denominator of Eq. (2.10) is always smaller than 1, with a divergence in the limit $v \to v_0$. For intermediate velocities, the effective time gap is approximately 10–20% *larger* than vT depending on the setting of s_0.

In the literature, the equilibrium state of homogeneous and stationary traffic is often formulated in macroscopic quantities such as traffic flow Q, (local) average velocity V and traffic density ρ. The translation from the microscopic net distance s into the density is

given by the *micro-macro relation*

$$s = \frac{1}{\rho} - l, \tag{2.12}$$

where l is the vehicle length. In equilibrium traffic, ρ is therefore given by s_e, the mean velocity is simply $V = v_e$ and the traffic flow follows from the hydrodynamic relation

$$Q = \rho V. \tag{2.13}$$

So, the equilibrium velocity v_e is needed as a function of the distance s_e. An analytical expression for the inverse of Eq. (2.10), i.e., the *equilibrium velocity* as a function of the gap, $v_e(s)$, is only available for the acceleration exponents $\delta = 1, 2$ or $\delta \to \infty$ [124]. For $\delta = 4$, we only have a parametric representation $\rho(v)$ with $v \in [0, v_0]$ resulting from Eqs. (2.12) and (2.10). Figure 2.6(a) and (b) show the equilibrium velocity-density relation $V_e(\rho)$ for the same parameter settings as in Fig. 2.5. The assumed vehicle length $l = 5\,\mathrm{m}$ together with the minimum jam distance $s_0 = 2\,\mathrm{m}$ results in a maximum density $\rho_{\max} = 1/(s_0+l) \approx 143\,\mathrm{vehicles/km}$. Using the relation (2.13), we obtain the so-called *fundamental diagram* between the traffic flow and the vehicle density, $Q(\rho) = V\rho(v)$ which is displayed in Fig. 2.6(c) and (d). Notice that Q is typically given in units of vehicles per hour and the density ρ in units of vehicles per km.

According to Eqs. (2.10) and (2.12), the *fundamental relations* of homogeneous traffic depend on the desired velocity v_0 (low density), the safety time gap T (high density) and the jam distance s_0 (jammed traffic). In the low-density limit $\rho \ll 1/(v_0 T)$, the equilibrium flow can be approximated by $Q \approx v_0\rho$. In the high density regime, one has a linear decrease of the flow,

$$Q(\rho) \approx \frac{1 - \rho(l + s_0)}{T}, \tag{2.14}$$

which can be used to determine the effective length $l + s_0$ and T. Notice that the vehicle length is not a model parameter but only a scaling quantity that determines the (static) maximum density $\rho_{\max}$ together with the IDM parameter s_0.

2.4 Collective Traffic Instability

Let us finally investigate the *collective traffic dynamics* of many driver-vehicle units on a road section. Under certain conditions and especially on freeways, the collective dynamics resulting from vehicle interactions can cause traffic instabilities, leading to the breakdown of traffic flow.

By simulation of a platoon of IDM vehicles following an externally controlled lead vehicle, we will now investigate the nonlinear dynamics that leads to a transition from free to congested traffic. We assume that the externally controlled first vehicle drives at $v_{\mathrm{lead}} =$

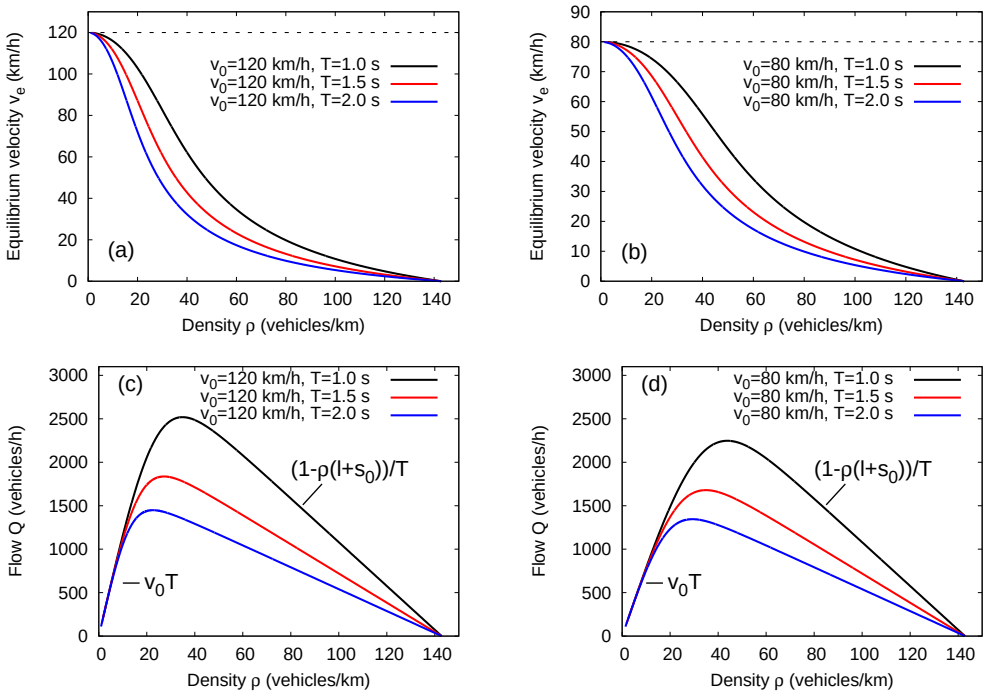

Figure 2.6: Equilibrium velocity-density relations of the IDM (top) and corresponding flow-density relations, so-called *fundamental diagrams* (bottom). The equilibrium properties depend on the minimum distance s_0 (here set to 2 m), the desired velocity v_0 (here displayed for 120 and 80 km/h) and the time gap T (here 1.0, 1.5 and 2.0 s). The safety time gap is the most important parameter determining the maximum flow (stationary freeway capacity).

80 km/h, and the drivers follow each other at their equilibrium distance $s_e \approx 39.4$ m. At $t = 110$ s, the first vehicle decelerates with $-2\,\mathrm{m/s^2}$ for a time period of 5 s. This braking maneuver reduces the velocity to $v_{\mathrm{lead}} = 44$ km/h and serves as initial *perturbation*. At $t = 120$ s, the first vehicle accelerates again to the former velocity of 80 km/h which is maintained for the rest of the simulation time. In order to study the influence on the traffic (in)stability, we vary the setting for the maximum acceleration a while the other IDM parameters used in these simulations are taken from Table 2.1.

Figure 2.7 shows the time series $v(t)$ and $\dot{v}(t)$ of the driving maneuvers of the externally controlled vehicle and the reaction of some selected vehicles further upstream in a one-lane scenario. Depending on the setting of the maximum acceleration, the collective dynamics is *stable* (see Figs. 2.7(a) and (b) for $a = 1.4\,\mathrm{m/s^2}$) or *unstable* (see Figs. 2.7(c) and (d) for $a = 0.4\,\mathrm{m/s^2}$).

For the simulation corresponding to unstable traffic, the trajectories $x_\alpha(t)$ of all vehicles α in the platoon are displayed in a time-space diagram shown in Fig. 2.8. The trajectory diagram shows the spatiotemporal emergence of a *stop-and-go wave* triggered by the braking

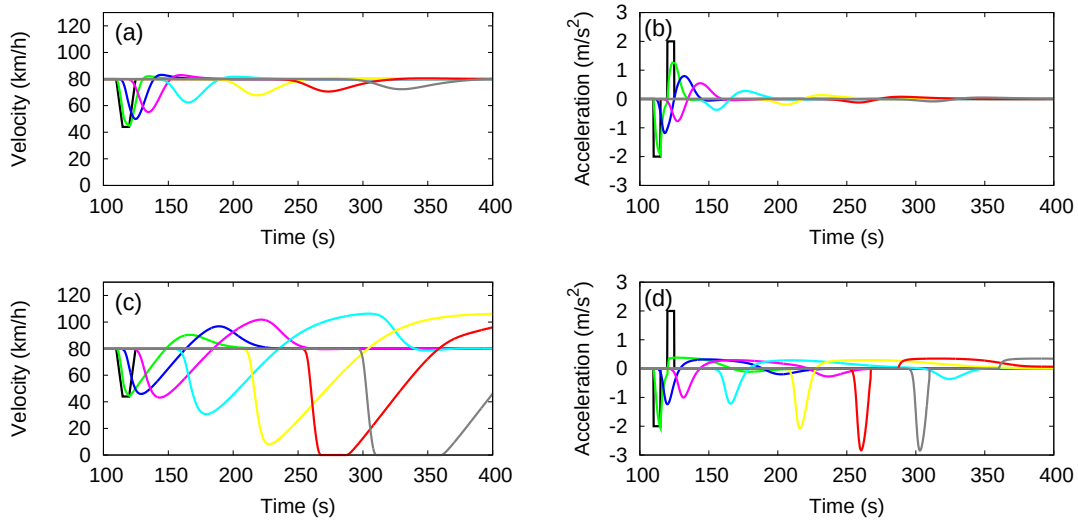

Figure 2.7: Time series $v(t)$ and $\dot{v}(t)$ for some vehicles of a platoon (car 1, 2, 5, 10, 25, 50 and 100) of identical IDM vehicles following an externally controlled lead vehicle. At $t = 110\,\mathrm{s}$, the first vehicle brakes with a constant deceleration of $-2\,\mathrm{m/s^2}$. This initial perturbation is followed by a similar constant acceleration at $t = 120\,\mathrm{s}$, leading again to the former speed of $v_{\mathrm{lead}} = 80\,\mathrm{km/h}$. The simulation corresponding to the acceleration parameter $a = 1.4\,\mathrm{m/s^2}$ results in a *stable* collective traffic dynamics [diagrams (a) and (b)] while a reduction to $a = 0.4\,\mathrm{m/s^2}$ [diagrams (c) and (d)] leads to an *unstable* dynamics which is characterized by increasing braking decelerations. Finally, vehicles further upstream in the platoon even decelerate to a standstill which is associated with the emergence of a *stop-and-go wave*. The other IDM parameters are taken from Table 2.1.

maneuver of the first vehicle at $(t = 110\,\mathrm{s}, x = 13.5\,\mathrm{km})$. Initially, the (small) perturbation travels further downstream. After a while, the (increased) perturbation starts propagating *upstream*, i.e., against the driving direction of the vehicle flow. This can be explained by the time delays that drivers need to react to the changing traffic situation: After the initial braking, the following driver needs some time to respond to this new situation by decelerating him- and herself. Thus, at the time she slowed down to the new velocity, the actual distance is lower than the required safety distance. Therefore, additional braking is necessary, leading to a lower velocity than the one of the vehicle introducing the perturbation. Moreover, the time to re-accelerate to the eventually restored speed of the leading vehicle takes even more time due to the *limited acceleration capabilities*. This response mechanism acts like a 'vicious circle': Each following driver has to reduce his or her velocity a bit more to regain the necessary safety distance which eventually leads to a standstill of some successive vehicles, i.e., to the emergence of a stop-and-go wave.

This *deterministic* mechanism leading to *collective traffic instabilities* due to finite acceleration capabilities is illustrated in Fig. 2.8. The maximum acceleration a corresponds to a velocity adaptation time of the order of $\tau_v = v_0/(4a)$. Thus, traffic becomes more unstable

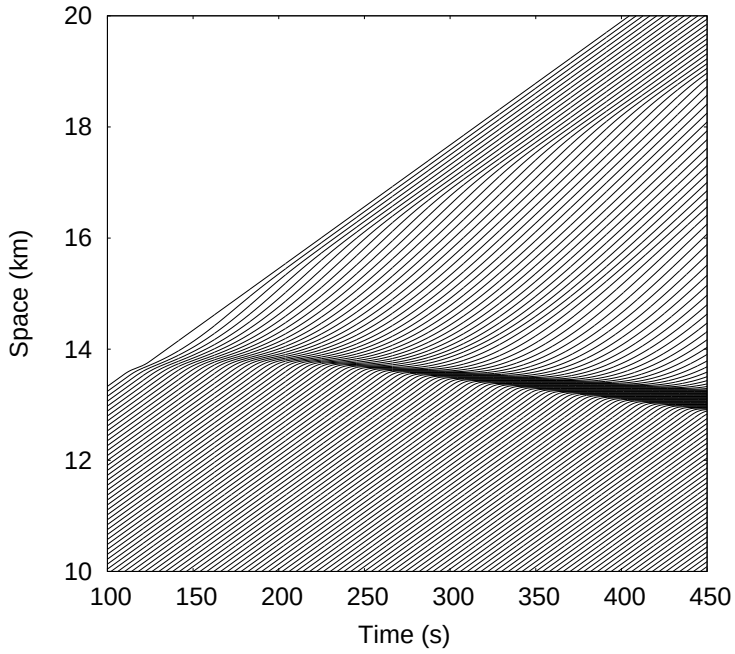

Figure 2.8: Time-space diagram of every second IDM trajectory $x_\alpha(t)$ corresponding to the results shown in Fig. 2.7(c) and (d) with an unstable setting of $a = 0.4\,\mathrm{m/s^2}$. In the simulation, a stop-and-go wave is emerging from the initial perturbation of the externally controlled first vehicle. The propagation speed of the stop-and-go wave against the driving direction is $V_g = \Delta x/\Delta t \approx 13\,\mathrm{km/h}$.

for decreasing values of a (increasing τ_v) because drivers re-adapt slower to the equilibrium speed after the triggered perturbation.[3] The propagation velocity of the downstream front of the stop-and-go wave can be determined from the time-space diagram as approximately 13 km/h which is in good agreement with empirical observations [56, 13] and the IDM is therefore able to reproduce this self-organized property of traffic flows. Notice that the propagation speed is arguable constant ($15 \pm 5\,\mathrm{km/h}$) all over the world.

2.5 Summary

This chapter introduces the Intelligent Driver Model (IDM) [124] which serves as basic model for this thesis. Let us summarize the essential model properties:

- The IDM acceleration is a smooth and continuous function incorporating different driving modes for all velocities in freeway traffic as well as city traffic. Besides

[3] In Chap. 4, we will show that the instability mechanism is robust with respect to typical (acceleration) fluctuations, and to a heterogeneous mixture of driver-vehicle units with statistically distributed values of T and v_0. For a more detailed analysis of the mechanisms of traffic instabilities, we refer to Sec. 4.2, where we also take into account reaction times and finite update times.

the distance to the leading vehicle and the actual velocity, the IDM also takes into account velocity differences, which play an essential stabilizing role in real traffic, especially when approaching traffic jams. Furthermore, considering velocity differences is necessary for a collision-free driving dynamics. The IDM is defined by its acceleration function introduced in Sec. 2.1.

- The IDM contains only a few parameters which all have a reasonable interpretation, are known to be relevant and are empirically measurable. Moreover, the fit parameters have realistic values which will be shown in Chap. 3 by means of calibration with respect to microscopic traffic data.

- The IDM has different regimes for braking and accelerating and shows a plausible microscopic acceleration and deceleration behavior of single driver-vehicle units as discussed in Sec. 2.2. The considered limiting cases offer clear interpretations of the model parameters.

- In equilibrium traffic, the IDM has a velocity-dependent equilibrium gap to the preceding vehicle corresponding to a unique flow-density relation, the so-called fundamental diagram (cf. Sec. 2.3). Moreover, it has been shown that the fundamental diagram and the stability properties of the IDM can be easily (and separately) calibrated to macroscopic empirical data.

- The IDM has been successful in reproducing the characteristic features of macroscopic traffic phenomena such as traffic breakdowns, the capacity drop, the scattering in the fundamental diagram and the propagation of stop-and-go waves or other patterns of congested traffic [124]. Moreover, the IDM shows realistic values of self-organized properties like the propagation velocity of localized clusters or the outflow from jams [56]. In Sec. 2.4, we have investigate in detail the collective dynamics and traffic instability which leads to the emergence of stop-and-go waves.

Let us finally illustrate the concept of follow-the-leader traffic models in terms of control theory. Figure 2.9 illustrates the nonlinear feedback loop of car-following models: The controllers are associated with the driver-vehicle units, the quantity to be controlled is the velocity of the own vehicle (or the distance to the leading vehicle), and the input stimuli are the observed distances and velocities, respectively. The nonlinear acceleration (gain) function (2.1) controls the actions to reach desired velocities or distances by means of accelerating or braking. Let us note that we have to solve the coupled system of *nonlinear ordinary differential equations* for a given set of driver-vehicle units. The IDM can be efficiently integrated numerically using a 'modified Euler' integration scheme. For numerical details, we refer to Chap. 6 on page 101.

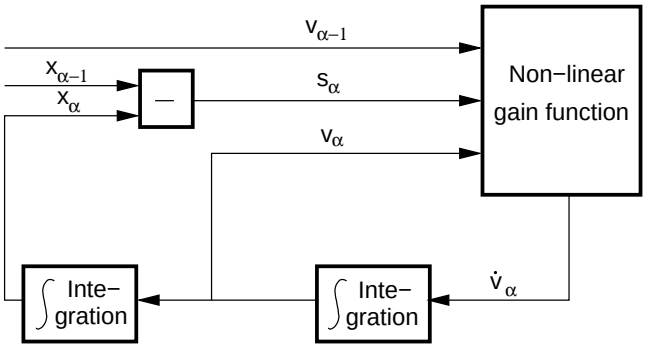

Figure 2.9: Elements of the nonlinear feedback loop of the vehicle dynamics described by car-following models: The actions of the driver-vehicle units α include (i) the input stimuli with respect to the leading vehicle, (ii) the acceleration (gain) function and (iii) two integrative elements. Notice that the velocity and the distance to the leader is the control quantity, respectively, while the nonlinear gain function calculates the instantaneous acceleration $\dot{v}(t)$.

3 Model Calibration and Validation

As microscopic traffic flow models are mainly used to describe collective phenomena such as traffic breakdowns, traffic instabilities and the propagation of stop-and-go waves, these models are traditionally calibrated with respect to macroscopic traffic data, e.g., one-minute flow and velocity data collected by double-loop detectors.

Nowadays, as microscopic traffic data have become more and more available, the problem of analyzing and comparing microscopic traffic flow models with real microscopic data has raised some interest in the literature [96, 91, 12, 98, 11, 113, 78]. Besides single-vehicle data of stationary detectors, the two main data categories are trajectory data and floating car data: *Trajectory data* contain the time series of the longitudinal motion $x_\alpha(t)$ of each vehicle α in an observed spatiotemporal area. As an example, Fig. 2.8 shows trajectory data generated from a microscopic simulation of the IDM. Empirical vehicle trajectory data are extracted from high-frequency digital images or videos that are recorded from an elevated observer position, e.g., from a helicopter [49] or a high-rise building [155]. In addition, the lateral motion $y_\alpha(t)$ and, in particular, the driving lane can be determined as well. Trajectory data contain the complete information of all vehicles on a certain road section. All surrounding vehicles in the neighboring lanes are known. On the other hand, the data collection is expensive and often limited to road sections smaller than 1 km.

Floating car data (FCD) are recorded by vehicles that 'float' with the traffic and serve as measuring stations. These vehicles are equipped with sensors and record variables such as speed and position for a particular trip. Based on this data, the vehicles compute a microscopic, local traffic situation which can be transmitted to the control center via mobile communication (e.g., cellular) networks [53]. If the vehicle is additionally equipped with an ACC system (cf. Sec. 1.1 on page 3), the distance to the car ahead and its velocity are also measured by the radar sensor at high temporal resolution. This measurement method facilitates observations over a long time interval. On the other hand, next-nearest neighbors and vehicles in the neighboring lanes are not gathered in contrast to trajectory data.

Since the primary task of a car-following model is to reproduce realistic car-following behavior, it is straightforward to compare a microscopic traffic model with the empirically measured driving behavior of human drivers which can be determined from both types of microscopic data. A car-following model describes the motion of the following vehicle in

response to the leading vehicle, so that it is possible to compare empirical with computed data of followers. Deviations between measured and simulated gaps are used to calibrate and validate the model. So, the following question arises: How well can a microscopic model reproduce the individual driving behavior? By a calibration study, we will now determine the optimal model parameters of the Intelligent Driver Model (IDM) that describe the FCD data best.

In Sec. 3.1, the FCD sets used for our calibration will be described in detail. Then, a method for adopting a car-following model to empirical FCD will be developed (Sec. 3.2). The setup for the microscopic calibration and the used objective functions will be discussed in Sec. 3.3. Section 3.4 describes the approach used to optimize the model parameters which is based on a genetic algorithm. Section 3.5 presents the calibrated IDM parameters. In a second step, the IDM will be validated by applying the calibrated parameter settings to the other FCD sets (Sec. 3.6). We conclude with a discussion of the results.

3.1 Floating Car Data Sets

For the following calibration study, we use three publicly available FCD sets that have been provided by the Robert Bosch GmbH [146]. The time series have been recorded in 1995 during an afternoon peak hour on a fairly straight one-lane road in Stuttgart, Germany. Unfortunately, the data sets do not give information about the individual drivers. The data have been recorded by a car equipped with a radar in front providing the relative speed and distance to the car ahead. The relative speed of the vehicle in front is measured directly via the Doppler effect. The data are recorded with a frequency of 10 Hz, i.e., with a time increment of 0.1 s. The device is hardly visible to other drivers (cf. Sec. 1.1). Some analysis can be found in the dissertation of Witte [135]. More details on the data processing are described in the doctoral thesis of Bleile [5].

Figure 3.1 shows the three time series used for the microscopic calibration and validation. The duration of the measurements are 250 s, 400 s and 300 s, respectively. All data sets show complex situations of daily city traffic with several acceleration and deceleration periods. All data sets even contain standstills due to traffic lights. The first two FCD sets are most of the time limited to low velocities below approximately 20 km/h, corresponding to small distances $s \lesssim 15\,\text{m}$. In the FCD set 3, the velocity varies in the range between 0 km/h and 60 km/h.

However, the differences in the velocity between the leader and the follower are small in all data sets. The accelerations $a(t)$ derived from the velocity by numerical differentiation are within a reasonable range of approximately $[-2, 2]\,\text{m/s}^2$. Note that the FCD sets only contain car-following behavior without a free acceleration to the desired velocity. More-

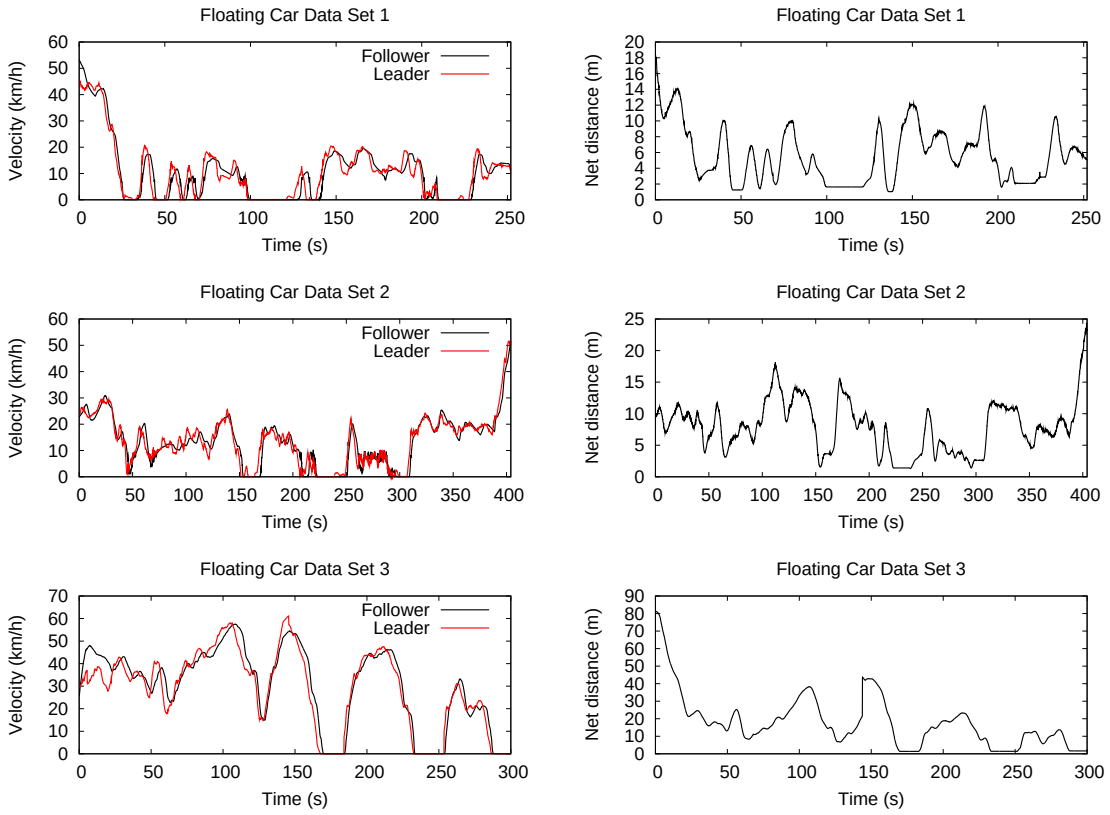

Figure 3.1: Velocity and net distance time series for three *floating car data* (FCD) sets recorded by the Robert Bosch GmbH in 1995. The data is publicly available via the DLR Clearing House website [146]. The sets show city traffic with several standstills due to traffic lights. The data set 3 exhibits a jump in the distance from approximately 20 m to 40 m at $t \approx 144$ s because the front car turned away.

over, the third FCD set exhibits a jump in the distance to the leader from approximately 20 m to 40 m at $t \approx 144$ s because the front car turned its direction.

3.2 Simulation Setup

Primarily, a car-following model describes the individual driving behavior in terms of the actual acceleration in response to the driving behavior of the leading vehicle (cf. Chap. 2). In the FCD sets discussed in the previous section, the velocity difference was measured (independently) by the follower. Since the velocity of the following FCD vehicle and the velocity difference are measured with high accuracy, the velocity of the leading car can approximately be determined as well. So, these data allow for a direct comparison between the measured driver behavior and trajectories simulated by a car-following model with the leading vehicle serving as externally controlled input. Initialized with the empirically

given distance and velocity differences, the microscopic model is used to compute the acceleration and, from this, the trajectory of the following car. The deviations between the empirically measured and simulated gaps are then used to calibrate and validate the model parameters.

The simulation setup directly corresponds to the car-following situation depicted in Fig. 2.1 on p. 16. More specifically, the car-following model defines the acceleration $\dot{v}^{\mathrm{sim}}(t)$ as a function of the own velocity $v^{\mathrm{sim}}(t)$, the gap to the leading vehicle $s^{\mathrm{sim}}(t)$ and the velocity of the leader $v_{\mathrm{lead}}^{\mathrm{data}}(t)$,

$$\dot{v}^{\mathrm{sim}}(t) = \dot{v}(s^{\mathrm{sim}}, v^{\mathrm{sim}}, v_{\mathrm{lead}}^{\mathrm{data}}). \tag{3.1}$$

While $v_{\mathrm{lead}}^{\mathrm{data}}$ is externally given, the velocity of the simulated vehicle and its distance to the leader are derived from the simulated acceleration function by integration:

$$v^{\mathrm{sim}}(t) = \int_0^t \dot{v}^{\mathrm{sim}}(t')\,\mathrm{d}t' \quad \text{and} \quad x^{\mathrm{sim}}(t) = \int_0^t v^{\mathrm{sim}}(t')\,\mathrm{d}t'. \tag{3.2}$$

Analogously, the trajectory of the leading vehicle in the simulation is given by the integrated velocity provided by the floating car data,

$$x_{\mathrm{lead}}^{\mathrm{data}}(t) = \int_0^t v_{\mathrm{lead}}^{\mathrm{data}}(t')\,\mathrm{d}t'. \tag{3.3}$$

The net distance to the leading vehicle is then given by the difference between the simulated trajectory $x^{\mathrm{sim}}(t)$ and the given position of the rear bumper of the leading vehicle $x_{\mathrm{lead}}^{\mathrm{data}}(t)$:

$$s^{\mathrm{sim}}(t) = x_{\mathrm{lead}}^{\mathrm{data}}(t) - x^{\mathrm{sim}}(t). \tag{3.4}$$

This can be directly compared to the gap $s^{\mathrm{data}}(t)$ provided by the data. As initial conditions for the Eqs. (3.2), the velocity and distance to the leading vehicle at the beginning of a simulation run are taken from the empirical data:

$$v^{\mathrm{sim}}(t=0) = v^{\mathrm{data}}(0) \quad \text{and} \quad s^{\mathrm{sim}}(t=0) = s^{\mathrm{data}}(0). \tag{3.5}$$

In addition, the distance $s^{\mathrm{sim}}(t)$ has to be reset to the value of the FCD when the leading object changes as a result of a lane change of one of the considered vehicles. For example, the leading vehicle of the FCD set 3 in Fig. 3.1 turns to another lane at $t \approx 144\,\mathrm{s}$ which leads to a jump in the net distance. At other times, the distance of the FCD is not used in the simulation. For the numerical integration in the simulation, we use the explicit integration scheme described in Chap. 6.

3.3 Error Measures

The calibration process aims at minimizing the difference between the measured driving behavior and the driving behavior simulated by the car-following model under consideration. Basically, any quantity can be used as error measure that is not fixed in the simulation, such as the velocity, the velocity difference or the net distance. In the following, we use the error in the net distance $s(t)$ for conceptual reasons: When optimizing with respect to s, the average velocity errors are automatically reduced as well. This does not hold the other way round, as the error in the distance may incrementally grow when optimizing with respect to differences in the velocities $v^{\mathrm{sim}}(t)$ and $v^{\mathrm{data}}_{\mathrm{follow}}(t)$.

For the parameter optimization, we need an *objective function* as a quantitative measure of the error between the simulated and observed trajectories. As the objective function has a direct impact on the calibration result, we consider three different error measures. The *relative error* is defined as a functional of the empirical and simulated time series, $s^{\mathrm{data}}(t)$ and $s^{\mathrm{sim}}(t)$:

$$\mathcal{F}_{\mathrm{rel}}[s^{\mathrm{sim}}] = \sqrt{\left\langle \left(\frac{s^{\mathrm{sim}} - s^{\mathrm{data}}}{s^{\mathrm{data}}} \right)^2 \right\rangle}. \tag{3.6}$$

Here, the expression $\langle \cdot \rangle$ means the temporal average of a time series $z(t)$ of duration ΔT, i.e.,

$$\langle z \rangle := \frac{1}{\Delta T} \int_0^{\Delta T} z(t)\, dt. \tag{3.7}$$

Since the relative error is weighted by the inverse distance, this measure is more sensitive to small distances s than to large distances. As example, a simulated gap of 10 m compared to a distance of 5 m in the empirical data results in a large error of 100%, whereas the same deviation of 5 m leads to an error of 5% only for a spacing of, for instance, 100 m which is typical for large velocities.

In addition, we define the *absolute error* as

$$\mathcal{F}_{\mathrm{abs}}[s^{\mathrm{sim}}] = \sqrt{\frac{\langle (s^{\mathrm{sim}} - s^{\mathrm{data}})^2 \rangle}{\langle s^{\mathrm{data}} \rangle^2}}. \tag{3.8}$$

As the denominator is averaged over the whole time series interval, the absolute error $\mathcal{F}_{\mathrm{abs}}[s^{\mathrm{sim}}]$ is less sensitive to small deviations from the empirical data than $\mathcal{F}_{\mathrm{rel}}[s^{\mathrm{sim}}]$. However, the absolute error measure is more sensitive to large differences in the numerator, i.e., for large distances s. Note that we have normalized both, the relative and the absolute error in order to make it independent of the duration ΔT of the considered time series. It also allows for a direct comparison between both error measures.

As the absolute error systematically overestimates errors for large net distances (at high velocities), while the relative error systematically overestimates deviations of the observed headway in the low velocity range, we have also studied a combination of both error measures. For this, we have defined the *'mixed error measure'*

$$\mathcal{F}_{\mathrm{mix}}[s^{\mathrm{sim}}] = \sqrt{\frac{1}{\langle |s^{\mathrm{data}}| \rangle} \left\langle \frac{(s^{\mathrm{sim}} - s^{\mathrm{data}})^2}{|s^{\mathrm{data}}|} \right\rangle}. \tag{3.9}$$

The dependence of the calibration results on the respective error measure is investigated in Sec. 3.5.

3.4 Nonlinear Optimization with a Genetic Algorithm

The calibration procedure aims at minimizing the differences between the floating car trajectories of human drivers and the simulated headways of a car-following model with a fixed parameter set. Finding an optimal parameter set of a car-following model with a nonlinear acceleration function such as the IDM, cf. Eq. (2.1), corresponds to a *nonlinear optimization problem*. In order to numerically find an approximative solution, we apply a genetic algorithm as a *search heuristic*. Genetic algorithms (GA) are a particular class of evolutionary algorithms that use techniques inspired by evolutionary biology such as inheritance, mutation, selection and recombination [28, 157]. The implemented GA proceeds as follows (cf. Ref. [156]):

- The evolution starts with a *population* of randomly generated *'individuals'*. In each *generation*, an entirely new population of individuals is created, based on the fitness scores of the members of the old generation. In our application, an 'individual' represents a parameter set of a car-following model and a population consists of N such sets. In contrast to the traditional representation of individuals by binary strings ('genome'), we treat a parameter as a real number.

- In each generation, the *fitness* of each individual in the population is evaluated. The fitness of an individual is determined via one of the objective functions proposed in Sec. 3.3. More specifically, the scaled fitness score is obtained from the objective score $\mathcal{F}$ by calculating the reciprocal value of $\mathcal{F}^2$. In addition, a penalty value is added for any vehicle collision during a simulation run.

- In the *selection process*, two individuals are stochastically selected from the current population, based on their fitness score and *recombined* to generate a new individual. After this recombination, the model parameters of the selected individuals are also randomly selected. In addition, the best individual is kept without any modification

to the next generation (*elitism*). Subsequently, the genes of all individuals, i.e., their model parameters, are varied randomly corresponding to a *mutation* that is controlled by a given probability. The resulting new generation is then used in the next iteration of the GA. For reasons of numerical efficiency, the parameter values are chosen within reasonable, user-defined limits.

- The termination criterion is implemented as a two-step process: Initially, a fixed number of generations is evaluated. Then, the evolution terminates after convergence which is specified by a constant best-of-generation score for at least a given number of generations.

The presented optimization algorithm is obviously less efficient than a conjugate gradient method such as the Nelder-Mead algorithm [87] which approximately finds an optimized parameter set if the objective function varies smoothly. However, like all general-purpose multidimensional optimization algorithms (without stochastic components), Nelder-Mead occasionally gets stuck in a local minimum. In contrast, the presented GA approach which is less specific in the search direction allows to escape from (small) local optima.

3.5 Calibration Results for the Intelligent Driver Model

In this section, we calibrate the Intelligent Driver Model (IDM) [124] to the three FCD sets presented in Sec. 3.1, using the nonlinear optimization algorithm discussed in the previous section. The simulation setup and the objective functions have already been introduced in Sec. 3.2. In order to restrict the parameter space for the optimization to reasonable and positive parameter values, we apply the following constraints for the minimum and maximum values: The desired velocity v_0 is restricted to $[1, 70]\,\mathrm{m/s}$, the safety time gap T to $[0.1, 5]\,\mathrm{s}$, the minimum distance s_0 to $[0.1, 8]\,\mathrm{m}$, the maximum acceleration a and the comfortable deceleration b to $[0.1, 6]\,\mathrm{m/s^2}$. Note that the acceleration exponent $\delta = 4$ was kept constant as usual (see cf. Chap. 2).

The calibration results for the three FC data sets (see Fig. 3.1) and the considered three objective functions $\mathcal{F}$ (Eqs. (3.6), (3.8) and (3.9)) are summarized in Table 3.1. Obviously, the calibrated IDM parameters vary from one FC data set to another, but they also vary with the considered objective function. Remarkably, all parameter values obtained from the calibration to the empirical data are of the correct size and within the expected parameter range. Particularly, the IDM parameter for the safety time gap T ($1\,\mathrm{s} \ldots 1.5\,\mathrm{s}$), the minimum distance s_0 ($1.25\,\mathrm{m} \ldots 3.5\,\mathrm{m}$) and the maximum acceleration a ($1\,\mathrm{m/s^2} \ldots 1.5\,\mathrm{m/s^2}$) turn out to be robust with respect to different driving situations and different objective functions. The resulting traffic dynamics for simulation runs with the calibrated IDM parameters are validated in Sec. 3.6.

	FCD set 1			FCD set 2			FCD set 3		
Measure	$\mathcal{F}_{\text{rel}}[s]$	$\mathcal{F}_{\text{mix}}[s]$	$\mathcal{F}_{\text{abs}}[s]$	$\mathcal{F}_{\text{rel}}[s]$	$\mathcal{F}_{\text{mix}}[s]$	$\mathcal{F}_{\text{abs}}[s]$	$\mathcal{F}_{\text{rel}}[s]$	$\mathcal{F}_{\text{mix}}[s]$	$\mathcal{F}_{\text{abs}}[s]$
Error [%]	24.1	20.8	20.7	28.7	26.2	25.7	18.0	13.0	11.2
v_0 [m/s]	69.9	70.0	70.0	70.0	70.0	68.9	16.0	16.1	16.2
T [s]	1.08	1.12	1.03	1.52	1.44	1.23	1.30	1.31	1.35
s_0 [m]	2.39	2.35	2.59	2.62	2.79	3.50	1.60	1.52	1.25
a [m/s^2]	1.01	1.23	1.43	0.953	0.973	1.09	1.58	1.56	1.55
b [m/s^2]	3.23	3.10	3.91	0.590	0.993	1.17	0.761	0.626	0.605

Table 3.1: Calibrated IDM parameters for three different floating car (FC) data sets and three different objective functions $\mathcal{F}$. The calibration error is between 11% and 29%. The IDM acceleration exponent $\delta = 4$ has been kept constant. All IDM parameters except v_0 show reasonable values. See the main text for a detailed discussion of the results.

Starting from the optimized IDM parameters, Fig. 3.2 shows the resulting error measures of the FCD sets 1 and 3 for a systematic variation of a single model parameter while keeping the other parameters constant. All error curves are smooth and significant parameters show only one global minimum. The solutions belonging to different objective functions are altogether in the same parameter range. This robustness of the IDM parameter space is an result of the calibration study. Furthermore, Fig. 3.3 shows contour plots of $\mathcal{F}_{\text{mix}}[s^{\text{sim}}]$ for the FCD set 3 for a simultaneous variation of two IDM parameters, reflecting the correlation between the model parameters. Similar to the results shown in Fig. 3.2, the shapes of the contour plots indicate that the IDM parameter space is smooth and exhibits only one global minimum for the multi-dimensional parameter space corresponding to a unique solution for the nonlinear optimization problem. Furthermore, the orthogonality of the contour lines indicate that the IDM parameters are not collinear.

Let us discuss our results for each IDM parameter in more detail. The IDM parameter for the *desired velocity* is estimated to be $v_0 = 57.6\,\text{km/h}$ for the FCD set 3. This value corresponds to the maximum velocity reached in the recorded driving situations. The other FCD sets result in $v_0 \approx 250\,\text{km/h}$ which is the maximum value allowed (as constraint) in the optimization algorithm. This unreasonably high value results from the fact that the FCD sets describe bound traffic without acceleration periods to the desired speed apart from data set 3, where the turning of a vehicle allowed for a free acceleration period (see Fig. 3.1 on page 31). There, the short free acceleration period leads to a distinct minimum in the corresponding error measure curve in Fig. 3.2. The error curves for the other data sets are flat up to $50 - 60\,\text{km/h}$ (Fig. 3.2), i.e., fully compatible with realistic values of the desired velocity.

The safety time gap T is the most important parameter as it adjusts the distance to the leading vehicle. The calibrated values within the range $1.0 \leq T \leq 1.5\,\text{s}$ are exactly in the expected range. In addition, T is very significant in the calibration process, as can

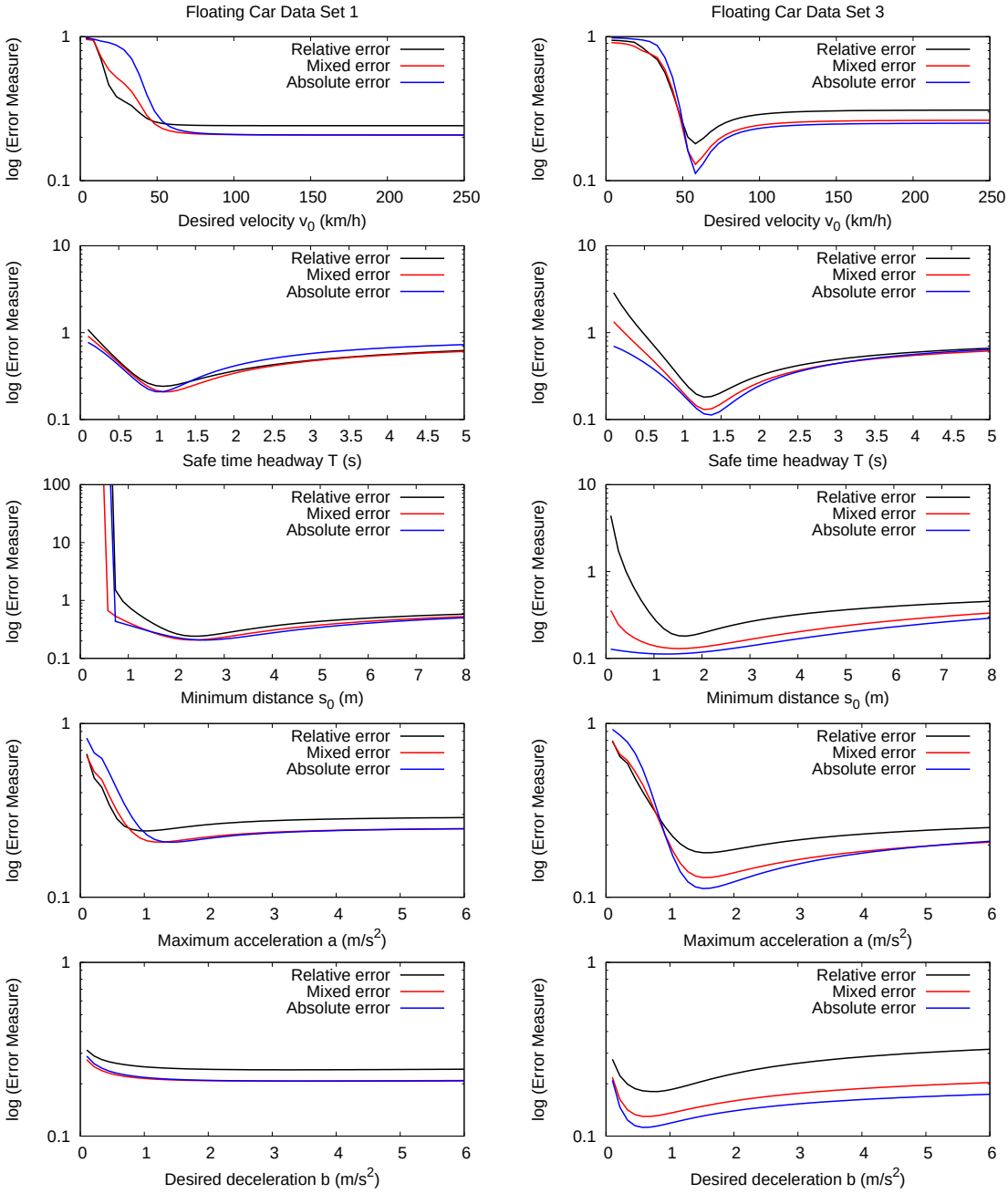

Figure 3.2: Systematic variation of one IDM parameter while keeping the other parameters at the optimal values listed in Table 3.1. The diagrams show the resulting error measures $\mathcal{F}_{\text{rel}}$, $\mathcal{F}_{\text{mix}}$ and $\mathcal{F}_{\text{abs}}$ for the FCD set 1 (left) and for the FCD set 3 (right), reflecting the sensitivity of the error measures with respect to variations of IDM parameters. Particularly, significant model parameters like T, s_0 and a show a distinct minimum. Remarkably, the solutions belonging to different objective functions are in the same parameter range which demonstrates the robustness of the calibration results for the IDM.

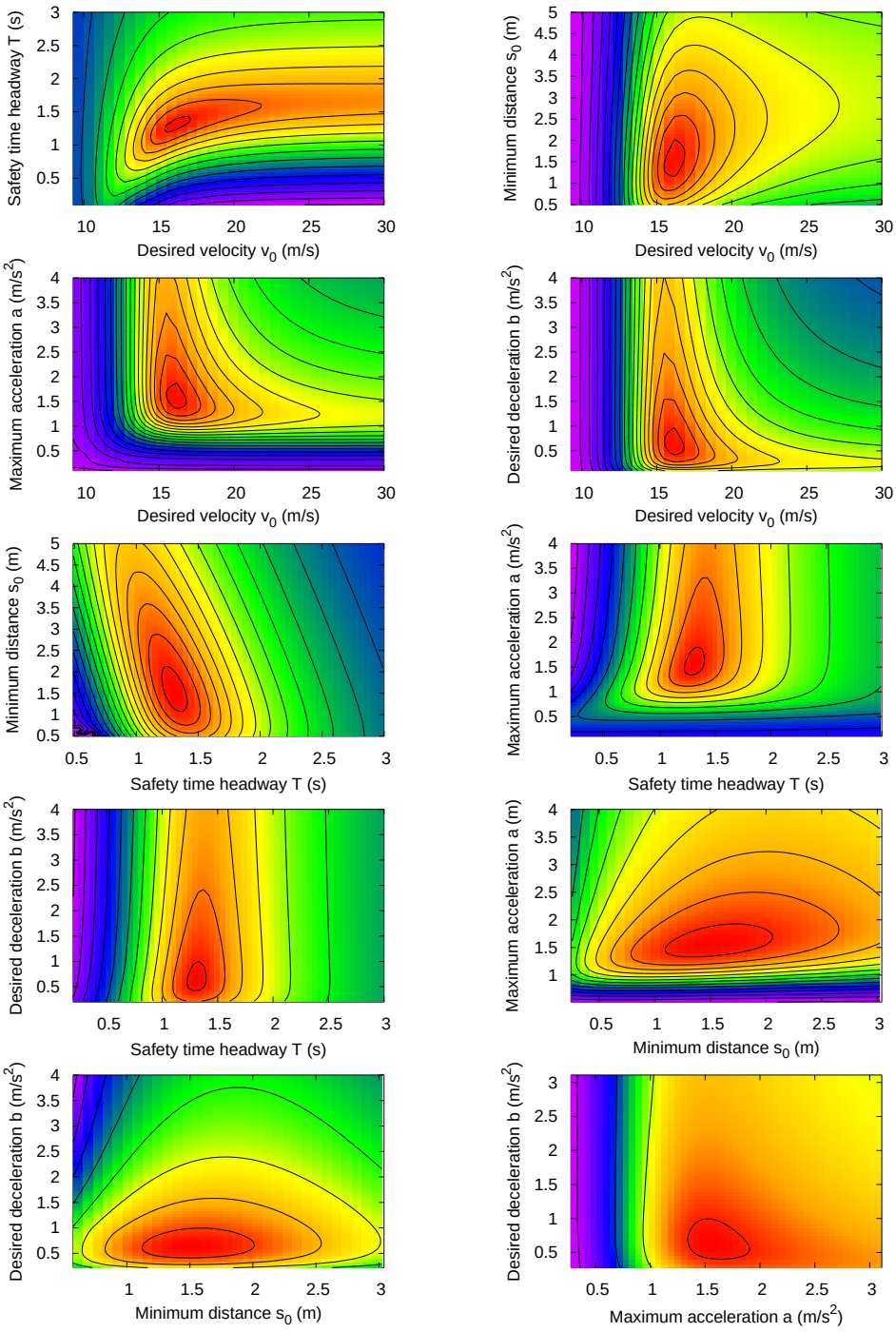

Figure 3.3: Contour plots with equidistant contour lines showing the error measure $\mathcal{F}_{\text{mix}}[s^{\text{sim}}]$ for the FCD set 3 as a result of a simultaneous variation of two IDM parameters while keeping the others constant at the optimum values given in Table 3.1. The IDM parameters are mainly uncorrelated as indicated by the orthogonality of the contour lines. The correlation between s_0 and T is explained by the equilibrium distance $s_0 + vT$, see Eq. (2.2).

be seen from the diagrams in Fig. 3.2, which show distinct minima around $T \approx 1.2\,\mathrm{s}$ and strong variations of the error measures when varying this parameter value. In addition, the gradients in the diagrams of Fig. 3.3 towards the optimum solutions indicate a similar characteristics. The parameter T is not correlated with the other IDM parameters except for the minimum distance s_0 which can partially compensate for T. This correlation is explained by the equilibrium gap that is given by $s_0 + vT$ (see Eq. (2.2)).

The considered FCD sets all contain standstills due to traffic lights. Therefore, the minimum distance s_0 can easily be determined with this data. The results for s_0 are between 1.3 m and 3.5 m, i.e. are exactly in the expected range for a minimum bumper-to-bumper distance when traffic comes to a standstill. Note that the relative error measure of s_0 for the FCD set 3 in Fig. 3.2 is more sensitive than the absolute error measure, as theoretically discussed in Sec. 3.3. As intended by its definition, the measure $\mathcal{F}_{\mathrm{mix}}$ is a compromise between the relative and the absolute objective function.

The IDM parameter for the maximum acceleration a is significant for the reproduction of the considered FCD sets. As shown in Fig. 3.2, too low and too high acceleration values increase the calibration error. The calibration results of $1 \leq a \leq 1.6\,\mathrm{m/s^2}$ are in the realistic range (see Chap. 2). The desired deceleration parameter b can *not* be reliably calibrated with the considered data sets because the data do not contain any situation where the following vehicle approaches the leader (from a large distance) with a noticeable velocity difference. The resulting values for b show the largest variation of all IDM parameters, as the error measures vary weakly (see the related diagrams in Figs. 3.2 and 3.3). For the FCD set 1, there is no minimum at all.

Finally, we discuss the effect of a non-constant driving style of human drivers which is also referred to as 'intra-driver variability' [92]. In the FCD set 3, the driver stops three times because of red traffic lights. The bumper-to-bumper distance is $s_{\mathrm{stop},1} = 1.39\,\mathrm{m}$ in the first time interval of $\Delta t_1 = 13.9\,\mathrm{s}$ duration, $s_{\mathrm{stop},2} = 1.42\,\mathrm{m}$ for the second time interval of $\Delta t_2 = 17.7\,\mathrm{s}$ duration and $s_{\mathrm{stop},3} = 1.64\,\mathrm{m}$ for the third time interval of $\Delta t_3 = 11.8\,\mathrm{s}$ duration. These data show that a deterministic car-following model only allows for an 'effective' (averaged) description of the human driving behavior. This results in parameter values that capture the 'mean' observed driving performance. Furthermore, we can calculate a theoretical lower bound for the relative error from these data. Considering the theoretical 'best case' of a perfect agreement between data and simulation for all times except for the three standstills, the relative error function depends only on s_0 and is given by

$$\xi(s_0) = \sum_{i=1}^{3} \alpha_i \left(\frac{s_0 - s_{\mathrm{stop,i}}}{s_{\mathrm{stop,i}}} \right)^2 , \tag{3.10}$$

where $\alpha_i = \Delta t_i / \Delta T$ is the weight for the ith stand-still relative to the total time interval $\Delta T = 300\,\mathrm{s}$ of the FCD set 3. A necessary condition for the optimal minimum distance

s_0^{opt} minimizing the error ξ is given by

$$\frac{\partial \xi}{\partial s_0} = \sum_{i=1}^{3} \frac{2\alpha_i (s_0 - s_{\mathrm{stop,i}})}{(s_{\mathrm{stop,i}})^2} \stackrel{!}{=} 0. \tag{3.11}$$

This equation can be easily solved analytically, resulting in

$$s_0^{\mathrm{opt}} \approx 1.458\,\mathrm{m}. \tag{3.12}$$

This optimal solution defines a theoretical lower bound (based on about 15% of the data of the considered time series) for the relative error measure of

$$\xi_{\min}(s_0^{\mathrm{opt}}) \approx 7.9\%. \tag{3.13}$$

This result indicates that the total calibration error of $\mathcal{F}_{\mathrm{rel}} = 18.0\,\%$ listed in Table 3.1 may be mainly attributed to the *intra-driver variability* [92], considering the fact that not only s_0 will slightly vary in time, but also other parameter values.

3.6 Model Validation

In the previous section, we calibrated the IDM model parameters by minimizing the deviation between the observed distance $s^{\mathrm{data}}(t)$ and the corresponding time series $s^{\mathrm{data}}(t)$ obtained from simulations with the IDM. In this section, we *validate* the obtained calibrated IDM parameter settings by applying these settings to the other FCD sets. Moreover, we discuss the resulting driving dynamics in order to prove that the model satisfies the requirements for its further applications.

Let us first validate the IDM in a quantitative way by simply simulating a FCD set using the parameters calibrated on the basis of another data set. We use the three optimal parameter settings listed in Table 3.1 and restrict ourselves to the 'mixed error' measure, see Eq. (3.9). Moreover, we calculate the arithmetic average of the parameter values. The mean parameter settings are listed in the caption of Table 3.2. Finally, we validate the typical IDM parameter settings proposed in Chap. 2, Table 2.1.

The obtained errors $\mathcal{F}_{\mathrm{mix}}[s^{\mathrm{sim}}]$ for the considered five parameter settings and the three FC data sets are listed in Table 3.2. The underlined errors refer to the parameter values corresponding to the best calibration results. This cross-comparison allows to evaluate the *inter-driver variability*, i.e., how much the resulting traffic dynamics varies when applying different parameter settings to the same FCD set.

Comparing the error for the averaged parameter set or for the standard parameter set (listed in Table 2.1 on page 17) with the errors for the parameters optimized for specific

	Parameter set 1	Parameter set 2	Parameter set 3	Mean parameters	'Default' parameters
FCD set 1	<u>20.8%</u>	28.7%	28.6%	21.8%	23.9%
FCD set 2	35.4%	<u>26.2%</u>	40.6%	31.0%	28.6%
FCD set 3	41.2%	26.9%	<u>13.0%</u>	29.6%	25.5%

Table 3.2: Resulting calibration and validation results for the error measure $\mathcal{F}_{\text{mix}}[s^{\text{sim}}]$ and the three considered FCD sets when using the calibrated parameter sets 1−3 (see Table 3.1). The mean parameter settings are $v_0 = 57.0\,\text{m/s}$, $T = 1.29\,\text{s}$, $s_0 = 2.22\,\text{m}$, $a = 1.25\,\text{m/s}^2$ and $b = 1.57\,\text{m/s}^2$. The 'default' IDM parameters are listed in Table 2.1 on page 17. The underlined errors correspond to the best calibration results.

driving situations and drivers, one can say that the IDM performs well and behaves very robust. The obtained errors for the 'mean' and the 'default' parameters are in the range between 22% and 31%, i.e., of the same order as for the calibrated parameter sets. These results are consistent with typical error ranges obtained in previous studies [96, 12, 98].

Let us finally compare the dynamics of the net distance $s(t)$ and the velocity $v(t)$ resulting from the calibrated IDM parameters with the empirical data of human drivers. These are shown in Fig. 3.4 for the FCD sets 1 and 2 and in Fig. 3.5 for the FCD set 3. The depicted simulations have been carried out with the optimal parameters regarding the mixed error measure $\mathcal{F}_{\text{mix}}$. The differences in the resulting traffic dynamics for the different error measures considered are negligible.

The frequent acceleration and deceleration periods contained in the FCD set 1 are reproduced by the IDM, although the differences in the distance reveal that the model sometimes over- and underestimates the headway of the human driver, cf. the diagrams in the left column of Fig. 3.4. The calibrated safety time gap parameter $T = 1.12\,\text{s}$ listed in Table 3.1 minimizes the overall error and approximates the 'average' driving dynamics of the human driver. The increasing deviation in the standstill around $t \approx 100\,\text{s}$ can be explained by a drift in the empirical data that we did not correct for.

The calibration of the FCD set 2 is associated with the largest error $\mathcal{F}_{\text{mix}} = 26.2\%$. The strong deviation of up to 8 meters between the calibrated IDM and the observed driving behavior of FCD set 2 at time $t \approx 115\,\text{s}$ (see diagrams in the right column of Fig. 3.4) indicates that the car-following model cannot explain why the human driver lets the gap to the leading vehicle increase. As a consequence of the optimization process, the time gap parameter of $T = 1.44\,\text{s}$ is somewhat too high so that the IDM keeps a larger distance to the leader than the human driver, e.g., in the situation around $t \approx 20\,\text{s}$ and for $t \approx 380\,\text{s}$.

Figure 3.5 shows that the IDM describes the human driver in the FCD set 3 very accurately.

For a direct comparison, the diagrams in the right column of the figure show the obtained time series for the 'default' IDM parameter settings. Notice that the object change in the data at $t \approx 144\,\mathrm{s}$ is considered in the calibration simulation by resetting s to the distance of the new leader. The largest deviation from the data is observed around $t \approx 55\,\mathrm{s}$. The gap to the leader increases as a result of a strong acceleration of the leader. This behavior is not reproduced by the IDM. Instead, the car-following model immediately reacts to the behavior of the leading car with a similar acceleration to keep the adjusted safety time gap. In the next instant, the leader has to brake which explains the observed behavior of the follower. This kind of *driver anticipation* is obviously not considered by the simple car-following approach. For a more elaborated modeling approach, we refer to Chap. 4.

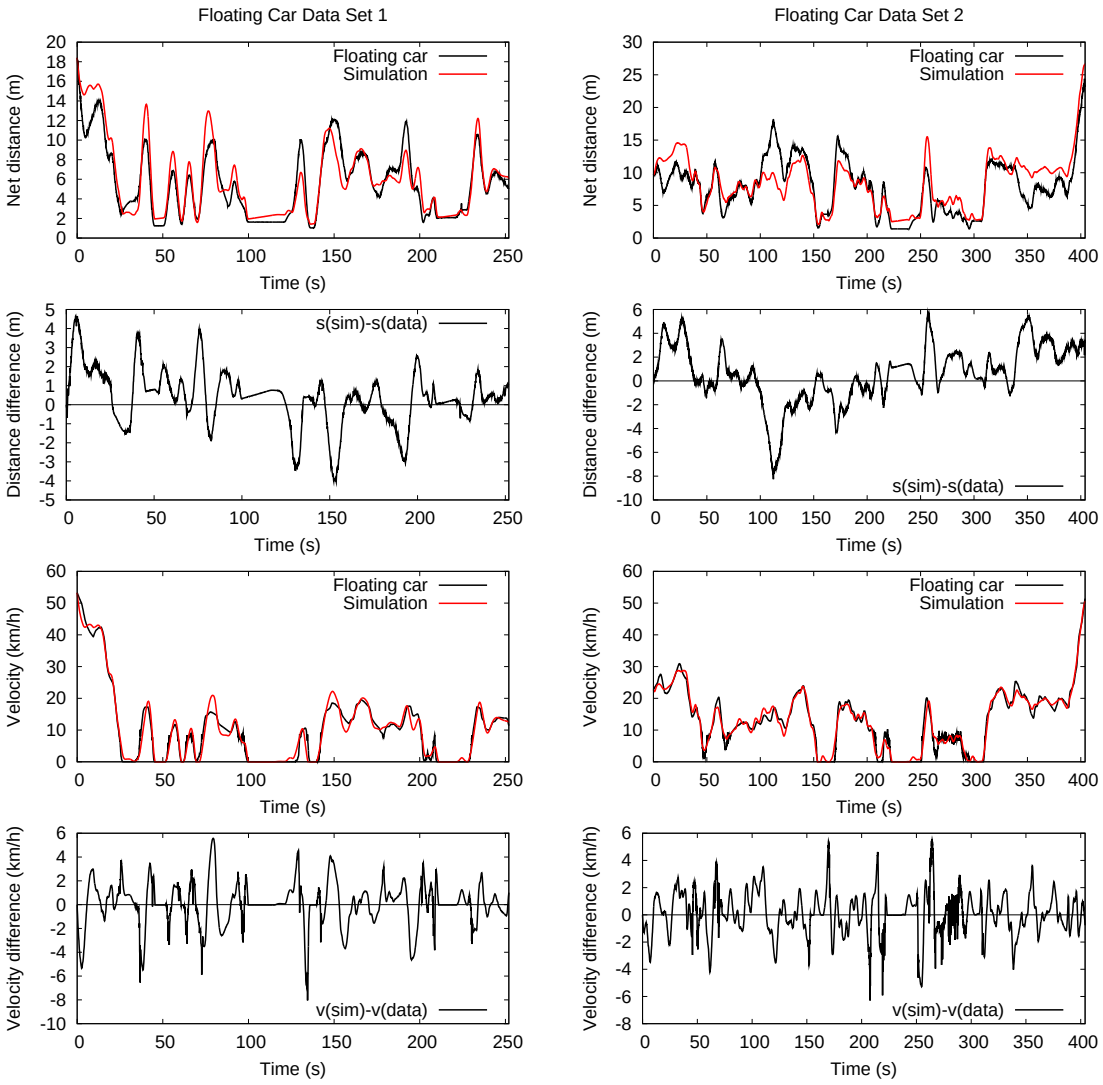

Figure 3.4: Resulting traffic dynamics of the calibrated IDM with the leading vehicle from the FCD sets 1 (left column) and 2 (right column). The simulation results are compared with the follower from the empirical data. The IDM parameters used in the simulations are taken from Table 3.1 for the error measure $\mathcal{F}_{\text{mix}}$.

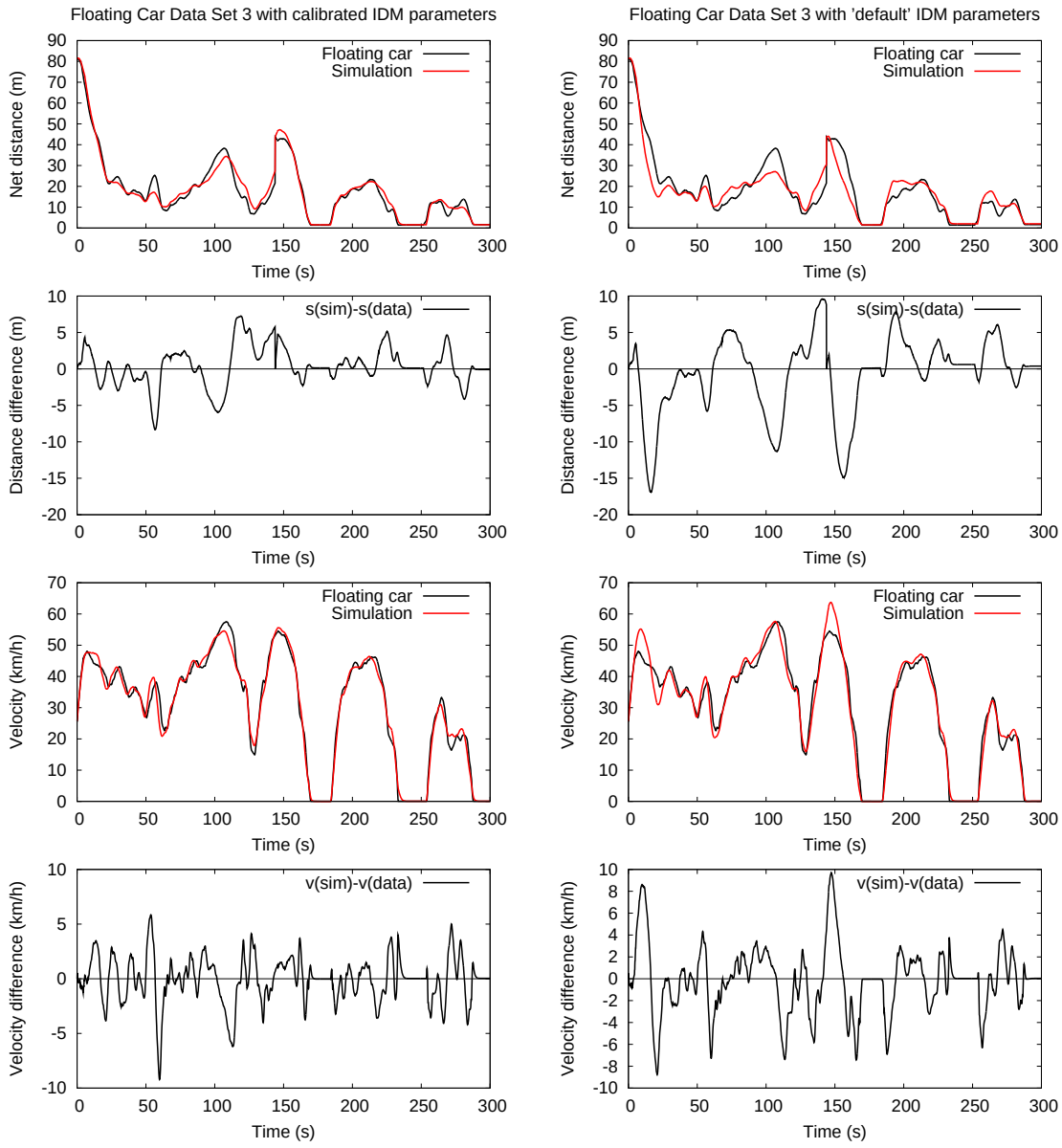

Figure 3.5: Simulation results of the IDM for the FCD set 3. Left: Calibrated parameters for $\mathcal{F}_{\text{mix}}$ given in Table 3.1. Right: 'Default' parameters of Table 2.1. See the main text for a detailed discussion.

3.7 Summary and Discussion

In this chapter, we have studied the car-following behavior of individual drivers in real city traffic on the basis of three floating car (FC) data sets recorded by a vehicle equipped with an ACC sensor. By means of a nonlinear optimization procedure based on a genetic algorithm, we have calibrated the IDM parameters by minimizing the deviations between the observed driving dynamics and the simulated trajectory when following the same leading vehicle. As the data sets mainly describe car-following situations in obstructed traffic and standstills, the IDM parameters T, s_0 and a are particularly significant and show distinct minima for the three proposed error measures, while the values of v_0 and b were hard to determine exactly by the FC data sets used. We have considered several criteria for the analysis of the IDM. Apart the fit error, we have investigated the variance, the significance of and the correlation between parameters as well. We have obtained the following main results:

- All calibrated IDM parameters show reasonable values within the expected range. For example, the time gap T is in the range between 1 s and 1.4 s corresponding to maximum free flows between 1800 and 2500 vehicles/h (cf. Sec. 2.3). The maximum acceleration a varies between 1.0 and 1.6 $\mathrm{m/s^2}$, cf. the investigation in Sec. 4.2.3. These calibration results are obtained for city traffic, but the settings can be applied to freeway traffic as well. Of course, the desired velocity v_0 has to be adapted accordingly.

- All IDM parameters are nearly uncorrelated (cf. Fig. 3.3) and the error measures are smooth functions of the model parameters. Only T and s_0 can partially compensate for each other due to their contribution to the desired distance, $s_0 + vT$, cf. Eq. (2.2) on page 15. The calibrated parameter settings are robust and consistent regarding the objective functions applied.

- The typical calibration errors are of the order of $10 - 30\%$ which is consistent with the findings in Ref. [96]. Human drivers do not drive constantly over time, i.e., their behavioral driving parameters change. As shown in-depth for the minimal distance s_0, this *intra-driver variability* accounts for a large part of the deviations between simulations and empirical observations.

- Another contribution to the overall error is given by *driver anticipation* which is not incorporated in car-following models (cf. Sec. 1.2). More complex microscopic traffic models take more than the immediate predecessor into account, or they incorporate non-stationary parameters because of driver adaptation processes [126, 122]. In the following Chap. 4, we will therefore consider these aspects for a more sophisticated

modeling approach. Note, however, that multi-leader anticipation requires trajectory data because the FC data is limited to the immediate predecessor.

- We validated the IDM by applying ('cross-comparing') the calibrated parameter settings to other FC data sets. The resulting IDM traffic dynamics turned out to be robust with respect to reasonable changes of parameter settings. In addition, the typical IDM settings for freeway traffic proposed in Table 2.1 on page 17 are consistent with the averaged settings obtained from our calibration to city traffic. The differences in the resulting traffic dynamics for different parameter settings can be attributed to the *inter-driver variability* [92]. Note that microscopic traffic models can easily cope with this kind of heterogeneity because different parameter values can be attributed to each individual driver-vehicle unit.

The understanding of the human driver behavior is important both for the improvement of microscopic traffic models and for the deployment of advanced driver assistance systems. The fact that the IDM is able to *effectively* reproduce the human driving behavior *on a microscopic scale* is particularly interesting because a real-world implementation of an ACC system based on the IDM has recently been presented by Volkswagen [67, 66]. Let us finally remark that the observed human driver behavior is not necessarily 'optimal' regarding an efficient and comfortable driving style. The most accurate reproduction of the human driving style should therefore not serve as the only (anyway relevant) criterion when designing automated driving assistance systems. In Part II, we will propose and evaluate an extension of ACC systems aimed at an actively jam-avoiding driving strategy. To this end, we will consider an automated adaptation of the driving characteristics according to the actual traffic situation.

4 The Human Driver Model

The nature of human driving behavior as compared to the 'automatic' response assumed by most microscopic traffic models is a controversial topic in traffic science [33, 8, 46, 85, 59, 15, 83]. Finite reaction times and limited estimation capabilities impair human driving performance and traffic stability as compared to automated driving, sometimes called 'adaptive cruise control' (ACC), cf. Sec. 1.1. However, unlike machines, human drivers routinely scan the traffic situation several vehicles ahead and anticipate future traffic situations leading. This can compensate for some weaknesses of human drivers and increase traffic stability (again).

The question arises, how these aspects affect the overall driving behavior and performance, and whether the stabilizing effects (such as anticipation) dominate over the destabilizing effects (like reaction times and estimation errors) or not, or whether they effectively cancel out each other. The answers to these questions are crucial for determining the influence of a growing number of vehicles equipped with ACC systems on the overall traffic flow which is the topic of Part II.

Single aspects of human driving behavior have been investigated in the past. An essential feature of human driving is a considerable *reaction time* which is a consequence of the physiological aspects of sensing, perceiving, deciding, and performing an action [107]. Th resulting reaction time (to unexpected situations) is of the order of 1 s and varies strongly between different drivers (age, gender), different stimuli, and different studies [29]. Clearly, reaction times contribute to traffic instabilities and, consequently, are an essential element in many traffic models [80]. In the most straightforward way, they are introduced as time delays into time-continuous car-following models which results in a coupled set of *delay-differential equations*. This approach has been pursued, e.g., for the Optimal Velocity Model (OVM) [3, 2], and for the Intelligent Driver Model (IDM) [124, 125]. However, the OVM with delay turns out to be accident-free only for unrealistically small reaction times [20]. To overcome this deficiency, Davis [21] has introduced (among other modifications) an anticipation of the expected future gap to the front vehicle, allowing accident-free driving at reaction times of 1 s. However, reaction times were not fully implemented in Ref. [21] since the own velocity which is one of the stimuli on the right-hand side of the acceleration equation, has been evaluated at the actual rather than at the delayed time. Another approach to model temporal anticipation consists in including the acceleration of the preceding vehicles in the input variables of the model. More commonly, however,

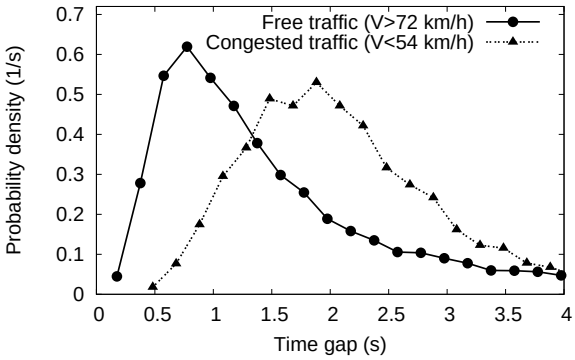

Figure 4.1: Empirical distribution of time gaps obtained from single-vehicle data from the left lane of the Dutch freeway A9 at a detector cross section 1.0 km upstream of an on-ramp. The free traffic data has been filtered with respect to average flows > 1000 vehicles/h/lane. Moreover, we distinguish between average velocities $V > 72\,\mathrm{km/h}$ (free traffic), and $V < 54\,\mathrm{km/h}$ (congested traffic). In congested traffic, the time gap distribution is shifted to higher values.

microscopic traffic models have been formulated in terms of *iterated coupled maps* such as the Gipps model [26] or the Newell model [88] or in terms of a *cellular automaton* such as the Nagel-Schreckenberg model [84]. In these two model classes, the update time step is considered as an explicit model parameter rather than an auxiliary parameter needed for numerical integration, and it is often interpreted as 'reaction time'.

To my knowledge, there exists no car-following model exhibiting platoon stability for reaction times (with respect to all stimuli) exceeding half of the time gap of the vehicles in the platoon. Human drivers, however, accomplish this task easily: In dense (not yet congested) traffic, the most probable time gaps on German or Dutch freeways are $0.9 - 1\,\mathrm{s}$ [64, 114] which is of the same order as the typical reaction time [29]. Moreover, single-vehicle data indicate that some drivers drive at gaps as low as $0.3\,\mathrm{s}$ which is below the reaction time of even a very attentive driver by a factor of 2 or more. Figure 4.1 shows data from a Dutch freeway, which have been filtered with respect to average velocities (and flows). Safe driving would not be possible at such time gaps and reaction times, when only the immediate vehicle in front was considered.

This suggests that human drivers achieve additional stability and safety by taking into account next-nearest neighbors and further vehicles ahead as well. Such 'spatial anticipation' or 'multi-anticipation' has been applied to the OVM [70] and to the Gipps model [24] as well as to some cellular automata model [63, 69]. As expected, the resulting models show a higher stability than the original model. However, the stability of the aforementioned models is still smaller than that of human driving. Furthermore, they display unrealistic behavior such as clustering in pairs [24] or too large propagation velocities of perturbations in congested traffic (i.e., $V_g \gg -15\,\mathrm{km/h}$) [70].

Imperfect estimation capabilities often serve as motivation or justification to introduce stochastic terms into microscopic traffic models such as the Gipps model [26]. Most cellular automata require fluctuating terms as well. In nearly all these cases, fluctuations are assumed to be δ-correlated in time and acting directly on the accelerations. An important feature of human estimation errors, however, is a certain *persistency*. If one underestimates, say, the distance at time t, the probability of underestimating it at some time later is high as well. Another source leading to temporally correlated acceleration noise lies in the tendency of human drivers to actively adapt to the traffic situation, i.e., to change the acceleration only at discrete times which is sometimes taken into account by the 'action point' concept [131].

In this chapter, we propose the *Human Driver Model* (HDM) in terms of four extensions to classical follow-the-leader models by incorporating into them (i) finite reaction times, (ii) estimation errors, (iii) spatial anticipation, and (iv) temporal anticipation. We formulate the HDM as a 'meta-model' that can be combined with a wide class of microscopic traffic models. The class of compatible models is characterized by continuous acceleration functions depending on the velocity, the gap, and the relative velocity with respect to the leading car and includes, for example, the OVM [3], the Gipps model [26], the velocity difference model [41, 51], the IDM [124], and the boundedly rational driver model [74, 75]. For matters of illustration, we will apply the Human Driver Model to the IDM (cf. Chap. 2).

The chapter is structured as follows: In Sec. 4.1, HDM in terms of the acceleration function of the underlying traffic model will be formulated. In Sec. 4.2, the asymptotic stability of vehicle platoons will be simulated as a function of the reaction time T' for different degrees of anticipation. There, we will investigate two causes of traffic instability: The time lag caused by finite accelerations (cf. also Sec. 2.4), and the delay caused by the finite reaction times of drivers. Furthermore, in Sec. 4.3, the macroscopic traffic dynamics for an open system containing a flow-conserving bottleneck will be simulated. A summary of the findings and a discussion will conclude the chapter (Sec. 4.4).

4.1 Modeling Human Driving Behavior

Let us now formulate the Human Driver Model (HDM) as a *meta-model* applicable to time-continuous microscopic traffic models (car-following models) of the general form

$$\frac{\mathrm{d}v_\alpha}{\mathrm{d}t} = \dot{v}^{\mathrm{mic}}\left(s_\alpha, v_\alpha, \Delta v_\alpha\right), \tag{4.1}$$

where the own velocity v_α, the net distance s_α, and the approaching rate $\Delta v_\alpha := v_\alpha - v_{\alpha-1}$ to the leading vehicle serve as stimuli determining the acceleration $\dot{v}^{\mathrm{mic}}$ (cf. Secs. 1.2 and

2.1). This class of basic models is characterized by (i) instantaneous reaction, (ii) reaction to the immediate predecessor only, and (iii) infinitely exact estimating capabilities of drivers regarding the input stimuli s, v, and Δv which also means that there are no fluctuations. In Sec. 8.1, we will discuss that, in some sense, such models describe driving behavior similar to adaptive cruise control systems. For the sake of simplicity, we will restrict ourselves here to single-lane longitudinal dynamics, while lane-changing models are discussed in Chap. 5.

4.1.1 Finite Reaction Time

A reaction time T' is incorporated in a time-continuous model of the type given by Eq. (4.1) simply by evaluating the right-hand side of Eq. (4.1) at a previous time $t - T'$. The numerical integration (cf. Chap. 6) now depends on both, the reaction time and the update time. In this way, one obtains a coupled set of *delay-differential equations*. If the reaction time is a multiple n of the update time interval, i.e., $T' = n\Delta t$, it is straightforward to generalize Eq. (4.1) by calculating all terms on the right-hand sides with the velocities and positions n time steps in the past. If T' is not a multiple of the update time interval, we propose a linear interpolation according to

$$x(t - T') = \beta x_{t-n-1} + (1 - \beta)x_{t-n}, \tag{4.2}$$

where x denotes any quantity on the right-hand side of (4.1) such as s_α, v_α or Δv_α. x_{t-n} denotes this quantity n time steps before the actual step. Here, n is the integer part of $T'/\Delta t$, and the weight factor of the linear interpolation is given by $\beta = T'/\Delta t - n$. We emphasize that *all* input stimuli s_α, v_α, and Δv_α are evaluated at the delayed time.

Note that the reaction time T' is sometimes set equal to the 'safe time gap' T. It is, however, essential to distinguish between these times conceptually. While the time gap T is a characteristic parameter of the driving style, the reaction time T' is essentially a *physiological parameter* and, consequently, weakly or not correlated with T. We point out that both, the time gap T and the reaction time T' are to be distinguished from the numerical update time step Δt which is sometimes interpreted as a reaction time as well. For example, in our simulations, an update time step of 2 s has about the same effect as a reaction time of 1 s, while the results are essentially identical for any update time step below 0.1 s. In Sec. 4.2.4, we investigate the interplay between reaction time and numerical update time step. The latter can be basically interpreted as a typical length of time periods during which drivers do not focus their attention on the driving task ('restricted attention span').

4.1.2 Imperfect Estimation Capabilities

We will now model estimation errors for the net distance s and the velocity difference Δv to the preceding vehicle. Since the velocity itself can be obtained by looking at the speed indicator, we neglect its estimation error. From empirical investigations (for an overview see Ref. [8]) it is known that the uncertainty of the estimation of Δv is proportional to the distance, i.e., one can estimate the time-to-collision (TTC) $s/|\Delta v|$ with a constant uncertainty.[1] For the distance itself, we specify the estimation error in a relative way by assuming a constant variation coefficient V_s of the errors. Furthermore, we take into account a finite persistence of estimation errors by modeling them as a Wiener process [25]. This leads to the following nonlinear stochastic processes for the distance and the velocity difference,

$$s^{\text{est}}(t) = s(t)\,\exp(V_s w_s(t)), \tag{4.3}$$

$$(\Delta v)^{\text{est}}(t) = \Delta v(t) + s(t)\,r_{\text{c}} w_{\Delta v}(t), \tag{4.4}$$

where $\exp(\cdot)$ denotes the exponential function, $V_s = \sigma_s/\langle s\rangle$ with $\sigma_s^2 = \langle (s - \langle s\rangle)^2\rangle$ is the variation coefficient of the distance estimate, and $1/r_{\text{c}}$ is a measure of the average estimation error of the time-to-collision. The stochastic variables $w_s(t)$ and $w_{\Delta v}(t)$ obey independent Wiener processes $w(t)$ of variance 1 [25] with correlation times τ defined by

$$\frac{\mathrm{d}w}{\mathrm{d}t} = -\frac{w}{\tau} + \sqrt{\frac{2}{\tau}}\,\xi(t) \tag{4.5}$$

with

$$\langle \xi\rangle = 0, \quad \langle \xi(t)\xi(t')\rangle = \delta(t - t'). \tag{4.6}$$

In the explicit numerical update from time step t to step $t + \Delta t$, we have implemented the Wiener processes by the approximation [25]

$$w_{t+\Delta t} = e^{-\Delta t/\tau} w_t + \sqrt{\frac{2\Delta t}{\tau}}\,\eta_t, \tag{4.7}$$

where the $\{\eta_t\}$ are independent realizations of a uniformly distributed quantity with zero mean and unit variance. By numerical validation we checked that the update scheme (4.7) satisfies the fluctuation-dissipation theorem $\langle w_t^2\rangle = 1$ and $\langle w_t w_{t'}\rangle = e^{-|t-t'|/\tau}$ for any update time interval satisfying $\Delta t \ll \tau$.

The stochastic sources V_s and r_c characterize the degree of the estimation uncertainty of the drivers, while τ denotes the correlation time of errors. The limit $\tau \to 0\,\text{s}$ corresponds to multiplicative white acceleration noise, while $\tau \to \infty$ corresponds to 'frozen'

[1] Generally, the estimation error includes a systematic bias as well. We have found, however, that our model is very robust with respect to reasonable biases in the distance and velocity-difference estimates.

error amplitudes, i.e., to *de facto* heterogeneous traffic. Simulations have shown that, in agreement with our expectations, traffic becomes more unstable with increasing values of the fluctuation strengths V_s and r_c. To compare the influence of the temporally correlated multiplicative HDM noise with more conventional white acceleration noise, we have repeated the simulations of Sec. 4.3 with the deterministic HDM ($V_s = r_c = 0$), augmented by an additive noise term $\sqrt{Q_a}\xi(t)$ on the right-hand side of the acceleration equation. Remarkably, values of the fluctuation strength Q_a can be found, for which the dynamics are essentially the same as for the more realistic stochastic terms described by V_s, r_c, and τ. Thus, the more realistic representation of sources of stochasticity in the HDM can be used to determine the appropriate strength Q_a of the simplified white noise representation.

It is interesting to compare the stochastic HDM expressions for imperfect estimation capabilities with other stochastic microscopic traffic flow models. While fluctuating terms were first introduced to traffic models more than 20 years ago [26], the most prominent example of stochastic traffic models are cellular automata (CA) of the Nagel-Schreckenberg type [84] and extensions thereof. There is, however, a qualitative difference compared to most continuous models: Fluctuation terms change the dynamics of many CA models qualitatively. Therefore, they must be carefully chosen to yield plausible results. In contrast, the qualitative dynamics of car-following models typically remain the same when fluctuations are added via the proposed HDM approach.

4.1.3 Temporal Anticipation

We assume that drivers are aware of their finite reaction time and anticipate the traffic situation accordingly. Besides anticipating the future distance [21], we will anticipate the future velocity using a *constant-acceleration heuristic*. The combined effects of a finite reaction time, estimation errors and temporal anticipation lead to the following input variables for the underlying microscopic model (4.1):

$$\frac{\mathrm{d}v}{\mathrm{d}t} = \dot{v}^{\mathrm{mic}}(s'_\alpha, v'_\alpha, \Delta v'_\alpha) \tag{4.8}$$

with

$$s'_\alpha(t) = \left[s_\alpha^{\mathrm{est}} - T'\Delta v_\alpha^{\mathrm{est}}\right]_{t-T'}, \tag{4.9}$$

$$v'_\alpha(t) = \left[v_\alpha^{\mathrm{est}} + T'a_\alpha\right]_{t-T'}, \tag{4.10}$$

and

$$\Delta v'_\alpha(t) = \Delta v_\alpha^{\mathrm{est}}(t - T'). \tag{4.11}$$

We did not apply the constant-acceleration heuristic for the anticipation of the future velocity difference or the future distance, as the accelerations of other vehicles cannot be

estimated reliably by human drivers. Instead, we have applied the simpler *constant-velocity heuristic* for these variables.

Notice that the anticipation terms discussed in this subsection (which do not contain any additional model parameters) are specifically designed to compensate for the reaction time by means of plausible heuristic. The impact of these anticipation terms will be studied in Sec. 4.2. They are to be distinguished from 'anticipation' terms in some models aimed at collision-free driving in 'worst-case' scenarios (sudden braking of the preceding vehicle to a standstill), when the braking deceleration is limited. Such terms typically depend on the velocity difference and are included, e.g., in the Gipps model, in the IDM, and in some cellular automata [69, 65], but notably not in the OVM. The HDM is most effective when using a basic model with a reasonable dependence on relative velocities.

4.1.4 Spatial Anticipation Several Vehicles Ahead

Let us now split up the acceleration of the underlying microscopic model into a single-vehicle acceleration on a nearly empty road depending on the considered vehicle α only, and a braking deceleration taking into account the vehicle-vehicle interaction with the preceding vehicle:[2]

$$\dot{v}^{\mathrm{mic}}(s_\alpha, v_\alpha, \Delta v_\alpha) := \dot{v}^{\mathrm{free}}(v_\alpha) + \dot{v}^{\mathrm{int}}(s_\alpha, v_\alpha, \Delta v_\alpha). \tag{4.12}$$

Next, we model the reaction to several vehicles ahead just by summing up the corresponding vehicle-vehicle pair interactions $\dot{v}^{\mathrm{int}}_{\alpha\beta}$ between vehicle β and vehicle α for the n_{a} nearest preceding vehicles β:[3]

$$\frac{\mathrm{d}}{\mathrm{d}t} v_\alpha(t) = \dot{v}^{\mathrm{free}}_\alpha + \sum_{\beta=\alpha-n_{\mathrm{a}}}^{\alpha-1} \dot{v}^{\mathrm{int}}_{\alpha\beta}. \tag{4.13}$$

All distances, velocities and velocity differences on the right-hand side are specified according to Eqs. (4.9) to (4.11). Each pair interaction between vehicle α and vehicle β is specified by

$$\dot{v}^{\mathrm{int}}_{\alpha\beta} = \dot{v}^{\mathrm{int}}\left(s_{\alpha\beta}, v_\alpha, v_\alpha - v_\beta\right), \tag{4.14}$$

[2] This decomposition of the acceleration will also be used in Chap. 5 to formulate a lane-changing model for a wide class of microscopic traffic models.

[3] The underlying modeling concept for this decomposition is a *social force approach*[82, 38]. Basically, there are two types of forces: A *driving force* to accelerate to the desired velocity, and repulsive *interaction forces* that are effective if one gets too close to the leader. When considering several leaders, it obviously makes no sense to change the driving force to reach the desired velocity since, by definition, this part of the acceleration is independent of any other vehicles. In contrast, it is intuitive to add further repulsive interaction forces if there are several leaders. Notice that the interaction force must decay sufficiently fast with the distance in order that the sum of the forces always stays finite.

where

$$s_{\alpha\beta} = \sum_{j=\beta+1}^{\alpha} s_j \tag{4.15}$$

is the sum of all *net* headways between the vehicles α and β because the (net) gaps determine the criticality of a situation.

4.1.5 Applying the HDM Extensions to the Intelligent Driver Model

In the following, we will apply the HDM extensions to the IDM, whose continuous acceleration function is given by Eq. (2.1) on page 15. Remarkably, there exists a closed-form solution of the multi-anticipative IDM equilibrium distance as a function of the velocity,

$$s_e(v) = \frac{\gamma s^*(v,0)}{\sqrt{1-\left(\frac{v}{v_0}\right)^\delta}}, \tag{4.16}$$

which is γ times the equilibrium distance of the IDM, where

$$\gamma(n_\mathrm{a}) = \sqrt{\sum_{\alpha=1}^{n_\mathrm{a}} \frac{1}{\alpha^2}}. \tag{4.17}$$

The equilibrium distance $s_e(v)$ can be transformed to that of the original IDM by renormalizing the relevant IDM parameters appearing in $s^*(v,0)$:

$$s_0^\mathrm{ren} = \frac{s_0}{\gamma}, \quad T^\mathrm{ren} = \frac{T}{\gamma}. \tag{4.18}$$

The above renormalisation will be applied to all simulations in this thesis. In the limiting case $n_a \to \infty$ (i.e., anticipation to arbitrarily many vehicles), we obtain $\lim_{n_\mathrm{a}\to\infty} \gamma(n_\mathrm{a}) = \pi/\sqrt{6} = 1.283$. This means that the combined effects of all non-nearest-neighbor interactions would lead to an increase in the equilibrium distance of just about 28%. According to Eq. (4.17), the largest impact results from the direct leader, while the second predecessor weights 11.8% relative to the first leader, the third predecessor 4.9%, etc. However, in case of a large velocity difference, non-nearest neighbors can contribute to Eq. (4.13) to a larger extend. Therefore, multi-anticipation is able to increase the stability, see Sec. 4.2 below.

4.1.6 Summary and Further Driver Adaptation Processes

From a control-theoretical point of view, the HDM extensions implement a continuous response to delayed (and noisy) input stimuli. The different stabilizing and destabilizing

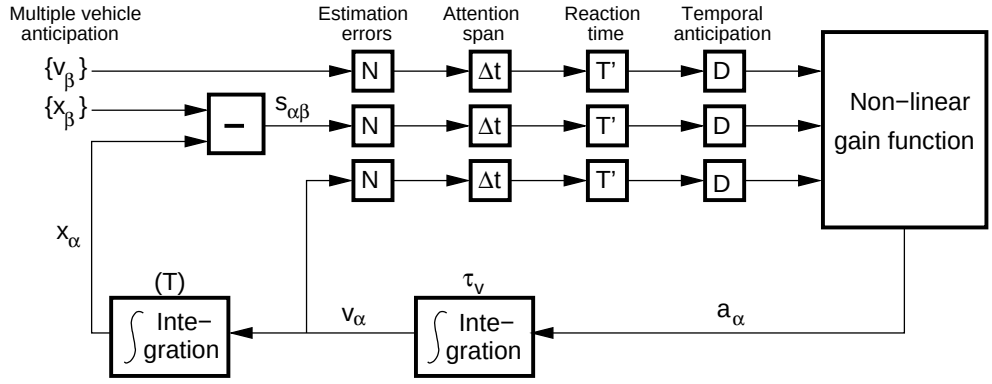

Figure 4.2: Elements of the feedback loop for the vehicle dynamics according to the Human Driver Model. The quantities to be controlled are the distance s_α and velocity v_α. The control is performed by the acceleration function of the model representing a nonlinear gain function. The feedback path from the acceleration to the quantities to be controlled contains three characteristic times. Besides integral elements incorporating the velocity adaptation time τ_v, the feedback contains delay elements representing the update time Δt and the reaction time T' needed to 'calculate' the acceleration function (cf. Sec. 4.2 for a detailed analysis). To include temporal anticipation, additional (nonlinear) derivative elements are incorporated into the control path. The whole circuit is perturbed by the leading vehicles represented by the external (and noisy) inputs x_β, and v_β.

factors of the driver's behavior and the vehicle dynamics constitute a *nonlinear feedback control system* as visualized in Fig. 4.2 (cf. the IDM control loop illustrated in Fig. 2.9 on page 28). More specifically, the controllers are the drivers, the quantities to be controlled are the velocity of the own vehicle and the distance to the leading vehicle, and the input stimuli are the observed distances and velocities, respectively.[4] Notice that the reaction time is represented by dead-time or delay elements. The actions in order to reach desired values of the velocity and distance consist in accelerating or braking according to a car-following model. In the framework of control theory, this acceleration is represented by a nonlinear *gain function*. Since only the acceleration can be controlled, the control path contains additional integral elements. To include anticipation, additional (nonlinear) derivative elements are required in the control path. The control path as illustrated in Fig. 4.2 contains several time delays which we will investigate in detail in the following Sec. 4.2.

Finally, it should be mentioned that the proposed HDM assumes a longitudinal human 'driving style' characterized by the reaction to the *immediate* traffic environment with in a time-independent way referring to constant parameter settings (which, of course, can be varied for each driver-vehicle unit in a microscopic traffic simulation). On a *longer time scale*, however, human drivers also adapt their driving style to the traffic situation, i.e., the

[4]Instead of the velocity difference, one can take the velocity $v_{\alpha-1}$ of the leading vehicle as equivalent input.

actual driving style depends on the traffic conditions during the last few minutes [10, 122]. For example, it is observed that most drivers increase their preferred temporal headway, after being stuck in congested traffic for some time, cf. Fig. 4.1. This is sometimes called 'frustration effect' [118, 34]. Accordingly, when larger gaps appear or when reaching the downstream front of the congestion area, human drivers accelerate less compared to a free-traffic situation.

This *memory effect* [122] can be modeled by assuming that, when encountering congested traffic characterized by a low 'level of service' $\lambda = v_\alpha/v_0$, drivers gradually adapt their driving style from a 'free-traffic mode' to a 'congested-traffic mode'. This typically involves a gradual change of some parameters of the underlying car-following model as a function of the new, slowly varying quantity $\lambda(t)$. Specifically, for the HDM-IDM combination, the parameters a and T valid for free traffic can be changed appropriately on a time scale of the order of a few minutes. For further details, we refer to Ref. [122].

In the remainder of this chapter, we will neglect this effect for matters of simplicity. Nevertheless, long-term adaptations of the driving style have a significant influence on the capacity and stability of traffic flow. In Part II, we will compensate for this capacity-reducing effect by proposing an automated strategy that depends on different traffic situations.

4.2 Collective Stability of Vehicle Platoons

It is well known in the theory of car-following models [33] and for macroscopic traffic models [123] that *collective instabilities* of traffic flow can occur even for zero reaction times and negligible update times. This is true even if a pair of vehicles always behaves locally stable. The reason is that, in an extended multi-particle system with many degrees of freedom, two concepts of linear stability have to be considered: *Local stability* is related to the response of a vehicle following the motion of the vehicle directly in front, i.e., to the dynamics of a pair of vehicles. *Asymptotic, string* or *collective stability* refers to the damping of a perturbation initially introduced by a leading vehicle along a platoon of following vehicles [80].[5] Generally, collective stability is a more restrictive criterion than local stability. It is relevant for the breakdown of traffic flow and traffic safety.

In traffic flow, the source of the string instability is the finite velocity adaptation time resulting from limited acceleration capabilities. As a consequence, perturbations amplify while propagating upstream in the platoon of vehicles and eventually lead to oscillating congested traffic (stop-and-go traffic). This is a commonly observed type of traffic congestion [102]. An examples of this instability mechanism for the (deterministic) IDM is shown in Fig. 2.8 on page 26.

In Sec. 4.2.2, we investigate the string stability of the HDM as a function of the reaction time T', the temporal anticipation and the number n_a of anticipated vehicles by simulating a platoon of vehicles following an externally controlled lead vehicle. We carefully distinguish between reaction time, adaptation time and update time and investigate the role of each of these times with respect to instabilities of traffic flow. First, we study how the stability is influenced by the reaction time and a finite acceleration capability (Sec. 4.2.3). Second, we investigate the interplay between reaction time and numerical update time (Sec. 4.2.4). Since we apply the same perturbation of the lead vehicle to all numerical investigations of this section, we start with a description of the simulation scenario in Sec. 4.2.1.

4.2.1 Simulation Setup and Applied Perturbation

We have simulated a platoon of 100 vehicles following a leader with externally prescribed velocity $v_{\text{lead}}(t)$. Initially, and for the first 1000 s of simulation time, the leader drives at velocity $v_{\text{lead}} = 25\,\text{m/s}$. Furthermore, all followers are in equilibrium, i.e., the initial velocities of all platoon vehicles are the same and their gaps are equal to $s_e(v_{\text{lead}})$ [cf. Eq. (4.16)]. That is, the initial accelerations are zero. Throughout this section, we neglect

[5] Note that the regime of string instability can be further subdivided into a region of *convective instability*, where perturbations grow, but finally are convected out of the system, and a region of *absolute instability*.

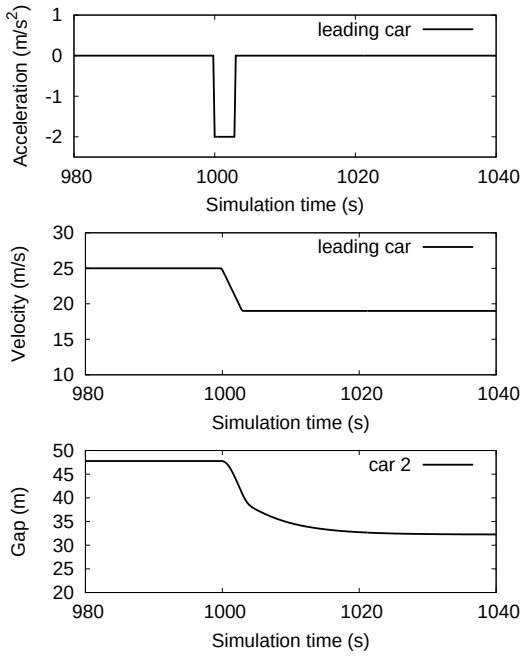

Figure 4.3: Time series of the acceleration and velocity for the externally controlled first vehicle of the vehicle platoon. The lead vehicle decelerates at $t = 1000\,\mathrm{s}$ with $-2\,\mathrm{m/s^2}$, inducing a perturbation to the platoon of vehicles. The distance of the second car is in equilibrium before the braking maneuver and adjusts to the new equilibrium distance after a while. This braking maneuver serves as perturbation in all simulations of this chapter.

fluctuations which will be considered in Sec. 4.3. To trigger possible instabilities, the externally controlled vehicle decelerates with $-2\,\mathrm{m/s^2}$ from $25\,\mathrm{m/s}$ to $19\,\mathrm{m/s}$ during the time interval $1000 \le t \le 1003\,\mathrm{s}$, and drives at $v'_{\mathrm{lead}} = 19\,\mathrm{m/s}$ afterwards until the simulation ends at $t = 2500\,\mathrm{s}$. This braking maneuver serves as *perturbation* for all simulations of this section. Figure 4.3 shows the time series of the acceleration and velocity of the lead vehicle and the distance to the lead vehicle of the second car in the platoon.

As the nonlinear dynamics resulting from this finite perturbation cannot be handled by linearization anymore, we investigate the system numerically. In all simulations, we have used the explicit integration scheme (6.4) on page 104, assuming constant accelerations between each update time interval Δt. The update time interval is set to $\Delta t = 0.1\,\mathrm{s}$, the vehicle length is $5\,\mathrm{m}$ and the 'standard' IDM parameters given in Table 2.1 on page 17 are used unless stated otherwise. We only set the maximum acceleration to $a = 1.4\,\mathrm{m/s^2}$. If the number of anticipated vehicles n_a is larger than the number of preceding vehicles (which can happen for the first vehicles of the platoon), then n_a is reduced to the maximum number of vehicles. As usual, we restrict the maximum braking deceleration to $9\,\mathrm{m/s^2}$ to consider the physical limit for the braking decelerations (cf. Chap. 2). Since we have observed such values finally leading to accidents only in simulations of unrealis-

tic parameter combinations, this limit has a negligible influence on the dynamics in the following sections.

4.2.2 Influence of Reaction Time and Anticipation

Let us now investigate the string stability of the HDM as a function of the reaction time T', the parameter-free temporal anticipation, and the number n_a of anticipated vehicles by means of simulation. The initial conditions, the model parameters and the driving maneuver of the leading vehicle which introduces the initial perturbation have been described in the previous Sec. 4.2.1. We distinguish the following three regimes of asymptotic or collective stability:

(i) *String stability* refers to the situation, where all perturbations introduced by the deceleration of the lead vehicles are damped away while propagating through the platoon of vehicles.

(ii) The *oscillatory regime* is characterized by string instability, where perturbations increase but do not lead to collisions between vehicles, i.e., negative net distances.

(iii) The *collision regime* refers to a situation where, finally, the instability results in a collision of two (or more) vehicles.

The condition for a simulation to be in the collision regime (iii) is fulfilled if there is *some* time t and *some* vehicle α such that $s_\alpha(t) < 0$. The condition for string stability is fulfilled if $|\dot{v}_\alpha(t)| < 3\,\mathrm{m/s^2}$ for all vehicles and at *all* times (including the period where the leading vehicle decelerates). Additionally, string stability requires that, for sufficiently long times after the braking maneuver, the accelerations of *all* vehicles converge to zero. Finally, if neither the conditions for the collision regime nor those for the stable regime are fulfilled, the simulation result is attributed to the oscillatory regime. For matters of illustration, we refer to Fig. 4.5 below.

By means of simulation, we have determined the string stability boundaries as a function of the reaction time T' and the platoon size of vehicles. Figure 4.4 shows the three stability regimes for four scenarios with different temporal and spatial anticipation:

(1) The first scenario with neither spatial anticipation ($n_a = 1$) nor temporal anticipation serves as reference. This case corresponds to conventional IDM car-following behavior with finite reaction time, cf. Sec. 4.1.1. A platoon of 100 vehicles is stable for reaction times of up to $T'_{\mathrm{c1}} = 0.9\,\mathrm{s}$. Test runs with larger platoon sizes (up to 1000 vehicles) did not result in different thresholds suggesting that stability for a platoon size of 100 essentially means string stability for arbitrarily large platoon sizes. For reaction times $T' > T'_{\mathrm{c2}} = 1.15\,\mathrm{s}$, the collective instability leads to accidents.

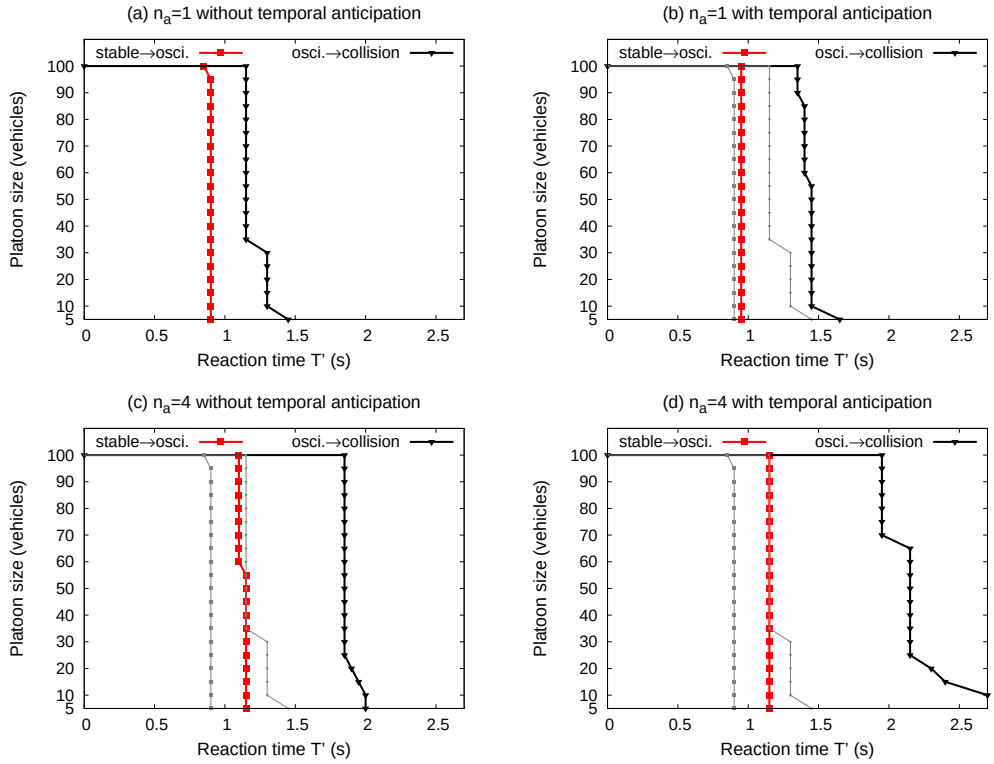

Figure 4.4: String stability regimes for a platoon of identical vehicles as a function of the platoon size and the reaction time T' for the scenarios (1) - (4). The graph (a) depicts scenario (1) assuming conventional follow-the-leader behavior ($n_a = 1$) without temporal anticipation; (b) with temporal anticipation and $n_a = 1$ (scenario (2)); (c) reaction to $n_a = 4$ vehicles without temporal anticipation (scenario (3)); (d) reaction to $n_a = 4$ vehicles with temporal anticipation (scenario (4)). In the diagrams (b)-(d), the first scenario of graph (a) is plotted with thin lines for purposes of comparison. The externally controlled first vehicle induced a perturbation according to Fig. 4.3. In the 'stable' phase, all perturbations are damped away. In the oscillatory regime, the perturbations increase, but do not lead to collisions.

(2) The second scenario extends the reference scenario by implementing temporal anticipation as specified in Sec. 4.1.3. While the stability limit, $T'_{c1} = 0.95\,\mathrm{s}$, is only slightly increased with respect to scenario (1), the collision limit $T'_{c2} = 1.4\,\mathrm{s}$ is increased significantly.

(3) The third simulation scenario implements spatial anticipation by looking $n_a = 4$ vehicles ahead (cf. Sec. 4.1.4). This spatial anticipation increases the stability and shifts both boundaries, T'_{c1} and T'_{c2} to significantly higher values.

(4) The forth scenario combines temporal and spatial anticipation ($n_a = 4$) which leads to the most stable system. Particularly, the second boundary is shifted to values of $T'_{c2} \geq 2\,\mathrm{s}$. Remarkably, the simulations show that, with suitable anticipation,

one could obtain *collision-free traffic even for reaction times exceeding the safety time gap* of $T = 1.5\,\mathrm{s}$. More detailed investigations for even larger reaction times reveal that collisions are triggered either directly by late reactions to deceleration maneuvers or indirectly as a consequence of the string instability. Further increasing the number of anticipated vehicles n_a does not change the thresholds significantly.

We have checked if these results are robust with respect to parameter changes and found no qualitative difference for other parameter sets within a reasonable range. For example, when changing the time gap from $T = 1.5\,\mathrm{s}$ to $T = 0.9\,\mathrm{s}$, the stability thresholds T'_{c1} and T'_{c2} reduce proportionally, i.e., T'_{c1} remains typically of the order of or slightly below T, while $T'_{c2} > T$.[6] Furthermore, we have also investigated the role of *statistically distributed reaction times*, assuming that every driver has a different reaction time T'_α within a range of $\pm 30\%$ around a mean value $\langle T'_\alpha \rangle = T'$ (cf. Chap. 6 for numerical details). Interestingly, the variation of the individual reaction times leads to a remarkably small change of the stability boundaries T'_{c1} and T'_{c2}.

In summary, these findings demonstrate the important influence of anticipation for the collective stability as modeled by the HDM. With a suitable spatial and temporal anticipation, we have obtained string stability for reaction times near (and even larger than) the safety time gap.

4.2.3 Traffic Instability due to Reaction Times and Finite Accelerations

Let us now investigate the influence of finite human reaction times T' and the time lag τ_v caused by finite accelerations of the vehicles. Obviously, both characteristic times influence the stability of traffic flow. Reaction times are an essential factor contributing to traffic instabilities as shown in Sec. 4.2.2. Clearly, stability always decreases when T' increases as explicitly shown in Sec. 4.2.2.[7]

In contrast to the reaction time, the velocity adaptation time τ_v (needed to accelerate to a new velocity) is already implicitly contained in the acceleration function (2.1) of the IDM. It results from limited acceleration capabilities modeled by the IDM parameter a. For low values of a, the lag time of velocity adaptations to the leading vehicles leads to collective instabilities already observed for zero reaction time (see Sec. 2.4).

In the following, we investigate the interplay between the reaction time T' and the adaptation time τ_v by simulating a vehicle platoon (see Sec. 4.2.1), using a constant update time

[6] Note that, in Ref. [125], a similar investigation has been carried out with a weaker braking perturbation of $-0.7\,\mathrm{m/s^2}$. Those results are in agreement with the findings presented here.

[7] As even adaptive cruise control (ACC) systems display relevant time delays in the control path that cannot be neglected [66, 79], a profound understanding of the dynamics and the instability mechanisms caused by time delays is needed.

of $\Delta t = 0.1\,\mathrm{s}$. The value for Δt is so low that the numerical results represent, to a good approximation, the exact solution of the set of delay-differential equations. The velocity adaptation time is mainly influenced by the acceleration, i.e., by the IDM and given by

$$\tau_v = \frac{v_0}{4a}, \tag{4.19}$$

where v_0 is the desired velocity and a the maximum acceleration parameter [60].

We have simulated the system for a fixed reaction time of $T' = 0.9\,\mathrm{s}$ and three values for the acceleration parameter a. The results are as follows:

(1) For $a = 1.0\,\mathrm{m/s^2}$, the system is *string stable*, i.e., the initial perturbation of $2\,\mathrm{m/s^2}$ dissipates quickly.

(2) After lowering the acceleration parameter to $a = 0.3\,\mathrm{m/s^2}$, the initial perturbation decreases for the first few vehicles (the system is *locally stable*), but it increases again for the subsequent vehicles, and finally leads to a traffic breakdown in the neighborhood of vehicle 100 at a simulated time $t \approx 1250$ s, i.e., the system is *string unstable* as shown in Fig. 4.5(a). After the first traffic breakdown, further stop-and-go waves develop as displayed in Fig. 4.6(a).

(3) Remarkably, after increasing the acceleration from the reference value $1.0\,\mathrm{m/s^2}$ to $a = 2.5\,\mathrm{m/s^2}$, the system becomes *string unstable as well*, cf. Fig. 4.5(b). Again, further stop-and-go waves develop in the course of time further upstream.

When varying the maximum acceleration capability, we come to the remarkable result that stability reaches its maximum for a certain range of values for a that depends on the reaction time T'. Traffic flow becomes more unstable if the value of the maximum acceleration is higher *or* lower than this value. We have checked if these results are robust with respect to parameter changes and found no qualitative difference for other parameter sets within a reasonable range. For example, when changing the time gap parameter from $T = 1.5$ s to $T = 0.9$ s, the stability thresholds reduce proportionally.

In any case, the results are markedly different from the case of zero reaction time where higher values of a (lower values of τ_v) *always* increase stability. This can be understood by recognizing that the 'classical' collective instability mechanism of the IDM (effective for high values of τ_v and only weakly depending on T') is *qualitatively different* from the second instability mechanism (active for low values of τ_v *and* high values of the reaction time). In the first case, the traffic breakdown is initially triggered by a *long-wavelength string instability* as can be seen from Fig. 4.5(a) in the plots for cars no. 10 and 20. Secondary instabilities of shorter wavelengths appear only in the nonlinear regime (car 50), before a complete breakdown is observed (car 80).

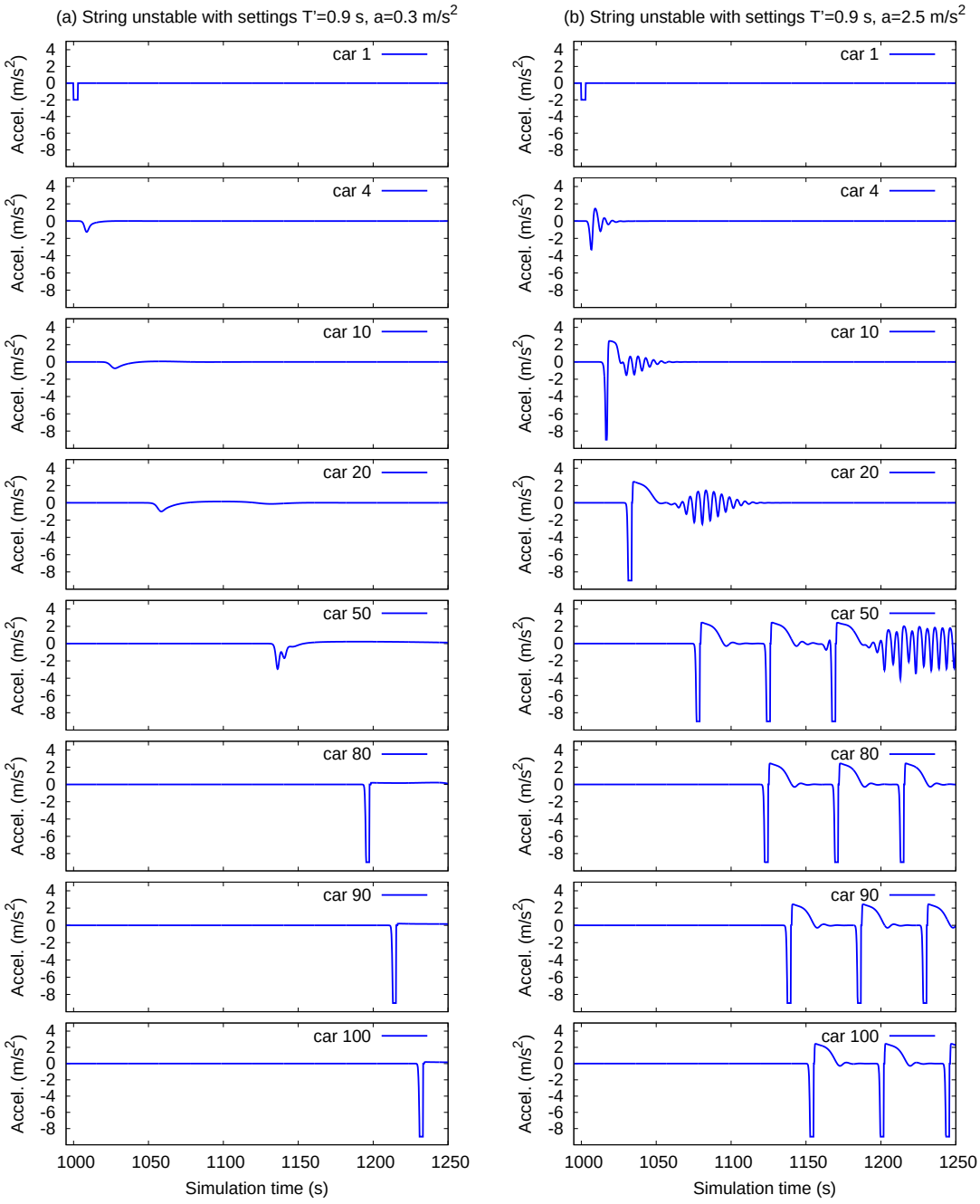

Figure 4.5: Time series of the acceleration with a reaction time of $T' = 0.9\,\mathrm{s}$. The maximum acceleration is reduced to $a = 0.3\,\mathrm{m/s^2}$ (left column) or increased to $a = 2.5\,\mathrm{m/s^2}$ (right column) showing unstable traffic (while $a = 1.0\,\mathrm{m/s^2}$ leads to stable traffic). (Left) The initial perturbation caused by the braking maneuver of the first vehicle is initially reduced (car 10), but then it increases while propagating upstream. This results in a stop-and-go wave for the car 100. (Right) The perturbation grows as well. The different instability mechanisms are discussed in the main text. In both scenarios, more stop-and-go waves are triggered as shown in Fig. 4.6.

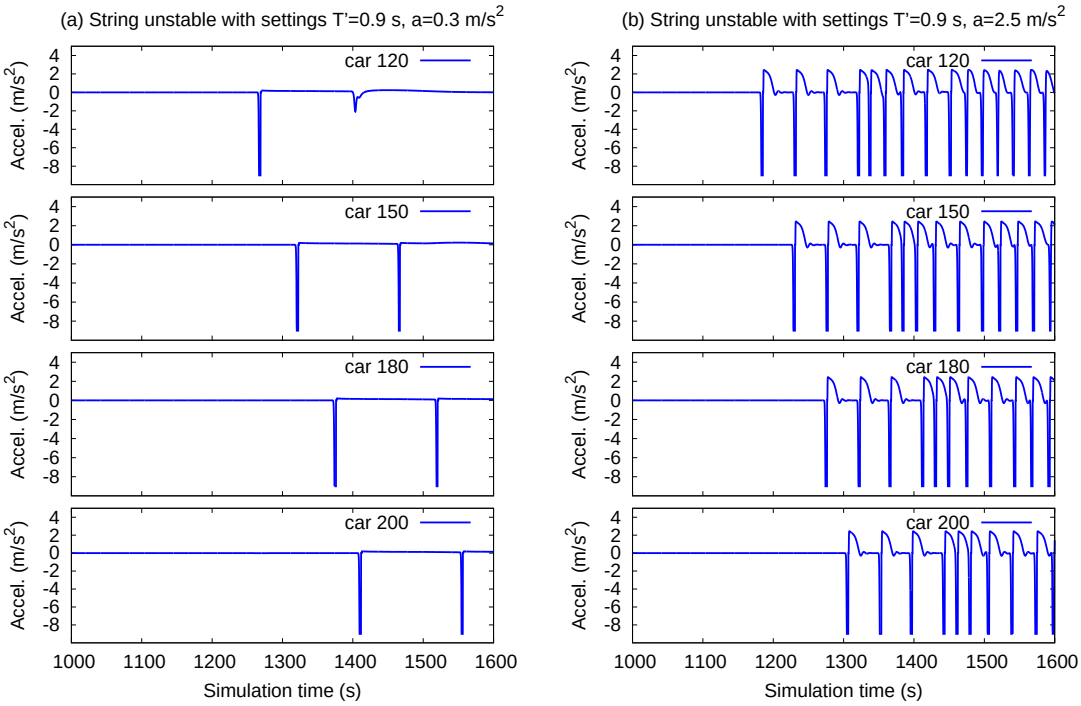

Figure 4.6: Patterns of emerging stop-and-go waves. The simulation is identical to that of Fig. 4.5, but vehicles further upstream are shown on a different time scale. The period of the stop-and-go waves is about 120 s for the simulation shown (on the left), while in the scenario on the right, the period is about 30 s.

In contrast, the second instability mechanism is initially triggered by a *short-wavelength local instability* as can be seen from Fig. 4.5(b) for the vehicles no. 1, 4 and 10. Further stop-and-go waves are triggered by the same mechanism later on. The range of the parameters T' and τ_v for the second mechanism is plausible when recognizing that the initial local instability is of the same type as that of simple feedback loops with delay-time elements, i.e., the velocity adaptation time in our context. Such systems become unstable if the ratio T'/τ_v exceeds a certain value of the order of unity that depends on the specific system. In contrast, the classical long-wavelength instability triggered by long velocity update times does not require a finite reaction time.

We have investigated this observation more systematically by calculating the instability of the system as a function of the reaction time and the acceleration parameter. To obtain a continuous measure for the instability, we have calculated the variance of the accelerations for the 20 floating cars 5, 10, 15, ..., 100 based on the time series for $t > 1000$ s, i.e., after the perturbation. The diagrams (a) and (c) of Fig. 4.7 show this instability measure as a function of T' for several fixed values of a. We get the following results:

- For $a \geq 1\,\mathrm{m/s^2}$, the system is stable for sufficiently small reaction time, and the in-

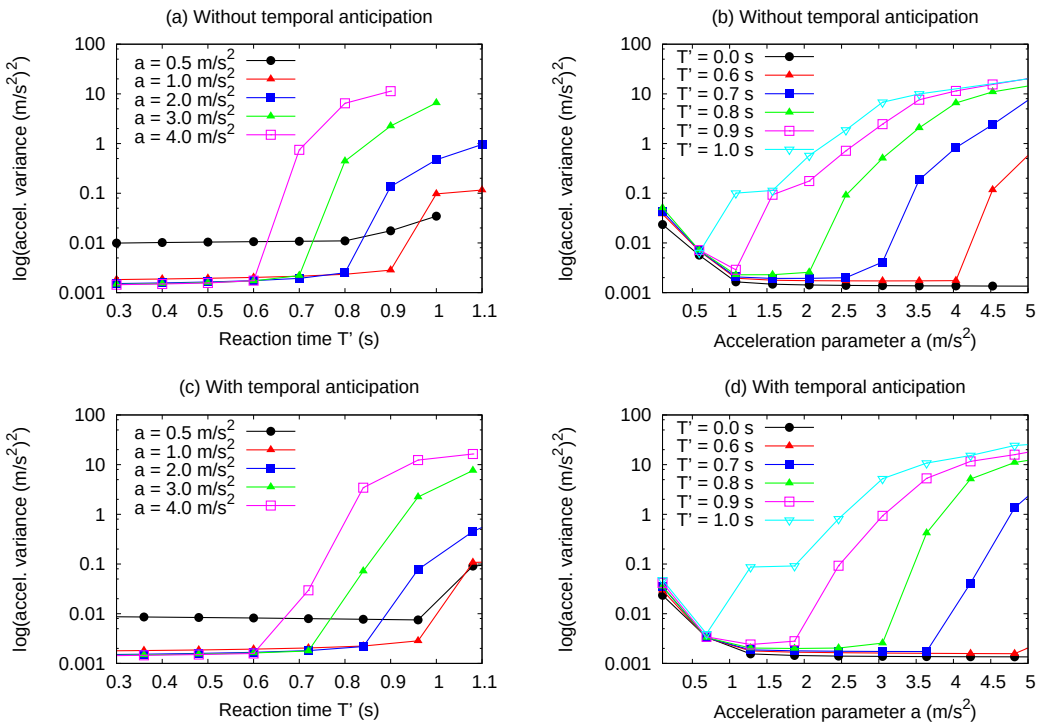

Figure 4.7: System instability measured by the variance of vehicle acceleration (see the main text for details) as a function of the reaction time T' (diagram a,c) and the maximum acceleration parameter a (b,d) for some fixed values of a and T', respectively. In (a) and (b), temporal anticipation has been switched off, while it has been turned on in (c) and (d). No spatial anticipation has been assumed. Notice that each point represents one simulation run.

stability threshold $T'_c(a)$ decreases with a. This is a signature of the short-wavelength instability mechanism.

- For $a = 0.5\,\mathrm{m/s^2}$, the system becomes unstable regardless of the value of T', and the instability measure has only a weak dependence on T'. This is a signature of the long-wavelength mechanism. Temporal anticipation slightly stabilizes the platoon dynamics.

Obviously, for a given reaction time T', there is a certain 'optimal' value for a or a range of values, where the system has maximum stability. This is depicted in Fig. 4.7(b) and (d) where the stability is plotted as a function of a for several fixed values of T':

- For $T' \leq 0.9\,\mathrm{s}$, the two mechanisms of instability are separated by an 'optimal' range of the parameter a where the system is completely stable. While, in the long-wavelength instability range $a \lesssim 0.6\,\mathrm{m/s^2}$, the instability measure depends only weakly on T', the critical acceleration a_c at the threshold of the short-wavelength

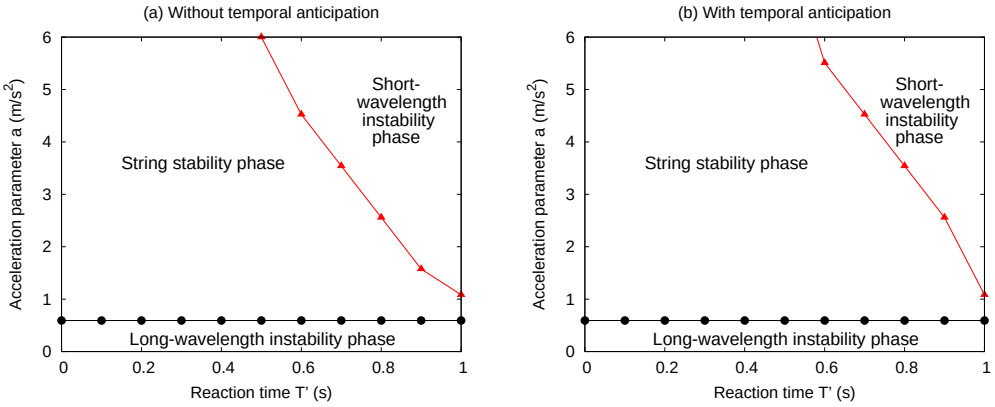

Figure 4.8: Phase diagram of stable and unstable traffic flow spanned by the reaction time T' and the acceleration parameter a. The initial perturbation leads to a long-wavelength collective instability for small values of a. For higher settings of a, the finite reaction time causes short-wavelength local instabilities. For a broad range of combinations of (T', a), the traffic dynamics of the vehicle platoon is stable. Temporal anticipation increases the range of stable settings of (T', a). Interestingly, for higher reaction times, an effectively *lower* value of a is able to reduce the instability of the system due to a delayed response to the input stimuli.

instability decreases strongly with increasing T'. For $T' < 0.6\,\mathrm{s}$, this instability mechanism is no longer observed for realistic values of a.

- For $T' = 1.0\,\mathrm{s}$, there is no longer a range of a with complete stability. Instead, both mechanisms seem to be effective simultaneously in the range of accelerations that was 'optimal' for $T' = 0.9\,\mathrm{s}$. Note that temporal anticipation increases the range of acceleration parameter values that correspond to stable platoon dynamics.

These findings are summarized in the phase diagram shown in Fig. 4.8 as a function of T' and a. Since the initial perturbation leads to a finite acceleration variance for stable traffic as well, the stable phase has been identified by values of the acceleration variance below $0.02\,\mathrm{m}^2/\mathrm{s}^4$.

4.2.4 Relation between Reaction Times and Numerical Update Times

In the simulations of Secs. 4.2.2 and 4.2.3, the update time step was chosen so small ($\Delta t = 0.1\,\mathrm{s}$) that even smaller update time steps of, e.g., $\Delta t = 0.01\,\mathrm{s}$, did not deliver significantly different results. However, investigating large update time steps is interesting, since both finite reaction times T' *and* update time steps Δt introduce delays in the reaction to the traffic situation, and the relative influence of both effects becomes important. *A priori*, it is not clear if both effects are dynamically equivalent and, if so, for which pairs

of values. Note that large values of Δt are desirable as they imply a better numerical efficiency.

We have systematically investigated the effects of various combinations of T' and Δt for the system of 100 vehicles and the perturbation discussed in Sec. 4.2.1. Figure 4.9 shows the results in form of a 'phase diagram' spanned by both times for various settings of the spatial anticipation parameter, $n_a = 1, \ldots, 4$, while keeping all other parameters constant (cf. Sec. 4.2.1). Furthermore, we have applied temporal anticipation in all simulations. The three dynamical phases are characterized by (i) no instabilities, (ii) accident-free instabilities which may be either of the short-wavelength or the collective long-wavelength type (see Sec. 4.2.3), (iii) instabilities that eventually lead to accidents. Notice that the phase boundaries for $\Delta t \approx 0\,\mathrm{s}$ in the diagrams 4.9(a) and (d) refer to the string stability regimes shown in Fig. 4.4(b) and (d) for a platoon size of 100 vehicles. As expected from the results presented in Sec. 4.2, the stability boundaries are shifted towards larger reaction times when increasing spatial anticipation from $n_a = 1$ to $n_a = 4$ vehicles. For larger values of n_a, the result does not change qualitatively anymore.

Interestingly, for a given value T_0 of either T' or Δt, the combination $(T' = T_0, \Delta t \approx 0)$ leads to a stronger destabilizing effect than the combination $(T' = 0\,\mathrm{s}, \Delta t = T_0)$. To explain this finding, it is essential to distinguish between the the two times conceptually:

(i) The limiting case $\Delta t \to 0$ for finite values $T' = T_0$ corresponds to the exact solution of the time-continuous model for a finite reaction time, i.e., to the delay-differential equation (4.2) (see the horizontal axes of the diagrams in Fig. 4.9).

(ii) The case $\Delta t = T_0$ and $T' = 0\,\mathrm{s}$ corresponds to the numerical solution of the model with zero reaction time, but for large integration time steps, i.e., to a coupled iterated map (see the vertical axes of the diagrams in Fig. 4.9).

Since the two limiting cases lead to qualitatively different mathematical models they are obviously not equivalent. Consequently, the phase boundaries of Fig. 4.9 are not symmetric with respect to the axes. In Fig. 4.9(a) for example, the parameter combination $(\Delta t = 1.2\,\mathrm{s}, T' = 0.6\,\mathrm{s})$ corresponds to stable traffic while $(\Delta t = 0.6\,\mathrm{s}, T' = 1.2\,\mathrm{s})$ leads to crashes. Therefore, for the same numerical values, the reaction time T' introduces stronger destabilizing effects than the update time interval Δt.

This can be explained by looking more closely at the two mechanisms. In case (i), the acceleration at any time t is calculated using the information available at $t - T_0$, i.e., the delay is always given by a considered value T_0. For the complementary case (ii), the update scheme (6.4) on page 104 corresponds to instantaneously updating the acceleration based on the actual information at time $t = nT_0$ with integer n, and driving with this acceleration for the whole next time step, i.e., not responding to any new information

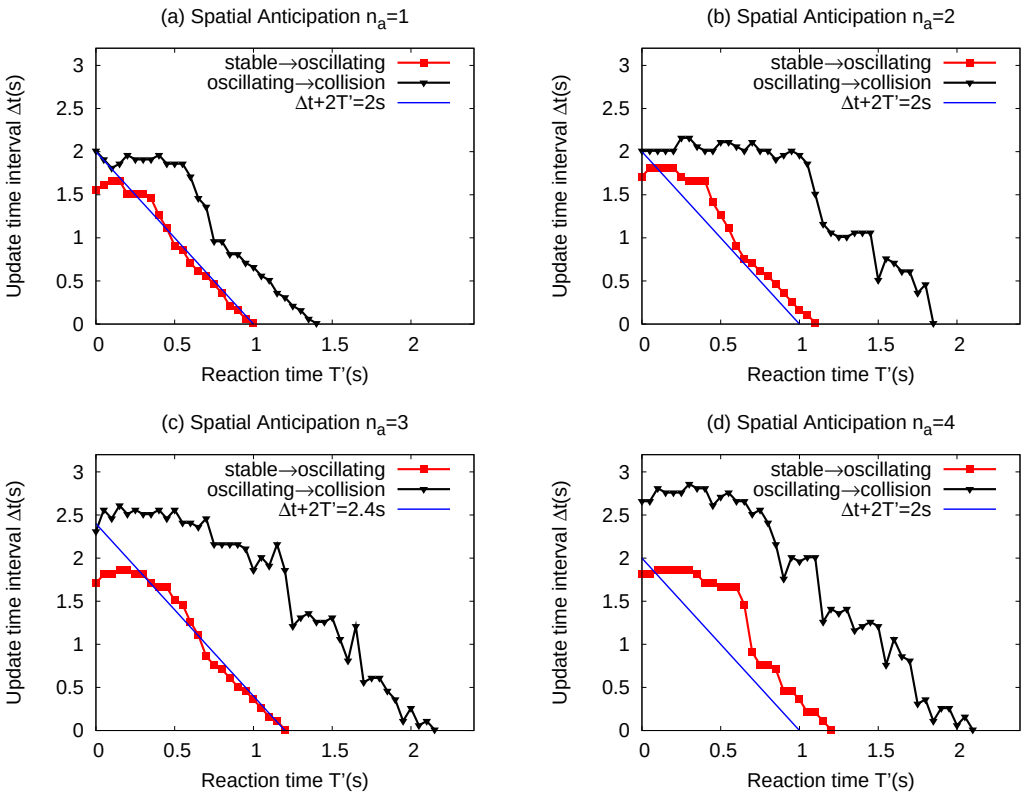

Figure 4.9: Phase diagrams of the three dynamical phases for a platoon size of 100 vehicles as a function of the reaction time T' and the numerical time discretization Δt. Diagram (a) refers to follow-the-leader behavior ($n_a = 1$), while stability is increased for spatial anticipation over $n_a > 1$ vehicles. Besides the numerical necessity for a finite update time step Δt, the value of Δt can be interpreted as 'attention span', i.e., as a typical length of time periods, during which drivers do not draw their attention to the driving task.

during that time. This corresponds to an effective delay time varying between 0 and T_0 as depicted in Fig. 4.10. Consequently, a reaction time $T' = T_0$ should have a *stronger destabilizing effect than an update time interval of the same numerical value*. This is consistent with the results shown in Fig. 4.9. Remarkably, the borderline between stable and oscillatory platoons is approximately given by the equation $\Delta t + 2T' = C$ with, e.g., $C = 2\,\mathrm{s}$ in Fig. 4.9(a). This means, the destabilizing effect of a finite reaction time is about twice as big as the one by a finite update time interval of the same numerical value or, *cum grano salis*, the *effective* reaction time T'_{eff} introduced by a finite update time interval Δt is about

$$T'_{\mathrm{eff}} \approx \frac{\Delta t}{2}. \tag{4.20}$$

Besides the numerical necessity for a finite time discretization Δt, the value of Δt can be interpreted as the typical length of time periods, during which drivers do not update their

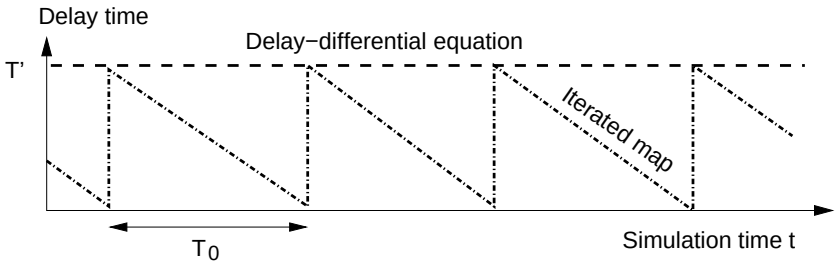

Figure 4.10: Illustration of the effective delay time as a function of the continuous simulation time for $T' = T_0$ and $\Delta t = 0$ (delay-differential equation, dashed), and for $T' = 0$ and $\Delta t = T_0$ (iterated map, solid).

response to changes in the traffic situation. In conjunction with the update scheme (6.4), drivers are assumed to evaluate the traffic situation at times that are multiples of Δt and to instantaneously adapt their acceleration to the new situation. It has been proposed that distractions and the 'restricted attention span' of human drivers play an important role in driving behavior [6]. Since the reaction time can be varied independently from the update time interval, the combined effects of distractions and finite reaction times can be investigated simultaneously.

4.3 Traffic Dynamics of an Open System with a Bottleneck

In the previous section, we have investigated the HDM with respect to string stability of a platoon of vehicles with a specific perturbation introduced by an externally controlled lead vehicle. In this section, we will examine the opposite effects of the driver reaction time T' and the spatial anticipation n_a on the stability of traffic and the occurring traffic states in a more complex situation, namely an open system containing a *flow-conserving bottleneck*, i.e., a road segment with a local decrease of capacity.

Specifically, we will consider a single-lane road section of total length 20 km with a bottleneck and open boundaries. Each simulation run covers a time interval of 3 h. We initialize the simulations with very light traffic of density 1 vehicle/km and set all initial velocities to 100 km/h. Note that the initial conditions are relevant only during the time interval needed by the vehicles to cross the road section, i.e., for about the first 15 minutes. Furthermore, we will assume identical drivers and vehicles of length $l = 5$ m, whose parameters are given in Table 4.1. The HDM has been used with the IDM as basic underlying model. The update time interval of the numerical integration is set to $\Delta t = 0.1$ s.

We will simulate idealized rush-hour conditions by increasing the inflow $Q_{\text{in}}(t)$ at the upstream boundary linearly from 100 veh/h at $t = 0$ to 2100 veh/h at $t = 1$ h, keeping the traffic demand constant afterwards. Since this demand exceeds the static road capacity $Q_{\text{theo}}^{\max} \approx 2000$ veh/h at the bottleneck (i.e., the maximum of the fundamental diagram, cf. Fig. 2.6 on page 24, and Fig. 4.12 below), a traffic breakdown is always triggered, irrespective of the stability of traffic. We have produced a *flow-conserving bottleneck* at 18 km $\leq x \leq$ 20 km by linearly increasing the IDM parameter T from 1.1 s to 1.65 s in the region 18.0 km $\leq x \leq$ 18.5 km, setting $T = 1.65$ s for 18.5 km $\leq x \leq$ 19.5 km, and linearly decreasing T again from 1.65 s to 1.1 s in the region 19.5 km $\leq x \leq$ 20.0 km. This leads to a reduced capacity in this area.[8]

4.3.1 Spatiotemporal Traffic Flow Dynamics

In our simulations, we have varied the driver reaction time T' within the range 0 to 1.7 s and the number n_a of vehicles considered in the spatial anticipation from 1 to 7. The other parameters of the HDM with the IDM as underlying car-following model are kept constant at the values listed in Table 4.1.

Figure 4.11 shows typical examples of the spatiotemporal traffic patterns occuring in the simulations. Specifically, a congested traffic state may be either localized or extended The criterion to discriminate between these two types of congested traffic is the width of the congested region which, for localized clusters, is constant (and typically less than 1 km),

[8] For a justification of this implementation of a flow-conserving bottlenecks, see, e.g., Ref. [40].

HDM Parameter	Value
Reaction time T'	$0 \ldots 1.7\,\mathrm{s}$
Number of anticipated vehicles n_a	$1 \ldots 7$
Relative distance error V_s	$5\,\%$
Inverse TTC error r_c	$0.01/\mathrm{s}$
Error correlation times τ_s, $\tau_{\Delta v}$	$20\,\mathrm{s}$

Table 4.1: Parameters of the HDM-IDM combination with the values used in the simulations of this section. The driver reaction time T' and the number n_a of vehicles considered in spatial anticipation are varied. The IDM parameters for the underlying car-following model are as follows: The desired velocity is $v_0 = 128\,\mathrm{km/h}$, the safety time gap $T = 1.1\,\mathrm{s}$, the maximum acceleration $a = 1.0\,\mathrm{m/s^2}$, the desired deceleration $b = 1.5\,\mathrm{m/s^2}$ and the jam distance $s_0 = 2\,\mathrm{m}$.

while the width of extended congested traffic is variable and depends particularly on the inflow.

Within extended congested traffic, there exist three dynamical phases separated by continuous phase transitions: (1) *oscillating congested traffic* (OCT), (2) *homogeneous congested traffic* (HCT) and (3) *triggered stop-and-go waves* (TSG). As order parameter to distinguish between OCT (cf. Fig. 4.11a) and HCT (cf. Fig. 4.11b), we have used the variance σ^2 of the temporal velocity variations in the congested region sufficiently upstream of the bottleneck. There, σ^2 is essentially constant with respect to space and time. While, in the case of HCT, σ^2 depends mainly on the fluctuating forces and remains below $1\,(\mathrm{m/s})^2$, it jumps to more than $100\,(\mathrm{m/s})^2$ and essentially becomes independent of the fluctuation strength in the case of OCT. In contrast to OCT, TSG states reach the free branch of the fundamental diagram, i.e., there are uncongested areas between the congested ones (cf. Fig. 4.12 below). Nevertheless, the OCT and TSG states are hard to distinguish, as they are not separated by a hysteretic phase transition, and the free branch between the 'stop-and-go' waves of TSG is approached exponentially, i.e., the definition of a somewhat arbitrary threshold is necessary to discriminate TSG from OCT states.

Furthermore, we have observed two different kinds of localized clusters: (1) *moving localized clusters* (MLC) and (2) *pinned localized clusters* (PLC). The transition between them is sharp. MLC move upstream at at a constant propagation velocity of about $V_g = -15\,\mathrm{km/h}$, while the location of PLCs is fixed at the bottleneck. In contrast to the IDM, for the HDM-IDM combination we have observed a coexistence of both localized dynamical phases (see Fig. 4.11d) as required by observations [102]. Note that the second stop-and-go wave in Fig. 4.11(d) is triggered by the boundary condition which acts as a further bottleneck here and is consistent with observations as well.

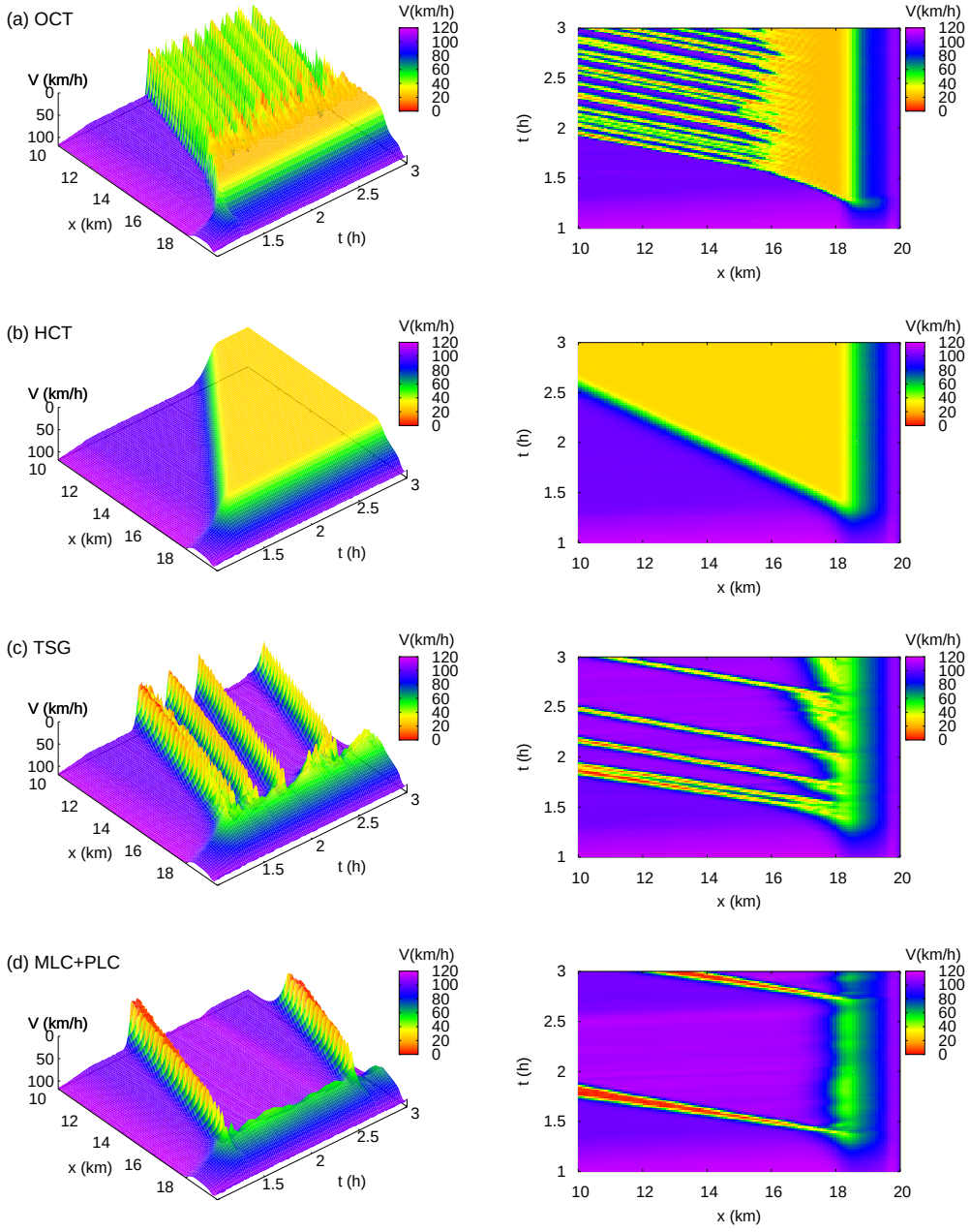

Figure 4.11: Spatiotemporal dynamics of typical traffic states of the phase diagram of Fig. 4.14. The macroscopic velocity field $V(x,t)$ is shown in a 3d plot (left column) and in a contour plot representation (right column). (a) The special case of the IDM with fluctuations ($n_a = 1$, reaction time $T' = 0\,\mathrm{s}$) leads to oscillatory congested traffic (OCT); (b) $n_a = 5$ anticipated vehicles and a reaction time $T' = 0.9\,\mathrm{s}$ leads to homogeneous congestion (HCT); even larger reaction times lead to (c) triggered stop-and-go traffic (TSG) ($n_a = 5$, $T' = 1.1\,\mathrm{s}$) or (d) a combination of moving localized clusters (MLCs) and a pinned localized cluster (PLC) ($n_a = 6$, $T' = 1.2\,\mathrm{s}$).

Remarkably, the destabilizing effects of finite reaction times can be compensated to a large extent by the spatial and temporal anticipation of the HDM such that the resulting stability and dynamics are similar to the IDM case of zero anticipation and no reaction time. This is illustrated by comparing Fig. 4.11(a) (no reaction time and no anticipation) with Fig. 4.11(c) (finite reaction time and anticipation). By comparing the simulation results in Fig. 4.11 with empirical traffic data from Ref. [102], one can see a qualitative agreement of the spatiotemporal dynamics in many respects. Particularly, (i) the congestion pattern is triggered by a bottleneck, (ii) the downstream front of the congestion pattern is stationary and located at the position of the bottleneck, (iii) traffic is essentially non-oscillatory in a region of about 1 km width near the bottleneck, (iv) further upstream, the congested traffic consists of stop-and-go waves propagating upstream at a constant velocity, while the period of the oscillations is variable. In addition to these qualitative aspects, there exists a nearly quantitative agreement with respect to the propagation velocity of $V_g \approx -15\,\mathrm{km/h}$. Notice that isolated and coexisting moving localized clusters (MLCs) and pinned localized clusters (PLCs) as shown in Fig. 4.11 have been observed in traffic data as well [102].

Figure 4.11(a) shows a complex traffic state with almost homogeneous congested traffic near the bottleneck and stop-and-go waves further upstream. This can be understood by distinguishing between linear and convective stability. Near the bottleneck, the congested traffic is linearly unstable, i.e., small perturbations created by the fluctuation terms of the model will grow. However, while growing, the perturbations travel upstream and are eventually propagating out of the system, leaving homogeneous congested traffic behind. This means, the congested region near the bottleneck is convectively stable. Thus, the sometimes observed complex transition from free traffic *via* homogeneous congested traffic ('synchronized traffic') to stop-and-go traffic can possibly be explained by fluctuation terms in the acceleration equation, connected with a congested region near the bottleneck that is linearly unstable, but convectively stable.[9]

4.3.2 Time Series and Flow-Density Relations

Figure 4.12 shows flow-density data of virtual detectors located at $x = 14\,\mathrm{km}$ and at $x = 17\,\mathrm{km}$ (5 km and 2 km upstream of the bottleneck, respectively) with a sampling period of 1 min. The data for OCT, 4.12(a) and TSG, 4.12(c), cover a two-dimensional area in the congested area which is in agreement with the *wide scattering* observed in empirical flow-density data [89, 4, 119].

Since the HDM has a unique equilibrium flow-density curve and since we have simulated

[9] Notice that, apart from fluctuations, Fig. 4.11(a) corresponds to a simulation of the underlying IDM. Since the nature of the fluctuations is not relevant (cf. Sec. 4.1.2), a similarly complex state can even be simulated with the purely deterministic IDM (or with other models) if other fluctuation sources are present, e.g., a fluctuating bottleneck strength.

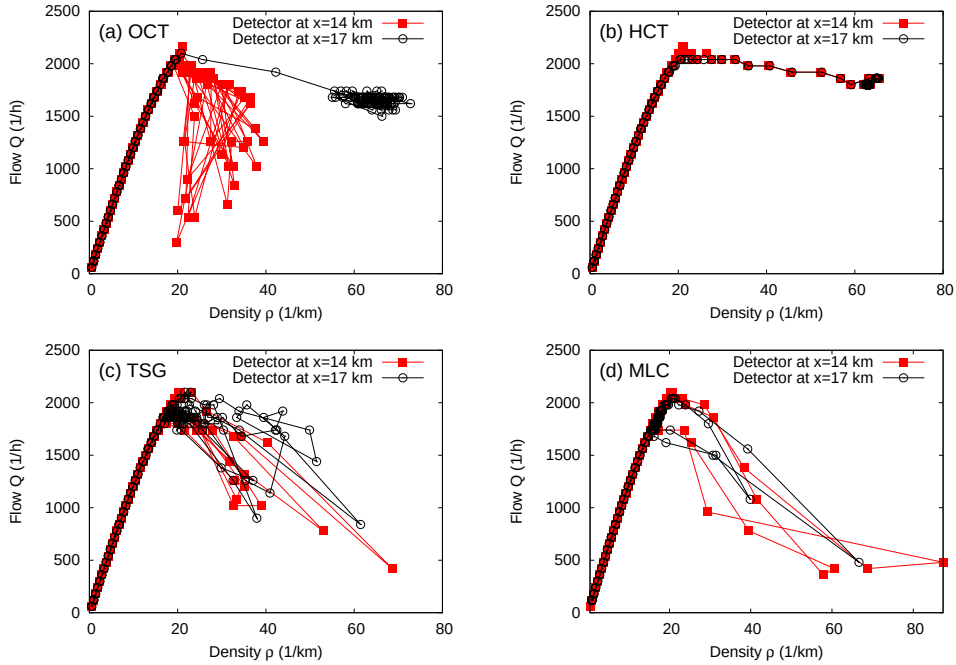

Figure 4.12: Simulated flow-density data at cross sections $x = 14\,\text{km}$ and $x = 17\,\text{km}$ measured by a virtual detector with a sampling interval of 60 s. The spatiotemporal dynamics of the depicted four simulation scenarios is shown in Fig. 4.11 on page 72.

identical driver-vehicle units, the observed scattering implies that the simulated congested traffic is out of equilibrium. In the simulations, possible forces bringing traffic out of equilibrium are the fluctuation terms of the HDM and traffic instabilities. It turns out that traffic instabilities contribute much more to the scattering of the flow-density data than the fluctuation terms.[10] Moreover, the distance from the equilibrium curve (and thus the area of scattering), is increased by long relaxation times back to equilibrium. These are implied by the adaptation of the driver behavior to the traffic environment as discussed in connection with the 'memory effect' in Sec. 4.1.6 (cf. Ref. [122]).

Figure 4.13 shows average velocity time series $V(t)$ of the same virtual detectors. Compared to the IDM with fluctuations in diagram 4.13(a), the finite reaction times and anticipations of the HDM lead to a larger period of velocity oscillations (about 8 min in the diagram 4.13c) compared to 4 min in diagram 4.13a) and to softer upstream congestion fronts, i.e., to lower velocity gradients. Remarkably, the periods and gradients of the velocity time series of the HDM agree well with those of real stop-and-go traffic data [102, 124], whereas the IDM and many other car-following models yield too short time periods.

[10] Note, however, that in real traffic the heterogeneity of the driving styles and vehicle types plays an important role as well [89, 4, 119].

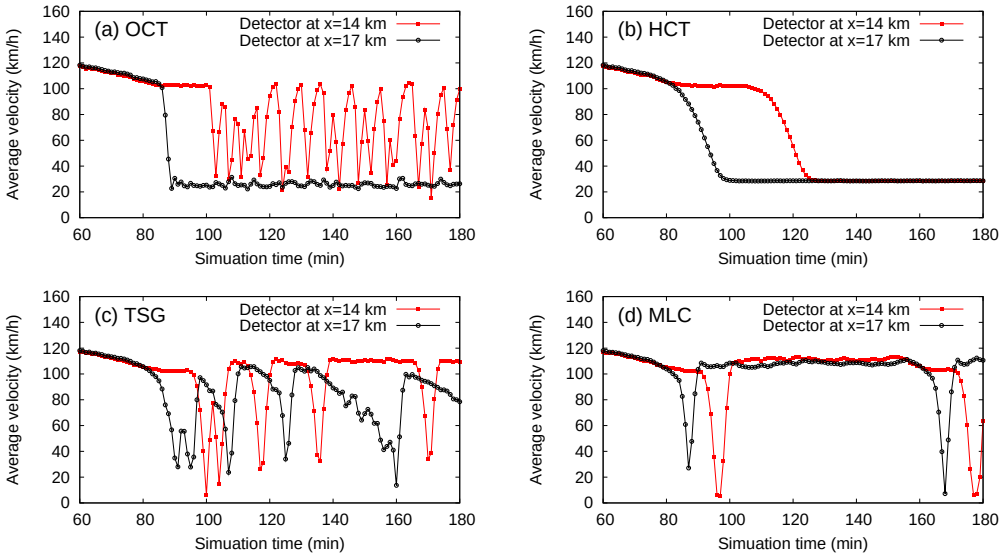

Figure 4.13: Velocity time series measured by virtual detectors located at $x = 14\,\mathrm{km}$ and $x = 17\,\mathrm{km}$ for the simulation scenarios discussed in Sec. 4.3.3. Notice the increase of the oscillation wavelength in the scenarios (c) and (d) with anticipation compared to (a) without anticipation which is in agreement with empirical observations.

Besides stability issues, the HDM simulation results agree better with empirical traffic data in the following aspects: (i) Compared to the underlying IDM, the HDM simulation shows larger oscillation periods and the transitions between 'stop' and 'go' are smoother. (ii) Coexisting PLCs and MLCs are observed both in the HDM and in real traffic data [102]. (iii) Near the bottleneck, the HDM regularly produces traffic of relatively high flow and density ('general pattern'), while one needs a fine-tuning of the parameters to produce these states with the IDM alone.

4.3.3 Phase Diagram of Congested Traffic States

Let us finally investigate the destabilizing influence of the reaction time T' and the stabilizing effects of n_a in a more systematic way. We have varied the number of vehicles used for the spatial anticipation from $n_a = 1$ to $n_a = 7$. For each value of n_a, we have varied the reaction time in steps of 0.05 s. By associating qualitatively different simulation results with different *dynamical traffic phases* as discussed in the previous Sec. 4.3.1, we have obtained a phase diagram in the space spanned by n_a and T', see Fig. 4.14. The lower left corner of Fig. 4.14 corresponds to the special case of the IDM with fluctuations, i.e., to the case of zero reaction time $T' = 0$ and consideration of the immediate front vehicle only, i.e., $n_a = 1$. In this case, the simulation results in OCT, see Fig. 4.11(a) as discussed before. Varying n_a and T' leads to the following main results:

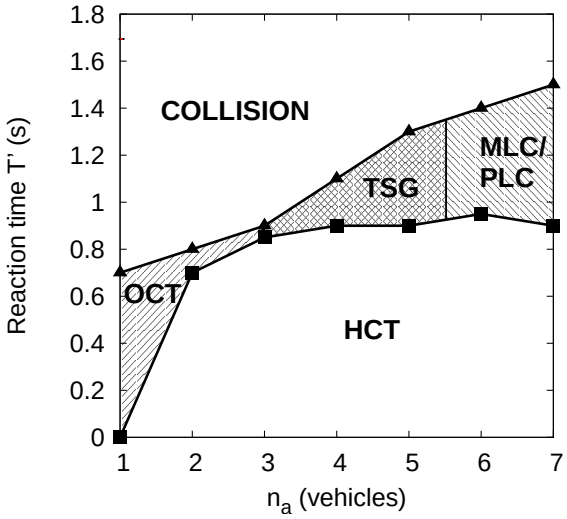

Figure 4.14: Phase diagram of congested traffic states in the phase space spanned by the number n_a of considered leaders and the reaction time T' in the open system with a bottleneck as described in the text. The dynamic phases HCT (homogeneous congested traffic), OCT (oscillatory congested traffic), TSG (triggered stop-and-go traffic) and MLC and PLC (moving and pinned localized clusters) are discussed in the main text.

- Traffic stability increases drastically, when spatial anticipation is increased from $n_a = 1$ to $n_a = 6$, while no significant (qualitative) changes are observed for $n_a > 6$.
- For a sufficiently large number of anticipated vehicles, the congestion pattern becomes stable, corresponding to homogeneous congested traffic (HCT), see Fig. 4.11(b).
- Increasing the reaction time T' destabilizes traffic and finally leads to crashes. For a given value of n_a, the critical threshold T'_{c2} for crashes is somewhat lower than in the simulations of Sec. 4.2.2 which is caused by the more complex simulation scenario and by the higher braking decelerations activated by the traffic breakdown. In contrast, the boundary to the HCT states essentially corresponds to the threshold T'_{c1} for string stability.
- Other extended congested traffic states are found as well. Triggered stop-and-go waves (TSG) are shown in Fig. 4.11(c). In addition, we found a (spatial) coexistence of moving localized clusters (MLC) and pinned localized clusters (PLC) in the course of the freeway, see Fig. 4.11(d).
- The results are robust against variations of the stochastic HDM parameters or when the correlated noise is replaced by white acceleration noise (cf. Sec. 4.1.2).

The phase diagram shown in Fig. 4.14 contained qualitatively the same spatiotemporal congested states as found in Refs. [35, 123, 124]. At first sight, this seems surprising. In these publications, the different phases are a consequence of different traffic demands on the main road and an on-ramp. Therefore, besides using a different model, the control parameters making up the phase space were *extrinsic* in the previous work, while the phase space is spanned by *intrinsic* model parameters (i.e., reaction time T' and the number of leading vehicles n_a) in the present work. Different traffic states can be produced not only by varying the 'bottleneck strength', but also by varying model parameters that influence stability. Thus, variations of both kinds of control parameters, i.e., extrinsic flow parameters and intrinsic capacity and stability limits, can lead to phase transitions.

4.4 Discussion and Conclusions

Finite reaction times and errors in estimating the input variables are essential factors of human driver behavior affecting the performance and stability of vehicular traffic. This applies not only to human drivers, but (to a smaller extent) also to realistic driver-assistance systems [66, 79]. Human drivers, on the other hand, compensate for these destabilizing effects by looking several vehicles ahead, anticipating the future traffic situation, and adapting to the traffic environment. Nevertheless, simple models such as the Optimal Velocity Model and its generalizations [3, 21, 51] or the IDM already allow to describe many, particularly macroscopic, aspects of the traffic dynamics. The question arises why, despite their conceptual shortcomings, these models work so well. This question becomes even more pressing because of the fact that all of the above models (including the IDM) produce unrealistic dynamics and collisions when simulating with realistic reaction times which are of the order of 1 s [29]. In this chapter we have shown that, to a large extent, *the destabilizing effects of reaction times and estimation errors can be compensated for by spatial and temporal anticipations*: For certain combinations of the relative strength of these effects, one obtains essentially the same collective longitudinal dynamics as without consideration of any of these effects. This result explains the good performance of the underlying simple car-following models. Note, however, that the wavelengths of the stop-and-go waves with the HDM extensions are larger and the transitions between 'stop' and 'go' are smoother than those of the IDM (and other car-following models) in agreement with observations. Obviously, multi-anticipation plays a role for the collective dynamics in real traffic.

In order to put the mutual balance of stabilizing and destabilizing effects into a more general context, we have proposed and studied the Human Driver Model (HDM) which is formulated as a *meta model* that can be used to extend a wide class of car-following models, where the acceleration depends only on the positions, velocities and accelerations

of the own and the preceding vehicle. The HDM explicitly takes into account the effects of (i) reaction times, (ii) imperfect estimation capabilities, (iii) temporal anticipation and (iv) multi-vehicle anticipation.[11] The HDM has two deterministic parameters, namely the reaction time T' and the number n_a of anticipated vehicles. The only stochastic contributions of the HDM come from modeling finite estimation capabilities. The stochastic sources V_s and r_c characterize the degree of the estimation uncertainty of the drivers, while τ denotes the correlation time of errors. All human-driver extensions are turned off and the original basic model is recovered by setting $T' = 0$, $n_a = 1$ and $V_s = r_c = 0$. By applying the HDM extensions to the IDM, we have provided quantitative details of the balance conditions and the remaining differences in the traffic dynamics. This involves validity criteria for the applicability of simpler car-following models.

In the context of microscopic traffic models, there are three characteristic time constants that influence the dynamics and stability of traffic flow: The reaction time T' of the drivers, the velocity adaptation time τ_v needed to accelerate to a new desired velocity, and the numerical update time Δt.[12] Based on the model-independent formulation of the HDM, we have investigated how these times interplay with each other and influence the instability mechanisms by simulating the local and string stability of a platoon of vehicles with the IDM as underlying acceleration model for various combinations of the three times.

When comparing the reaction time with the velocity adaptation time τ_v, we have obtained the interesting result that the 'optimal' acceleration (and deceleration) to obtain a maximum stability depends on the reaction time: The higher the reaction time, the lower the optimal accelerations. Therefore, a finite reaction time of 1 s can be partially compensated by an *optimized*, i.e., *effectively lowered* acceleration capability.

We found that, in fact, the reaction time and the update time have a similar dynamical effect since both introduce instabilities *via* the local short-wavelength mechanism, while the velocity adaptation time triggers instabilities *via* collective long-wavelength instabilities. Consequently, it is correct to interpret the update time of iterated maps (such as the Gipps model [26] or the Newell model [88]) as a measure for the reaction time, although, obviously, iterated maps are qualitatively different from delay-differential equations. Remarkably, the numerical update time is dynamically equivalent to about *half* the reaction time. Consequently, a reaction time T' has a stronger destabilizing effect than an update

[11] Moreover, human drivers also adapt their driving style to the traffic situation on a *longer time scale* such that the actual driving style depends on the traffic conditions during the last few minutes ('frustration effect') [122, 126].

[12] Note that even a fourth time scale, namely the 'safety time gap' between two vehicles, is connected with but different from the reaction time. We emphasize that, in general, the 'desired' time gap T of the IDM is not equivalent to any of the three other times T', Δt or τ_v. While the safety time gap T is a characteristic parameter of the driving style, the reaction time T' is essentially a *physiological parameter* and, consequently, at most weakly correlated with T. The time gap T has, however, a strong influence on the stability of traffic flow since it determines the upper limit for the cumulative time delays of the control path from the acceleration to the desired distance.

time interval of the same numerical value.

5 The Lane-Changing Model MOBIL

So far, we have successfully applied single-lane car-following models to describe traffic dynamics. Particularly, collective phenomena such as traffic instabilities and the spatiotemporal dynamics of congested traffic can be well understood within the scope of single-lane traffic models. There are, however, situations where lane changes play an essential role such as modeling on-ramp and off-ramp bottlenecks. Moreover, real traffic consists of different types of vehicles, e.g., cars and trucks. For obvious reasons, such heterogeneous traffic streams can only be described realistically within a multi-lane modeling framework, allowing faster vehicles to improve their driving conditions by passing slower vehicles. Consequently, lane-changing models are an important component of any microscopic multi-lane traffic simulation software (cf. the following Chap. 6).

This chapter is structured as follows: Sec. 5.1 will provide an introduction and motivation of the presented modeling approach. In Sec. 5.2, the lane-changing model MOBIL will be formulated both for symmetric ('US') and asymmetric ('European') passing rules. In Sec. 5.3, the MOBIL rules will be applied to multi-lane traffic simulations with open boundary conditions in combination with the Intelligent Driver Model (Chap. 2) as underlying longitudinal car-following model. Finally, we will conclude with a discussion of the proposed model and a generalization of the MOBIL concept to other decision processes occuring in traffic simulations, e.g., when approaching traffic lights and yielding right of way (Sec. 5.4).

5.1 Introduction to the Modeling Approach

Recently, freeway lane-changing has received increased attention [68, 43, 16, 132, 9, 86]. Since lane-changing maneuvers often act as initial perturbations, it is crucial to understand their impact on the capacity, stability and breakdown of traffic flows. Particularly near bottleneck sections such as on-ramps and off-ramps, lane changing is often a significant ingredient to trigger a traffic breakdown (provided that the traffic volume is high). Additionally, the drivers' lane-changing behavior has direct influence on traffic safety.

Despite its great significance, lane-changing has by far not been studied as extensively as the longitudinal acceleration and deceleration behavior. One reason for this is the scarcity of reliable data [44, 7], because neither cross-sectional data from detectors nor

floating car data are sufficient to empirically determine typical lane-changing properties such as the rate of lane changes or the gaps and velocities of the cars affected by a lane change. Therefore, only a few empirical studies about lane-changing rates as a function of traffic flow or density are available [110, 141]. Recent progress in video tracking methods, however, allows for a collection of high-quality trajectory data from aerial observations [49, 155]. These 2D data will become more and more available in the future and will allow for a more profound understanding of the microscopic lane-changing processes.

The modeling of lane changes is typically considered as a multi-step process: On a *strategic* level, the driver knows about his or her route in a network which influences the lane choice, e.g., with regard to lane blockages, on-ramps, off-ramps or other mandatory merges [115]. In the *tactical* stage, an intended lane change is prepared and initiated by advance accelerations or decelerations of the driver and possibly by coordination of drivers on the target lane [43]. In the *operational* stage, the driver determines whether an immediate lane change would be both safe and desired [27]. This choice has been often described by gap-acceptance models, in which drivers compare the available gaps to the smallest acceptable gap, the critical gap. In general, critical gaps depend on the speed of the subject vehicle, on the relative speed with respect to those of the lead and the lag vehicles in the adjacent lane and on the type of lane change [116]. Most lane-changing models in the literature classify lane changes as either mandatory or discretionary [27, 139, 1, 116, 31, 109]. While mandatory changes are performed for strategic reasons, the driver's motivation for discretionary lane changes is a perceived improvement of the driving conditions in the target lane compared to the respective current situation.

This thesis chapter presents a lane-changing model for microscopic car-following models which only deals with the *operational* decision process. When considering a lane change, we assume that a driver makes a trade-off between the expected own advantage and the disadvantage imposed on other drivers. In particular, the model takes the follower in the target lane into account. For a driver considering a lane change, the *subjective utility* of a change increases with the gap to the new leader on the target lane. However, if the velocity of this potential leader is lower, it may be favorable to stay in the present lane in spite of the smaller gap. A criterion for the utility including *both* situations is the difference of the expected *accelerations* (or *decelerations*) after and before the lane change. In this work, we therefore propose to use as utility function this acceleration difference, evaluated with an underlying microscopic longitudinal traffic model. Our approach assumes that the higher the acceleration on a given lane, the nearer it is to the 'ideal' acceleration on an empty road and the more attractive it is to the driver. Therefore, the basic idea of the proposed lane-changing model is to formulate the anticipated advantages and disadvantages of a prospective lane change in terms of single-lane accelerations.

Compared to explicit gap-based lane-changing models, the formulation in terms of accel-

erations of a longitudinal model has several advantages:

- The assessment of the traffic situation is transferred to the acceleration function of the car-following model which allows for a compact and widely applicable model formulation with a small number of additional parameters. In contrast to the classical gap-acceptance approach, critical gaps are not explicitly taken into account.
- It is ensured that both longitudinal and lane-changing models are consistent with each other. For example, if the longitudinal model is collision-free, the combined models will be accident-free as well.
- Any features of the longitudinal model such as anticipation is automatically transferred to the lane-changing model.

Apart from using accelerations as utility functions, the main novel feature of the proposed lane-changing model consists in taking into account the (dis-)advantage of the followers via a *politeness parameter*. By adjusting this parameter, the motivations for lane-changing can be varied from purely egoistic to a more altruistic behavior. Particularly, there exists a value where lane changes are carried out only if this increases the weighted accelerations of the lane-changing driver and *all* affected neighbors. This strategy can be paraphrased by the acronym *'Minimizing Overall Braking Induced by Lane Changes'* (MOBIL). In the following, we will refer to our concept by this acronym, regardless of the value of the politeness parameter.

Note that all lane-changing models cited before assume egoistic behavior. With the politeness factor one can model two common lane-changing behavior. First, even if both the safety criterion and the 'egoistic' incentive criterion are satisfied, most drivers will not change lanes for a marginal advantage if this obstructs other drivers. Secondly, in countries with asymmetric lane-changing rules, 'pushy' drivers on a 'fast lane' may induce a slower driver in front to change to a slower lane in order to be no longer obstructed (typically, passing on the 'slow' lane is forbidden in these countries).

5.2 Model Formulation

As introduced in Sec. 1.2, the acceleration of car-following models is of the general form

$$a_\alpha := \frac{\mathrm{d}v_\alpha}{\mathrm{d}t} = a(s_\alpha,\, v_\alpha,\, \Delta v_\alpha). \tag{5.1}$$

That is, the motion of a single driver-vehicle unit α depends on its velocity v_α, the gap s_α to the front vehicle $(\alpha - 1)$ and the relative velocity $\Delta v_\alpha = v_\alpha - v_{\alpha-1}$. Some examples are Optimal Velocity Model [3], the IDM (see Chap. 2) or the Velocity Difference Model [41,

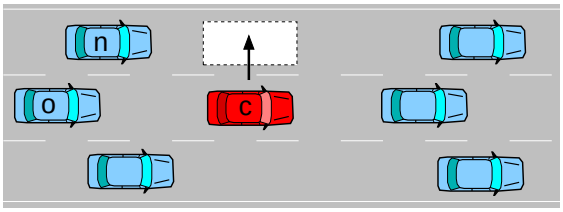

Figure 5.1: Sketch of the nearest neighbors of a central vehicle c considering a lane change to the left. The new and old successors are denoted by n and o, respectively. Accelerations after a possible change are denoted with a tilde.

51]. In the following, we will formulate MOBIL for this class of models. Generalizations to models taking into account more than one predecessor or an explicit reaction time as the HDM (cf. Chap. 4) are straightforward.[1]

A specific lane change, e.g., from the center lane to the outer (passing) lane as shown in Fig. 5.1, generally depends on the leader and the follower on the present and the target lane, respectively. In order to formulate the lane-changing criteria, we use the following notation: For a vehicle c considering a lane change, the followers on the target and present lane are represented by n and o, respectively. The acceleration a_c denotes the acceleration of vehicle c on the actual lane, while $\tilde{a}_c$ refers to the situation on the target lane, i.e., to the expected acceleration of vehicle c on the target lane for the same position and velocity. Likewise, $\tilde{a}_o$ and $\tilde{a}_n$ denote the acceleration of the old and new followers after the lane change of vehicle c. Notice that the leader on the target lane is the nearest vehicle on this lane for which the position is $x > x_c$. Likewise for the followers for which $x < x_c$. This also applies for the case where the vehicles on neighboring lanes are nearly side by side and a possible change would lead to negative gaps. In this case, the longitudinal model must return a very high braking deceleration such that such lane changes are excluded by the criteria to be discussed below.

5.2.1 Safety Criterion

Like other lane-changing models [27], we consider an *incentive* to change lanes and additional *safety constraints*. Our safety criterion checks the possibility of executing a lane change by considering the effect on the follower n in the target lane as depicted in Fig. 5.2.[2] Formulated in terms of longitudinal accelerations, the safety criterion guarantees that, after the lane change, the deceleration $\tilde{a}_n$ of this vehicle does not exceed a given safe value

[1] The question about the role of reaction times is of minor importance for lane-changing decision. In a good approximation, one can even neglect the delay for a lane-changing decision because the driver's anticipation will compensate for the reaction time.

[2] The 'critical gap' to the new leader for the subject vehicle c is evaluated by the MOBIL incentive criterion, see below.

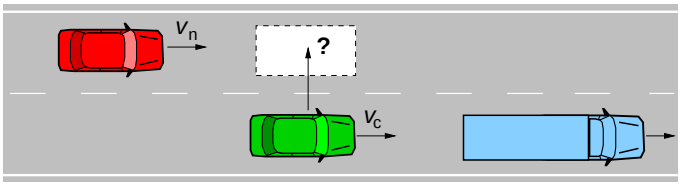

Figure 5.2: Illustration of the safety criterion (5.2) when considering a lane change: The acceleration of the follower n in the new (left) lane has to be larger than the threshold $-b_{\text{safe}}$. Therefore, the parameter b_{safe} sets a lower bound to the perturbation strength due to lane changes.

b_{safe}, i.e.,

$$\tilde{a}_n \geq -b_{\text{safe}}. \tag{5.2}$$

Although formulated as a simple inequality, this condition implicitly contains all the dependencies reflected by the longitudinal car-following model, as the acceleration $\tilde{a}_n(t)$ typically depends on the gap, the velocity and the approaching rate, cf. Eq. (5.1). That is, if the longitudinal model has a built-in sensitivity with respect to *velocity differences*, this dependency is inherited to lane-changing decisions. In this way, larger gaps between the following vehicle in the target lane and the own position are required to satisfy the safety constraint if the following vehicle is faster than the changing vehicle. In contrast, smaller gaps are acceptable if the following vehicle is slower. Compared to conventional gap-acceptance models, this approach depends on gaps only indirectly, via the dependence on the longitudinal acceleration.

By formulating the criterion in terms of safe braking decelerations of the longitudinal model, collisions due to lane changes are *automatically* excluded. For realistic longitudinal models, b_{safe} should be well below the maximum possible deceleration $b_{\max}$ which is about $9\,\text{m/s}^2$ on dry road surfaces.[3] Increasing the value for b_{safe} generally leads to stronger perturbations due to individual lane changes, but the braking reaction of the follower on the target lane is always limited by the value of b_{safe}. This is relevant in traffic simulations due to the fact that performing a lane change implies a discontinuous change in the input parameters in the acceleration function of the new follower.

5.2.2 Incentive Criterion for Symmetric Lane-Changing Rules

An actual lane change is only executed if, besides the safety criterion, the incentive criterion is simultaneously fulfilled. The *incentive criterion* typically determines whether a lane change improves the individual local traffic situation of a driver. In the presented model, we propose an incentive criterion that includes a consideration of the immediately affected

[3] Note that the maximum safe deceleration b_{safe} prevents accidents even in the case of totally selfish drivers as long as its value is not greater than the maximum possible deceleration $b_{\max}$ of the underlying longitudinal model.

neighbors as well (see Fig. 5.3). A *politeness factor* p determines to which degree these vehicles influence the lane-changing decision of a driver. For symmetric overtaking rules, we neglect differences between the lanes and propose the following incentive criterion for a lane-changing decision of the driver of vehicle c:

$$\underbrace{\tilde{a}_c - a_c}_{\text{driver}} + p\left(\underbrace{\tilde{a}_n - a_n}_{\text{new follower}} + \underbrace{\tilde{a}_o - a_o}_{\text{old follower}}\right) > \Delta a_{\text{th}}. \tag{5.3}$$

The first two terms denote the advantage (utility) of a possible lane change for the driver him- or herself, where $\tilde{a}_c$ refers to the new acceleration for vehicle c after a prospective lane change. The considered lane change is attractive if the driver can accelerate more, i.e., go faster in the new lane. The third term with the prefactor p is an innovation of the presented model. It denotes the total advantage (acceleration gain – or loss, if negative) of the two immediately affected neighbors, weighted with the politeness factor p (see Fig. 5.3). It can of course be argued to take into account only the new follower, at least to give him more weight than to the old follower, who will anyway find him- or herself in an advantageous situation after the lane change of the leading vehicle. However, it is straightforward to adapt Eq. (5.3) accordingly. Finally, the switching threshold Δa_{th} on the right-hand side of Eq. (5.3) models a certain inertia and prevents lane changes if the overall advantage is only marginal compared to a 'keep lane' directive.

In summary, the incentive criterion is fulfilled if the own advantage (acceleration gain) is greater than the weighted sum of the disadvantages (acceleration losses) of the new and old successors and the threshold Δa_{th}.[4] Note that the threshold Δa_{th} influences the lane-changing behavior *globally*, while the politeness parameter affects the lane-changing behavior locally, i.e., with respect to the involved neighbors. As for the safety constraint (5.2), our incentive criterion is more general than a simple gap-based rule. If the longitudinal model is sensitive to velocity differences, there may be an incentive for a lane change even if the gap on the new lane is smaller – provided that the leader on the new lane is faster.

The generalization to traffic on more than two lanes per direction is straightforward. If, for a vehicle on a center lane, the incentive criterion is satisfied for both neighboring lanes, the change is performed to the lane where the incentive is larger.

Since the disadvantages of other drivers and the own advantage are balanced via the politeness factor p, the lane-changing model contains typical strategic features of classical game theory. The value of p can be interpreted as the degree of altruism. It can vary

[4] In fact, the incentive criterion (5.3) automatically includes a 'safety component' for the lane-changing vehicle. Even for the most aggressive parameter settings ($p = 0$ and $\Delta a_{\text{th}} = 0$), lanes are only changed if, on the new lane, the acceleration is higher or, equivalently, the necessary braking deceleration is lower than on the present lane (it may, nevertheless, be greater than $b_{\max}$). Consequently, criterion (5.3) can only be true if the new lane is 'safer' than the old lane. The only requirement for the acceleration model is that, in dangerous situations, it should return a braking deceleration that increases when the situation becomes more critical – a condition that any reasonable longitudinal model should fulfill.

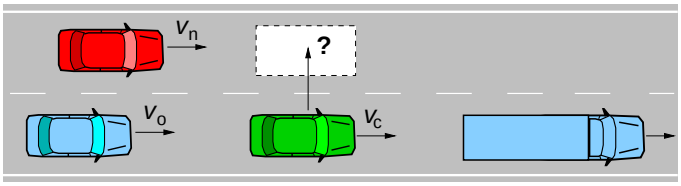

Figure 5.3: Illustration of the decision process for a lane change to the left lane with symmetric MOBIL rules. The incentive criterion (5.3) compares the acceleration of the considered vehicle c in the actual and, virtually, in the left lane. The proposed model also takes into account the following driver-vehicle units by weighting their old and new accelerations with the politeness parameter p.

from $p = 0$ (for selfish lane-hoppers) to $p > 1$ for altruistic drivers, who do not change if that would deteriorate the traffic situation of the followers. They would even perform disadvantageous lane changes if this would improve the situation of the followers sufficiently. In the special case $p = 1$ and $\Delta a_{\text{th}} = 0$, the incentive criterion simplifies to

$$\tilde{a}_c + \tilde{a}_n + \tilde{a}_o > a_c + a_n + a_o. \tag{5.4}$$

Thus, lane changes are only performed, when they increase the sum of accelerations of all involved vehicles which corresponds to the concept of *'Minimizing Overall Braking Induced by Lane Changes'* (MOBIL) in the strict sense. When setting the safe braking threshold to the desired braking deceleration, i.e., $b_{\text{safe}} = b$, the strict MOBIL strategy corresponding to $p = 1$ has no free parameters and might therefore be considered as a 'minimal model' for lane-changing decisions.

5.2.3 Incentive Criterion for Asymmetric Passing Rules

In most European countries, the driving rules for lane usage are restricted by legislation. We now formulate an asymmetric lane-changing criterion for two-lane freeways and assume, without loss of generality, that the right lane is the default lane, i.e., we implement a 'keep-right' directive.[5] Specifically, we presuppose the following 'European' traffic rules:

(i) *Passing rule*: Passing on the right-hand lane is forbidden, unless traffic flow is bound or congested, in which case the symmetric rule (5.3) applies. We treat any vehicle driving at a velocity below some suitably specified velocity v_{crit}, e.g., $v_{\text{crit}} = 60\,\text{km/h}$, as driving in bound or congested traffic.

(ii) *Lane usage rule*: The right lane is the default lane. The left lane should only be used for the purpose of overtaking.

[5] The reformulation for left-oriented traffic describing, e.g., traffic rules in the UK as well as the generalization to more than two lanes are straightforward.

The passing rule is implemented by replacing the longitudinal dynamics on the right-hand lane by the condition

$$a_c^{\mathrm{Eur}} = \begin{cases} \min(a_c, \tilde{a}_c) & \text{if } v_c > \tilde{v}_{\mathrm{lead}} > v_{\mathrm{crit}}, \\ a_{\mathrm{c}} & \text{otherwise,} \end{cases} \tag{5.5}$$

where $\tilde{a}_c$ corresponds to the acceleration on the left lane and $\tilde{v}_{\mathrm{lead}}$ denotes the velocity of the front vehicle on the left-hand lane. The passing rule influences the acceleration on the right-hand lane only (i) if there is no congested traffic ($\tilde{v}_{\mathrm{lead}} > v_{\mathrm{crit}}$), (ii) if the front vehicle on the left-hand lane is slower ($v_c > \tilde{v}_{\mathrm{lead}}$) and (iii) if the acceleration $\tilde{a}_c$ for following this vehicle would be lower than the single-lane acceleration a_c in the actual situation. Notice that the condition $v_c > \tilde{v}_{\mathrm{lead}}$ prevents that vehicles on the right-hand lane brake whenever they are passed.

The 'keep-right' directive of the lane-usage rule is implemented by a constant bias Δa_{bias} in addition to the threshold Δa_{th}. Furthermore, we neglect the disadvantage (or advantage) of the successor in the right lane in Eq. (5.3) because the left lane has priority[6], see Fig. 5.4. Explicitly speaking, the resulting asymmetric incentive criterion for lane changes from left to right reads

$$\tilde{a}_c^{\mathrm{Eur}} - a_c + p\,(\tilde{a}_o - a_o) > \Delta a_{\mathrm{th}} - \Delta a_{\mathrm{bias}}, \tag{5.6}$$

while the incentive criterion for a lane change from right to left is given by

$$\tilde{a}_c - a_c^{\mathrm{Eur}} + p\,(\tilde{a}_n - a_n) > \Delta a_{\mathrm{th}} + \Delta a_{\mathrm{bias}}. \tag{5.7}$$

Again, the quantities with a tilde refer to the new situation after a prospective lane change. While the parameter Δa_{bias} is small, it clearly has to be larger than the threshold Δa_{th}. Otherwise, the switching threshold would prevent changes to the right-hand lane even on an empty road.

Neglecting the follower on the right-hand lane allows to model the following situation: Via the politeness factor p, a driver on the right lane considering a lane change to the left takes into account the *disadvantage* of the approaching vehicle in the target lane. This can prevent the considered lane change, even if the lane change is not critical which is assured by the safety criterion (5.2). This feature of the MOBIL lane-changing model realistically reflects a perceptive and anticipative driving behavior, as commonly observed for asymmetric passing rules. Furthermore, by taking into account only the follower on the faster (left) lane via the politeness factor p, one models a selective *dynamic pressure* to change lanes that faster (possibly tailgating) drivers on the fast (left) lane exert on their slower predecessors, see Fig. 5.4. This is a frequently observed behavior on European freeways, particularly on Germany freeways with their wide distribution of desired velocities. Notice

[6]This does not mean that this vehicle will be ignored, because the safety criterion is applied in any case.

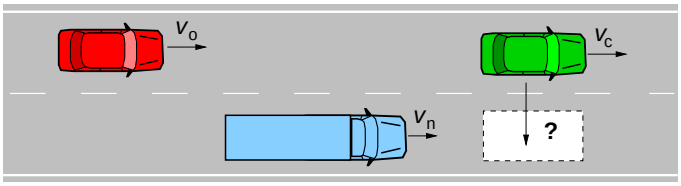

Figure 5.4: The asymmetric incentive criterion additionally includes only the following driver-vehicle unit in the (left) passing lane. The sketch illustrates the 'dynamic pressure' which is imposed by a fast follower o to the vehicle c. The succeeding driver may induce a lane change of vehicle c to the right lane if the disadvantage (of being hindered) exceeds the own disadvantage in the right lane. This 'passive cooperation' of the subject c is frequently observed in countries with asymmetric lane-changing rules, e.g., after having passed a slow truck. Notice that the decision process for a lane change to the left is similar to the situation depicted in Fig. 5.3.

that, in any case, the safety criterion (5.2) prevents a critical lane change to the slower lane.

5.3 Multi-Lane Traffic Simulations

We will now apply the MOBIL concept to computer simulations of a two-lane freeway. As underlying acceleration model, we will use the Intelligent Driver Model (IDM) as described in Chap. 2. The sensitivity of the IDM to velocity differences automatically results in lane-changing rules that depend on velocity differences as well. Particularly, a lane change may be favorable even if the gap on the target lane is smaller, provided that the velocity of the leading vehicle on that lane is higher.

The lane-changing behavior does not only depend on the lane-changing and the car-following model, but also on the heterogeneity of the driver-vehicle units and on the infrastructure. Particularly, for identical driver-vehicle units on a homogeneous ring road, a stationary state would be reached soon. To avoid this artifact, we have introduced heterogeneity by implementing two types of vehicles. The slower 'trucks' differ in their reduced desired velocity $v_0 = 80\,\mathrm{km/h}$ compared to the faster 'cars' ($v_0 = 120\,\mathrm{km/h}$). We have assumed uniformly distributed velocities *within* each class as well. More specifically, we assumed velocities between 64 km/h and 96 km/h for trucks, and between 96 km/h and 144 km/h for cars. We assumed a truck fraction of 20% and the vehicle length was assumed to be 4 m for cars and 12 m for trucks. Moreover, we have used the following further IDM parameters: The safety time gap was set to $T = 1.2\,\mathrm{s}$, the maximum acceleration to $a = 1.5\,\mathrm{m/s^2}$, the desired deceleration to $b = 2\,\mathrm{m/s^2}$ and the minimum distance to $s_0 = 2\,\mathrm{m}$. The values of the MOBIL parameters used in the simulations are listed in Table 5.1.

The incentive criterion is evaluated in each numerical update step in the simulation, i.e.,

MOBIL Parameter	Value
Politeness factor p	$0 \ldots 1$
Changing threshold Δa_{th}	$0.1\,\text{m/s}^2$
Maximum safe deceleration b_{safe}	$4.0\,\text{m/s}^2$
Bias for right lane Δa_{bias}	$0.3\,\text{m/s}^2$

Table 5.1: Parameters of the MOBIL lane-changing model. The politeness parameter p of the incentive criterion mainly determines the lane-changing rate. The changing threshold Δa_{th} prevents lane changes of marginal advantage. The maximum safe deceleration b_{safe} serves as additional safety criterion. The value of b_{safe} is chosen considerably below the physically possible maximum deceleration of about $9\,\text{m/s}^2$ on dry roads. In the case of asymmetric ('European') lane-changing rules, the additional bias Δa_{bias} models a preferred lane-usage of the default lane. The values are used in the simulations in combination with the Intelligent Driver Model (IDM).

the drivers continuously check their incentives. If a lane change is favorable *and* safe, the lane change is performed immediately, i.e., the transition time from the present lane to the target lane is neglected. Notice that this implies a discontinuous acceleration for the considered vehicle and also for the old and new successors. However, as the velocity is given by integrating up the acceleration, the velocities of all vehicles (and the accelerations of all other vehicles not directly involved in the lane change) remain continuous in time.[7] We have checked the simulation results for different numerical update steps ($\Delta t = 0.25$, 0.1 and 0.01 s). However, we found only a negligible quantitative difference of the lane-changing rates, regardless of the density and the value of p (see Fig. 5.5).

Notice that the discrete nature of the lane-changes could potentially lead to situations where slight differences in the input quantities lead to huge effects, i.e., lane changes or not at a given time t. By simulations, however, we verified that the frequency of such events is of the order of the update time step. That is, the multi-lane model based on the IDM and MOBIL is mathematically consistent in the sense that the numerical results for a limited simulation period converge in the limit $\Delta t \to 0\,\text{s}$.[8] This is remarkable since, to our knowledge, there is no published lane-changing model that does not explicitly depend on the numerical update step. For the following simulations, we have applied the 'modified Euler' integration scheme with an update interval Δt of 0.25 s for updating the longitudinal dynamics (see Chap. 6).

When evaluating the MOBIL accelerations of the old and new followers, one has, in prin-

[7] Of course, it is possible to enforce continuous acceleration changes as well, but this is not important here.

[8] Therefore, the local consistency order 1 remains valid with respect to a suitable norm such as $||x||_p = \int_{t_0}^{t_1} dt|x|^p$ where $p > 0$ and $x(t)$ is, e.g., the deviation between $s(t)$ for finite Δt and the exact solution.

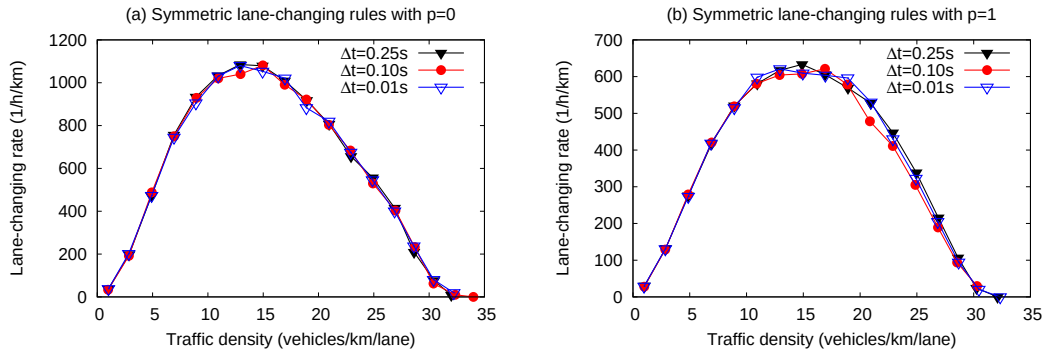

Figure 5.5: Lane-changing rate for various numerical update steps $\Delta t = 0.01,\ 0.1,$ and $0.25\,\mathrm{s}$ in an open system. The diagrams show that the frequency of (discretionary) lane changes is independent from Δt regardless of the traffic density and the setting of the politeness parameter p (see the main text). For the simulation scenario and the measurement of the lane-changing rate (here for a road segment of 1 km located around $x = 5.5\,\mathrm{km}$), we refer to Sec. 5.3.2 on page 92.

ciple, the freedom to evaluate the accelerations, using the own model parameter set or that of the respective successors. Clearly, using the driving parameters of the followers is in line with the reasoning behind MOBIL, although they are not directly observable by the driver planning a lane change. However, strong cues are given to the driver both by the vehicle type (truck, family car, sports car) and by the past driving style. Therefore, we evaluate all MOBIL accelerations with the model parameters of the driver-vehicle unit, for which the respective acceleration is relevant.

5.3.1 Spatial Distribution of the Lane-Changing Rate

In this section, we apply the proposed lane-changing model in simulations of discretionary and mandatory lane changes. We have simulated a two-lane road section of 10 km length with open boundary conditions. For an open system, the inflow at the upstream boundary is the natural control parameter. The inflow at the upstream boundary has been kept constant at 1000 vehicles/h/lane. Furthermore, we have assumed an on-ramp (of merging length 300 m) centered at the location $x = 7.5$ km with a constant inflow of 500 vehicles/h.

The *mandatory merge* from the on-ramp to the right lane of the freeway is modeled by a 'virtual vehicle' standing at the end of the merging lane which is otherwise treated as a third, i.e., additional lane. Due to the imposed deceleration in order to avoid a collision in case the merging cannot be performed in time, the attractiveness of the merging lane automatically decreases. Consequently, the incentive to merge to the freeway increases, when approaching the standing vehicle. To support lane-changing in this situation, we assume an egoistic behavior of merging vehicles by temporarily setting $p = 0$.

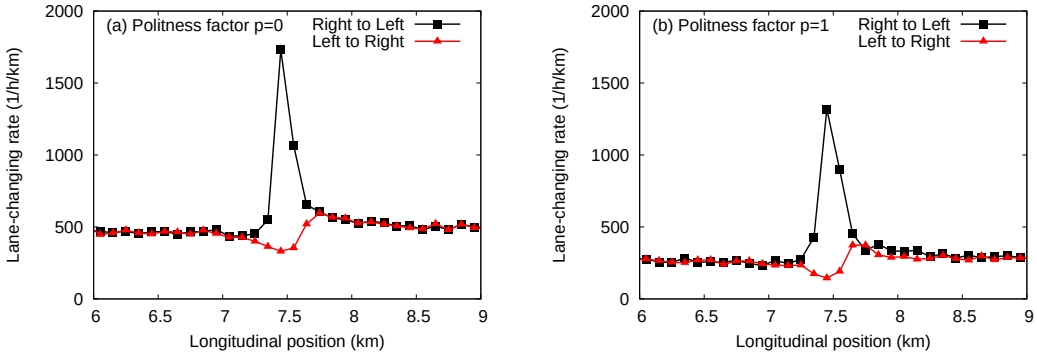

Figure 5.6: Distributions of the lane-changing rate as a function of the longitudinal spatial coordinate for $p = 0$ (left) and $p = 1$ (right).

The simulation results are evaluated in Fig. 5.6 which shows the distribution of lane-changing events as a function of the longitudinal coordinate. The lane-changing rate measures the performed lane changes per kilometer and hour. The setting of p only determines the absolute number of lane changes, but does not change the qualitative behavior. For any value of p, the lane-changing rate is nearly homogeneously distributed sufficiently far up- and downstream of the on-ramp. In a range of about 500 m around the center of the on-ramp located at $x = 7.5$ km, the number of lane changes to the left lane is increased by approximately a factor of 4, while the changes to the right lane are slightly reduced. Thus, the on-ramp locally induces a strongly increased activity of *discretionary lane changes* from the right to the left lane, while the number of lane changes from the left to the right is reduced. Since vehicles merge from the on-ramp to the right lane of the freeway, the right lane becomes less attractive for vehicles on the freeway upstream of the merging zone. This demonstrates the strong dependence of lane-changing behavior on spatial inhomogeneities of the road. The *relative* increase is even higher for 'polite' drivers ($p = 1$) compared to 'egoistic' ones (i.e., for $p = 0$). This is plausible because, due to the conservation of the vehicle number and the symmetry between the lanes, the area between the upper and lower curves of Fig. 5.6(a) and (b) must be equal to the on-ramp flow. Note that the lane-changing rate is slightly increased downstream of the on-ramp because of the increased traffic density (see the lane-changing rate as a function of traffic density in the following Sec. 5.3.2).

5.3.2 Lane-Changing Rate as Function of the Traffic Density

Let us now investigate the lane-changing rate as a function of the traffic density for open road systems. A method to locally measure the lane-changing rate and the traffic density in a microscopic simulation is as follows: The road is divided into subsections, e.g., of

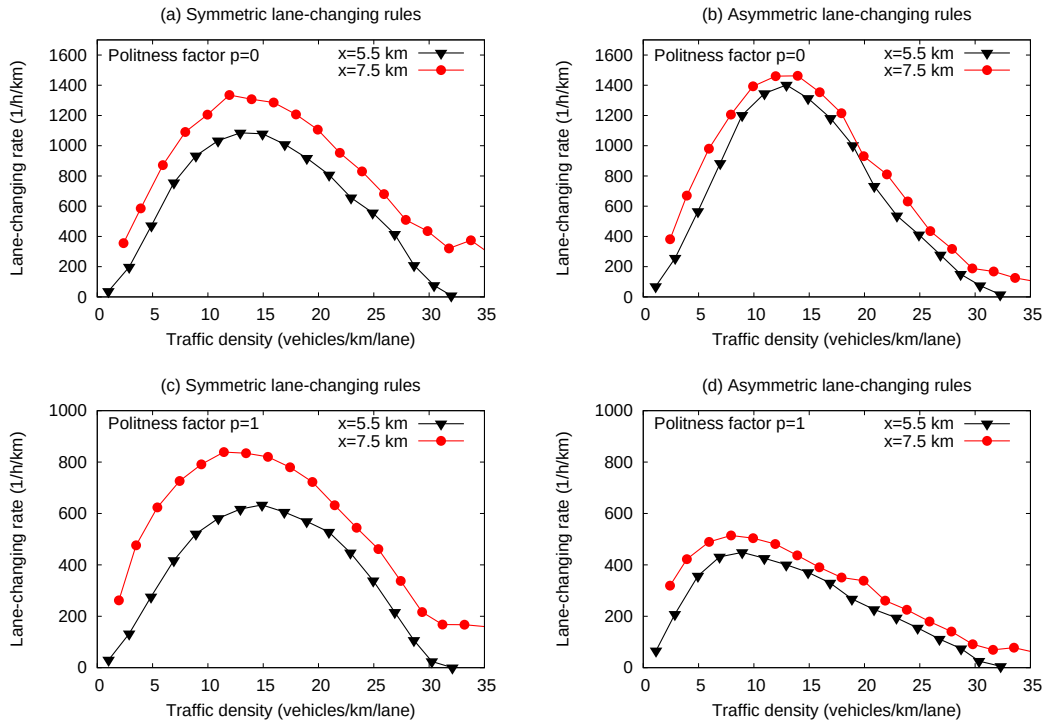

Figure 5.7: Lane-changing rates for symmetric lane-changing rules (left) and asymmetric ones (right) as a function of traffic density. In the simulations, the politeness parameter has been either set to $p = 0$ (top) or $p = 1$ (bottom). Furthermore, the diagrams show the lane-changing rates measured in two 1 km long road sections of the 10 km long road section. As shown in the diagrams, the maximum lane-changing rate is mainly determined by the politeness factor. Furthermore, an on-ramp at location $x = 7.5\,\text{km}$ with a merging zone of 300 m increases the lane-changes locally.

length $\Delta x = 1\,\text{km}$ and time is divided into time intervals of duration $\Delta t = 1\,\text{min}$. For each spatiotemporal element $[\Delta x \Delta t]$ obtained in this way, the number n of lane changes and the average density ρ is determined. The lane-changing rate is then given by

$$r(\rho) = \frac{n}{\Delta x \Delta t}. \tag{5.8}$$

Finally, we average over all lane-changing rates belonging to the same density interval $[\rho, \rho + \Delta\rho]$. Taking different values of Δx, Δt or $\Delta\rho$ did not changed the results qualitatively.

We have run multiple simulations with inflows varying from 100 vehicles/h/lane up to 1800 vehicles/h/lane and a constant ramp flow of $Q_{\text{rmp}} = 500$ vehicles/h (for the simulation setup, see Sec. 5.3.1). The lane-changing rates on two road sections for politeness factors of $p = 0$ and $p = 1$ and for symmetric and asymmetric lane-changing rules are shown in Fig. 5.7. Our results are as follows:

- The lane-changing rates increase for traffic densities $1\,\text{km/lane} < \rho < 10/\text{km/lane}$. A more detailed analysis reveals a quadratic dependency for sufficiently small densities (see Sec. 5.3.3 below).
- The maximum lane-changing rates are obtained for intermediate densities. The maximum is located between 10/km/lane (for $p = 1$ and asymmetric rules) and 15/km/lane (in the other cases).
- The peak value strongly depends on the value of the politeness parameter. For $p = 0$, the maximum lane-changing rate is about 1100 vehicles/h/km for symmetric rules and 1400/h/km for asymmetric ones. For $p = 1$, the maximum lane-changing rate is only about 600 vehicles/h/km for symmetric rules and 450/h/km for asymmetric ones. Further simulations show that already a small positive value $p > 0$ reduces the maximum rate of lane changes significantly.
- For a further increase of the traffic density, the lane-changing rates decrease, because velocity differences between neighboring lanes are reduced ('synchronized traffic', see below). For density values around 30 vehicles/km/lane, the lane-changing rates on the homogeneous road section around $x = 5.5\,\text{km}$ are negligible, because changing lanes is not profitable or possible anymore due to a lack of suitable gaps. This observation could be attributed to the 'moving like a solid block' effect proposed in Ref. [36].
- The curves of the lane-changing rates measured at the homogeneous road section around $x = 5.5\,\text{km}$ and the section at $x = 7.5\,\text{km}$ (which includes the merging area) show similar shapes. However, due to the vehicles that merge from the on-ramp to the freeway, the lane-changing rate is systematically shifted to higher values (cf. Sec. 5.3.1).
- Even at high traffic densities, the lane-changing rate does not drop to zero. There are still about 100–200 lane changes per hour and kilometer.

The politeness parameter p is the most important parameter determining the lane-changing rate. Let us, nevertheless, discuss the influence of the other MOBIL parameters as well. The lane-changing threshold Δa_{th} influences the peak of the curve weakly, but it does not change $r(\rho)$ qualitatively. For example, increasing Δa_{th} from 0.1 to $0.3\,\text{m/s}^2$ reduces the maximum number of lane changes by approximately 100/h/km. Moreover, the influence of the maximum safe deceleration b_{safe} is negligible within a reasonable range of braking accelerations from $-9\,\text{m/s}^2$ to $-b$, as the IDM braking strategy limits braking decelerations to the 'comfortable deceleration' b in nearly all situations (cf. Sec. 2.2).

Let us finally discuss the mean velocities as a function of the traffic density for the lane-changing rates shown in Fig. 5.7. We have implemented 'virtual' cross sections in order

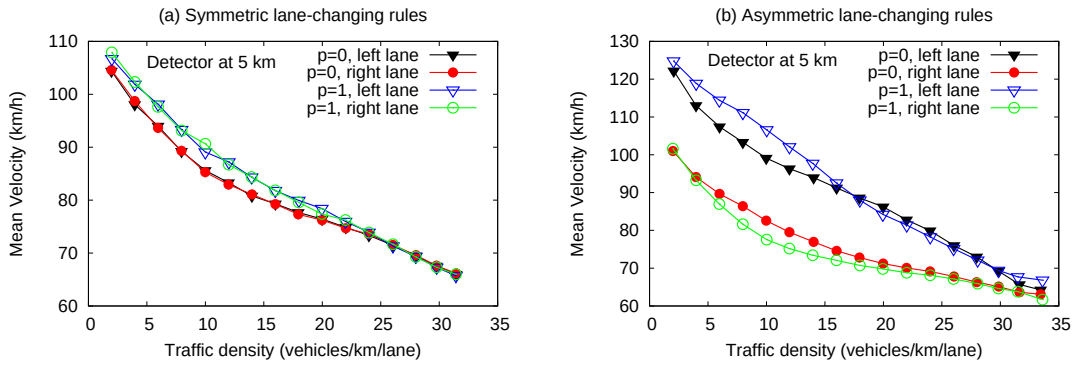

Figure 5.8: Lane-resolved 1-minute velocity averages of simulated detector data at the cross section $x = 5\,\mathrm{km}$ for (a) symmetric and (b) asymmetric MOBIL rules. The simulation results correspond to the lane-changing rates shown in Fig. 5.7 for politeness parameters of $p = 0$ and $p = 1$.

to aggregate the data over 1-minute intervals in order to mimic real-world double-loop detector measurements. For each sample interval, we have recorded the lane-resolved traffic flow Q_i and determined the arithmetic velocity averages V_i. The density ρ was calculated via the hydrodynamic relation $Q = \rho V$ from the lane-averaged quantities $Q = \sum_{i=1}^{L} Q_i$ and $V = \sum_{i=1}^{L} (Q_i V_i)/Q$ for the simulated road consisting of $L = 2$ lanes. Finally, we have averaged over all data belonging to the same density class (of class width $\Delta\rho = 2\,/\mathrm{km/lane}$).

Figure 5.8 shows the velocities of the left and the right lane measured with a detector located at $x = 5\,\mathrm{km}$ for symmetric and asymmetric lane-changing rules and for politeness parameters of $p = 0$ and $p = 1$. In our simulations, traffic is always free with means speeds of about $V \geq 65\,\mathrm{km/h}$. For symmetric lane-changing rules, the velocity is primarily synchronized in all lanes for all densities due to the lack of any lane preference, see Fig. 5.8(a). In contrast, the difference in the average velocities in different lanes (see Fig. 5.8b) is a consequence of the asymmetric lane-changing rules, i.e., of the parameter Δa_{bias}. The initially equally distributed trucks are mostly found on the right-most lane. The separation results in a different velocity-density relation for the fast (left) lane and the slow (right) lane, as shown in Fig. 5.8(b). For both lane-changing scenarios, the velocity differences decrease with growing traffic density.

The influence of the politeness factor p is as follows:

- For symmetric lane-changing behavior, the 'altruistic' lane-changing behavior corresponding to $p = 1$ increases the mean speed in *both* lanes for traffic densities of about $\rho \leq 20\,/\mathrm{km/lane}$. Therefore, the suppression of disadvantageous lane changes for the neighbors [see Eq. (5.4)] improves the overall traffic performance. In contrast, an 'egoistic' lane-changing behavior ($p = 0$) results in higher average travel times.

- For asymmetric MOBIL rules, the lane-changing behavior corresponding to $p = 1$ leads to more pronounced velocity differences between the lanes. While the speed in the passing (left) lane is higher than in the case $p = 0$, the speed in the slow (right) lane is reduced. Notice that these variations only occur for intermediate traffic densities, i.e., when lane changes lead to interactions between vehicles in neighboring lanes. When a driver-vehicle unit considers to change to the fast lane, the disadvantage of the follower in the target lane is included (and weighted) by the politeness factor. An unselfish driver, therefore, stays in the slower lane to avoid the perturbation of the faster vehicles in the left lane.

- However, for symmetric *and* asymmetric MOBIL rules, the differences between the lane-changing behavior for different settings of the politeness parameter p disappear for densities $\rho > 20\,/\mathrm{km/lane}$. This result is consistent with the measured lane-changing rate shown in Fig. 5.7, as the number of lane changes decreases with growing density due to a lack of suitable gaps, independent of the politeness value.

5.3.3 Lane-Changing Rate for Small Traffic Densities

Let us study the lane-changing rate for sufficiently small densities in more detail. In light traffic, changing lanes in order to pass slower vehicles ahead is possible without delays in nearly all cases. Therefore, we are able to derive an analytical expression for the resulting lane-changing rate which also allows for a check of the software implementation. For this, we assume a homogeneous road section with n lanes. The overall density ρ is assumed to be symmetrically distributed among the lanes and the velocity distribution is described by the probability density $f(v)$. Let us consider vehicles driving at a constant speed v encountering slower vehicles driving at $v' < v$. The (differential) rate for encountering a vehicle within the velocity interval $[v', v' + dv']$ is given by the relative flow $dQ' = (v - v')\rho f(v')dv'$. On average, only the fraction $1/n$ of this differential flow belongs to vehicles on the same lane, thereby obstructing the vehicle driving at speed v and initiating a lane change of this vehicle. Integrating over all velocities $v' < v$ leads to the following average lane-changing frequency of cars driving at speed v:

$$w(v) = \frac{1}{n} \int_0^v dv' \, (v - v')\rho f(v'). \tag{5.9}$$

The mean lane-changing rate R of an ensemble of vehicles is, therefore, given by the expression

$$R = \rho \langle w \rangle = \frac{\rho^2}{n} \int_0^\infty dv \int_0^v dv' f(v) f(v') (v - v') \tag{5.10}$$

$$= \frac{\rho^2}{2n} \int_0^\infty dv \int_0^\infty dv' f(v) f(v') |v - v'| \tag{5.11}$$

$$= \frac{\rho^2}{2n} \langle |v - v'| \rangle, \tag{5.12}$$

where we have used the standard expression for the bivariate expectation value of independent stochastic variables in the last step. In case of just two vehicle types with occurrence frequencies p_1 and $p_2 = 1 - p_1$ driving at constant speeds v_1 and v_2, respectively, the expectation value can be estimated as $\langle |v - v'| \rangle = 2 p_1 p_2 |v_1 - v_2|$.

Let us now compare the theoretical lane-changing rate at a density $\rho' = \rho/n$ per lane,

$$R = n \rho'^2 \, p_1 p_2 \, |v_1 - v_2|, \tag{5.13}$$

to our simulations. The vehicles are initially distributed with regular distances and randomly chosen lanes on a $n = 2$ or 3 lane road with periodic boundary conditions. The changing threshold Δa_{th} is set to zero according to the simplifications made in the analytical calculations. In Fig. 5.9, the simulation results for the averages and variations are compared with the analytical curve from Eq. (5.13). For densities $\rho < 3$/km/lane, the analytical expression describes the simulated lane-changing rate very accurately. For $\rho > 3$/km/lane, the simulated lane-changing rate stays below the expected theoretical curve, because the free traffic assumption becomes invalid. Since the density is approximately homogeneous in space and time, these results are independent from the values $(\Delta x, \Delta t)$ used for the spatiotemporal measurement of the lane-changing rate.

5.4 Conclusions and Outlook

Lane-changing models are an important component of any microscopic traffic simulation software. Most of the published and implemented lane-changing models follow a rule-based approach with different gap-acceptance conditions and, consequently, different lane-changing behaviors in different situations. Due to the variety of possible driving conditions associated with discretionary and mandatory lane changes, this approach often tends to lead to complex models with many parameters.

In this chapter, we have presented the general concept MOBIL defining lane-changing

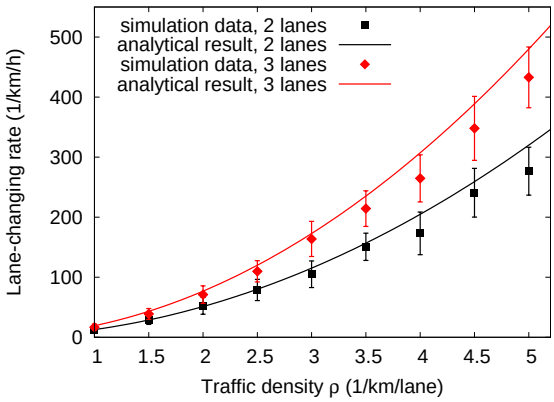

Figure 5.9: Lane-changing rates on a 2- or 3-lane freeway under free-flow conditions according to simulations (symbols) and analytical calculations (solid lines). Equation (5.13) reproduces the simulation data within the error bands for densities $\rho < 3$/km/lane, while the deviation from the free-traffic assumptions becomes significant for higher densities: The simulated lane-changing rate is lower than the analytic expression, because the assumption that an immediate lane change would always be possible breaks down.

models for a broad class of car-following models. The basic idea of MOBIL is to measure both the attractiveness of a given lane, i.e., its *utility* and the risk associated with lane changes in terms of accelerations. This means, both the incentive criterion and safety constraints can be expressed in terms of the acceleration function of the underlying car-following model. This allows for an efficient and compact formulation of the lane-changing model with a small number of additional parameters. As a consequence, the properties of the car-following model, e.g., any dependence on relative velocities or the exclusion of collisions are transferred to the lane-changing behavior. Moreover, the model is able to describe mandatory and discretionary lane changes as well as symmetric and asymmetric lane changes in a unified and consistent way. By virtue of the acceleration-based decisions, the lane changes are more anticipative than those of gap-based models. For example, if a leading vehicle on a possible target lane is faster than the own leader, MOBIL in combination with the IDM may suggest a lane change even if the lead gap on the target lane is smaller than that on the actual lane. In a way, MOBIL *anticipates* that the gap will be larger in the future.

As a novel feature, the proposed model takes into account other drivers via a *politeness factor* p. The politeness factor characterizes the degree of (passive) cooperativeness among drivers. That is, a driver takes a lane-changing decision by considering its expected effects on other drivers. More specifically, even advantageous lane changes will not be performed if the personal advantage is smaller than the disadvantage to the traffic environment, multiplied by p. Furthermore, a 'pushy' driver is able to initiate a lane change of his or her leader which is a commonly observed driving behavior in countries with asymmetric

lane-changing rules and dedicated passing lanes (cf. Fig. 5.4).

The MOBIL concept has only a few parameters and each parameter is associated with an intuitive meaning. The safety criterion is simply described by a critical acceleration threshold b_{safe}. The threshold Δa_{th} prevents lane-changing in case of marginal advantages. For the asymmetric incentive criterion, an additional bias parameter Δa_{bias} differentiates between default and passing lanes. The optional politeness parameter p weights the accelerations and decelerations of the vehicles directly affected by a lane change. The parameters $b_{\text{safe}}, \Delta a_{\text{th}}$ and Δa_{bias} are given in units of the acceleration and are directly *measurable* quantities. Moreover, the politeness factor could also be empirically determined and measured by comparing the situation before and after the lane change of the affected vehicles.[9] By means of simulations, we have investigated the lane-changing rate of an open road system with an on-ramp in combination with the Intelligent Driver Model (IDM), leading to deterministic lane-changing behavior. The lane-changing rate is mainly determined by the politeness factor p, but depends also on the considered location of the road section. As shown in the simulations, the lane-changing rate is locally increased at the location of a road inhomogeneity which is related to mandatory lane changes.

We emphasize that MOBIL is meant to represent only the last 'operational' decision, whether to immediately perform a lane change or not. In reality, a lane-changing decision also includes strategical and tactical aspects in preparation for this final step which are particularly relevant for congested traffic and for mandatory lane changes. For example, tactical behavior may involve accelerations (or decelerations) of the own vehicle or of vehicles in the target lane in preparation for an expected lane change. Such behavior corresponds to an *active* cooperation between the drivers.

Finally, extensions of the proposed acceleration-based concept to other decision processes that occur in traffic network simulation software are possible as well. For example, when approaching a traffic light that switches from green to yellow, one has to decide whether to stop in front of the signal or to pass it with unchanged speed. In the framework of MOBIL, the 'stop' decision will be based on the safe braking deceleration b_{safe}. Similar considerations apply when deciding whether it is safe enough to cross an unsignalized intersection [37], to yield right of way when turning or to start an overtaking maneuver on the opposite lane of a two-way rural road.

[9] Obviously, an empirical study of lane changes in order to calibrate and validate the model would be the next step. This could, in principle, be done with highly resolved trajectory data [49, 155].

6 Microscopic Multi-Lane Traffic Simulator

So far, we have proposed models that describe the longitudinal movement and the lane-changing decisions of individual driver-vehicle units. Let us now describe the software framework that integrates these components into a microscopic multi-lane simulator for freeway traffic.[1] Note that the programming of own simulation tools provides the basis for scientific research, because it allows for full control and dedicated evaluation of the models. For example, in Part II we will study the impact of future driver assistance systems that are based on a traffic-state dependent driving strategy. The technical implementation corresponds to a car-following model with *time-dependent* parameters which requires an integrated simulation approach. Furthermore, we will integrate a module for inter-vehicle communication in order to combine vehicular traffic with new communication applications. Note that commercial traffic simulation software such as PTV-VISSIM™ [145], AIMSUN™ [142] or PARAMICS™ [143] is not yet suited to tackle these current research questions.

In particular, we present a microscopic multi-lane traffic simulator that has been implemented in JAVA™ with a graphical user interface (GUI) and graphical animation. The simulator makes use of the object-oriented programming paradigm by representing and abstracting functional units as classes. Examples for classes are, e.g., the longitudinal (acceleration) model, the lane-changing decision model, the ACC model, the graphical representation of a vehicle, etc. Furthermore, each object as a representative of a class includes data elements allowing for the consideration of individual characteristics (such as driving 'conservatively' or 'aggressively') and vehicle types (such as cars and trucks, or equipment with ACC or not, etc.).

The structure of the microscopic traffic simulator is shown in Fig. 6.1. The *input data layer* defines the simulation settings which can be provided by input files encoded in XML (extensible markup language), by the command line or via the GUI. In Sec. 6.1, we will discuss these input channels in more detail. The *main simulation loop* is organized by the 'Simulation Controller' which keeps track of the program operations and user actions. This central control unit calls the different model classes such as the road-section object, the container class structure of driver-vehicle units, the vehicle generator at the boundaries

[1] As it is customary in the field of software development, the presented 'general purpose' simulation tool is the result of team work over several years and has been developed in tight collaboration with Dr. Martin Treiber, who has started this project. Furthermore, only the general concept can be outlined here.

(see Sec. 6.2), etc. The numerical integration of the underlying locally coupled system of nonlinear differential equations is executed in the 'SimCore' class (see Sec. 6.2 for the explicit integration scheme). The *simulation results* can be visualized by 2D and 3D computer graphics on the screen or as a video. Furthermore, they can be written to data files (see Sec. 6.4).

6.1 Input Data for a Simulation Project

In order to specify a simulation project, some input data are required: The properties of the considered road section, the parameters of the used longitudinal models, the lane-changing parameters, the heterogeneity of the driver-vehicle units representing the variety of vehicles and drivers, options for a user-specified output, etc. In our traffic simulator, input parameters and data can be provided by the following channels:

- The *graphical user interface* (GUI) allows for an interactive control of a traffic simulation. Changes in the parameters by the user directly influence the simulation run. The screenshots in Fig. 6.2 on page 104 show examples of interactive control panels.
- The command line is read when starting the program. When calling the simulation program from an automated shell script, the command line easily allows for repeated runs with varying simulation parameters or projects as described in the following.
- A simulation project can be completely controlled by an input file which is read by a XML parser. A part of a XML project specification is shown in Fig. 6.3. Additionally, time-dependent boundary conditions (see Sec. 6.3) can be provided by separate input files.

6.2 Numerical Integration Scheme

Microscopic traffic flow models describe the motion of individual driver-vehicle units α. This thesis focuses on the subclass of time-continuous microscopic models where the acceleration $\mathrm{d}v_\alpha/\mathrm{d}t$ of a vehicle α is of the form

$$\frac{\mathrm{d}v_\alpha}{\mathrm{d}t} = f(v_\alpha, s_{\alpha\beta_1}, \Delta v_{\alpha\beta_1}, \ldots, s_{\alpha\beta_N}, \Delta v_{\alpha\beta_N}). \tag{6.1}$$

This means the acceleration function f of a vehicle α depends on the own velocity v_α and on the distances $s_{\alpha\beta}$ and velocity differences $\Delta v_{\alpha\beta}$ to a given number of preceding vehicles $\beta_1, \ldots, \beta_N$. For example, the Human Driver Model (HDM) proposed in Chap. 4 depends

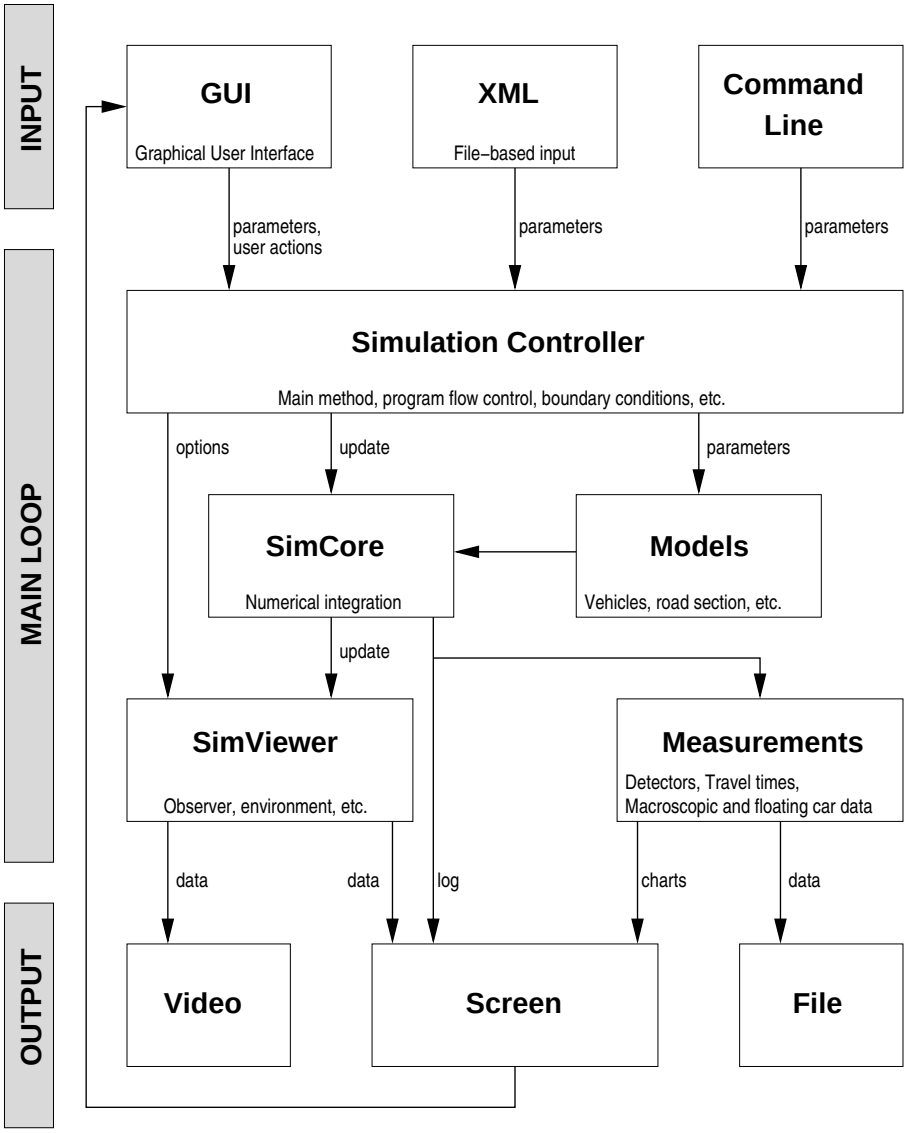

Figure 6.1: Illustration of the structure of the microscopic traffic simulator. The input data defining a simulation setting can be provided by XML-based data files, the command line or the graphical user interface (GUI). The main simulation loop is organized by the 'Simulation Controller', which controls the different program classes, the numerical integrator ('SimCore'), the graphical visualization ('SimViewer'), and the output classes corresponding to measurements of several microscopic and macroscopic quantities. The latter are written into file and may also be plotted on the screen. Furthermore, the single vehicles can be directly graphically visualized on the screen or, alternatively, recorded as a video stream.

on multiple leading vehicles β_i. The Intelligent Driver Model (IDM) [124] defined by (2.1) in Chap. 2 belongs to the subclass of car-following models which take into account only

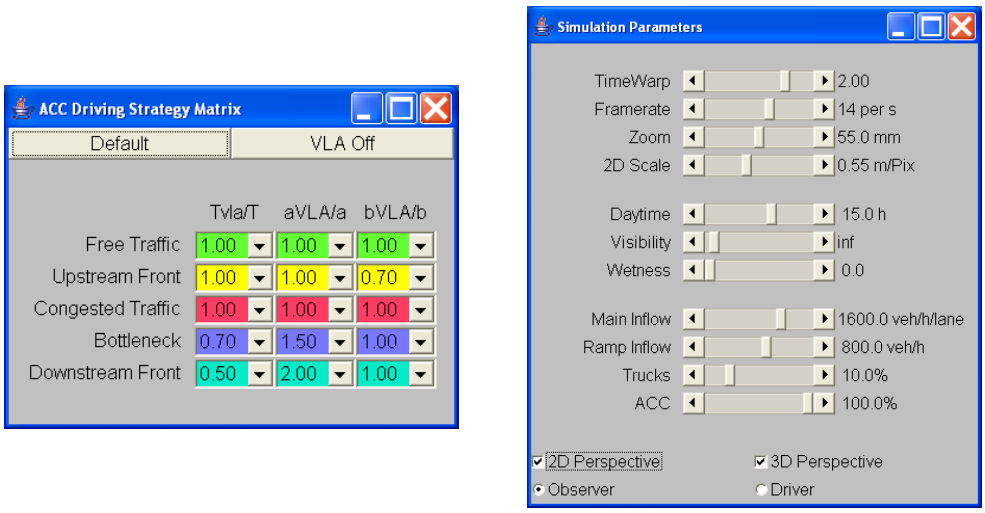

Figure 6.2: Two examples of GUI control panels for the driving strategy of ACC-equipped vehicles (left) and the general simulation parameters and display options (right).

the direct leader resulting in expressions of the form

$$\frac{\mathrm{d}v_\alpha}{\mathrm{d}t} = f\left(s_\alpha, v_\alpha, \Delta v_\alpha\right), \tag{6.2}$$

i.e., the acceleration only depends on the own velocity v_α, the gap s_α, and the velocity difference (approaching rate) $\Delta v_\alpha = v_\alpha - v_{\alpha-1}$ to the leading vehicle $(\alpha - 1)$. Notice that the models described by (6.1) or (6.2) are instantaneous in time and uniquely defined by the acceleration function f. We assume that the vehicle indices α are ordered such that $(\alpha - 1)$ denotes the preceding vehicle throughout the thesis.

Together with the gap $s_\alpha(t) = x_{\alpha-1}(t) - x_\alpha(t) - l_{\alpha-1}$ and the general equation of motion,

$$\frac{\mathrm{d}x_\alpha}{\mathrm{d}t} = v_\alpha, \tag{6.3}$$

Eq. (6.2) represents a (locally) coupled system of *ordinary differential equations* (ODEs) for the positions x_α and velocities v_α of all vehicles. As the considered acceleration functions f are nonlinear, we have to solve the set of ODEs by means of numerical integration with given initial values. In the context of car-following models, it is natural to use an explicit scheme assuming constant *accelerations* within each update time interval Δt. This leads to the explicit numerical update rules

$$\begin{aligned} v_\alpha(t + \Delta t) &= v_\alpha(t) + \dot{v}_\alpha(t)\Delta t, \\ x_\alpha(t + \Delta t) &= x_\alpha(t) + v_\alpha(t)\Delta t + \tfrac{1}{2}\dot{v}_\alpha(t)(\Delta t)^2, \end{aligned} \tag{6.4}$$

where $\dot{v}_\alpha(t)$ is an abbreviation for $f\left(s_\alpha(t), v_\alpha(t), \Delta v_\alpha(t)\right)$. For $\Delta t \to 0$, this scheme locally

```
<?xml version="1.0" encoding="ISO-8859-1"?>
<JSIMULATION_PROJECT>

<GENERAL with_defined_seed="true" crash_test="true" with_graph_output="true">
  <WINDOW_SIZE width="800" height="600" />
  <VISUALIZATION  with_two_mainroads="false" with_2d="true" with_3d="true"/>
</GENERAL>

<SCENARIO choiceScenario="1" roadlength_m="5000" lanes="3" is_ringroad="false">
    <INFLOW_MAIN file="onramp.BCup"/>
    <INFLOW_RAMP init_q_invh="750" />
</SCENARIO>

<HETEROGEN perc_vla="0" perc_truck="0.0" />

<MODELS b_max_ms2="9">
  <CARS length_m="4" vmax_kmh="200" >
      <IDM v0_kmh="120" T="1.2" s0="2" a="1.5" b="2.0"/>
  </CARS>
</MODELS>

<DETECTORS t_sample_s="60" with_aggr_data="true" rel_positions="0.7, 0.9"/>

</JSIMULATION_PROJECT>
```

Figure 6.3: Clipping of simulation project specification encoded in XML (extensible markup language).

converges to the exact solution of (6.2) with consistency order 1 for the velocities ('Euler update', cf. Ref. [95]) and consistency order 2 for the positions ('modified Euler update') with respect to the L^2-norm.[2] Because of the intuitive meaning of this update procedure in the context of traffic, the update rule (6.4) or similar rules are sometimes considered as part of the model itself rather than as a numerical approximation. Popular examples of such *coupled map models* include the Newell model [88] and the Gipps model [26]. A typical update time interval Δt for the IDM is between 0.1 and 0.2 s. Nevertheless, the IDM is approximately numerically stable up to an update interval of $\Delta t \approx T/2$, i.e., half of the time gap parameter.

An explicit reaction time T' is incorporated in a time-continuous model of the type given by Eq. (6.2) by evaluating the right-hand side at a previous time $t-T'$. In this way, one obtains a coupled set of *delay-differential equations* (DDEs). The numerical integration according to (6.4) now depends on both, the reaction time and the update time interval. If the reaction time is a multiple of the update time interval, i.e., $T' = n\Delta t$, it is straightforward to generalize equations (6.4) by calculating all terms on the right-hand sides with the

[2] A time-continuous traffic model is mathematically consistent if a unique local solution exists and if a numerical update scheme exists whose solution locally converges to this solution, when the update time interval goes to zero. It has the consistency order q if $||\epsilon|| = O(\Delta t^q)$ for $\Delta t \to 0$ where ϵ denotes the deviation of the numerical solution for x_α or v_α with respect to the exact solution, and $||\cdot||$ is some functional norm such as the L^2-Norm.

velocities and positions n time steps in the past. To this end, we save the past update steps in form of a 'cyclic buffer'. If T' is not a multiple of the update time interval Δt, we propose a linear interpolation according to

$$x(t - T') = \beta x_{t-n-1} + (1 - \beta) x_{t-n}, \tag{6.5}$$

where x denotes any quantity on the right-hand side of Eq. (6.2) such as s_α, v_α or Δv_α. Furthermore, x_{t-n} denotes this quantity taken n time steps before the actual step t (cf. Sec. 4.1.1). Here, n is the integer part of $T'/\Delta t$, and the weight factor of the linear interpolation is given by $\beta = T'/\Delta t - n$. As initial conditions, DDEs require values for the dependent variables over a whole time interval T'.

6.3 Boundary and Initial Conditions

The mathematical problem is not yet completely specified by the set of ODEs or DDEs. In addition, certain boundary (and initial) conditions have to be satisfied. For our system of driver-vehicle units, we distinguish two system classes:

- A *closed system* (a ring road) is defined by an initial value problem. The control parameter is the homogeneous traffic density ρ_h which essentially determines the long-term behavior of the system.
- For an *open system*, the inflow to the main road is the natural control parameter, i.e., the inflow at the upstream boundary, where the vehicles are introduced into the system with a given velocity. The actual implementation, however, is more complicated. For example, one has to satisfy the traffic demand at the upstream boundary without generating an artificial 'dynamic' bottleneck or causing collisions of entering vehicles. Furthermore, there exist situations where downstream boundary conditions become relevant as well, e.g., when introducing a stop-and-go wave. The details of the initial conditions are not relevant unless they lead to an immediate breakdown of traffic flow.

Note that realistic traffic systems are represented by open systems rather than closed systems. For example, road inhomogeneities like on-ramps or off-ramps are, *by definition*, modeled as sources or sinks. In most simulations, the inflow at the upstream boundary is a time-dependent function $Q(t)$, for example when simulating a rush-hour scenario with an increasing traffic demand. Additionally, information about the heterogeneity of the traffic flow, e.g., the percentage of 'trucks' or vehicles equipped with ACC systems, needs to be considered as well. In order to limit the amount of necessary input data, we evaluate the given quantities at a given simulation time by interpolation.

6.4 Definition and Measurement of Traffic-Related Quantities

In a microscopic traffic simulation, the positions and velocities of all vehicles are known in each time step. Therefore, several microscopic and (aggregated) macroscopic traffic-related quantities can be gathered and either displayed in real-time on the screen or written into data files. In the following, we summarize some common traffic quantities and refer to some examples for matters of illustration. Note that the following quantities are also measurable in reality.

Floating car data: A single vehicle in a microscopic simulation can be considered as a 'floating car' which gathers information about its own trajectory and, additionally, data of its direct environment such as the distance to the leading vehicle, etc. In Chap. 3, empirical and simulated time-series of floating car data (FCD) are extensively investigated, see, e.g., Fig. 3.5 on page 44.

Travel times: A common method used to estimate the current travel time is by summing up the travel time derived from speed measurements at different sections of the road simultaneously. The instantaneous travel time calculation assumes that present travel conditions would prevail for vehicles entering the road section at this moment. We define the instantaneous travel time of a road segment $[x_{\text{start}}, x_{\text{end}}]$ by

$$\tau_{\text{inst}}(t) = \int_{x_{\text{start}}}^{x_{\text{end}}} \frac{\mathrm{d}x}{V(x,t)}. \tag{6.6}$$

In a microscopic simulation, the average velocity $V(x,t)$ can be approximated from the velocities v_i and the integral by the sum over the gaps $\Delta x_\alpha = x_{\alpha-1} - x_\alpha$ of all vehicles α according to

$$\tau_{\text{inst}}(t) = \sum_{\alpha} \frac{\Delta x_\alpha(t)}{v_\alpha(t)}. \tag{6.7}$$

Moreover, the cumulative travel time is simply the vehicle number on the simulated section integrated over time. Note that $\tau_{\text{inst}}(t)$ mainly reflects the perspective of the drivers, while the cumulative travel time is a performance measure of the overall system that can be associated with the economic costs of traffic jams. Furthermore, the travel time is the most important variable of an user-oriented measure of the quality of service [32]. Examples for both quantities can be found in Fig. 8.7 on page 132.

Detector data: For a direct comparison with empirical double-loop detector data in our simulations, 'virtual detectors' mimic the real-world measurement process. At a given

cross-section, passage times and velocities of crossing vehicles are recorded (single-vehicle detector data) or the data are aggregated over a given sampling interval (typically 1 min). Data from virtual detector loops can be found, e.g., in Fig. 8.8 on page 133.

Spatiotemporal data: The spatiotemporal density $\rho(x,t)$ can be obtained from the microscopic quantities of the vehicles α by the generalized micro-macro relationship (2.12)

$$\rho\left(x_\alpha + \frac{l_{\alpha-1} + s_\alpha}{2}\right) = \frac{1}{l_\alpha + s_\alpha}. \tag{6.8}$$

While x_α denotes the vehicle position, s_α represents the spacing to the leader, and l_α the lengths of the vehicles. Moreover, the spatiotemporal velocity field $V(x,t)$ is analogously determined from the vehicle speeds. Note that the spatiotemporal dynamics can also be reconstructed from cross-sectional data by interpolation [121].

6.5 Graphical Visualization

The microscopic simulation of the vehicular traffic dynamics can be intuitively presented by computer graphics. The animated visualization of vehicle trajectories in the course of time demonstrate both, the individual interactions and the resulting collective dynamics. In particular, the graphical visualization turns out to be an important tool when developing and testing lane-changing models for their plausibility, because lane-changing maneuvers can be rather complex (cf. Chap. 5).[3] Furthermore, computer animations have become an important tool for a fast and intuitive understanding of the system dynamics within the project INVENT (App. B), for example, the knowledge transfer of scientific results by means of visualization was very helpful and efficient.

Our traffic simulator offers a fast and dynamic visualization in 2D and 3D. The graphics engine has been developed by M. Treiber based on the ADVANCED WINDOW TOOLKIT™ provided by SUN MICROSYSTEMS™. As an example for the 2D mode, Fig. 6.4 shows in parallel two simulation scenarios (with and without ACC equipped vehicles) for matters of direct comparison.[4] Notice that the instantaneous simulation of two independent simulation instances will be used to simulate inter-vehicle communication, where 'transverse' message propagation requires vehicles traveling in the opposite driving direction (see Sec. 8.4 on page 138). Furthermore, the 3D mode offers two observer perspectives: Figure 6.5 illustrates the 'cockpit perspective' of a driving vehicle on the road. A system

[3] Moreover, some aspects of the proposed lane-changing model MOBIL in Chap. 5 (such as the 'dynamic pressure' exerted by 'pushy' drivers on slower leaders in the fast lane) can be directly observed by visualization.

[4] Interactive elements such as the 'driving strategy matrix' (cf. Sec. 7.1) allow for a direct evaluation of parameter changes of the vehicles equipped with ACC systems.

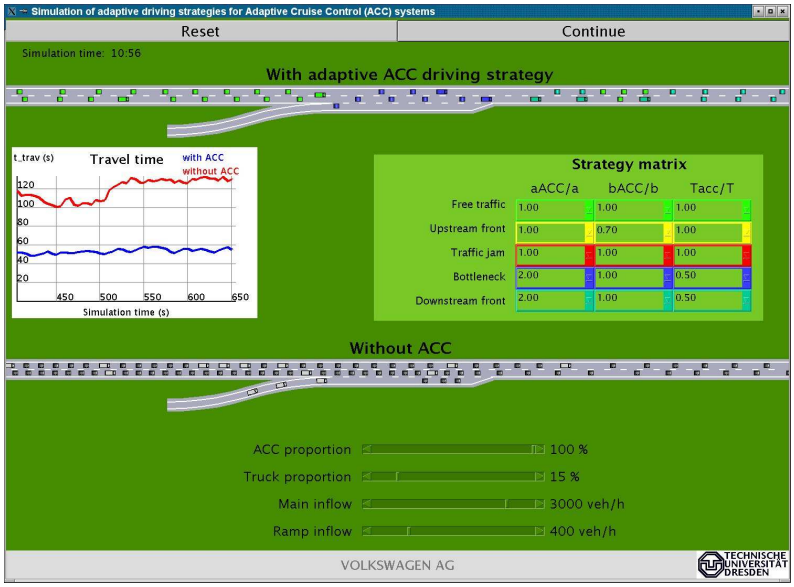

Figure 6.4: Screenshot of our traffic simulator as used in the INVENT project [151] with two independent simulation runs for a direct comparison and evaluation of the applied ACC strategy.

at rest allows for an observation from an arbitrary spatial perspective as illustrated in Fig. 8.12 on page 139.

Figure 6.5: Example for the 3D animation of the driver perspective. Two independent driving directions allow for the simulation of inter-vehicle communication. Notice that the *Coffeemeter* invented by M. Treiber visualizes the acceleration and the jerk (i.e., the changes of all acceleration with time) which are difficult to visualize by other means. Figure 8.12 on page 139 illustrates the observer perspective.

Part II

Traffic-Adaptive Cruise Control and its Impact on Traffic Flow

7 Model of a Traffic-Adaptive Cruise Control System

In this chapter, we generalize the concept of adaptive cruise control (ACC) (cf. Sec. 1.1) to a *traffic assistance* system, in which vehicles automatically adapt the ACC parameters to improve the traffic flow and road capacity, thereby decreasing traffic congestion while retaining driving comfort. In order to resolve possible conflicts between the objectives of comfort and road capacity, we propose a *driving strategy that adapts the ACC driving characteristics to the local traffic situation*. In contrast to conventional ACC systems, the driving behavior of the proposed traffic assistance system, i.e., the acceleration, is determined by a two-step process:

1. The *operational level* consists in responding to changes of the ACC *input quantities* s (net distance to the preceding vehicle), v (vehicle's own velocity) and Δv (velocity difference). The time scale is of the order of seconds and the spatial range is limited to the immediate vehicle ahead.

2. On the *strategic level*, the traffic situation is determined locally and the driving style is adapted accordingly by changing a number of ACC *parameters*. The parameter settings related to the detected traffic state change typically on time scales of minutes and in a range of typically a few hundred meters. This is analogous to manual changes of the desired velocity or the time gap in conventional ACC systems which, of course, are possible in the proposed system as well.

Specifically, we consider a finite set of five traffic situations: (i) Moving in free traffic, (ii) approaching an upstream congestion front, (iii) moving in congested traffic, (iv) leaving the downstream congestion front and (v) passing infrastructural bottleneck sections (such as work zones or intersections). These traffic situations have to be detected autonomously by each ACC-equipped vehicle. A detection algorithm determines which of the five traffic situations mentioned above applies best to the actual traffic situation. Since autonomous detection alone is only possible with delays, we also consider supplementing the local information by means of roadside-to-car and inter-vehicle communication between suitably equipped vehicles [103, 140, 104].

The proposed traffic assistance system consists of several system components as displayed in Fig. 7.1: The main operational layer is the ACC system, calculating the acceleration $\dot{v}(t)$ in response to the input sensor data. The novel feature of the proposed system is

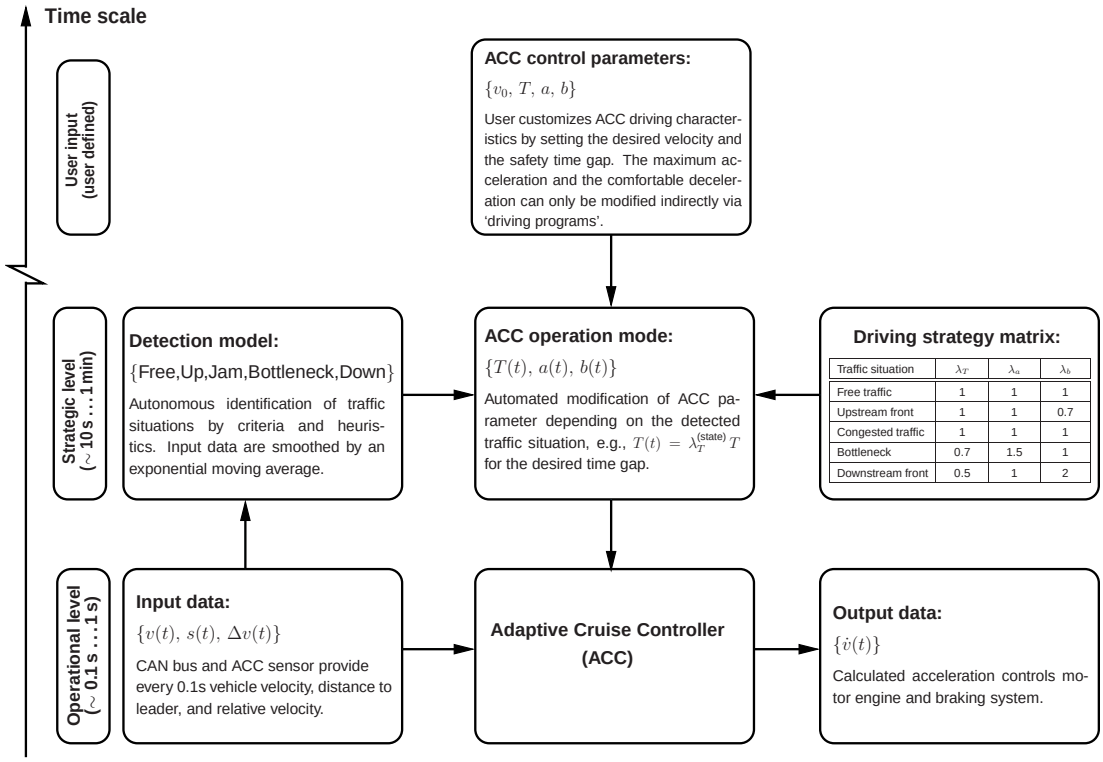

Figure 7.1: Overview of the components of the proposed traffic-adaptive cruise control system. The *operational level* controlling the dynamics on short time scales corresponds to conventional ACC systems. The *strategic layer* containing the novel elements of our concept controls the dynamics on time scales of the order of minutes. It is coupled to the operational level via changes of the ACC model parameters, e.g., T (time gap), a (maximum acceleration) and b (comfortable deceleration). Additionally, the driver is able to customize the driving characteristics by setting the desired velocity v_0 and the time gap T as in conventional ACC systems. Therefore, changes of T by the strategic level are specified relative to the driver settings.

the strategic layer which implements changes in the driving style in response to the local traffic situation by changing a number of parameters of the ACC system. An algorithm automatically detects the local traffic situation in real time, based on local information. The *driving strategy matrix* associates the driving characteristics, i.e., the parameters of the ACC controller, with the local traffic conditions classified in a discrete set of five 'traffic conditions'.

In the following sections, the system components of the proposed traffic-adaptive ACC system will be discussed in more detail. In Sec. 7.1, a general concept for a driving strategy will be introduced that is capable of improving the traffic flow efficiency, while retaining the comfort and safety for the driver. In Sec. 7.2, such a strategy will be implemented, i.e., the elements of the driving strategy in terms of the strategy matrix will be specified. In Sec. 7.3, the detection model for determining the traffic situation based on the evaluation of

the locally available floating car data will be described. Finally, the additional use of non-local information sources such as inter-vehicle and infrastructure-to-car communication for an improved detection of the local traffic state will be discussed (Sec. 7.4).

7.1 Considerations for a Comfortable and Efficient Driving Strategy

The design of an ACC-based traffic assistance system is subject to several, partly contradictory, objectives. On the one hand, the resulting driving behavior must be safe and comfortable for the driver. This implies comparatively large gaps and low accelerations. On the other hand, the performance of traffic flow is enhanced by smaller time gaps T and larger accelerations. Moreover, simulations show that higher accelerations increase both the *traffic stability* and the *dynamic bottleneck capacity*, i.e., the outflow from congested traffic as will be shown in Secs. 9.1 and 9.2. Our approach to solve this conflict of goals is based on the following observations:

- Most traffic flow breakdowns are initiated at some sort of road inhomogeneities or infrastructure-based bottlenecks such as on-ramps, off-ramps or sections of road works. For example, Schönhof *et al.* [102, 73] have observed these characteristics by investigating 245 breakdowns of traffic flow at several different bottlenecks of the German freeway A5 near Frankfurt/Main.
- An effective measure to avoid or delay traffic breakdowns is to homogenize the traffic flow. To this end, large velocity differences are to be avoided.
- Once a traffic breakdown has occurred, the further dynamics of the resulting congestion pattern is uniquely determined by the traffic demand (which is outside the scope of this investigation) and by the average driving style in the immediate neighborhood of the downstream congestion front [18]. In many cases, the downstream front is fixed and located near a bottleneck, as found in empirical investigations [102, 52, 55, 56, 57].
- Traffic safety is (indirectly) increased by reducing the spatial velocity gradient at the upstream front of traffic congestion, thereby reducing the risk of rear-end collisions.

In the context of the ACC-based traffic assistance system, we make use of these observations by *only temporarily changing the comfortable settings of the ACC system in specific traffic situations.* The situations in which this is necessary have to be determined autonomously by the equipped vehicle. To this end, we propose the following discrete set of five traffic states and the corresponding actions:

1. **Free traffic**: This is the default situation in which the ACC characteristics correspond to 'conventional' ACC systems. The ACC settings are determined solely by the maximum individual driving comfort. Since each driver can set his or her own parameters for the time gap and the desired velocity, this may lead to different settings of the ACC systems.

2. **Upstream jam front**: Here, the objective is to increase safety by reducing velocity gradients. When compared with the default situation, this implies earlier braking when approaching slow vehicles.

3. **Congested traffic**: Since drivers cannot influence the development of traffic congestion in the bulk of a traffic jam, the ACC settings are reverted to their default values.

4. **Downstream jam front**: In order to increase the dynamic bottleneck capacity, accelerations are increased and time gaps are temporarily decreased. Note that this handling rule is analogous to the driving behavior at a traffic light which switches from red to green: For a high discharge rate from the queue, it is necessary that the drivers are attentive and accelerate as quickly as possible.

5. **Bottleneck sections**: Here, the objective is to locally increase the capacity, i.e., to *dynamically 'fill the capacity gap'*. This requires a temporary reduction of the time gap which can be associated with an attentive driving behavior while passing a bottleneck section.

Note that the operational ACC layer always assures a safe approaching process regardless of the ACC settings for a certain detected traffic state. It is to emphasize that the total fraction of time periods during which the ACC settings deviate from the default state is usually only a few percent. Nevertheless, we will show in the Chaps. 8 and 9 that even a small percentage of equipped vehicles driving according to the above ACC strategy substantially decreases the size and duration of congestion and, thus, reduces the travel times in a relevant way.

Figure 7.2 illustrates typical sequences of these five traffic states. In free traffic conditions, the 'bottleneck state' is activated when passing a (stationary) bottleneck, e.g., an on-ramp. When traveling through congested traffic, the drivers initially experience the 'upstream front' (the tail of the queue). Then, they drive through 'congested traffic' conditions until they reach the head of the queue which corresponds to the 'downstream traffic state'.

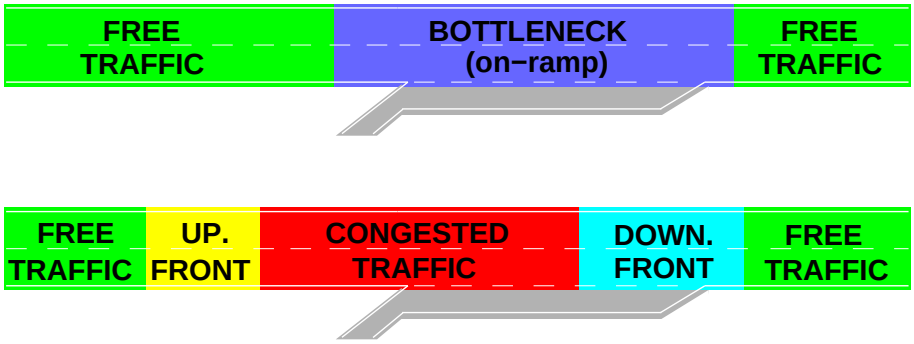

Figure 7.2: Typical sequences of traffic states. Top: The 'free traffic state' is the default under free traffic conditions. The 'bottleneck state' is activated when passing infrastructural bottleneck sections such as construction sites or intersections. Bottom: When traveling through congested traffic, drivers typically experience the sequence 'upstream jam front' → 'congested traffic' → 'downstream jam front'.

7.2 Implementation of the Traffic-Adaptive Cruise Control

For an implementation and simulation of the proposed system components, we require a representation of ACC systems in terms of a microscopic traffic model. In order to be a suitable and realistic candidate for simulating ACC systems, car-following models must meet several criteria: First of all, the car-following dynamics must be collision-free, at least, if this is physically possible. The dynamics should correspond to a natural and smooth driving behavior. Adaptations to new traffic situations (for example, when the preceeding vehicle brakes or another vehicle cuts in) should be performed without any oscillations and as comfortable as safety allows. Each model parameter should have an intuitive meaning and plausible values after calibration. Ideally, the parameter list should include the desired velocity v_0 and the desired time gap T which are preset by the driver in typical ACC systems. These criteria are, e.g., met by the Intelligent Driver Model (IDM), which has been introduced in Chap. 2. We will make use of this direct correspondence for the simulation of ACC vehicles in the following chapters when representing idealized ACC vehicles by the IDM.[1]

The implementation of the proposed traffic-adaptive driving strategy for the IDM is straightforward because three of five IDM parameters directly correspond to different aspects of the adaptation strategy: The *acceleration parameter* a gives an upper limit for the acceleration $\dot{v}(t)$ of the ACC-controlled vehicle. Consequently, this parameter is increased when leaving congestion, i.e., when the state 'downstream front' has been detected. The *comfortable deceleration* b characterizes the deceleration when approaching

[1] Note that the modeling assumption is profoundly reasonable because a real-world implementation of an ACC based on the IDM has recently been successfully implemented and presented by Volkswagen [67] (see Sec. 1.1 of the Introduction as well).

Traffic situation	λ_T	λ_a	λ_b	Driving behavior
Free traffic	1	1	1	Default/Comfort
Upstream front	1	1	0.7	Increased safety
Congested traffic	1	1	1	Default/Comfort
Bottleneck	0.7	1.5	1	Breakdown prevention
Downstream front	0.5	2	1	High dynamic capacity

Table 7.1: The *driving strategy matrix* summarizes the implementation of the ACC driving strategy. Each of the traffic situations corresponds to a different set of ACC control parameters. We represent the ACC driving characteristics by the *time gap* T, the *maximum acceleration* a and the *comfortable deceleration* b which are model parameters of the Intelligent Driver Model (IDM). λ_T, λ_a and λ_b are the multiplication factors in relation (7.1). For example, $\lambda_T = 0.7$ denotes a reduction of the default safety time gap T by 30% in bottleneck situations.

slower or standing vehicles. Obviously, in order to be able to brake with lower decelerations, one has to initiate the braking maneuver earlier. Since this smoothes upstream fronts of congestion, the parameter b is decreased when the state 'upstream front' has been detected. Notice that, irrespective of the value of b, the IDM deceleration (and thus the deceleration of the ACC vehicle) exceeds b if this is necessary to avoid collisions. Finally, the *safety time gap* T is decreased if one of the states 'bottleneck' or 'downstream front' is detected.

In order to be acceptable to drivers, the system parameters need to be changed in a way that preserves the individual preferences of the different users of the system and also the driving characteristics of different vehicle categories such as cars and trucks. In particular, the preferred time gap T can be changed both by the driver and by the event-driven automatic adaptation (cf. Fig. 7.1 on page 114). This can be fulfilled by formulating the changes in terms of *multiplication factors* λ_a, λ_b and λ_T defined by the relations

$$a^{(\mathrm{s})} = \lambda_a^{(\mathrm{s})}\, a, \quad b^{(\mathrm{s})} = \lambda_b^{(\mathrm{s})}\, b, \quad T^{(\mathrm{s})} = \lambda_T^{(\mathrm{s})}\, T, \tag{7.1}$$

where the superscripts (s) denote one of the five traffic situations, to which the respective value applies. Furthermore, a, b and T denote the default values of the IDM parameters.

In summary, this implementation can be formulated in terms of a *strategy matrix* as depicted in Table 7.1. Of course, all changes are subject to restrictions by legislation (e.g., the lower limit for T) or by the vehicle type such as an upper limit for a, particularly for trucks.

7.3 Detection Algorithm for a Vehicle-Based Identification of Traffic States

Let us now present a detection model for an automated, vehicle-based identification of the local traffic situation as required for the proposed automated driving strategy. Our detection model is based on locally available velocity time series data of the own vehicle and the leading car, whereas the velocity of the leader is measured by the radar sensor of the ACC system. For the sake of simplicity we only focus on the vehicle's own velocity, although both velocities can be treated similarly and used to determine a weighted average.[2] Due to short-term fluctuations, the time series data require a smoothing in time in order to reduce the level of variations that, if left unsmoothed, would trigger false transition signals to other traffic states. In our traffic simulator used for the simulations in Chapters 8 and 9, we have used an exponential moving average (EMA) for a measured quantity $x(t)$,

$$x_{\mathrm{EMA}}(t) = \frac{1}{\tau} \int_{-\infty}^{t} dt' e^{-(t-t')/\tau}\, x(t') \tag{7.2}$$

with a relaxation time of $\tau = 5\,\mathrm{s}$. The EMA allows for an efficient real-time update by solving the corresponding ordinary differential equation

$$\frac{d}{dt} x_{\mathrm{EMA}} = \frac{x(t) - x_{\mathrm{EMA}}(t)}{\tau}. \tag{7.3}$$

For an identification of the proposed five traffic states we define the following criteria: The *free traffic state* is characterized by a sufficiently high average velocity, i.e.,

$$v_{\mathrm{EMA}}(t) > v_{\mathrm{free}}, \tag{7.4}$$

where $v_{\mathrm{free}} = 60\,\mathrm{km/h}$ is a typical threshold value. In contrast, the *congested traffic state* is characterized by a low average velocity, namely

$$v_{\mathrm{EMA}}(t) < v_{\mathrm{cong}}, \tag{7.5}$$

with a threshold of $v_{\mathrm{cong}} = 40\,\mathrm{km/h}$. The detection of an upstream or downstream jam front relies on a *change* in speed compared to the exponentially averaged past of the speed. Approaching an *upstream jam front* is therefore characterized by

$$v(t) - v_{\mathrm{EMA}}(t) < -\Delta v_{\mathrm{up}}, \tag{7.6}$$

[2] The actual implementation is more elaborated and proprietary. It takes into account the available information about the leader as well.

whereas a *downstream front* is identified by an acceleration period, i.e.,

$$v(t) - v_{\mathrm{EMA}}(t) > \Delta v_{\mathrm{down}}. \tag{7.7}$$

Both thresholds are of the order of $\Delta v_{\mathrm{up}} = \Delta v_{\mathrm{down}} = 10\,\mathrm{km/h}$.

The identification of the *bottleneck state* requires information about the infrastructure because bottlenecks are typically associated with spatial modifications in the freeway design such as on-ramps, off-ramps, lane closures, gradients or construction sites (cf. Sec. 7.1). We assume that this information is provided by a digital map database containing the position of a bottleneck $(x_{\mathrm{begin}}, x_{\mathrm{end}})$ in combination with a positioning device (i.e., a receiver using a satellite navigation system such as the Global Positioning System (GPS)) which provides the actual vehicle position $x(t)$ [23]. This information allows for an identification of the bottleneck state by the spatial criteria[3]

$$x(t) > x_{\mathrm{begin}} \quad \text{AND} \quad x(t) < x_{\mathrm{end}}, \tag{7.8}$$

where x_{begin} is a position about 100 m upstream of the actual bottleneck and x_{end} a location somewhat downstream of its end (cf. Fig. 7.2).

It is possible that no criterion is fulfilled or, conversely, multiple criteria are met simultaneously. Therefore, we need a *heuristic* for the discrete choice problem. From our visualized traffic simulations (cf. Chap. 6 and, e.g., Fig. 8.1 on page 124), we found that the following decision order is the most appropriate one: *downstream front* → *bottleneck* → *traffic jam* → *upstream front* → *free traffic* → *no change*. This priority order also reflects the relevance of the driving strategy associated with these traffic states for an efficient traffic flow. A more sophisticated heuristic would consist in a dynamic adaptation of the thresholds used in the criteria of Eqs. (7.4) to (7.7), e.g., based on non-local information via inter-vehicle communication or vehicle-infrastructure communication as will be discussed in the next section (cf. Fig. 7.3).

7.4 Inclusion of Inter-Vehicle and Infrastructure-to-Car Communication

So far, the detection model is exclusively based on *local information* that is provided autonomously by the vehicle's own floating car data, the ACC radar sensor data and a

[3] In the case of very light traffic volumes, the adaptation to the 'bottleneck state' is not very effective because there is no need for improvement in this case. Consequently, the information 'near a bottleneck' should no longer have priority over the information 'free traffic'. The traffic-adaptive ACC should always operate in the 'free traffic' regime in this case, i.e., it should reduce to a conventional ACC system with fixed (user-defined) parameters.

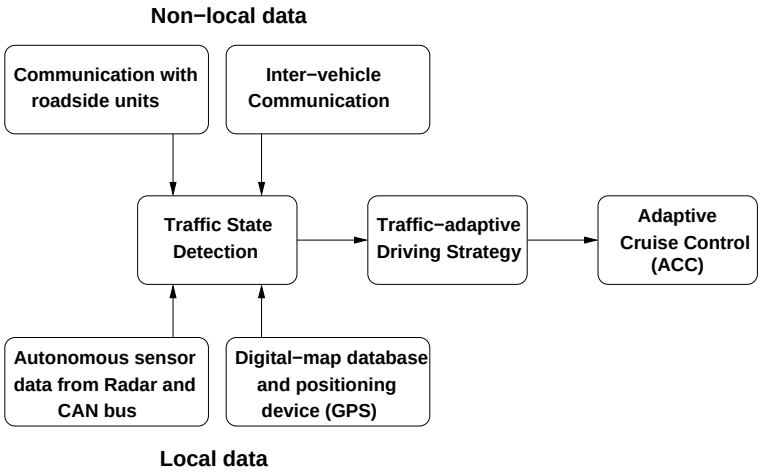

Figure 7.3: The autonomous detection and identification of the local traffic state is primarily based on local data provided by the ACC radar sensor and the GPS positioning device in combination with a digital map. Non-local data available from inter-vehicle communication or communication with a stationary 'roadside unit' can improve the sensitivity and reliability of the detection model (see also Fig. 8.12 for purpose of illustration).

satellite positioning device (cf. Fig. 7.3). Let us briefly discuss the principal limitations of this approach. An autonomous detection in real-time according to Eqs. (7.4) to (7.7) has to struggle with a time delay due to the exponential moving average that is of the order of τ. In addition, a transition time between two states is necessary for the subjective driving comfort (which is of the order of 5 s as well). Therefore, the resulting retardation makes the autonomous adaptation to the traffic condition nearly ineffective if they are not triggered by a known bottleneck (cf. Fig. 9.10 on page 155 for explicit simulations). For example, the adaptation towards a smooth deceleration behavior when approaching a dynamically propagating upstream congestion front requires the knowledge of its position at an early stage in order to be able to switch to the new driving strategy in time. Even more important, however, for the overall traffic performance is the activation of the traffic state 'downstream jam front' when leaving the jam (cf. Sec. 9.2).

For a more advanced vehicle-based traffic state estimation, non-local information can be additionally incorporated in order to improve the detection speed and quality. For example, *inter-vehicle communication* (IVC) based on the Dedicated Short Range Communication (DRSC) standard [144] is a promising extension, providing up-to-date information about *dynamic* up- and downstream fronts of congested traffic which cannot be estimated without delay by local measurements. Furthermore, in the case of a *temporary bottleneck* such as an accident that is not listed in the digital map database, the information about the location could be provided by communication with a stationary sender (so-called 'roadside unit', RSU) upstream of the bottleneck, corresponding to *infrastructure-to-car*

communication. In a feasibility study in Sec. 8.4, we will demonstrate how traffic-related messages can be transmitted by IVC and how the non-local information can be used for an improved traffic-state detection. Note that we do not use IVC for a direct *control* of ACC, but we merely incorporate additional, non-local information sources for an improved traffic-state estimation.

8 Integrated Simulation of Traffic-Adaptive Cruise Control

Since large-scale field experiments are scarcely feasible, the effects of upcoming driver assistance systems on the collective traffic dynamics are usually assessed by means of traffic simulations. In particular, the microscopic modeling approach allows for a natural representation of heterogeneous traffic and for a detailed specification of the parameters and proportions of cars and trucks. In order to investigate the impact of the proposed ACC-based traffic assistance system, we consider a mixed traffic flow consisting of vehicles with activated ACC systems and manually controlled driver-vehicle units. For realistic scenarios, only a small proportion of vehicles will be equipped with ACC systems.

The proposed components of the traffic-adaptive cruise control have been integrated in the microscopic simulation framework (presented in Chap. 6) allowing for the following *'simulation-in-the-loop'* method: Each vehicle equipped with ACC determines the local traffic situation autonomously by evaluating its own floating car data (as a result of the surrounding traffic). Depending on the detected traffic state, the *individual* ACC parameters T, a and b are changed by the multipliers of the driving strategy matrix listed in Table 7.1 on page 118. Consequently, the automatic adaptation of the individual driving style of single vehicles induces an intended *feedback* to the traffic dynamics of the overall system which is our object of investigation. Figure 8.1 shows a screenshot of the traffic simulation software.

As microscopic traffic model we use for both, equipped and non-equipped vehicles, the Intelligent Driver Model (IDM) introduced in Chap. 2, with the parameter sets for cars and trucks given in Table 8.1. Furthermore, lane-changing is a required ingredient for realistic simulations of multi-lane freeway traffic and merging zones like on-ramps. Lane changes have been simulated with the algorithm MOBIL (see Chap. 5) which is based on the expected advantage in the new lane in terms of the gain in possible acceleration or the avoidance of deceleration as calculated with the longitudinal driving model. Notice that the ACC system only controls longitudinal driving. For this reason, we use the same lane-changing parameters for ACC vehicles listed in Table 5.1 on page 90 (with politeness factor $p = 0.2$).

The rest of this chapter is structured as follows: In Sec. 8.1 we start with an analysis of the traffic models used to represent ACC and manually controlled vehicles and give a justifica-

Figure 8.1: Screenshot of the traffic simulator, showing the on-ramp scenario studied in Sec. 8.2. In our visualization, the current traffic state of each ACC vehicle is displayed by a changing vehicle color allowing for a direct, visual assessment of the respective detected state. In contrast, non-ACC vehicles are displayed in gray color. The parameters of the strategy matrix can be changed interactively by the researcher in order to test new strategy matrices directly. For purpose of illustration, two simulation runs are displayed. In the upper simulation, 100% of the vehicles are equipped with the ACC-based traffic assistance system. The reference case without ACC equipped vehicles displayed in the lower simulation window shows congested traffic at the bottleneck. In both simulations, the same time-dependent upstream boundary conditions, i.e., identical inflows have been used.

tion for modeling both types of vehicles with the same model. In the following subsections, we evaluate the impact of the proportion of vehicles equipped with ACC systems on the capacity and stability of traffic flow. We consider an on-ramp bottleneck (in Sec. 8.2) and an uphill gradient bottleneck (Sec. 8.3). Furthermore, we apply different boundary conditions to the open system and investigate different degrees of inter-driver heterogeneity. In Sec. 8.4, we finally simulate event-driven message information propagation by inter-vehicle communication for an autonomous detection and prediction of dynamic jam fronts.

8.1 Modeling Automated and Manual Driving Behavior

When dealing with traffic simulations for describing the effects of ACC-based driving, one has to take into account the operational differences between human drivers and ACC-controlled vehicles. Let us start with the representation of real-world ACC systems by

Model Parameter	Car	Truck
Desired velocity v_0	120 km/h	85 km/h
Safety time headway T	1.5 s	2.0 s
Maximum acceleration a	1.4 m/s^2	0.7 m/s^2
Desired deceleration b	2.0 m/s^2	2.0 m/s^2
Jam distance s_0	2.0 m	2.0 m

Table 8.1: Model parameters of the Intelligent Driver Model (IDM) for cars and trucks used in this chapter. The vehicle length has been set to 4 m for cars and 12 m for trucks, respectively. Vehicles equipped with the ACC system adapt their parameters T, a and b to the detected traffic situation summarized by the strategy matrix in Table 7.1 on page 118.

means of a microscopic traffic model. From a control-theoretical point of view, the input quantities of an ACC system, i.e., the vehicle's own speed, the distance to the car ahead and the velocity difference are exactly those of many car-following models. Moreover, as the ACC's radar detection time is generally negligible, ACC systems determine the instantaneous acceleration $\dot{v}(t)$ as a function of the actual velocity $v(t)$, the gap $s(t)$ and the approaching rate $\Delta v(t)$ to the leading vehicle. This corresponds directly to the formulation of car-following models which are limited in their reaction to the direct leader. In the following simulations, we therefore represent ACC-controlled vehicles by the IDM (cf. Chap. 2). From a traffic modeler's point of view, it is interesting that this correspondence can also be applied the other way round: A real-world implementation of an ACC system based on the IDM has recently been presented by Volkswagen within the German research project INVENT (cf. App. B).[1]

While the car-following approximation is perfectly suited to model the dynamics of ACC-controlled vehicles, the *human* driving style differs from it in essential points. The *finite reaction times* of humans and limited attention spans result in a delayed response to the traffic situation. Imperfect estimation capabilities result in perception errors. However, human drivers routinely scan the traffic situation several vehicles ahead, while the ACC sensors are restricted to the immediate vehicle in front. Furthermore, human drivers *anticipate* future traffic situations by making use of further cues and by forming hypotheses such as assuming constant accelerations of neighboring vehicles for the next few seconds. These aspects have explicitly been considered in the HDM approach presented in Chap. 4.

In order to investigate the influence of different modeling approaches to the representation

[1] Clearly, when implementing a concrete ACC system, one has to take into account present imperfections of ACC systems due to the vehicle's delayed response action in the control path (as opposed to the measurement process), resulting in time delays as well [66].

of ACC and human-like driving behavior, we have carried out simulations with a varying proportion of ACC-equipped vehicles represented by the IDM (with parameters listed in Table 8.1) and human drivers modeled by the HDM (with a reaction time of 0.9 s and $n_a = 3$ as number of anticipated vehicles). The simulated freeway section was 15 km long and an on-ramp as typical representative for a stationary bottleneck was located at $x = 12$ km. We have simulated idealized rush-hour conditions by linearly increasing (and afterwards decreasing) the inflow at the upstream boundary. In order to begin with, we have considered the most simple case of one lane with traffic only consisting of cars. For more details on the simulation setup, we refer to Sec. 8.2, in which the same boundary conditions will be used in a three-lane freeway scenario.

Figure 8.2 shows the resulting spatiotemporal dynamics for ACC penetrations of 0%, 10%, 20% and 30%. The diagrams in the left column correspond to a mix of HDM and IDM models, while the right column shows simulations exclusively based on the IDM using the same boundary conditions. Although the HDM leads to smoother upstream jam fronts, both simulation approaches show a similar spatiotemporal traffic dynamics: The simulation runs without ACC vehicles show a traffic breakdown after $t \approx 1$ h at the on-ramp due to the increasing incoming traffic at the upstream boundary. Moreover, an increasing proportion of ACC-equipped vehicles implementing the automated traffic-adaptive driving strategy (cf. Table 7.1) leads to a distinct reduction of traffic congestion. A proportion of even 10% ACC vehicles improves the traffic flow, while the traffic jam disappears completely for a proportion of ACC vehicles of 30%.

The comparison of the simulations, in which drivers have been either simulated by the IDM or the HDM, indicates that the overall macroscopic traffic dynamics does *not* depend on the details of the specific modeling approach. Furthermore, the positive impact of the traffic-adaptive ACC vehicles on the collective dynamics arises in both settings showing the generality of the traffic-adaptive driving strategy. Despite the differences between both models, the IDM based on the simple car-following approximation is able to essentially reproduce the macroscopic dynamics of the more complex HDM approach.[2] This finding is in agreement with the analysis of the HDM in Chap. 4. There, the result was that the destabilizing effects of reaction times and estimation errors are (to a large extent) be compensated for by spatial and temporal anticipations. Consequently we may conclude that, although the mode of operation is fundamentally different, ACC-equipped vehicles and manually controlled vehicles exhibit a similar *effective* driving behavior with respect to *collective properties* such as the stability of traffic flow, traffic performance (measured in terms of capacity) or the emergence and propagation of traffic congestion.[3]

[2] Note that, also on a microscopic level, the IDM has been able to reproduce the trajectories of human drivers to a satisfying extent (see Chap. 3).

[3] One might even speculate that hypothetical mixed future traffic consisting predominantly of automated vehicles will exhibit macroscopic dynamics similar to that of the actual traffic, although the driving

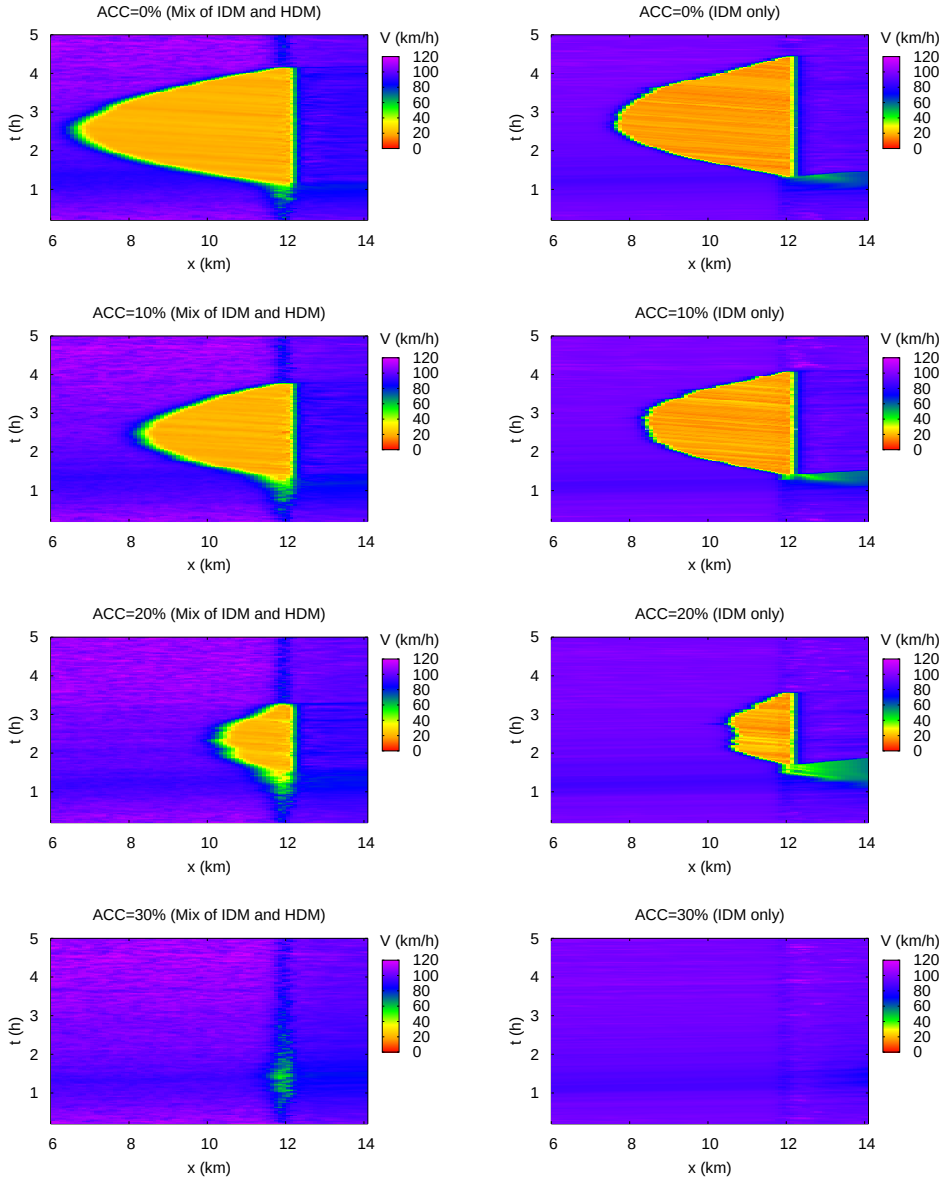

Figure 8.2: Spatiotemporal dynamics of the average velocity for various proportions of ACC vehicles which implement the traffic-adaptive driving strategy (cf. Chap. 7). The contour diagrams display the local velocity as a function of the longitudinal location x and time t. The simulations in the left column are carried out with a mixture of HDM vehicles (representing manual driving) and IDM vehicles (representing automated driving by means of ACC). The diagrams in the right column show simulations for the same boundary conditions, using the IDM also for human drivers. Both scenarios show a similar jam formation with a stationary downstream front pinned at the on-ramp at $x = 12\,\mathrm{km}$. Even a small increase of the percentage of traffic-adaptive ACC vehicles leads to a reduction of traffic congestion in both sets of simulations.

strategy would be markedly different.

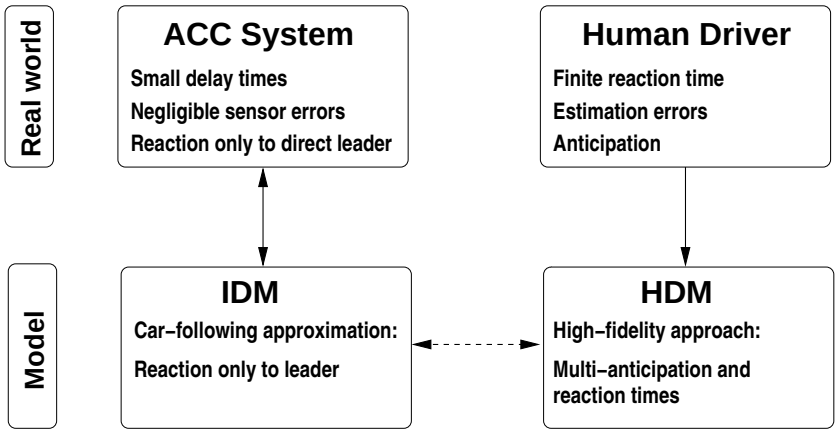

Figure 8.3: Summary of the modeling approach: Because the mode of operation of ACC systems directly corresponds to the control task of a car-following model, we associate the IDM with an 'ideal' ACC system, i.e., with perfect sensors and negligible power train response times. A detailed representation of manual driving requires a more complex modeling approach. The main aspects of human driving behavior are captured by the HDM. On a macroscopic level, however, the HDM and the IDM show a similar *effective* traffic dynamics (cf. Chap. 4).

The generality of the concept which does not depend on the details of the underlying traffic models has been demonstrated in Fig. 8.2. In the remainder of this chapter, the influence of the proposed automated driving strategy using ACC systems on *macroscopic properties* of traffic flow will be investigated. As it is primarily intended as a 'proof of concept' only, it is well justified to simulate human drivers with car-following models such as the IDM instead of using more complex models such as the HDM. The advantage of using simple models for both human-driven and automated vehicles lies in the reduced number of parameters that need to be calibrated. Moreover, the simulation results are easier to interpret and to review. Figure 8.3 summarizes our modeling approach.

8.2 Simulations with an On-Ramp Bottleneck

In this section, we will study an open road system with an on-ramp as a typical representative for a stationary bottleneck. We will consider a three-lane freeway section of 15 km length. The center of the on-ramp is located at $x = 12\,\text{km}$ and the merging zone has a length of 300 m.

Spatiotemporal dynamics under idealized rush-hour conditions: In a first scenario, we have simulated *idealized rush-hour conditions* by linearly increasing the inflow at the upstream boundary over a period of 1 hour from 1000 veh/h/lane to 1700 veh/h/lane. Afterwards, we have linearly decreased the traffic volume to 1000 veh/h/lane over a period

of 3 hours until the simulation has been stopped after a duration of 5 hours. Furthermore, we have assumed a constant ramp flow of 250 veh/h/lane and an overall truck fraction of 10%. Since the maximum overall flow of 1950 veh/h/lane exceeds the road capacity, a traffic breakdown is typically provoked at the bottleneck around 1:40 h. Figure 8.4 shows the resulting spatiotemporal dynamics for ACC equipment rates of 0%, 10%, 20% and 30%, respectively. For the purpose of better illustration, we have plotted the lane-averaged mean velocity upside down. Note that the downstream front of the traffic jam is stationary and localized at the on-ramp. After the breakdown of traffic flow, a queue builds up in upstream direction. The parabola-shaped jam formation reflects the applied upstream boundary conditions.

Similar to the results of the one-lane scenario shown in Fig. 8.2, an increased proportion of ACC-equipped vehicles in three-lane simulations leads to a reduction of the traffic jam. A proportion of even 10% ACC vehicles improves the traffic flow significantly. In contrast to the one-lane scenario studied in Fig. 8.2, the traffic jam is not yet completely avoided by an ACC proportion of 30%, although the time-dependent traffic demand per lane and the ramp flow are identical. The reason is that the consideration of the slower trucks reduces the average maximum throughput and the dynamic capacity of the system (cf. Chap. 9

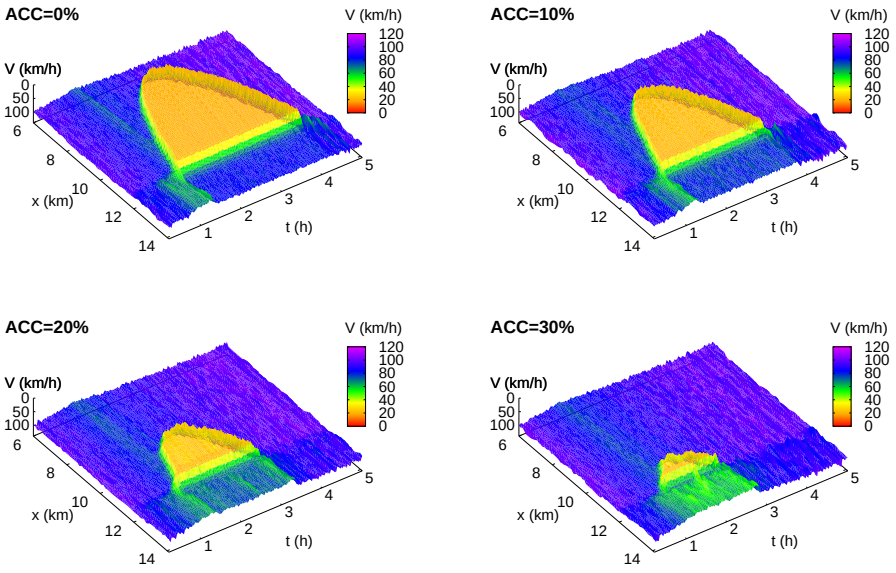

Figure 8.4: Spatiotemporal traffic dynamics of a three-lane freeway around an on-ramp located at $x = 12$ km for different proportions of ACC vehicles, represented by the lane-averaged velocity upside down. The simulations show the positive impact of ACC-equipped vehicles applying an adaptive driving strategy introduced in Chap. 7. The inflow at the upstream boundary is first increased and afterwards decreased to represent idealized rush-hour conditions.

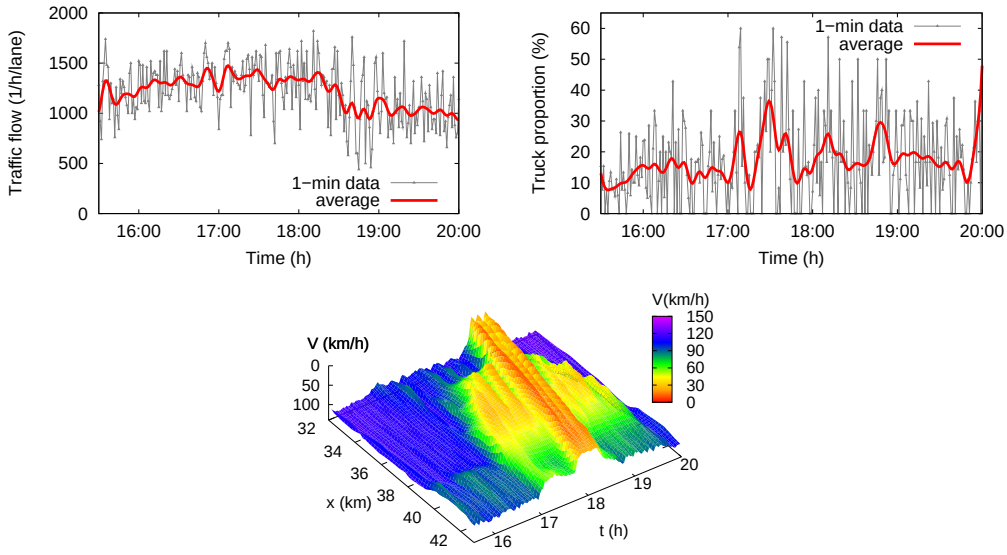

Figure 8.5: Top: Time series of empirical 1-min loop detector data of the lane-averaged traffic flow and truck proportion used as upstream boundary conditions in our traffic simulations. The data show the afternoon rush-hour peak on the German autobahn A8 from Munich to Salzburg (Austria). The moving averages (red thick lines) are only plotted for a better overview over the strongly fluctuating quantities. Bottom: Average spatiotemporal velocity reconstructed from cross-sectional detector data with the 'Adaptive Smoothing Method' [121] showing oscillating congested traffic during the afternoon rush-hour. An incident leading to a temporary lane closing further downstream causes even denser congested traffic that propagates through the region of oscillating traffic.

below).

Spatiotemporal dynamics with empirical boundary conditions: The traffic volume at the upstream boundary is the natural control parameter of the considered freeway section. For a more realistic traffic scenario, we have therefore used *empirical detector data* from the German freeway A8 from Munich to Salzburg (Austria) as upstream boundary condition. Figure 8.5 shows the 1-min data of the lane-averaged traffic flow and the proportion of trucks during the evening rush-hour between 15:30 h and 20:00 h. Note that, in the real-world data, traffic further downstream of the detector was congested between 17:00 h and 19:30 h due to a combination of an on-ramp and an uphill gradient, as illustrated in Fig. 8.5 as well. Moreover, we have assumed a constant ramp flow of 250 veh/h/lane with 10% trucks.[4]

We have studied the impact of the proposed traffic assistance system by carrying out several simulations with varying proportions of vehicles equipped with ACC systems, see

[4] In Sec. 8.3, we will use the same boundary conditions in combination with an uphill gradient.

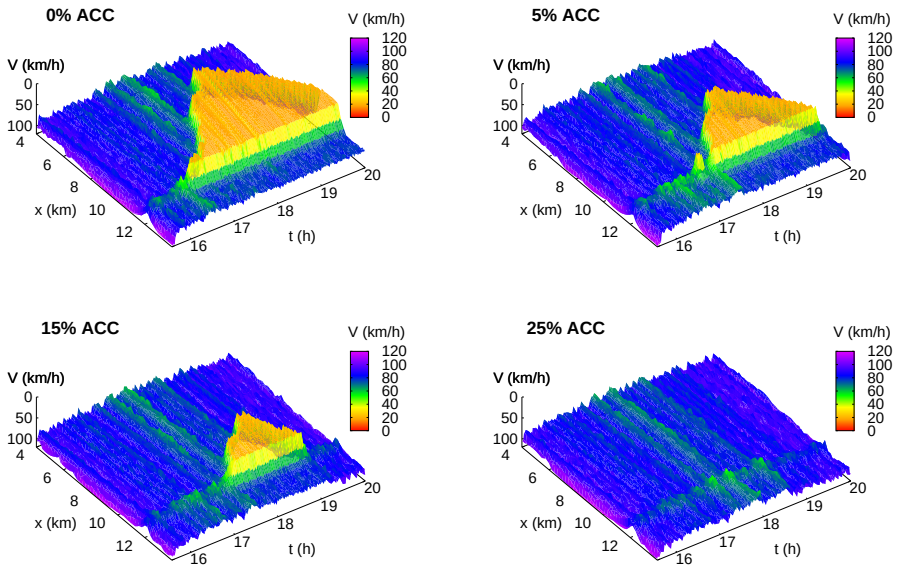

Figure 8.6: Spatiotemporal traffic dynamics represented by the lane-averaged velocity around an on-ramp located at $x = 12\,\text{km}$ on a three-lane freeway for different proportions of ACC vehicles. The inflow at the upstream boundary was taken from empirical 1-min detector data during the evening rush-hour, as shown in Fig. 8.5. The simulations demonstrate the positive impact of the traffic-adaptive cruise control system introduced in Chap. 7.

Fig. 8.6. Again, we have plotted the lane-averaged mean velocity upside down for the purpose of intuitive illustration of congested traffic. The simulation scenario without ACC vehicles shows a traffic breakdown at the on-ramp around $t = 17{:}00\,\text{h}$ which is due to the increasing incoming traffic at the upstream boundary during the rush-hour. The other three diagrams of Fig. 8.6 show simulation results for an increasing proportion of ACC-equipped vehicles which reduces traffic congestion significantly. A proportion of even 5% ACC vehicles improves the traffic flow due to a delayed traffic breakdown. This demonstrates the efficiency of the proposed automated driving strategy and its positive effect on capacity even for small penetration levels. Note that an equipment level of 25% ACC vehicles avoids the traffic breakdown in this scenario nearly completely.

Instantaneous and cumulative travel time: Let us now consider the travel time as the most important variable of an user-oriented measure of the level of service [32]. The *instantaneous* travel time of a given road segment is defined by Eq. (6.7) on page 107 which is an estimate for the actual travel time of a single driver. Moreover, the *cumulative* travel time of all simulated vehicles is defined by the respective number of vehicles on the simulated road section, integrated over time (cf. Chap. 6 for details). Note that

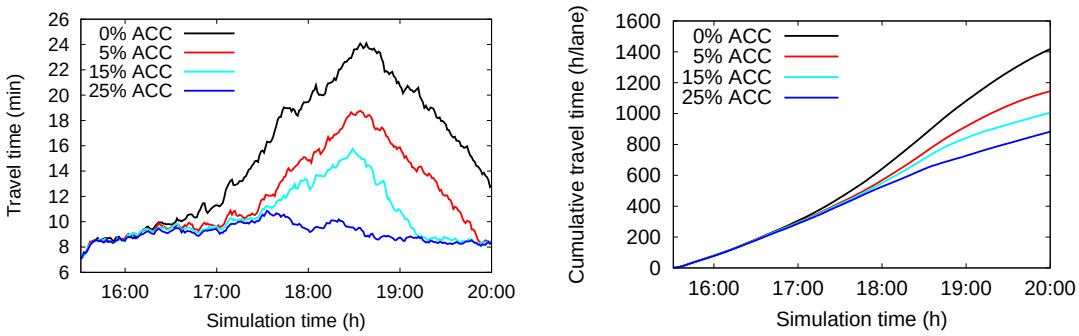

Figure 8.7: Instantaneous and cumulative travel times for different ACC equipment levels. The instantaneous travel time reflects the strong effect of a traffic breakdown on individual drivers, while the cumulative travel time indicates the impact of congestion on the overall system. During the peak of traffic congestion, the travel time is approximately tripled compared to the travel time under free flow conditions (approximately 8 min). A proportion of 25% ACC vehicles prevents the traffic breakdown completely.

$\tau_{\text{inst}}(t)$ mainly reflects the perspective of the drivers, while the cumulative travel time is a performance measure for the overall system.

Figure 8.7 displays the instantaneous and cumulative travel times for the simulation runs shown before in Fig. 8.6. Obviously, the breakdown of the traffic flow has a strong effect on the travel time. For example, the cumulative travel time without ACC vehicles amounts to about 1400 h per lane, whereas the scenario with 25% ACC vehicles results only in approximately 850 h/lane. Therefore, the traffic breakdown leads to an increase of the overall travel time by 60% compared to free flow conditions. As in the on-ramp scenario, the travel time of individual drivers at the peak of congestion (i.e., at $t \approx 18{:}45$ h) is even tripled when compared with the situation without congestion. The time series of the instantaneous travel times indicate that an increased ACC proportion delays the breakdown of traffic flow. Even for 5% ACC vehicles, the onset of traffic congestion is shifted by 20 min when compared with the traffic breakdown at $t \approx 17{:}00$ h in the scenario without ACC vehicles.

The results in Fig. 8.7 demonstrate that both the instantaneous and the cumulative travel time are sensitive measures for the impact of traffic congestion and, thus, the level of service. In contrast to other macroscopic quantities such as traffic flow or average velocity, the travel time sums up over *all vehicles* in the simulation and weights their influence directly in terms of the travel time. As shown in our simulations, even a slightly increased capacity due to the traffic-adaptive driving strategy of a small fraction of ACC-equipped vehicles can have a significant positive impact on system's performance.

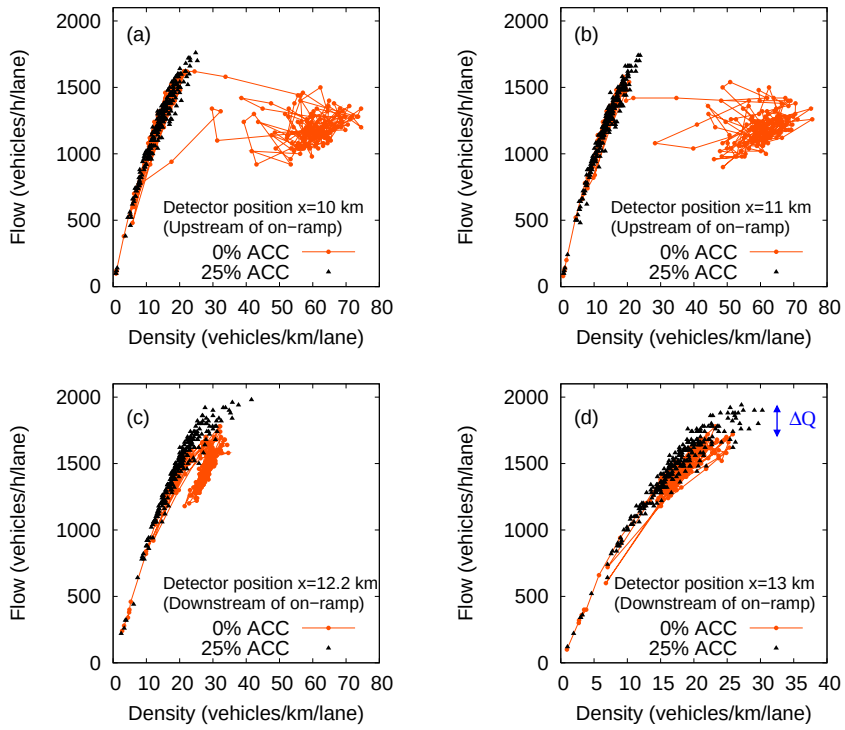

Figure 8.8: Flow-density relations of 1-min data for several cross-sections up- and downstream of an on-ramp located at $x = 12\,\text{km}$. Results of the simulations without ACC vehicles are directly compared with results for an ACC equipment level of 25%. Due to the local increase of capacity by the ACC driving strategy, the latter can practically avoid a traffic breakdown.

Flow-density relations: Let us additionally study the spatiotemporal traffic dynamics by investigating flow-density data. In order to facilitate a direct comparison with the data collected from double-loop detectors, we have applied the same data aggregation technique by introducing 'virtual detectors' mimicking real-world cross-sectional measurements (cf. Chap. 6). We have recorded the traffic flow Q and the mean velocity V within 1-min sampling intervals. Furthermore, we have determined the density ρ via the hydrodynamic relation $Q = \rho V$. All quantities are averaged over the three lanes of the simulated road section. Figure 8.8 shows the resulting flow-density relations for several cross-sections located up- and downstream of the on-ramp. For direct comparison, we have displayed the data of the simulations of Fig. 8.6 with an ACC proportion of 25% and without ACC vehicles in the same plots.

Upstream of the bottleneck (see Fig. 8.8a and b), the flow-density data show a branch of free traffic flow $Q \approx V_0\rho$ for densities $\rho < 30\,\text{veh/km/lane}$ (with an average free speed of $V_0 \approx 90\,\text{km/h}$) and a widely scattered area of congested traffic for $\rho > 30\,\text{veh/km/lane}$. In addition, Fig. 8.9 depicts data from detectors together with the equilibrium flow-density relation of cars and trucks, i.e., their *fundamental diagrams* (cf. Sec. 2.3 on page 20). Since

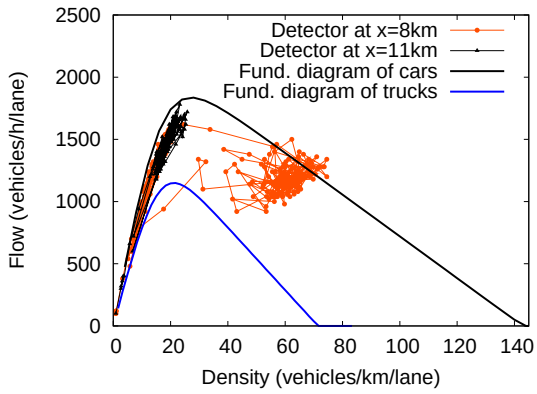

Figure 8.9: Flow-density data from a simulation without ACC vehicles together with the equilibrium flow-density curves (*fundamental diagrams*) for cars and trucks used in the simulations. The detector data points in the simulation are shifted towards the equilibrium curve of cars because the proportion of trucks is notably smaller than the one of cars.

the proportion of trucks is significantly smaller than those of cars, the detector data points are shifted towards the equilibrium curve of cars.

The data of the detectors located downstream (Fig. 8.8c and d) of the on-ramp show that the maximum flow in free traffic has been increased in the simulation scenario with 25% ACC vehicles when compared with the simulation without ACC-equipped vehicles. The increase ΔQ is achieved by the improved driving strategy in the traffic state 'bottleneck' (which increases the maximum throughput) and the 'downstream' state when leaving the jam (which increases the outflow from traffic congestion). Consequently, the breakdown of traffic flow is retarded (or even avoided) and the increased outflow (i.e, the *dynamic capacity*) leads to a faster relieve of traffic congestion. Note that, in Chap. 9, we will systematically investigate both of these capacities, relevant for characterizing the traffic dynamics in free and congested traffic.

8.3 Simulations with an Uphill Gradient Bottleneck

Let us now investigate a traffic scenario with an uphill gradient, which represents a *flow-conserving* bottleneck. As in the previous Sec. 8.2, we have simulated a freeway section of 15 km length with 3 lanes. The uphill region with a gradient slope is modeled by locally increasing the safety time headway parameter by 40% for all vehicles in a range of 1000 m around the bottleneck location at $x = 12.5$ km, with smooth linear transitions over 300 m. Again, we have used the empirical detector data from the German freeway A8 East from Munich to Salzburg (Austria) as time-dependent upstream boundary conditions (see Fig. 8.5 on page 130).

Figure 8.10 shows the spatiotemporal dynamics of the lane-averaged velocity for various proportions of ACC vehicles. The simulation scenario without ACC vehicles shows a traffic breakdown at $t \approx 16{:}30$ h at the upstream front of the uphill bottleneck at $x = 12$ km because of the increasing traffic volume during the rush-hour. The other diagrams of Fig. 8.10 show the simulation results for an increasing ACC proportion. Increasing the proportion of ACC vehicles applying the traffic-adaptive ACC driving strategy reduces traffic congestion significantly. An equipment level of 30% ACC vehicles avoids a traffic breakdown in this scenario completely.

For purpose of comparison with the findings in the previous section, let us also consider the travel time as important variable for a user-oriented level of service [32]. As indicated in Fig. 8.11, a breakdown of traffic flow has a strong effect on travel times. For example, the cumulative travel time without ACC vehicles amounts to about 1400 h/lane, whereas the scenario with 30% ACC vehicles results in approximately 1000 h. Therefore, the traffic breakdown leads to an increase of the overall travel time by 40% compared to free flow conditions. In comparison, the travel time of individual drivers at the peak of congestion (i.e., at $t \approx 18{:}45$ h) is even tripled when compared with the uncongested situation. Increasing the proportion of ACC vehicles reduces the travel times significantly due to the reduction in the lengths of the traffic jam.

These results are similar to the simulations for an on-ramp bottleneck studied in the previous Sec. 8.2. Therefore, we have shown that a vehicle-based ACC concept, which dynamically increases the *local* capacity near the bottleneck, is applicable to different kinds of bottlenecks such as an on-ramp or an uphill gradient.

We have chosen the rush-hour scenario in order to demonstrate the qualitative difference between free and congested traffic conditions, i.e., to reveal the maximum impact of an traffic-adaptive driving strategy. As shown by means of simulations, the overall traffic dynamics, particularly the travel times, are not significantly affected by ACC vehicles under free flow conditions. In contrast, under congested conditions (significantly after the time of break down), the proposed concept has a significant positive influence, because it

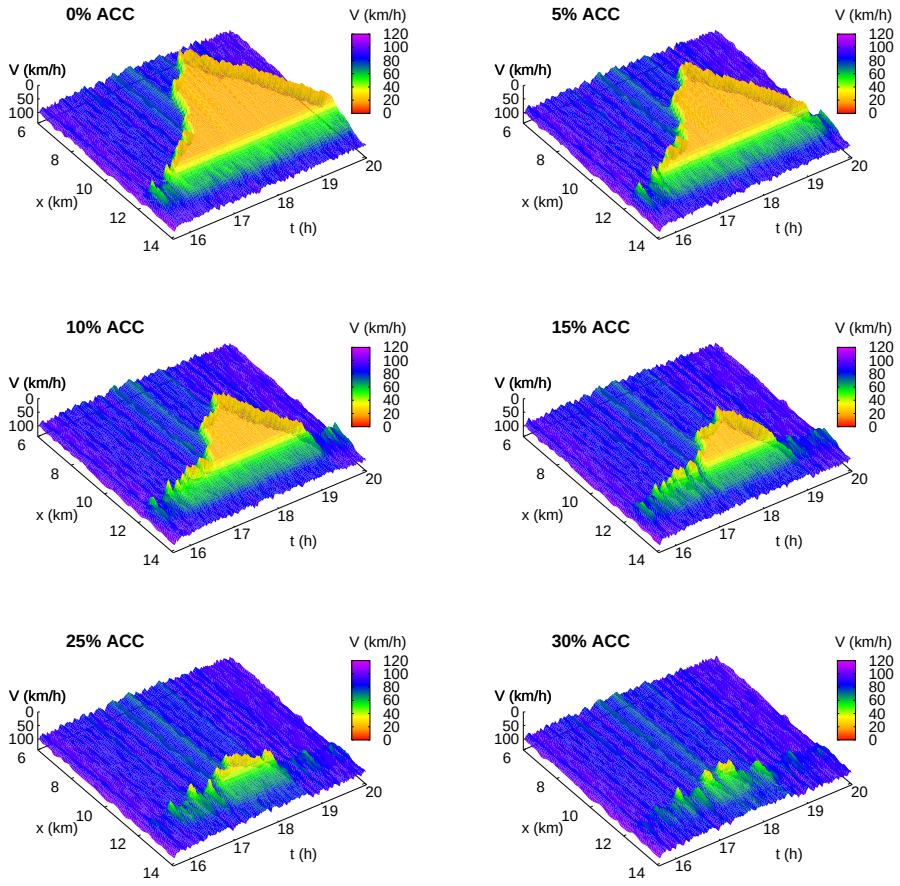

Figure 8.10: Spatiotemporal traffic dynamics upstream of an uphill gradient located between $x = 12\,\text{km}$ and $x = 13\,\text{km}$, for different proportions of ACC vehicles. The diagrams represent the lane-averaged velocity for a three-lane freeway upside down. In the simulations, the inflow at the upstream boundary is specified according to empirical 1-min detector data during an evening rush-hour, see Fig. 8.5. Increasing the proportion of ACC vehicles applying the traffic-adaptive ACC driving strategy can reduce traffic congestion significantly.

is designed to increase the outflow from congested regions. As a consequence, it reduces both the maximum length of congestion and its duration in time.

Let us finally summarize the factors that contribute to an enhanced system performance with a relevant reduction of travel times:

- An increased percentage of ACC vehicles leads to a delay of the breakdown of traffic flow. The reason is that the traffic-adaptive driving strategy of ACC systems is designed to increase the maximum free flow and, thus, to *'fill the capacity gap'* at the bottleneck. In Chap. 9, we will systematically investigate this relationship.

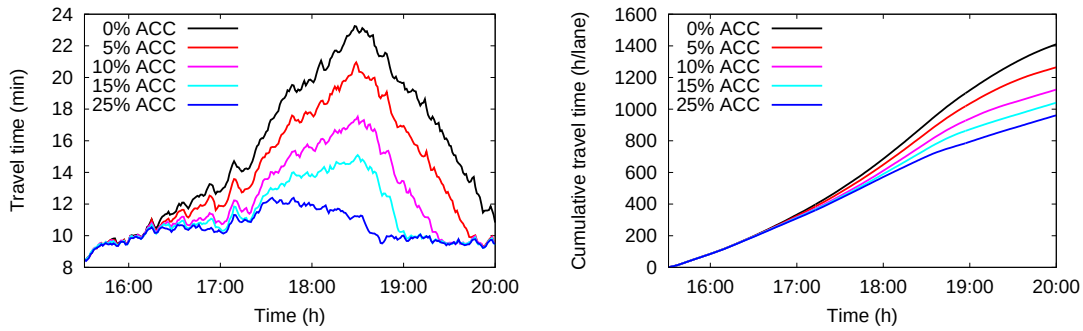

Figure 8.11: Current and cumulative travel times for different ACC equipment levels corresponding to simulations of a three-lane freeway with an uphill gradient, see Fig. 8.10. The left diagram shows the strong effect of a traffic breakdown on the resulting travel times, while the cumulative travel time indicates the impact of congestion on the overall system.

- A delayed onset of traffic congestion results in a significantly reduced maximum queue length, given the same inflow further upstream. Note that we treated the traffic demand at the upstream boundary as a constant (external) parameter.
- A reduced queue length leads, in turn, to an earlier dissolution of the traffic jam. Moreover, an increase of the outflow at the downstream end of the queue improves its dissolution.

8.4 Detection of Dynamic Congestion Fronts by Inter-Vehicle Communication

As already discussed in Sec. 7.4, the information about *temporary* bottlenecks, e.g., accidents or dynamic (i.e., moving) congestion fronts cannot be estimated without delay by local measurements only. A possible solution to this problem is the use of inter-vehicle communication (IVC) which is widely regarded as a promising concept for a fast transmission of information between vehicles. It implies applications for improved traffic safety and advanced driver information systems [140, 103, 104, 134, 136, 137]. In contrast to conventional communication channels which operate with a *centralized* broadcasting concept via radio or mobile-phone services, IVC is designed as a *local service* based on the Dedicated Short Range Communication (DRSC) standard [144], enabling data transmission at a frequency of 5.8 GHz. These devices broadcast messages which are received by all other equipped vehicles within a *limited broadcasting range* $r_{\max}$. As IVC message transmission is not controlled by a central station, no further communication infrastructure is needed. For example, wireless local-area networks (WLAN) have already shown their suitability for IVC with typical broadcasting ranges of $200-500\,\mathrm{m}$ [108, 93, 138]. In addition, short-range broadcasting technology also allows for an integration of the additional feature of a vehicle-infrastructure communication, using stationary senders ('roadside units') as illustrated in Fig. 8.12.

In general, there are two strategies, how a message can be transported upstream via IVC: Either a message 'hops' from an equipped car to a subsequent equipped car within the same driving direction (*'longitudinal hopping'*) or the message is transmitted to an IVC-equipped vehicle of the other driving direction which transports the message upstream and delivers it back by broadcasting it to cars of the original driving direction (*'transversal hopping'* or *'store-and-forward'*), cf. Fig. 8.12. The problem of the longitudinal hopping process is that it does not work well for low equipment rates due to the limited broadcasting range $r_{\max}$ [103]. A concept using IVC for traffic-state detection must therefore tackle the problem that both the required transport distances into upstream direction and the distances between two equipped vehicles are typically larger than the broadcasting range. The transversal hopping mechanism overcomes this problem by using vehicles of the opposite driving direction as relay stations. Hence, it is even capable of a reliable and fast information propagation in the cases of low equipment levels (some percent of the vehicle fleet).

Figure 8.13 shows the probability distribution for successful message propagation according to simulations of a typical traffic situation (with an overall traffic density of $\rho = 29$,veh./km in each direction and an average velocity of $V \approx 85\,\mathrm{km/h}$). The numerical results agree well with the theoretical expectations based on analytical calculations (for details and

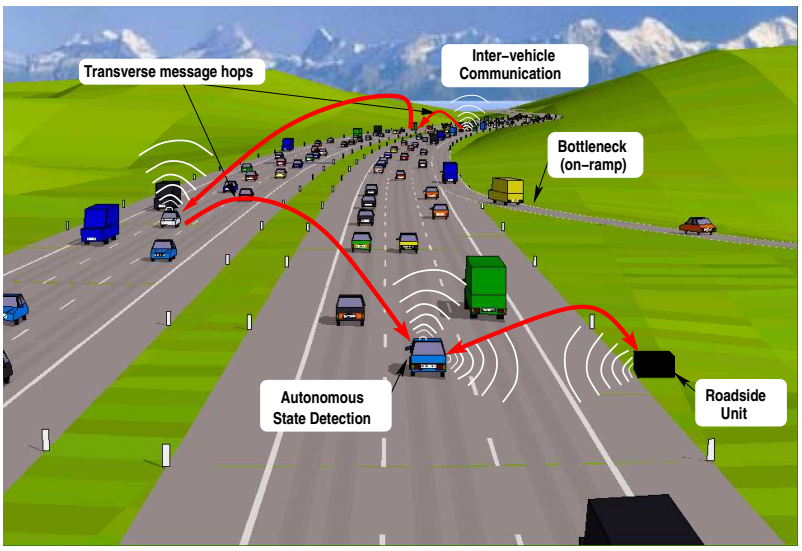

Figure 8.12: Illustration of various local and non-local data sources for vehicle-based traffic state detection. In particular, traffic-related messages can be propagated by inter-vehicle communication: Broadcasted messages can either be received by a subsequent car via 'longitudinal hopping' or may be picked up by a transmitter car in the opposite driving direction via 'transversal hopping'. In the latter case, the message travels with the transmitter upstream until it is delivered back to the original driving direction by a further transversal hop. Furthermore, equipped vehicles can communicate with stationary senders ('roadside units') along the freeway.

the derivation of the analytical results, see Ref. [103]). For example, even for an ACC proportion of $\alpha = 5\%$, 80% of the messages have been transmitted to equipped vehicles at a location at least $r_u = 1\,\mathrm{km}$ upstream within a time interval of approximately $t \leq 60\,\mathrm{s}$. The reason for the robustness of the message propagation statistics is that the frequency for encountering another equipped vehicle in the opposite driving direction (even in the case of a low equipment rate) is relatively high because the vehicles in the opposite directions move with a large relative velocity. In contrast, the gaps between equipped vehicles within the same driving direction do not change significantly over time which results in a low *connectivity* for the longitudinal message hopping process in the case of low equipment levels.

For purpose of demonstration, let us now simulate the whole chain of message propagation by means of IVC:

1. The generation of traffic-related messages by individual vehicles,
2. the transmission of up-to-date information in upstream direction using transversal message hopping via the opposite driving direction and
3. the receipt of the messages for predicting the future traffic situation further downstream.

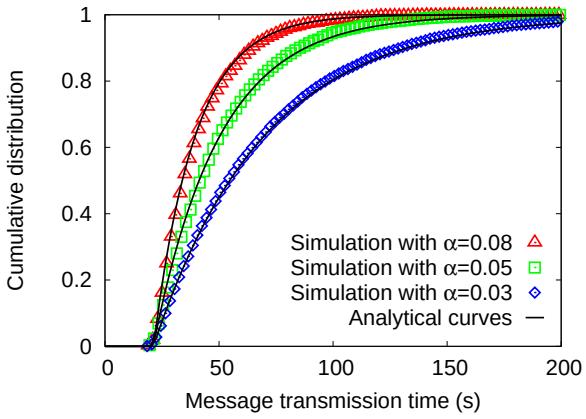

Figure 8.13: Cumulative distributions of transmission times for various equipment rates α via inter-vehicle communication with a broadcasting range $r_{\max}$ of 250 m and a minimum propagation distance r_u of 1 km. Symbols correspond to simulation results and solid curves to analytical results [103]. The analytical results were well reproduced by explicit simulations of the transversal message hopping processes. By using the equipped vehicles of the opposite driving direction as transmitter cars, the message propagation is fast and reliable. For example, 80% of the messages have been transmitted to equipped vehicles at least $r_u = 1$ km upstream within approximately 60 s even for an ACC proportion of $\alpha = 5\%$.

The simulation is based on a small fraction (3%) of vehicles equipped with IVC. Note that the provision of non-local information can be used to improve the autonomous traffic state detection proposed in Sec. 7.3.

The presented microscopic traffic simulator (cf. Chap. 6) simulates two independent freeways in opposite direction and generates the underlying vehicular dynamics as illustrated in Fig 8.12. We consider a scenario with an assumed fraction of only 3% communicating vehicles. Each equipped vehicle detects jam fronts and generates traffic-related messages based on the locally available floating car data. In order to this end, the simulation software has been extended by a 'message pool module' which organizes the book-keeping of message broadcast and reception between equipped cars within a limited broadcasting range $r_{\max}$. In Fig. 8.14, we have set $r_{\max} = 10$ m for purpose of illustration. As the routing in this system is obviously given by the two traffic streams in opposite directions, no further rules are necessary for modeling the message exchange process.

The resulting trajectories of equipped vehicles in both driving directions together with the generation of messages and their reception by a considered vehicle are illustrated in Fig. 8.14. There, a temporary road blockage triggered a stop-and-go wave reflected by horizontal trajectory curves in one driving direction, while the traffic flow in the opposite driving direction was free. When cars encountered the propagating stop-and-go wave, they started to broadcast messages about the detected position and time of the upstream jam front and the following downstream jam front. The event-driven messages were received

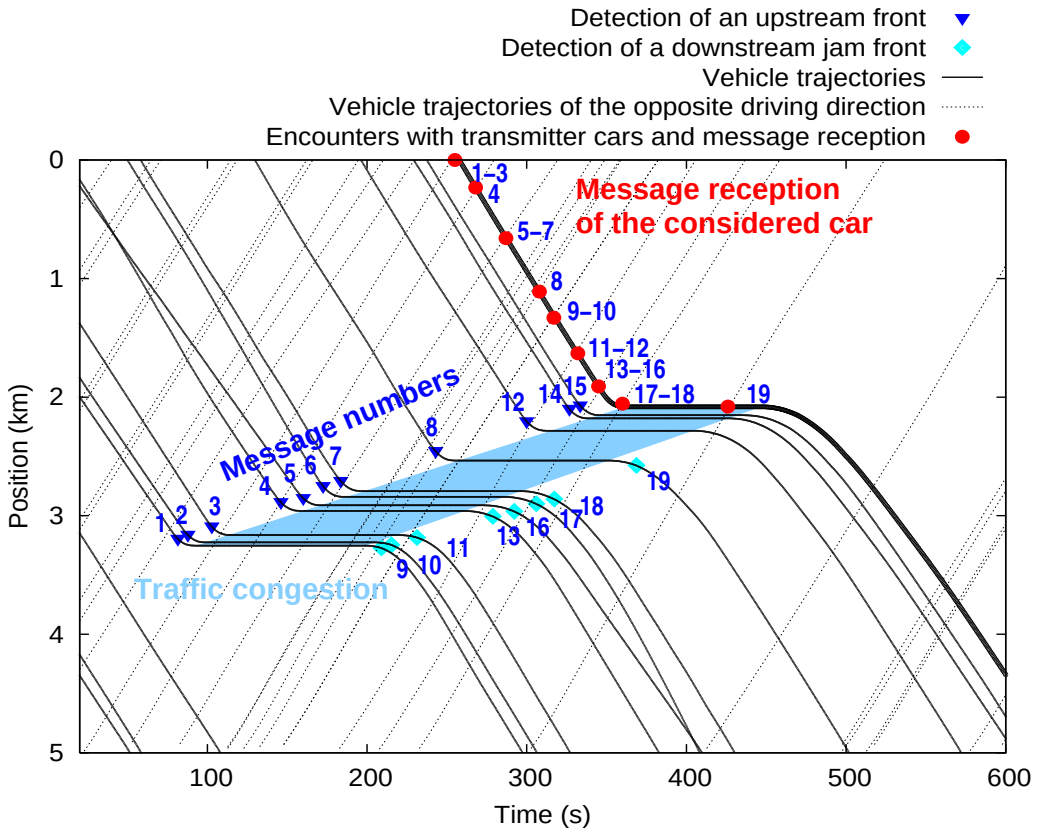

Figure 8.14: Space-time diagram of the simulated traffic scenario. The trajectories of the 3% IVC-equipped vehicles are displayed by solid or dotted lines, depending on the driving direction. The vehicles in the other driving direction serve as transmitter cars for the message propagation, using the transversal hopping mechanism. For purpose of illustration, a small broadcasting range has been chosen. A temporary road blockage triggers a stop-and-go wave indicated by horizontal trajectory slopes in one driving direction. When cars reach the front of a moving jam, they broadcast messages containing the detected position and time, both for the upstream jam front and the following downstream jam front. The generated messages marked by numbers. They are received some time later by the considered vehicle further upstream (thick solid line). The trajectories of the subsequent vehicles of the considered car are not shown. The crossing trajectories of equipped vehicles (e.g., in the upper-left corner of the diagram) reflect passing maneuvers due to different desired velocities.

and carried forward by vehicles in the other driving direction via the transversal hopping mechanism. Eventually, the messages are received by equipped vehicles further upstream.

As shown in Fig. 8.14, the considered vehicle received the first message about the upcoming traffic congestion already 2 km before reaching the traffic jam. Further received messages from other equipped vehicles could be used to confirm and update the traffic situation further downstream. Thus, based on a suitable prediction algorithm, each equipped vehicle could autonomously forecast the moving jam fronts by extrapolating the spatiotemporal information of the messages. In the considered simulation scenario, the upstream jam

fronts were very accurately predicted with errors of ±50 m already 1 km ahead of the jam, while the errors for the predicted downstream jam amounted to ±100 m. Obviously, the quality of the jam-front anticipation improves with the number and the timeliness of the incoming messages. More details about the used prediction algorithm can be found in Ref. [104].

Finally it should be mentioned that the received and interpreted information about the upcoming traffic situation cannot only be used for an improved autonomous detection, but also offers promising possibilities for advanced traveler information systems. Interestingly, in a survey among approximately thousand Dutch motorists, about 90% of the drivers declared that they would appreciate information about the downstream traffic conditions such as congestion, road works, etc. [127].

9 Influence of the ACC Equipment Level on Traffic Capacities

In this chapter, the impact of a systematically increasing proportion of ACC-equipped vehicles on the variables relevant for the traffic performance will be investigated. In free flow, the *maximum throughput* is determined by the maximum flow obtained until the traffic flow breaks down, while in congested traffic it is given by the *dynamic capacity* (i.e., the downstream outflow from a traffic jam). These capacities will be studied in Secs. 9.1 and 9.2. In Sec. 9.3, the cumulative travel time will be considered. Furthermore, the influence of the heterogeneity of the vehicle fleet and the influence of the λ-factors of the proposed driving strategy matrix will be analyzed. Throughout this chapter, we will consider a similar simulation scenario as in Sec. 8.2, with a two-lane freeway and an on-ramp serving as bottleneck. Since the considered quantities result from traffic simulations, a statistical method has been developed that evaluates the gradual change in the ACC equipment level together with the variation in the traffic quantities observed in the simulations. The corresponding smoothing method is based on weighted linear regression and documented in App. A on page 165.

9.1 Maximum Flow in Free Traffic

In this section, the system dynamics until the traffic flow breaks down will be examined in detail. In particular, we will focus on the influence of the external parameters such as the safety time gap T and the proportion of ACC-equipped vehicles. As shown in the previous Chap. 8, a traffic flow breakdown involves a significant reduction of traffic capacity which, in turn, leads to a drastic rise in travel times. Therefore, the traffic state 'passing a bottleneck section' in the ACC driving strategy matrix aims at an suppression (or, at least, at a delay) of the traffic flow collapse by lowering the time gap T in combination with an increased acceleration a (cf. Sec. 7.1). Note that a local reduction in the road capacity is the *defining characteristics* of a bottleneck. Consequently, the proposed driving style in the bottleneck section should lead to a *dynamic homogenization* of the road capacity, thereby allowing for a higher maximum flow at the bottleneck.

The relevant measure for assessing the efficiency of the proposed driving strategy 'passing a bottleneck section' is the maximum possible flow until the traffic flow breaks down. An

upper bound for this quantity C, defined as maximum number of vehicles per unit time and lane, is given by the inverse of the time gap, i.e., $C < 1/T$. According to Eq. (2.14), however, the theoretical maximum flow also depends on the effective length $l_{\text{eff}} = l + s_0$ (which is given by the vehicle length l plus the minimum bumper-to-bumper distance s_0) of a driver-vehicle unit, resulting in

$$Q_{\max}^{\text{theo}} = \frac{1}{T}\left(1 - \frac{l_{\text{eff}}}{v_0 T + l_{\text{eff}}}\right). \tag{9.1}$$

Note that this *static road capacity* $Q_{\max}^{\text{theo}}$ corresponds to the maximum of a *triangular* fundamental diagram. In the case of the IDM (with a finite acceleration), the theoretical maximum is even lower (cf. Sec. 2.3 on page 20). Generally, the *maximum free flow* $Q_{\max}^{\text{free}}$ before traffic breaks down is a *dynamic* quantity that depends on the traffic stability as well. Typically, this quantity is lower than $Q_{\max}^{\text{theo}}$. In summary, we have the inequalities

$$\frac{1}{T} > Q_{\max}^{\text{theo}}(\text{triangular}) \geq Q_{\max}^{\text{theo}}(\text{IDM}) \geq Q_{\max}^{\text{free}} \geq Q_{\text{out}}. \tag{9.2}$$

The *dynamic capacity* Q_{out} (which characterizes the outflow from a traffic jam) will be considered in the following Sec. 9.2. Note that the equality signs are only obtained in the limit of perfectly stable traffic.

In the following, we will therefore analyze the maximum free flow $Q_{\max}^{\text{free}}$ resulting from traffic simulations. To this end, we have considered a similar simulation scenario as in Sec. 8.2 with a two-lane freeway and an on-ramp serving as a bottleneck. The inflow at the upstream boundary was increased at a constant rate of $\dot{Q} = 700\,\text{veh/h}^2$, while the ramp flow was kept constant with 250 veh/h/lane. We have checked other progression rates as well, but only found a marginal difference. In order to determine the maximum free flow, we have used the following criterion: A traffic breakdown is detected if more than 20 vehicles on the main road are driving slower than a critical velocity $v_{\text{crit}} = 30\,\text{km/h}$. Once a traffic breakdown was detected, we used the flow of the actual 1-min aggregate of a 'virtual' detector (cf. Sec. 6.4) located downstream of the on-ramp for measuring the maximum flow.

Probability of traffic flow breakdown: The maximum free flow $Q_{\max}^{\text{free}}$ results from a measurement process which is based on 1-min aggregation intervals. As the underlying complex traffic simulation involves nonlinear models, discrete lane change decisions, random influences (such as the determining of the vehicle type while inserting at the upstream boundary etc.), it is expected that $Q_{\max}^{\text{free}}$ will vary stochastically leading to different results, also for identical boundary and initial conditions.[1] Consequently, we will consider

[1] Assuming a random seed of the computer's pseudorandom number generator.

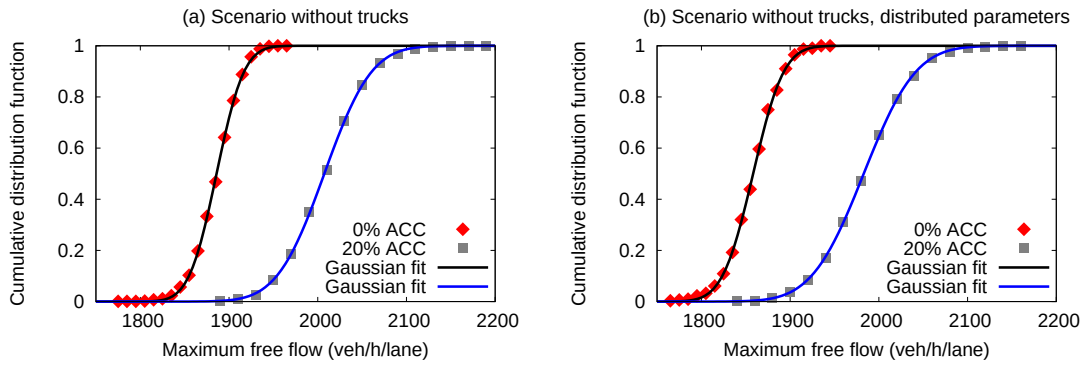

Figure 9.1: Traffic breakdown probability for an ACC equipment rate of 0% and 20%, respectively, and for different degrees of heterogeneity due to stochastically distributed parameters (see main text). The diagrams show the cumulative distribution functions of the maximum free flow $Q_{\max}^{\text{free}}$ resulting from 1000 simulation runs and numerical fits for the cumulative Gaussian distribution $N(x;\mu,\sigma^2)$. An increased proportion of ACC vehicles shifts the maximum flow at which the traffic flow breaks down to larger values. The fit parameters are listed in Table 9.1.

the maximum free flow as a *random variable* which reflects the probabilistic nature of a traffic flow breakdown also observed in real traffic [94, 58].

The statistical properties of $Q_{\max}^{\text{free}}$ have been investigated by means of repeated simulation runs. Overall, we have simulated eight scenarios. In order to begin with, we have varied the mixture of the vehicle fleet by considering different vehicle types. In particular, we have examined scenarios without trucks and with a total truck percentage of 10%, and, in addition, without ACC-equipped vehicles and with an ACC equipment level of 20%. Furthermore, we have considered *inter-driver variability* by assigning uniformly and independently distributed values to the parameters v_0, T, a and b of width $\pm 20\%$, i.e., the averages of the parameter values have been left unchanged and the width of the distributions have been set to 20% (i.e., the individual values vary between 80% and 120% of the average parameter value).

Each scenario has been simulated 1000 times to derive the statistical properties of the maximum free flow. The resulting cumulative distribution functions for $Q_{\max}^{\text{free}}$ reflecting the probability of a traffic flow breakdown are shown in Fig. 9.1 (for the scenarios without trucks) and in Fig. 9.2 (for the scenarios with 10% trucks).

As the measurement of the maximum free flow yields a distribution of finite variance and results from many stochastic contributions, the resulting cumulative distribution function follows the *Central Limit Theorem*[2] and can be fitted numerically with the integrated (and

[2]The Central Limit Theorem states that the sum of independent statistical variables will be approximately normally distributed if all variances are finite and if each individual variance is much smaller that the summed variance.

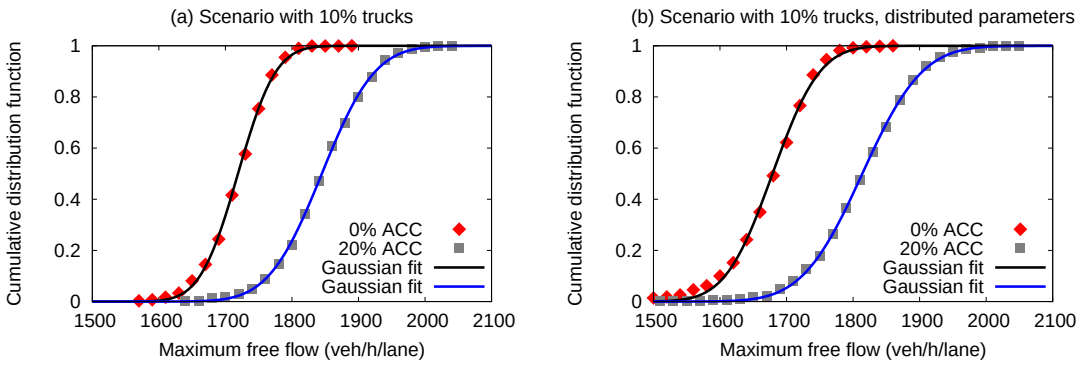

Figure 9.2: Cumulative distribution functions of the maximum free flow $Q_{\max}^{\text{free}}$ for similar traffic scenarios as shown in Fig. 9.1. In addition to the simulations shown in Fig. 9.1, we have considered 10% trucks. The numerically fitted parameters of the cumulative Gaussian distributions are listed in Table 9.1.

normalized) Gaussian function

$$N(x;\mu,\sigma^2) = \frac{1}{\sigma\sqrt{2\pi}} \int_{-\infty}^{x} e^{\frac{(t-\mu)^2}{2\sigma^2}}\, dt, \tag{9.3}$$

where μ is the mean value and σ^2 the variance. The fit parameters are listed in Table 9.1. The main results are as follows:

- The Gaussian distribution function $N(x;\mu,\sigma^2)$ fits the simulation results well (see Figs. 9.1 and 9.2). The maximum free flow $Q_{\max}^{\text{free}}$ follows a normal distribution. Thus, the fit parameters μ and σ^2 are good estimators for the mean value and the variance of the Gaussian distribution.

- In all considered scenarios, an increased proportion of ACC vehicles shifts the maximum throughput to a larger value μ. This shows the positive impact of the traffic-adaptive driving strategy on the traffic efficiency. In particular, the temporary change of the driving characteristics while passing the bottleneck helps to increase the maximum throughput by 6–8% in the considered scenarios (with an ACC equipment level of $\alpha = 20\%$). Note that we will furthermore investigate this performance increase as a function of the equipment level α below.

- The considered traffic scenarios show different degrees of heterogeneity, i.e., mixtures of various vehicle types (cars and trucks, equipped with ACC system or not). Moreover, v_0, T, a and b are stochastically distributed as mentioned above. An increase in the degree of heterogeneity leads to larger fluctuations in the traffic flow which, in turn, results in a larger variation σ of the random variable $Q_{\max}^{\text{free}}$ and also

Simulation scenario	ACC fraction	μ/(h/lane)	σ^2/(h/lane)^2
0% trucks	0% ACC	1887	35^2
0% trucks	20% ACC	2007	59^2
10% trucks	0% ACC	1719	63^2
10% trucks	20% ACC	1845	89^2
0% trucks, distr. parameters	0% ACC	1858	38^2
0% trucks, distr. parameters	20% ACC	1983	65^2
10% trucks, distr. parameters	0% ACC	1679	79^2
10% trucks, distr. parameters	20% ACC	1814	100^2

Table 9.1: Parameters of the cumulative Gaussian distribution $N(x;\mu,\sigma^2)$ for different simulation scenarios shown in Figs. 9.1 and 9.2. The Gaussian distributions have been numerically fitted to the data for the maximum free flow $Q_{\max}^{\text{free}}$ resulting from 1000 simulation runs. An increase in the degree of heterogeneity (due to different types of vehicles or stochastically distributed parameters) results in a larger variation σ of flow at which traffic breaks down.

to a slightly reduced mean value. Note that $Q_{\max}^{\text{free}}$ varies even in simulations with identical cars which can be associated with deterministic chaos [106].

- As the consideration of ACC-equipped vehicles with their adaptive (i.e., *time-dependent*) parameter choice increases the level of heterogeneity in a significant way, the variation σ is increased compared to the values without ACC vehicles. This finding makes it clear that the impact of ACC-equipped vehicles on the traffic dynamics must be studied with a realistic level of heterogeneity, e.g., in a multi-lane freeway scenario considering cars and trucks. Otherwise, the assessment of ACC systems may erroneously lead to negative results.

Maximum free flow as a function of the ACC proportion: Let us now investigate the maximum free flow as a function of the ACC proportion α. To this end, we have gradually increased α in a range from 0 to 50% using the same scenario as described above. In Fig. 9.3, the result of each simulation run is represented by a point. As expected from our previous findings, the values of the maximum free flow $Q_{\max}^{\text{free}}$ vary stochastically. For better illustration, we have therefore developed a *weighted linear regression method* which calculates the expectation value and the standard deviation as a *continuous* function of α. This allows for an intuitive assessment of the variation by means of a 'variation band' around the expectation value. The only parameter of this evaluation procedure is the

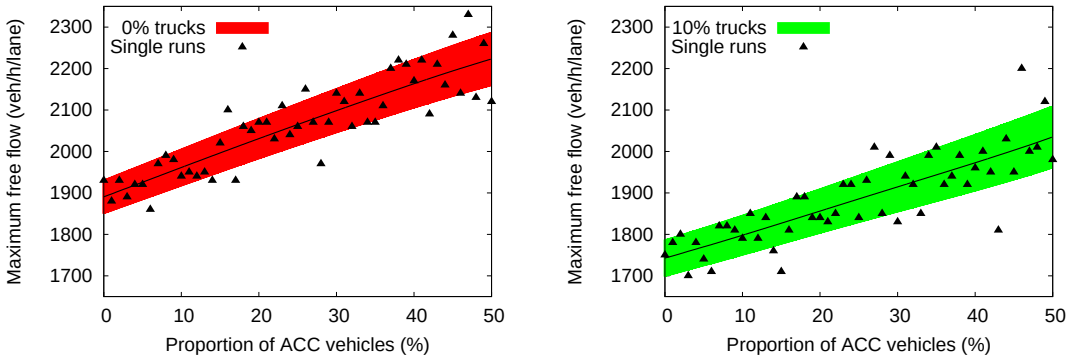

Figure 9.3: Maximum free flow as a function of the ACC percentage α without (left) and with 10% trucks (right). The single simulation runs are depicted by symbols and vary stochastically. Using a linear regression with a local weight of width $\delta = 0.1$ (cf. App. A), we have calculated the expectation value and the variation of the simulation data. Note that the genuine cumulative distributions for $\alpha = 0\%$ and $\alpha = 20\%$ are shown in Fig. 9.1.

width δ of the smoothing kernel. Here, we have used $\delta = 0.1$. The numerical method is explained and derived in detail in App. A on page 165.

Figure 9.3 shows the results for a traffic scenario without trucks and a scenario with 10% trucks. As expected, increasing the proportion of trucks with their higher safety time gap T (cf. Table 8.1) reduces the maximum free flow. However, the average value of the maximum free flow increases with growing ACC equipment level α. The gain in the maximum free flow is basically proportional to α.

Figure 9.4 summarizes the simulation results for various truck proportions (0%, 10% and 20%). In addition, we have plotted the *relative increase* $q_{\max}^{\text{free}}$ of the maximum flow compared to the situation with non-equipped vehicles,

$$q_{\max}^{\text{free}} = \frac{Q_{\max}^{\text{free}}(\alpha)}{Q_{\max}^{\text{free}}(0)}. \tag{9.4}$$

This quantity allows for a direct comparison between the different simulation scenarios. For example, the gain in the maximum free flow varies between approximately 16% and 21% for a given ACC portion of 50%. For an ACC portion of 20%, the maximum free flow increases by approximately 7%. Although this appears to be a small rise, one should not underestimate its impact on the resulting traffic dynamics. As we have shown in the previous Chap. 8 in different simulation scenarios, an ACC proportion of 20% prevents (or, at least, delays) the traffic flow breakdown. Comparing this to the reference simulation without 'intelligent' ACC-equipped vehicles, individual travel times vary by a factor of 2 or 3! As the gain in the maximum free flow is basically proportional to α, the quantity $q_{\max}^{\text{free}}/\alpha$ is approximately constant and describes the *relative gain* in $Q_{\max}^{\text{free}}$ per ACC portion

α. The values for the simulations shown in Fig. 9.4 are in the range between 0.32 and 0.42.

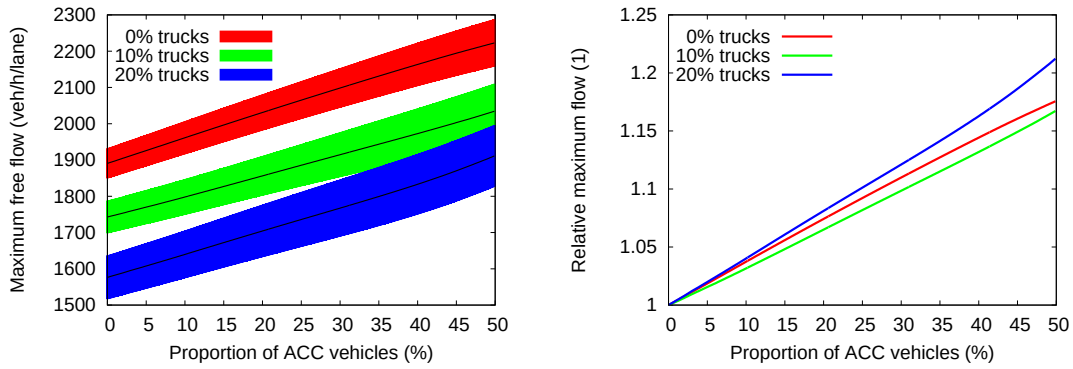

Figure 9.4: Left: Maximum free flow until traffic breaks down as a function of the ACC proportion for various truck fractions. Increasing the portion of trucks decreases the maximum free flow. (Right) Relative growth according to Eq. (9.4) allowing for a direct comparison. Note that even a rise of the maximum free flow by 5% (e.g., for an ACC portion of 15%) leads to a large reduction in individual travel times as demonstrated in Chap. 8.

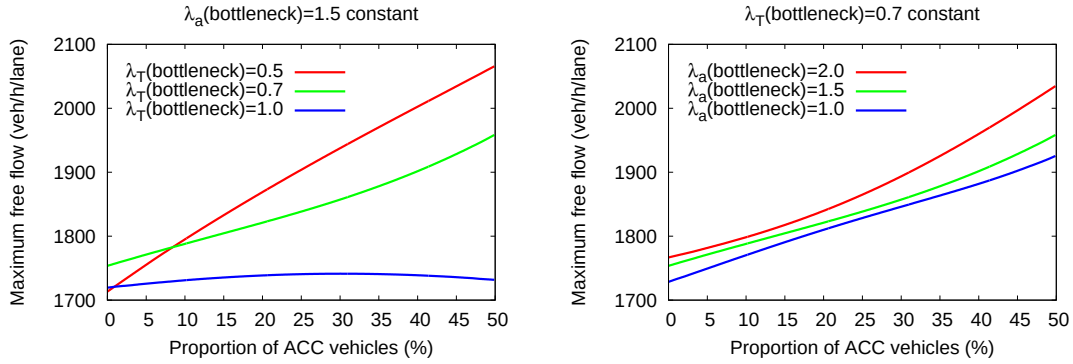

Figure 9.5: Maximum free flow as a function of the ACC proportion for the simulation scenario with 10% trucks. The ACC driving strategy in the 'bottleneck' state is varied: The left diagram shows various settings for λ_T while keeping the maximum acceleration a constant. The right diagram refers to simulations with varying λ_a for a constant time gap T. With increasing ACC penetration rate, the crucial influence of the time gap becomes obvious while the impact of a in the 'bottleneck' state does not influence the maximum free flow in a relevant way. Note that the green lines (derived with the numerical method documented in App. A) correspond to the default settings of the proposed strategy matrix listed in Table 7.1.

Maximum flow for different driving strategy parameters: Besides the proportions of trucks and ACC-equipped vehicles, the traffic performance is influenced by the multiplication factors λ of the ACC driving strategy in the bottleneck state. In particular, the

maximum free flow depends on the modification λ_T of the time gap and λ_a of the maximum acceleration in the 'bottleneck' state. As 'default' values, we have chosen $\lambda_T^{\text{bottle}} = 0.7$ and $\lambda_a^{\text{bottle}} = 1.5$ (see Table 7.1 on page 118). While considering the aforementioned simulation scenario with 10% trucks, we have varied these driving strategy parameters in the 'bottleneck' state. The results shown in Fig. 9.5 are as follows:

- The safety time gap T has a strong impact on the maximum free flow as displayed in the left diagram of Fig. 9.5 (while keeping $\lambda_a^{\text{bottle}} = 1.5$ constant). A further reduction of the ACC time gap by $\lambda_T = 0.5$ leads to a stronger increase in the maximum free flow when considering a growing ACC proportion compared to the 'default' setting $\lambda_T = 0.7$. Note that this is consistent with Eq. (9.1). Moreover, the modification of a alone while keeping T unchanged ($\lambda_T = 1$) does not improve the maximum free flow.
- The maximum acceleration a has clearly a smaller effect on the maximum free flow than T, as displayed in the right diagram of Fig. 9.5. While keeping λ_T constant, different settings such as $\lambda_a = 1$, 1.5 or 2 do not change the resulting maximum free flow in a relevant way. So, the throughput can only be efficiently increased in combination with smaller time gaps (corresponding to lower values of T), but not by increasing the acceleration a alone.

Maximum free flow as a function of the time gap: Finally, we have investigated the influence of the time gap T which is according to Eq. (9.1) the most important parameter for the *static* road capacity. The simulation results for the *observed* maximum free flow $Q_{\text{max}}^{\text{free}}$ as a function of the safety time gap T are shown in Fig. 9.6. We have simulated a homogeneous vehicle fleet consisting of cars only. The single simulation runs are depicted by symbols. For a concise illustration of the stochastic variations, we have again used the weighted linear regression method, with a width of $\delta = 0.3$ (cf. App. A).

Obviously, the maximum free flow decreases with increasing T. The dynamic quantity $Q_{\text{max}}^{\text{free}}$ remains always lower than the theoretical capacity $Q_{\text{max}}^{\text{theo}}$ given by Eq. (9.1) which is only obtained for perfectly stable traffic and serves as a theoretical upper bound (cf. Eq. (9.2)). Furthermore, as the difference between $Q_{\text{max}}^{\text{theo}}$ and the dynamic maximum free flow increases for lower values of T, one finds that smaller values of T reduce stability as well.

9.2 Dynamic Capacity after a Traffic Breakdown

Let us now investigate the system dynamics *after* a breakdown of traffic flow. Traffic jam formation is determined by the *difference* of the upstream inflow Q_{in} (i.e., the traffic

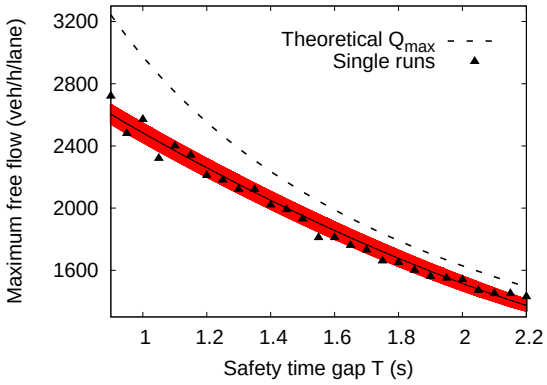

Figure 9.6: Maximum free flow as a function of the safety time gap T which is the most important parameter for the maximum throughput. The static maximum road capacity according to Eq. (9.1) is indicated by dashed lines. The maximum free flow as a *dynamic* quantity is typically lower, but depends on the traffic stability as well. Symbols indicate results of single simulation runs, while the solid lines correspond to averages over several simulations and the associated bands to plus/minus one standard deviation.

demand) and the outflow Q_{out} from the downstream jam front (i.e., the head of the queue) which is also called 'dynamic capacity'. On the long run, a given traffic demand can only be influenced by a different route choice of the drivers in the network which is not within the scope of this investigation. Consequently, a short-term reduction of traffic congestion can only be obtained by increasing the outflow. This is the intention of the proposed traffic state 'downstream jam front' (cf. Sec. 7.1) which aims at a brisk leaving of the queue by increasing the maximum acceleration a and decreasing the safety time gap T of the ACC system.

In this section, we investigate the impact of such an ACC driving strategy on the *dynamic capacity* which is the crucial quantity during traffic congestion [18]. We use the same simulation setup (of a two-lane freeway with an on-ramp) as in the previous section. Whenever a traffic breakdown was provoked by the increasing inflow, we aggregate the flow data of the 'virtual detector' 1 km downstream of the bottleneck within an interval of 10 minutes.

Dynamic capacity as a function of the ACC proportion: Figure 9.7 shows the resulting dynamic capacity for a variable percentage of ACC vehicles in a scenario without trucks and in a scenario with 10% trucks. Single simulation runs are depicted by symbols, while the average and the variation band were calculated from the scattering values with the weighted linear regression method using a width $\delta = 0.1$ (cf. App. A). As intended by the proposed driving strategy of ACC-equipped vehicles, the dynamic capacity increases with growing ACC equipment rate.

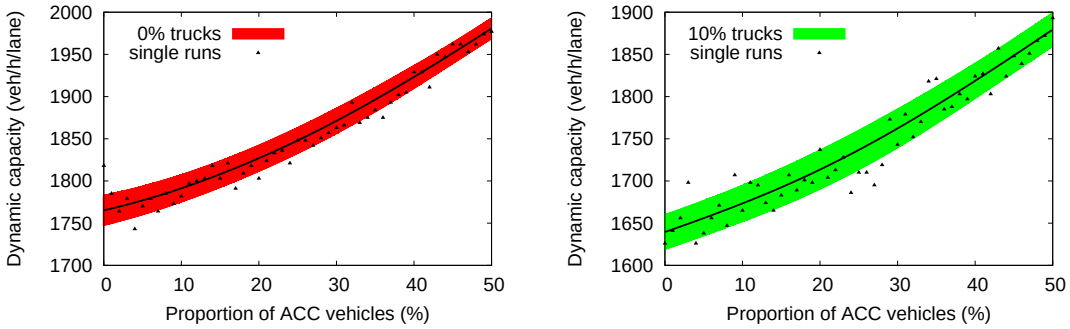

Figure 9.7: Dynamic capacity as a function of the percentage of ACC vehicles (left) without trucks and (right) with 10% trucks. The outflow from a traffic jam increases with a growing number of ACC-equipped vehicles. The single simulation runs (symbols) have been smoothed with the weighted linear regression method using a width of $\delta = 0.1$.

Figure 9.8 compares the results for different truck proportions. Furthermore, we have defined the *relative increase of the dynamic capacity* $q_{\text{out}}(\alpha)$ by a given ACC equipment level α by

$$q_{\text{out}}(\alpha) = \frac{Q_{\text{out}}(\alpha)}{Q_{\text{out}}(0)}. \tag{9.5}$$

The relative increase of q_{out} for $\alpha = 50\%$ is between 12% and 16% and therefore somewhat lower than the increase of the maximum free capacity (cf. Sec. 9.1). Interestingly, the dynamic capacity does not increase linearly as the measured maximum free capacity displayed in Fig. 9.3 on page 148, but faster. Consequently, the relative increase $q_{\text{out}}(\alpha)$ grows for higher ACC equipment rates α. This can be understood by an 'obstruction effect' caused by slower accelerating drivers (in particular, trucks) which hinder faster (ACC) vehicles.

Furthermore, we can compare the maximum free capacity $Q_{\text{max}}^{\text{free}}$ displayed in Fig. 9.3 on page 148 with the dynamic capacity Q_{out} which is lower than $Q_{\text{max}}^{\text{free}}$. The difference between both traffic quantities is referred to as *capacity drop*.[3] We found that the values of the relative capacity drop are between 5 and 15% for various simulations.

Dynamic capacity for different driving strategy parameters: The increase of the dynamic capacity is based on the proposed driving strategy for the traffic regime 'downstream jam front'. The ACC-equipped vehicles increase their maximum acceleration a in combination with a decrease in time gap T (cf. Table 7.1 on page 118). In Fig. 9.9, simulation results are shown for varying relative factors λ_a and λ_T for the relevant traffic state 'down-

[3] The capacity drop is the crucial quantity determining the performance (loss) in throughput of the freeway transportation system. Note that the capacity drop accounts for the persistence of traffic jams once the traffic flow has broken down. Realistic values for the capacity drop are between 5% and 20% [55, 14, 19, 62].

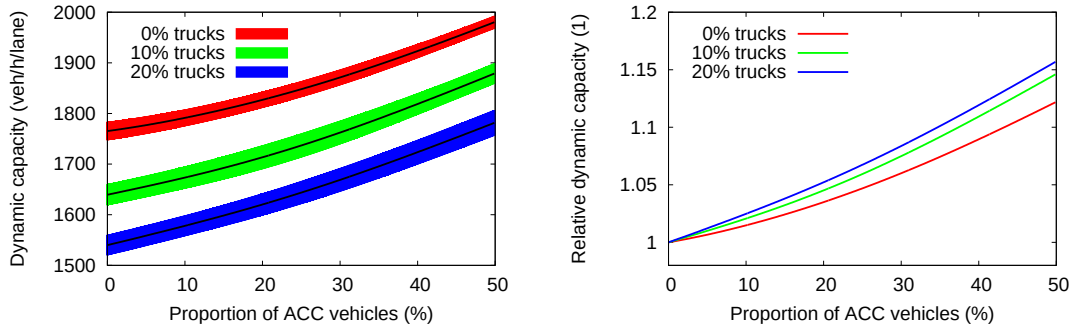

Figure 9.8: Left: Dynamic capacity as a function of the ACC equipment level for different truck proportions. The ACC driving strategy associated with the traffic state 'downstream jam front' increases the dynamic capacity for a growing ACC equipment rate. The lower acceleration capability of trucks (cf. Table 8.1) leads to a lower dynamic capacity. Right: The relative increase in the outflow is in the range of 12-15% for a considered ACC portion of 50%.

stream jam front' (using a scenario with 10% trucks). The default values $\lambda_a^{\text{down}} = 2$ and $\lambda_T^{\text{down}} = 0.5$ correspond to the results shown before in Fig. 9.7. The simulation results show that the dynamic capacity is only increased in a relevant way by adapting *a and T* simultaneously.

Dynamic capacity of moving downstream jam fronts: Empirical investigations have shown that most of the traffic flow breakdowns are located at permanent bottlenecks and the downstream jam front is almost always located ('pinned') at the bottleneck [102, 73].[4] Based on the assumption that the position of a stationary bottleneck (e.g., an on-ramp) is provided by a digital map database, the autonomous detection algorithm reliably estimates the downstream jam front leading to an increase of the dynamic capacity as shown before. Nevertheless, as mentioned in Sec. 7.4, non-stationary (i.e., *moving*) jam fronts are more difficult to detect on the basis of local information only. We will explicitly investigate this using the simulation scenario depicted in Fig. 8.14 on page 141: A triggered stop-and-go wave is moving in upstream direction. The downstream jam front is detected using the criterion (7.7) on page 120 for the velocity. Due to the required smoothing of the data input using the exponential moving average, the autonomous real-time detection of the 'downstream' state is delayed by the order of the relaxation parameter τ, i.e., 5 s in our case.

This delay makes the adaptation to the traffic state ineffective, as illustrated in Fig. 9.10 for various truck fractions: The simulation results clearly show that the dynamic capacity is *not* increased by the ACC driving strategy in this case. Of course, a more sensitive detection of the downstream front, e.g., by lowering the relaxation time τ of the real-time

[4] Further examples from traffic simulations are shown in Figs. 8.6 on page 131 or 8.10 on page 136.

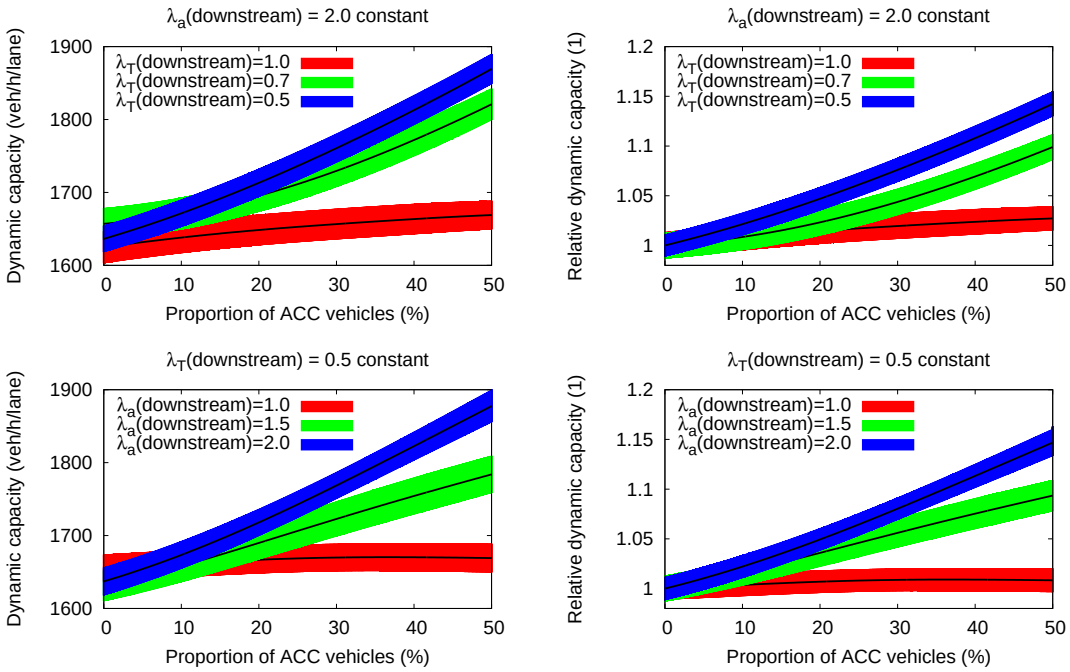

Figure 9.9: Dynamic capacity for various parameter values of the ACC adaption in the 'downstream jam front' traffic state. Top: Variation of the relative time gap λ_T keeping the relative maximum acceleration constant ($\lambda_a = 2$). Bottom: Variation of λ_a while keeping λ_T constant at the default value 0.5. The simulation results show that the dynamic capacity is increased in a relevant way only by adapting a in combination with T.

EMA (7.2), would allow for an increase of the dynamic capacity within certain limits, but this would also lead to significantly more detection errors. Consequently, it is crucial for an efficient relieve of traffic congestion to switch to the 'downstream' driving regime in an anticipative and timely way. The required non-local information about moving jam fronts can be provided by inter-vehicle communication (as we have explicitly evaluated in Sec. 8.4) or communication with a roadside unit (RSU). Obviously, it would be ideal for a fast and reliable detection of the traffic state to 'fuse' several data sources.

9.3 Cumulative Travel Time as Function of the ACC Proportion

In this section, we will finally study the overall performance and robustness of the presented simulation results as a function of the ACC equipment rate. To this end, we consider the cumulative travel time which has turned out to be a sensitive performance measure (cf. Sec. 8.2). Again, we have used the scenario with a two-lane freeway and an on-ramp in order to perform simulation runs. We have varied the ACC proportion between 0 and 50%.

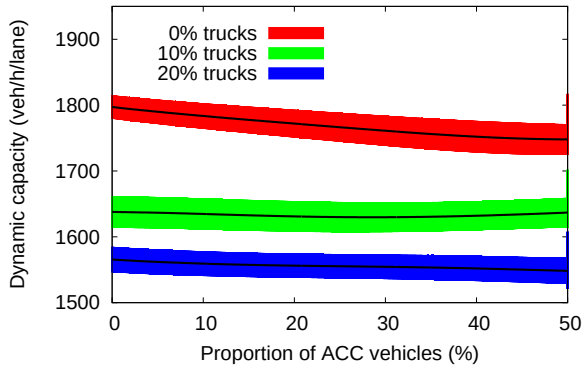

Figure 9.10: Dynamic capacity for a simulation scenario with a *moving* downstream jam front (stop-and-go wave, cf. Fig. 8.14) for three different truck percentages. The autonomous on-board detection of the regime 'downstream jam front' based on local information only does *not* increase the dynamic capacity because of time delays in the real-time averaging. A timely detection of non-stationary jam fronts requires non-local information, e.g., provided by inter-vehicle communication or communication with roadside units (cf. Sec. 8.4).

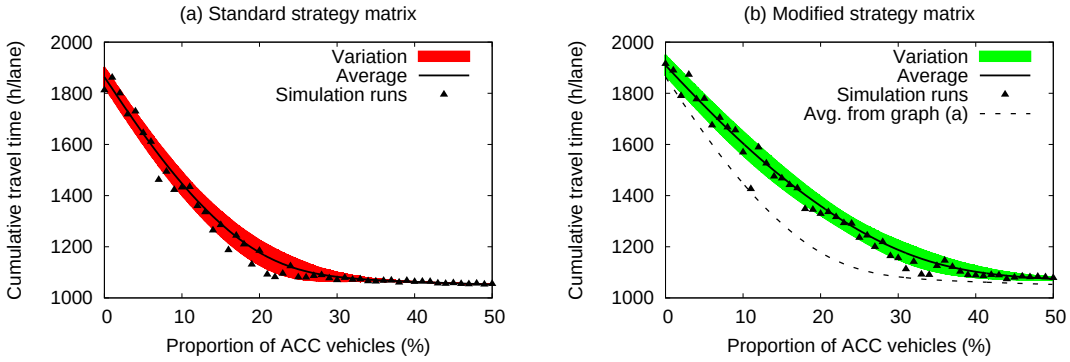

Figure 9.11: Cumulative travel time as a function of the proportion of ACC vehicles for the 'standard' ACC strategy matrix documented in Table 7.1 on page 118 (left diagram) and for a strategy matrix with the settings $\lambda_T = 0.8$ and $\lambda_a = 1.2$ in the 'bottleneck state' and $\lambda_T = 0.7$ and $\lambda_a = 1.5$ in the 'downstream state' (right). Both simulated systems show a similar monotonous reduction until the value corresponding to free traffic is reached. Due to the smaller modification factors λ, the strategy matrix in the right diagram is less effective in avoiding traffic jams. However, the reductions are significant in both cases even for low ACC equipment rates.

The resulting realizations of the cumulative travel time for the simulation runs are shown in the diagrams of Fig. 9.11. Additionally, we have calculated the average travel time and its variation by the weighted linear regression with a smoothing width of $\delta = 0.05$ with respect to the proportion of ACC vehicles (cf. App. A). The left diagram in Fig. 9.11 refers to an ACC strategy matrix with 'standard' factors λ as listed in Table 7.1 on page 118. The right diagram shows simulation results for an ACC strategy matrix with

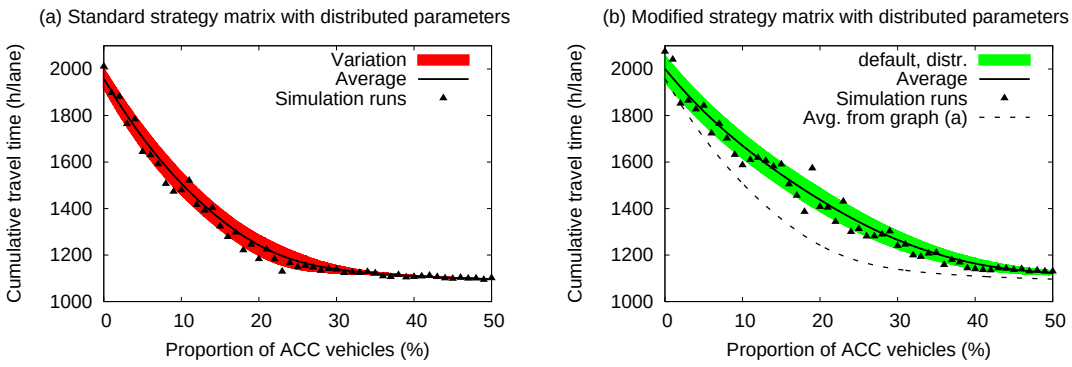

Figure 9.12: Cumulative travel time as a function of the proportion of ACC vehicles with uniformly distributed driving parameters of width ±20% (see main text), but for otherwise identical simulation scenarios as in Fig. 9.11.

lower modification factors, namely, $\lambda_T = 0.8$ and $\lambda_a = 1.2$ for the 'bottleneck state' and $\lambda_T = 0.7$ and $\lambda_a = 1.5$ for the 'downstream state'.

Both diagrams show an analogous system behavior: The cumulative travel times decrease *consistently* when increasing the fraction of ACC vehicles, until the travel time for free traffic is reached. For the 'standard' ACC strategy, the traffic jam is completely avoided for ACC percentages of at least 25%. As expected, the decrease of the cumulative travel time is shifted towards higher ACC equipment rates in the case of a lower relative reduction λ_T of the ACC time gap, given the same boundary conditions. However, the traffic flow breakdown is avoided in the latter case for ACC proportions $\geq 35\%$. Remarkably, in both scenarios the cumulative travel time already decreases significantly in both scenarios with low equipment levels of only a few percent of ACC vehicles.

Furthermore, the influence of the stochasticity is significantly lower than in the measurements of capacities: For example, in Fig. 9.11(left), the average cumulative travel time drops by one standard deviation per 1% of ACC vehicles, while the corresponding capacities in Fig. 9.3 increase by one standard deviation per 5–10% of ACC vehicles. This demonstrates the robustness of the proposed vehicle-based strategy for a better traffic performance. Moreover, the high effectiveness even for low equipment levels promises good chances for a successful introduction of such driving assistance systems.

Finally, we have investigated the effects of statistically distributed parameters in order to represent individual differences in the driving behavior. Figure 9.12 shows simulation results with uniformly distributed values of the parameters v_0, T, a and b within an interval of ±20% (cf. Sec. 9.1). Similar to the simulations shown in Fig. 9.11, we have obtained a reduction of traffic congestion with an increasing ACC proportion which demonstrates the robustness of the proposed adaptive driving strategy with respect to heterogeneous

driver-vehicle behavior. The somewhat higher total travel times compared to simulations without statistically distributed parameters can be explained by the fraction of vehicles driving with a lower desired velocity v_0 or a larger time headway T. Note that, for dense traffic conditions, these slower vehicles also determine the overall driving behavior of driver-vehicle units with higher desired velocities.

10 Summary and Conclusions

As mentioned in the Introduction, adaptive cruise control (ACC) systems are already available on the market. They will spread in the future and the next generation of ACC systems is expected to extend their range of applicability to low speeds including 'follow-to-stop' functionality. This offers a realistic perspective for a decentralized traffic optimization strategy based on ACC-equipped vehicles [61]. However, up to now, ACC systems were mainly optimized for the user's driving comfort and safety. With a growing level of distribution, the design of ACC systems which also consider their impact on traffic dynamics will be crucial for the next ACC generations.

In order to ensure that ACC systems are implemented in ways that improve, rather than degrade, traffic conditions, we have proposed an extension of ACC systems towards a *traffic-adaptive cruise control* with an actively jam-avoiding driving strategy. The main innovation of the proposed driver assistance system is the extension of ACC systems (which implement a continuous adaptation of the acceleration in response to the leading vehicle) by an additional adaptation of the driving characteristics on a longer time scale, based on information about the traffic situation. While the default operational state in free traffic conditions corresponds to conventional ACC systems, the ACC control parameters are automatically switched, according to the detected traffic situation, in a way that preserves the individual settings and preferences of the different drivers. Since, most of the time, the system operates in states corresponding to a conventional ACC system, the driving comfort is only minimally diminished in favor of a higher traffic capacity.[1]

In order to resolve conflicting objectives between driving comfort and road capacity, the strategy is based on a finite set of five different traffic situations which are associated with different sets of ACC control parameters. This concerns the safety time gap, the maximum acceleration and the comfortable deceleration. Based on local information, the proposed system autonomously detects the traffic state and automatically adapts its driving style, i.e., the acceleration characteristics of the underlying ACC system.

A concrete specification of a traffic-adaptive cruise control system has been presented. The three components of the concept are the ACC itself, implemented in form of a car-following model, an algorithm for the automatic real-time detection of the traffic situation based on

[1] In other (more abstract) words, the proposed concept of a traffic-adaptive driving strategy can be considered as a novel and independent dimension in the functional state space of any ACC system with a sufficiently large parameter space that allows for the implementation of different driving strategies.

local information and a 'strategy matrix' which connects the driving characteristics (i.e., the parameters of the ACC system) to the actual traffic conditions. We integrated the components in the microscopic simulation framework presented in Chap. 6 for simulating 'in-the-loop' the autonomous traffic-state detection (which requires surrounding traffic as input) and the feedback of a given proportion of ACC-equipped vehicles on the overall traffic dynamics.

As the impact of future driver assistance systems on the collective characteristics of traffic flow can only be evaluated by means of computer simulations, the presented traffic simulations serves as a first 'proof of concept'. Our simulations were based on the assumption that only a small fraction of ACC vehicles adapts their parameters according to the proposed *jam-avoiding* driving strategy, while the manually controlled vehicles applied a time-independent, constant driving style. The simulations of a freeway section with an on-ramp showed that, reducing the time gap locally when passing a bottleneck and at the downstream front of a traffic jam is sufficient to obtain efficient traffic flow, while most of the time our proposed ACC system is driving with natural parameter settings. As a bottleneck is *defined* by a local capacity reduction, the automatic reduction of the time gap of ACC-equipped vehicles at a bottleneck manages to fill the 'capacity gap', at least partially. As a consequence, the probability of a traffic flow breakdown is reduced. Together with an increased dynamic capacity, this results on average in reduced queue lengths during congested traffic. For example, the simulations of the afternoon rush-hour on a German autobahn demonstrate that even an ACC equipment level of 10% improves the traffic flow quality and reduces the travel times of the drivers in a relevant way.

We showed that the presented approach is also applicable to other kinds of bottlenecks such as an uphill gradient. Furthermore, the presented results are largely independent of details of the model and the heterogeneity of driver-vehicle units. Moreover, the traffic-adaptive ACC has significantly positive effects both for traffic demands at the brick of a breakdown and well beyond it. Our simulations showed that the proposed driving strategy increase both the *traffic stability* and the *dynamic capacity* (i.e., the outflow from congested traffic at the bottleneck which is typically lower than the maximum free flow). A reduction of this *capacity drop* is crucial for a faster relieve from traffic congestion. A systematic increase of the ACC equipment level for different simulation settings predicts a monotonous decrease of the cumulative travel time. Note that this is crucial for a gradual and successful introduction of the proposed 'intelligent' ACC system into the market.

A concrete vehicle implementation of a traffic-adaptive ACC-based system has already been presented by Volkswagen within the German research initiative INVENT. Current research focusses on the implementation of the autonomous detection of different traffic situations and transitions between driving strategies in real test vehicles. The ongoing exchange between traffic engineers and traffic modelers will hopefully improve both our

theoretical understanding and the applications for future advanced driver assistance systems.

Furthermore, the presented findings demonstrate the impact of the individual driver behavior on the overall traffic dynamics. This is also relevant for manual driving, because human drivers generally respond to the local traffic conditions as well [126]. For example, subconscious adaptation processes *decrease* the local capacity which has been interpreted as 'frustration effect' [122]. Consequently, it would be desirable to teach driver behaviors that are beneficial to the overall system (such as attentive driving at bottlenecks and prompt acceleration when leaving a jam) in driving lessons, in addition to established topics such as trainings in economic and safe driving.

It has pointed out that the autonomous detection algorithm of ACC vehicles can be improved by non-local information provided by inter-vehicle communication (IVC) and by communication with stationary roadside units which are both promising vehicle-based applications for wireless communication technologies and a vehicle-infrastructure integration in the context of Intelligent Transportation Systems (ITS). In order to evaluate these future application scenarios combining car with information technology, advanced simulation software will become more important as a tool in all stages of development. We have integrated a communication module into our microscopic traffic simulation software in order to simulate communication between vehicles. The software has been validated by comparing the simulated connectivity with analytical calculations for the message propagation probability. It has been shown that information about the position of jam fronts could be reliably distributed even for vehicle equipment rates as low as 3%. This result opens a promising perspective for advanced driver information services. The information can also be used to extend the functionality of today's ACC systems to *intelligent* assistance systems which use non-local data as well. First real-world applications will be demonstrated in the German ITS project Aktiv [150].

Appendix

A Data Smoothing with Weighted Linear Regression

When dealing with simulations, one often varies a single model parameter and plots it against a second quantity resulting from the simulation run. Frequently, the simulation result fluctuates because of stochastic elements in the model or in the initial and boundary conditions, or simply because of the sensitive dependence of the result on the parameters (*deterministic chaos* [106]). Since a single run takes a finite amout of time, it is disadvantageous to rerun the simulation frequently to derive the statistical properties of a quantity's variation. Furthermore, many simulation runs with the same parameters do not provide additional insights if the 'fluctuations' are mainly due to the sensitive dependence on varying parameter values. Here, we propose a statistical method that combines the gradual change in the independent model parameter x with the derivation of the variation in the resulting fluctuating quantity y without running multiple simulations for the same parameter value x. Applications of this smoothing method based on weighted linear regression are, e.g., shown in Chap. 9. Figures A.1 and A.2 below give further examples.

Suppose we are fitting n data points $\{x_i, y_i\}$, $i = 1, \ldots, n$ to a linear model with two parameters a and b,

$$\hat{y}(x) = \hat{y}(x; a, b) = a + bx. \tag{A.1}$$

A global measure for the goodness of fit is the sum of squared errors $y_i - \hat{y}(x_i)$, where the values y_i are measured, and the values x_i of the dependent variable are known exactly. The best-fitting curve for the *linear regression* can be obtained by the method of least squares, i.e., by minimizing the error function

$$\mathcal{F}(a, b) = \sum_{i=1}^{n} (y_i - a - bx_i)^2 \tag{A.2}$$

with respect to the fit parameters a and b. The solution of the system of linear equations is given by

$$b = b(\{x_i, y_i\}) = \frac{\langle xy \rangle - \langle x \rangle \langle y \rangle}{\langle x^2 \rangle - \langle x \rangle^2}, \tag{A.3}$$

$$a = a(\{x_i, y_i\}) = \frac{\langle x^2 \rangle \langle y \rangle - \langle x \rangle \langle xy \rangle}{\langle x^2 \rangle - \langle x \rangle^2}, \tag{A.4}$$

where the arithmetic average $\langle z \rangle$ of the measured data points $\{z_i\}$ is defined by

$$\langle z \rangle := \frac{1}{n} \sum_{i=1}^{n} z_i. \tag{A.5}$$

Let us now generalize the linear regression by using a *locally weighted average*

$$\langle z \rangle(x) := \sum_{i=1}^{n} w(x - x_i)\, z_i, \tag{A.6}$$

where the weights $w(x - x_i)$ are defined through a sufficiently localized function K:

$$w(x - x_i) = \frac{K(x - x_i)}{\sum\limits_{j=1}^{n} K(x - x_j)}. \tag{A.7}$$

As the expression (A.6) is evaluated locally for any value x, the dependence on x is transferred to the linear fit parameters (A.3) and (A.4) in addition to their dependence on the set of data points $\{x_i, y_i\}$, i.e.,

$$a(x) = a(x; \{x_i, y_i\}), \tag{A.8}$$

$$b(x) = b(x; \{x_i, y_i\}). \tag{A.9}$$

Therefore, the weighted linear regression based on weights centered at x' reads

$$\hat{y}(x, x') = a(x') + b(x')x. \tag{A.10}$$

For plotting y against x, the special case of centering the averages at $x' = x$ is relevant. With $a(x) = \langle y \rangle(x) - b(x)\, x$, we obtain

$$\hat{y}(x, x) = a(x) + b(x)\, x = \langle y \rangle(x). \tag{A.11}$$

Furthermore, the residual error $y_i - \hat{y}(x_i)$ is also weighted by the discrete convolution (A.6), resulting in

$$\sigma^2(x) = \sum_{i=1}^{n} w_i(x) \left[y_i - a(x) - b(x) x_i \right]^2. \tag{A.12}$$

Notice that the 'error band' $\sigma(x)$ describes the standard deviation of variations of the quantity y on length scales smaller than the width of the smoothing kernel K. For stochastic simulations, this is simultaneously an estimate of the fluctuations for given values of x.

In the following, we illustrate this method using a *Gaussian kernel* with the standard

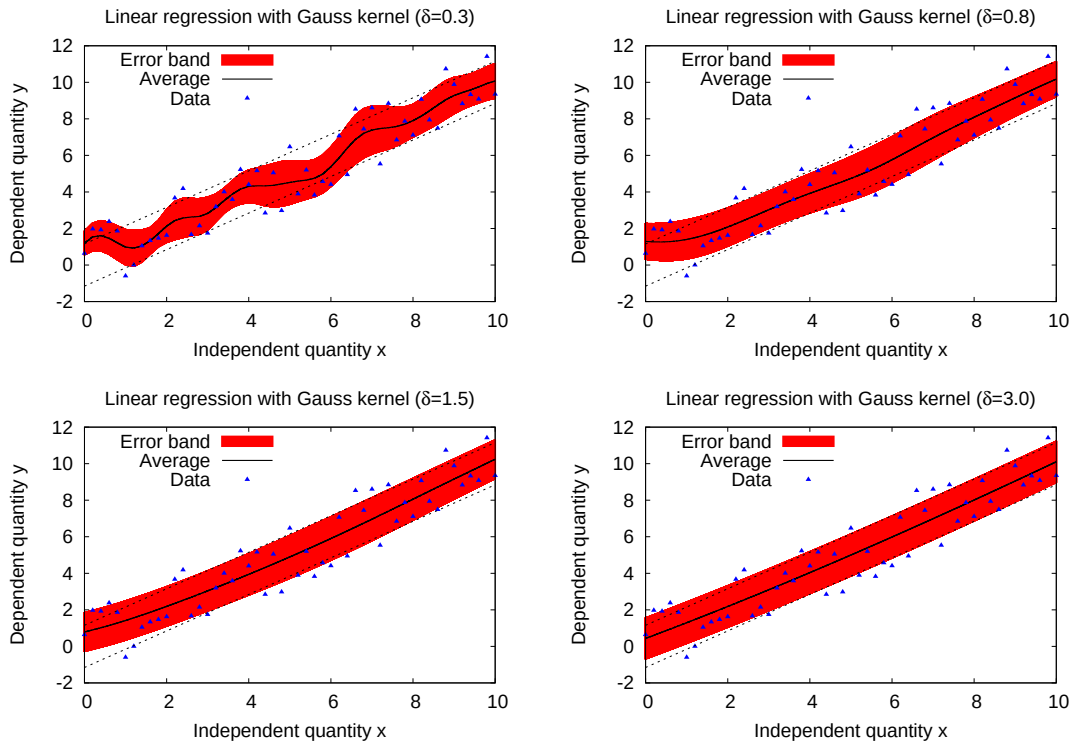

Figure A.1: Demonstration of the proposed weighted linear regression method: the discrete data set $\{x_i, y_i\}$ is generated with a linear trend and some noise with a standard deviation represented by dotted lines. The smoothing method calculates the locally fitted average trend and the variation denoted as 'error band'. The used Gaussian kernel contains only one single parameter, which is the width δ. This width is varied in the displayed graphs. The value $\delta = 3$ identifies the correct error band of $\pm\sqrt{4/3}$ almost exactly, but $\delta = 0.8$ yields acceptable error bands as well, while $\delta = 0.3$ is too sensitive to stochastic fluctuations.

variation δ as weight function[1],

$$K(x) = e^{-\frac{x^2}{2\delta^2}}. \tag{A.13}$$

Notice that the definition (A.7) of the weighted average does not require the weighting kernel to be normalized. The width of the Gaussian kernel δ is the only parameter of the numerical smoothing method. Note that, again, we obtain the common linear regression (A.1) in the limit $\delta \to \infty$.

In the following, we present the average $\langle y \rangle(x)$ according to Eq. (A.11) and the variation $\sigma(x)$ according to Eq. (A.12) for two examples. In Fig. A.1, the data set $\{x_i, y_i\}$ is generated by a linear function $y = x + \xi$ with uniformly distributed noise $\xi \sim G(-2, 2)$ and $x_i \in [0, 10]$. The width of the smoothing kernel determines how many neighboring data points are taken into account for a specific x. The graphs show the resulting fit functions

[1] A symmetric exponential $\exp(-|x|)$, a triangular function, or even a rectangular function could serve as weight function as well.

and the variations (errors) for $\delta = 0.3, 0.8, 1.5$, and 3.0. The variation of the data set (displayed as shaded 'error band' in each graph) is based on the local neigborhood. Note that this is a very efficient method to estimate statistical properties without carrying out repeated simulation runs with identical parameter settings. Particularly, the half-width of the error band is consistent with the true standard deviation $\sigma \approx \sqrt{\frac{4}{3}}$ and does not depend on δ, which would be the case if the error band was determined by the local variance $\left\langle (y - \langle y(x) \rangle)^2 \right\rangle (x)$.

In Fig. A.2, the underlying data set is generated by the s-shaped function $y = \tanh(x) + \xi$ with uniformly distributed noise $\xi \sim G(-0.4, 0.4)$ and $x \in [-5, 5]$. For $\delta = 0.5$, the linear regression is sufficiently localized to capture the s-shape trend of the data set. For $\delta = 2$, the smoothing interval is expanded, resulting in a primarily linear fit. Therefore, when dealing with nonlinear trends, the choice of the smoothing kernel width δ is a trade-off between smoothing fluctuations and capturing systematic local changes $\{x_i, y_i\}$. In any case, the error band $\sigma(x)$ directly gives the variation in the measurements *without* carrying out simulation runs with the same parameter settings repeatedly.

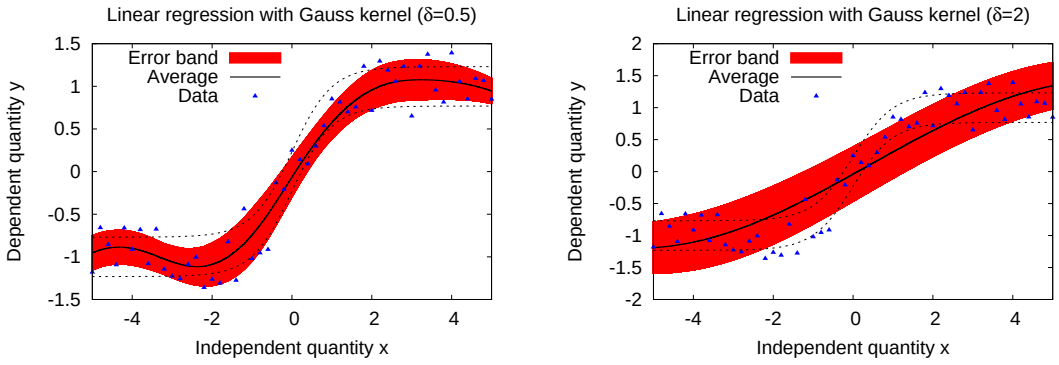

Figure A.2: Smoothed local (linear) trend and variation for synthetic data resulting from a tanh with additional noise. The standard deviation $\pm 0.4\sqrt{\frac{1}{3}}$ is plotted by dotted lines. The s-shaped curve is better captured by a more localized Gaussian kernel (width $\delta = 0.5$) compared to a broader smoothing width ($\delta = 2$). The data variation is depicted by the shaded 'error band' (A.12).

B The German Research Project INVENT

The German research initiative INVENT[1] was a four-year program running from 2001 till 2005. The project aimed at the development and deployment of novel technologies and traffic concepts for vehicle-based intelligent transportation systems (ITS). Several pilot applications and new functions for safer and more efficient future traffic systems were demonstrated. Moreover, the stakeholders also identified and established new technological standards.

INVENT continued previous cooperative projects in traffic research such as PROMETHEUS, MOTIV, and SANDY. The project was initiated and supported by the Federal Ministry for Research and Education (BMBF), which covered 45% of the total investments of 76 Million Euros. Apart from the big German automobile manufacturers, the project consortium also included companies from the sectors of telecommunication, information technology, electronics, and logistics. In addition to the industrial partners, research institutions and universities contributed to the projects as subcontractors. The Chair for Traffic Modelling and Econometrics of Dirk Helbing at Technische Universität Dresden contributed to the project as subcontractor of Volkswagen.

As illustrated in Fig. B.1, the project was divided into three research areas, with eight subprojects each: The project *Traffic Management in Transport and Logistics* designed, e.g., solutions for dynamic planning of courier service delivery routes by taking into account the current traffic situation. The project *Driver Assistance – Active Safety* focused on the development of a new generation of driver assistance systems using latest sensor technologies for driver information, but also for intervening in the drive train by automated braking and steering in emergency situations. For example, assistance systems for intersections, active pedestrian protection and lateral vehicle control were demonstrated.

The *Traffic Management 2010* subproject comprised sophisticated traffic management strategies for a new generation of navigation systems using machine intelligence and dynamic route guidance. Large-scale field tests and prototype applications were implemented in Magdeburg and Munich. To this end, data from, e.g., traffic signals, road induction loops, video monitoring, and floating car data were combined to obtain a reliable information basis.

[1] The abbreviation INVENT stands for 'Intelligenter Verkehr und nutzergerechte Technik', which is translated as 'intelligent traffic and user-friendly technology'.

Figure B.1: The research initiative INVENT was organized into three projects focusing on safety, traffic management, and logistics. These projects included eight subprojects each. The projects focused on the development and investigation of new technologies that will help to avoid accidents and reduce congestion. Parts of the thesis were developed in tight cooperation with Volkswagen within the subproject *Traffic Management 2010*. More information is provided on the website `www.invent-online.de`.

A more vehicle-based approach for an actively jam-avoiding strategy was considered in the subproject called 'Traffic Performance Assistance'.[2] The goal was to operate traffic flow more smoothly and to relieve traffic jams by means of advanced driver assistance systems. These future systems are designed to collect and combine data dynamically to reconstruct the actual traffic state. In addition, these assistance systems were considered to provide inter-vehicle communication (IVC), thus allowing to inform and warn subsequent vehicles. Hence, this subproject was intended as a platform for new applications of IVC technology. Together with the TU Dresden, Volkswagen demonstrated how this traffic information can be used for an anticipatory automated driving based on ACC systems [67]. The concept and an evaluation of the system benefits are presented in the second part of this thesis.

[2] In German: 'Verkehrsleistungsassistenz' (VLA).

C List of Symbols

Symbol	Unit	Annotation
ρ	1/km	Traffic density
Q	1/h	Traffic flow
V	m/s, km/h	Macroscopic average velocity
V_g	m/s, km/h	Average propagation velocity of stop-and-go waves
x_α	m	Longitudinal position of driver-vehicle unit α
l_α	m	Length of driver-vehicle unit α
v_α	m/s	Velocity of driver-vehicle unit α
$\dot{v}_\alpha$	m/s^2	Acceleration of driver-vehicle unit α, $\dot{v} := \frac{\mathrm{d}v}{\mathrm{d}t}$
Δv_α	m/s, km/h	Velocity difference of driver-vehicle unit α to leader
Δt	s	Numerical update time
δ		Width of the smoothing kernel of the weighted linear regression method (cf. App. A)
	Intelligent Driver Model (Chapters 2 and 3)	
v_0	m/s, km/h	Desired velocity
T	s	Parameter for the safety time gap
s_0	m	Minimum distance parameter
a	m/s^2	Parameter for the maximum acceleration
b	m/s^2	Parameter for the desired deceleration
$b_{\max}$	m/s^2	Maximum (physical) braking acceleration

Human Driver Model (Chapter 4)

Symbol	Unit	Annotation
T'	s	Reaction time
n_a	1	Number of anticipated vehicles
V_s	1	Relative distance error
r_c	1/s	Inverse time-to-collision error
τ_s, $\tau_{\Delta v}$	s	Perception error correlation times

Lane-Changing Model MOBIL (Chapter 5)

p	1	Politeness parameter
a_{thres}	m/s^2	Changing threshold parameter
a_{bias}	m/s^2	Bias for right lane
a_{thres}	m/s^2	Maximum safe deceleration

Traffic-Adaptive Cruise Control and Inter-Vehicle Communication (Part II)

λ_T	1	Relative time gap parameter
λ_a	1	Relative acceleration parameter
λ_b	1	Relative deceleration parameter
α	1	ACC proportion in traffic flow
r_{max}	m	Broadcast range for distributing messages
r_u	m	Minimum required distance of message propagation in upstream direction
τ	s	Relaxation time constant of the exponential moving average

D List of Abbreviations

Abbreviation	Annotation
ABS	Anti-lock braking system
ACC	Adaptive/Automatic/Advanced cruise control
ADAS	Advanced Driver Assistance System
AHS	Automated Highway System
DDE	Delay-differential equation
DSRC	Dedicated Short Range Communication
EMA	Exponential moving average
ESC, ESP	Electronic Stability Control, Electronic Stability Program
FC, FCD	Floating Car, Floating Car Data
GUI	Graphical user interface
GPS	Global Positioning System
HDM	Human Driver Model
IDM	Intelligent Driver Model
IVC	Inter-vehicle communication
ICT	Information and Communication Technology
ITS	Intelligent Transportation Systems (and Services)
LDW	Lane departure warning system
MOBIL	'Minimizing Overall Braking Induced by Lane Changes'
ODE	Ordinary-differential equation
OVM	Optimal Velocity Model
RSU	Roadside unit
WLAN	Wireless local-area networks
XML	Extensible markup language

Bibliography

[1] K. I. Ahmed (1999) Modeling drivers' acceleration and lane change behavior. Ph.D. thesis, Massachusetts Institute of Technology.

[2] M. Bando, K. Hasebe, K. Nakanishi, and A. Nakayama (1998) Analysis of optimal velocity model with explicit delay. *Physical Review E* 58, 5429.

[3] M. Bando, K. Hasebe, A. Nakayama, A. Shibata, and Y. Sugiyama (1995) Dynamical model of traffic congestion and numerical simulation. *Physical Review E* 51, 1035–1042.

[4] J. H. Banks (1999) An investigation of some characteristics of congested flow. *Transportation Research Record* 1678, 128–134.

[5] T. Bleile (1999) Modellierung des Fahrzeugfolgeverhaltens im innerstädtischen PKW-Verkehr. Dissertation, Universität Stuttgart.

[6] E. Boer (1999) Car following from the driver's perspective. *Transportation Research Part F: Traffic Psychology and Behaviour* 2, 201–206.

[7] M. Brackstone and M. McDonald, The microscopic modelling of traffic flow: Weaknesses and potential developments. In: D. E. Wolf, M. Schreckenberg, and A. Bachem (Editors), *Traffic and Granular Flow* (World Scientific, Singapore, 1996), pages 151–165.

[8] M. Brackstone and M. McDonald (1999) Car-following: A historical review. *Transportation Research Part F: Traffic Psychology and Behaviour* 2, 181–196.

[9] M. Brackstone, M. McDonald, and J. Wu, Lane changing on the motorway: Factors affecting its occurrence, and their implications. In: *Proceedings of the 9th International Conference on Road Transportation Information and Control* (Conference Publication No. 454, London, 1998), pages 160–164.

[10] W. Brilon and M. Ponzlet, Application of traffic flow models. In: D. E. Wolf, M. Schreckenberg, and A. Bachem (Editors), *Traffic and Granular Flow* (World Scientific, Singapore, 1996), pages 23–40.

[11] E. Brockfeld, R. D. Kühne, A. Skabardonis, and P. Wagner (2003) Toward benchmarking of microscopic traffic flow models. *Transportation Research Record* 1852, 124–129.

[12] E. Brockfeld, R. D. Kühne, and P. Wagner (2004) Calibration and validation of microscopic traffic flow models. *Transportation Research Record* 1876, 62–70.

[13] M. Cassidy and M. Mauch (2001) An observed traffic pattern in long freeway queues. *Transportation Research Part A: Policy and Practice* 35, 149–162.

[14] M. J. Cassidy and R. L. Bertini (1999) Some traffic features at freeway bottlenecks. *Transportation Research Part B: Methodological* 33, 25–42.

[15] D. Chowdhury, D. Santen, and A. Schadschneider (2000) Statistical physics of vehicular traffic and some related systems. *Physics Reports* 329, 199–329.

[16] B. Coifman, S. Krishnamurthy, and X. Wang, Lane-changing maneuvers consuming freeway capacity. In: S. Hoogendoorn, S. Luding, P. Bovy, M. Schreckenberg, and D. Wolf (Editors), *Traffic and Granular Flow '03* (Springer, Berlin, 2005), pages 3–14.

[17] C. Daganzo, *Fundamentals of Transportation and Traffic Operations* (Pergamon-Elsevier, Oxford, U.K., 1997).

[18] C. Daganzo, M. Cassidy, and R. Bertini (1999) Possible explanations of phase transitions in highway traffic. *Transportation Research Part B: Methodological* 33, 365–379.

[19] C. Daganzo, M. Cassidy, and R. Bertini (1999) Some traffic features at freeway bottlenecks. *Transportation Research Part B: Methodological* 33, 25–42.

[20] L. Davis (2002) Comment on "Analysis of optimal velocity model with explicit delay". *Physical Review E* 66, 038101.

[21] L. Davis (2003) Modifications of the optimal velocity traffic model to include delay due to driver reaction time. *Physica A* 319, 557–567.

[22] L. Davis (2004) Effect of adaptive cruise control systems on traffic flow. *Physical Review E* 69, 066110.

[23] C. Drane and C. Rizos, *Positioning Systems in Intelligent Transportation Systems* (Artech House, Norwood, USA, 1998).

[24] N. Eissfeldt and P. Wagner (2003) Effects of anticipatory driving in a traffic flow model. *European Physical Journal B* 33, 121–129.

[25] C. Gardiner, *Handbook of Stochastic Methods* (Springer, N.Y., 1990).

[26] P. G. Gipps (1981) A behavioural car-following model for computer simulation. *Transportation Research Part B: Methodological* 15, 105–111.

[27] P. G. Gipps (1986) A model for the structure of lane-changing decisions. *Transportation Research Part B: Methodological* 20, 403–414.

[28] D. E. Goldberg, *Genetic algorithms in search, optimization, and machine learning* (Addision-Wesley, 1989).

[29] M. Green (2000) "How long does it take to stop?" Methodological analysis of driver perception-brake times. *Transportation Human Factors* 2, 195–216.

[30] B. Greenshields, A study of traffic capacity. In: *Proceedings of the Highway Research Board, Vol. 14* (Highway Research Board, Washington, D.C., 1959), pages 228–477.

[31] A. Halati, H. Lieu, and S. Walker, CORSIM - Corridor traffic simulation model. In: R. F. Benekohal (Editor), *Proceedings of the Traffic Congestion and Traffic Safety in the 21th Century Conference* (ASCE, New York, 1997), pages 570–576.

[32] F. Hall, S. Wakefield, and A. Al-Kaisy (2000) Freeway Quality of Service: What really matters to drivers. *Transportation Research Record* 1776, 17–23.

[33] D. Helbing (2001) Traffic and related self-driven many-particle systems. *Reviews of Modern Physics* 73, 1067–1141.

[34] D. Helbing, I. J. Farkas, D. Fasold, M. Treiber, and T. Vicsek, Critical discussion of "synchronized flow", pedestrian evacuation, and optimization of production processes. In: *Traffic and Granular Flow '01* (Springer, Berlin, 2002), pages 511–530.

[35] D. Helbing, A. Hennecke, and M. Treiber (1999) Phase diagram of traffic states in the presence of inhomogeneities. *Physical Review Letters* 82, 4360–4363.

[36] D. Helbing and B. A. Huberman (1998) Coherent moving states in highway traffic. *Nature* 396, 738–740.

[37] D. Helbing, R. Jiang, and M. Treiber (2005) Analytical investigation of oscillations in intersecting flows of pedestrian and vehicle traffic. *Physical Review E* 72, 046130.

[38] D. Helbing and P. Molnár (1995) Social force model for pedestrian dynamics. *Physical Review E* 51, 4282–4286.

[39] D. Helbing and M. Schreckenberg (1999) Cellular automata simulating experimental properties of traffic flows. *Physical Review E* 59, R2505–R2508.

[40] D. Helbing and M. Treiber (2002) Critical discussion of "synchronized flow". *Cooper@tive Tr@nsport@tion Dyn@mics* 1, 2.1–2.24. (Internet Journal, `www.TrafficForum.org/journal`).

[41] W. Helly, Simulation of bottlenecks in single lane traffic flow. In: General Motors Research Loratories (Editor), *Proceedings of the Symposium on the Theory of Traffic Flow* (Elsevier, New York, 1959), pages 207–238.

[42] K. Henning and E. Preuschoff (Editors), *Einsatzszenarien für Fahrerassistenzsysteme im Güterverkehr und deren Bewertung*, volume 531 (VDI Verlag, Düsseldorf, 2003).

[43] P. Hidas (2005) Modelling vehicle interactions in microscopic traffic simulation of merging and weaving. *Transportation Research Part C: Emerging Technologies* 13, 37–62.

[44] P. Hidas and P. Wagner, Review of data collection methods for microscopic traffic simulation. In: *World Conference on Transport Research* (WCTR, Istanbul, Turkey, 2004).

[45] M. Hoedemaeker and K. A. Brookhuis (1998) Behavioural adaptation to driving with an adaptive cruise control (ACC). *Transportation Research Part F: Traffic Psychology and Behaviour* 1(2), 95–106.

[46] E. Holland (1998) A generalised stability criterion for motorway traffic. *Transportation Research Part B: Methodological* 32, 141–154.

[47] S. Hoogendoorn and P. Bovy (2001) State-of-the-art of vehicular traffic flow modelling. *Proceedings of the Institution of Mechanical Engineers, Part I: Journal of Systems and Control Engineering* 215(4), 283–303.

[48] S. P. Hoogendoorn and M. M. Minderhoud (2002) Motorway flow quality impacts of advanced driver assistance systems. *Transportation Research Record* 1800, 69–77.

[49] S. P. Hoogendoorn, H. J. V. Zuylen, M. Schreuder, B. Gorte, and G. Vosselman (2003) Microscopic traffic data collection by remote sensing. *Transportation Research Record* 1855, 121–128.

[50] P. A. Ioannou, *Automated highway systems* (Springer, New York, 1997).

[51] R. Jiang, Q. Wu, and Z. Zhu (2001) Full velocity difference model for a car-following theory. *Physical Review E* 64, 017101.

[52] B. Kerner (1998) Experimental features of self-organization in traffic flow. *Physical Review Letters* 81, 3797–3800.

[53] B. Kerner, C. Demir, R. Herrtwich, S. Klenov, H. Rehborn, M. Aleksic, and A. Haug, Traffic state detection with floating car data in road networks. In: *Proceedings of the 8th international IEEE conference on Intelligent Transportation Systems* (Vienna, 2005), page 700.

[54] B. Kerner and P. Konhäuser (1994) Structure and parameters of clusters in traffic flow. *Physical Review E* 50, 54–83.

[55] B. Kerner and H. Rehborn (1996) Experimental features and characteristics of traffic jams. *Physical Review E* 53, R1297–R1300.

[56] B. Kerner and H. Rehborn (1996) Experimental properties of complexity in traffic flow. *Physical Review E* 53, R4275–R4278.

[57] B. Kerner and H. Rehborn (1997) Experimental properties of phase transitions in traffic flow. *Physical Review Letters* 79, 4030–4033.

[58] B. S. Kerner (2000) Theory of breakdown phenomenon at highway bottlenecks. *Transportation Research Record* 1710, 136–144.

[59] B. S. Kerner, *The Physics of Traffic* (Springer, Heidelberg, 2004).

[60] A. Kesting and M. Treiber (2007) How reaction time, update time and adaptation time influence the stability of traffic flow. *Computer-Aided Civil and Infrastructure Engineering* 23, 125–137.

[61] A. Kesting, M. Treiber, S. Lämmer, M. Schönhof, and D. Helbing, Decentralized approaches to adaptive traffic control and an extended level of service concept. In: K. Gürlebeck and C. Könke (Editors), *Proceedings of the 17th International Conference on the Applications of Computer Science and Mathematics in Architecture and Civil Engineering* (Bauhaus University Weimar, 2006).

[62] A. Kesting, M. Treiber, M. Schönhof, F. Kranke, and D. Helbing, Jam-avoiding adaptive cruise control (ACC) and its impact on traffic dynamics. In: A. Schadschneider, T. Pöschel, R. Kühne, M. Schreckenberg, and D. E. Wolf (Editors), *Traffic and Granular Flow '05* (Springer, Berlin, 2007), pages 633–643.

[63] W. Knospe, L. Santen, A. Schadschneider, and M. Schreckenberg (2001) Human behaviour as origin of traffic phases. *Physical Review E* 65, 015101.

[64] W. Knospe, L. Santen, A. Schadschneider, and M. Schreckenberg (2002) Single-vehicle data of highway traffic: Microscopic description of traffic phases. *Physical Review E* 65, 056133.

[65] W. Knospe, L. Santen, A. Schandschneider, and M. Schreckenberg (1998) Disorder effects in cellular automata for two-lane traffic. *Physica A* 265, 614–633.

[66] F. Kranke, H. Poppe, M. Treiber, and A. Kesting, Fahrerassistenzsysteme zur aktiven Stauvermeidung im Straßenverkehr. In: M. Lienkamp (Editor), *VDI-Berichte zur 22. VDI/VW Gemeinschaftstagung: Integrierte Sicherheit und Fahrerassistenzsysteme*, volume 1960 (Verein Deutscher Ingenieure (VDI), Wolfsburg, 2006), page 375.

[67] F. Kranke and H.-J. Stauss (2006). Forschungsinitiative INVENT: Intelligenter Verkehr und nutzergerechte Technik. Schlussbericht VM 2010 zu dem Teilprojekt VLA – Verkehrsleitungsassistenz. Projektbericht der Volkswagen AG.

[68] J. A. Laval and C. F. Daganzo (2006) Lane-changing in traffic streams. *Transportation Research Part B: Methodological* 40(3), 251–264.

[69] H. K. Lee, R. Barlovic, M. Schreckenberg, and D. Kim (2004) Mechanical restriction versus human overreaction triggering congested traffic states. *Physical Review Letters* 92, 238702.

[70] H. Lenz, C. Wagner, and R. Sollacher (1999) Multi-anticipative car-following model. *European Physical Journal B* 7, 331–335.

[71] W. Leutzbach, *Introduction to the Theory of Traffic Flow* (Springer, Berlin, 1988).

[72] M. Lighthill and G. Whitham (1955) On kinematic waves: II. A theory of traffic on long crowded roads. *Proc. Roy. Soc. of London A* 229, 317–345.

[73] R. V. Lindgren, R. L. Bertini, D. Helbing, and M. Schönhof (2006) Toward demonstrating the predictability of bottleneck activation on German autobahns. *Transportation Research Record* 1965, 12–22.

[74] I. Lubashevsky, P. Wagner, and R. Mahnke (2003) Bounded rational driver models. *European Physical Journal B* 32, 243.

[75] I. Lubashevsky, P. Wagner, and R. Mahnke (2003) Rational-driver approximation in car-following theory. *Physical Review E* 68, 056109.

[76] S. Maerivoet and B. DeMoor (2005) Cellular automata models of road traffic. *Physics Reports* 419, 1–64.

[77] S. Maerivoet and B. D. Moor (2005). Transportation planning and traffic flow models. preprint `physics/0507127`.

[78] D. Manstetten, W. Krautter, and T. Schwab, Traffic simulation supporting urban control system development. In: *Proceedings of the 4th World Congress in Intelligent Transport Systems* (Berlin, 1997).

[79] G. Marsden, M. McDonald, and M. Brackstone (2001) Towards an understanding of adaptive cruise control. *Transportation Research Part C: Emerging Technologies* 9, 33–51.

[80] A. D. May, *Traffic Flow Fundamentals* (Prentice Hall, Eaglewood Cliffs, N.Y., 1990).

[81] M. M. Minderhoud, *Supported Driving: Impacts on Motorway Traffic Flow* (Delft University Press, Delft, 1999).

[82] E. W. Montroll (1978) Social dynamics and the quantifying of social forces. *Proceedings of the National Academy of Sciences of the United States of America* 75(10), 4633–4637.

[83] T. Nagatani (2002) The physics of traffic jams. *Reports of Progress in Physics* 65, 1331–1386.

[84] K. Nagel and M. Schreckenberg (1992) A cellular automaton model for freeway traffic. *J. Phys. I France* 2, 2221–2229.

[85] K. Nagel, P. Wagner, and R. Woesler (2003) Still flowing: Old and new approaches for traffic flow modeling. *Operations Research* 51, 681–710.

[86] K. Nagel, D. Wolf, P. Wagner, and P. Simon (1998) Two-lane traffic rules for cellular automata: A systematic approach. *Physical Review E* 58, 1425–1437.

[87] J. Nelder and R. Mead (1965) A simplex method for function minimization. *Computer Journal* 7, 308–313.

[88] G. Newell (1961) Nonlinear effects in the dynamics of car following. *Operations Research* 9, 209.

[89] K. Nishinari, M. Treiber, and D. Helbing (2003) Interpreting the wide scattering of synchronized traffic data by time gap statistics. *Physical Review E* 68, 067101.

[90] J. D. D. Ortúzar and L. G. Willumsen, *Modelling Transport* (Wiley, 2001).

[91] S. J. Ossen and S. P. Hoogendoorn (2005) Car-following behavior analysis from microscopic trajectory data. *Transportation Research Record* 1934, 13–21.

[92] S. J. Ossen, S. P. Hoogendoorn, and B. G. Gorte (2007) Inter-driver differences in car-following: A vehicle trajectory based study. *Transportation Research Record* 1965, 121–129.

[93] J. Ott and D. Kutscher, Drive-thru internet: IEEE 802.11b for "automobile" users. In: *Proceedings of Infocom 2004, Twenty-third AnnualJoint Conference of the IEEE Computer and Communications Societies* (2004), pages 362–373.

[94] B. Persaud, S. Yagar, and R. Brownlee (1998) Exploration of the breakdown phenomenon in freeway traffic. *Transportation Research Record* 1634, 64–69.

[95] W. H. Press, S. A. Teukolsky, W. T. Vetterling, and B. P. Flannery, *Numerical Recipes in C: The Art of Scientific Computing*. 2nd edition (Cambridge University Press, Cambridge, 1992).

[96] V. Punzo and F. Simonelli (2005) Analysis and comparision of microscopic flow models with real traffic microscopic data. *Transportation Research Record* 1934, 53–63.

[97] R. Rajamani, *Vehicle Dynamics And Control* (Springer, New York, 2005).

[98] P. Ranjitkar, T. Nakatsuji, and M. Asano (2004) Performance evaluation of microscopic flow models with test track data. *Transportation Research Record* 1876, 90–100.

[99] B. Rao and P. Varaiya (1993) Flow benefits of autonomous intelligent cruise control in mixed manual and automated traffic. *Transportation Research Record* 1408, 35–43.

[100] P. Richards (1956) Shock waves on the highway. *Operations Research* 4, 42–51.

[101] W. Schnabel and D. Lohse, *Grundlagen der Straßenverkehrstechnik und der Verkehrsplanung, Band 2: Verkehrsplanung* (Verlag für Bauwesen, 1997).

[102] M. Schönhof and D. Helbing (2007) Empirical features of congested traffic states and their implications for traffic modeling. *Transportation Science* 41, 1–32.

[103] M. Schönhof, A. Kesting, M. Treiber, and D. Helbing (2006) Coupled vehicle and information flows: Message transport on a dynamic vehicle network. *Physica A* 363, 73–81.

[104] M. Schönhof, M. Treiber, A. Kesting, and D. Helbing (2007) Autonomous detection and anticipation of jam fronts from messages propagated by intervehicle communication. *Transportation Research Record* 1999, 3–12.

[105] D. Schrank and T. Lomax, *The 2005 Urban Mobility Report* (Texas Transportation Institute, Texas A & M University, 2005).

[106] H. G. Schuster, *Deterministic Chaos* (Verlag Chemie (VCH), Weinheim, Germany, 1984).

[107] R. Shiffrin and W. Schneider (1977) Controlled and automatic human information processing II: Perceptual learning, automatic attending, and a general theory. *Psychological Review* 84, 127–190.

[108] J. P. Singh, N. Bambos, B. Srinivasan, and D. Clawin, Wireless LAN performance under varied stress conditions in vehicular traffic scenarios. In: *IEEE Vehicular Technology Conference* (2002), pages 743 – 747.

[109] A. Skabardonis (2002) Simulation of freeway weaving areas. *Transportation Research Record* 1802, 115–124.

[110] U. Sparmann, Spurwechselvorgänge auf zweispurigen BAB-Richtungsfahrbahnen. In: *Forschung, Straßenbau und Straßenverkehrstechnik*, volume 263 (Bundesminister für Verkehr, Bonn-Bad Godesberg, 1978).

[111] N. A. Stanton (1998) Vehicle automation and driving performance. *Ergonomics* 41(7), 1014–1028.

[112] C. Tampère and B. van Arem (2001) Traffic flow theory and its applications in automated vehicle control: A review. *IEEE Intelligent Transportation Systems Proceedings* , 391–397.

[113] B. Tilch and D. Helbing (1998) Generalized force model of traffic dynamics. *Physical Review E* 58, 133–138.

[114] B. Tilch and D. Helbing, Evaluation of single vehicle data in dependence of the vehicle-type, lane, and site. In: D. Helbing, H. Herrmann, M. Schreckenberg, and D. Wolf (Editors), *Traffic and Granular Flow '99* (Springer, Berlin, 2000), pages 333–338.

[115] T. Toledo, C. F. Choudhury, and M. E. Ben-Akiva (2005) Lane-changing model with explicit target lane choice. *Transportation Research Record* 1934, 157–165.

[116] T. Toledo, H. N. Koutsopoulos, and M. E. Ben-Akiva (2003) Modeling integrated lane-changing behavior. *Transportation Research Record* 1857, 30–38.

[117] Transportation Research Board (1998). National Automated Highway System Research Program: A Review, *Special Report 253*.

[118] M. Treiber and D. Helbing (1999). Explanation of observed features of self-organization in traffic flow, preprint `cond-mat/9901239`.

[119] M. Treiber and D. Helbing (1999) Macroscopic simulation of widely scattered synchronized traffic states. *Journal of Physics A: Mathematical and General* 32(1), L17–L23.

[120] M. Treiber and D. Helbing (2001) Microsimulations of freeway traffic including control measures. *Automatisierungstechnik* 49, 478–484.

[121] M. Treiber and D. Helbing (2002) Reconstructing the spatio-temporal traffic dynamics from stationary detector data. *Cooper@tive Tr@nsport@tion Dyn@mics* 1, 3.1–3.24. (Internet Journal, `www.TrafficForum.org/journal`).

[122] M. Treiber and D. Helbing (2003) Memory effects in microscopic traffic models and wide scattering in flow-density data. *Physical Review E* 68, 046119.

[123] M. Treiber, A. Hennecke, and D. Helbing (1999) Derivation, properties, and simulation of a gas-kinetic-based, non-local traffic model. *Physical Review E* 59, 239–253.

[124] M. Treiber, A. Hennecke, and D. Helbing (2000) Congested traffic states in empirical observations and microscopic simulations. *Physical Review E* 62, 1805–1824.

[125] M. Treiber, A. Kesting, and D. Helbing (2006) Delays, inaccuracies and anticipation in microscopic traffic models. *Physica A* 360, 71–88.

[126] M. Treiber, A. Kesting, and D. Helbing (2006) Understanding widely scattered traffic flows, the capacity drop, and platoons as effects of variance-driven time gaps. *Physical Review E* 74, 016123.

[127] C. van Driel, M. Hoedemaeker, and B. van Arem (2007) Impacts of a congestion assistant on driving behaviour and acceptance using a driving simulator. *Transportation Research Part F: Traffic Psychology and Behaviour* 10, 139–152.

[128] J. VanderWerf, S. Shladover, N. Kourjanskaia, M. Miller, and H. Krishnan (2001) Modeling effects of driver control assistance systems on traffic. *Transportation Research Record* 1748, 167–174.

[129] J. VanderWerf, S. Shladover, M. Miller, and N. Kourjanskaia (2002) Effects of adaptive cruise control systems on highway traffic flow capacity. *Transportation Research Record* 1800, 78–84.

[130] P. Varaiya (1993) Smart cars on smart roads: Problems of control. *IEEE Transactions on Automatic Control* 38(2), 195.

[131] P. Wagner and I. Lubashevsky (2003) Empirical basis for car-following theory development. *preprint* `cond-mat/0311192` .

[132] H. Wei, J. Lee, Q. Li, and C. J. Li (2000) Observation-based lane-vehicle-assignment hierarchy for microscopic simulation on an urban street network. *Transportation Research Record* 1710, 96–103.

[133] R. Wiedemann, Simulation des Straßenverkehrsflusses. In: *Heft 8 der Schriftenreihe des IfV* (Institut für Verkehrswesen, Universität Karlsruhe, 1974).

[134] L. Wischhof, A. Ebner, and H. Rohling (2005) Information dissemination in self-organizing intervehicle networks. *IEEE Transactions on Intelligent Transportation Systems* 6, 90–101.

[135] S. Witte (1996) Simulationsuntersuchungen zum Einfluss von Fahrverhalten und technischen Abstandsregelsystemen auf den Kolonnenverkehr. Dissertation, Universität Karlsruhe.

[136] H. Wu, R. Fujimoto, and G. Riley, Analytical models for information propagation in vehicle-to-vehicle networks. In: *Vehicular Technology Conference*, volume 6 (2004), pages 4548–4552.

[137] H. Wu, J. Lee, M. Hunter, R. Fujimoto, R. L. Guensler, and J. Ko (2005) Efficiency of simulated vehicle-to-vehicle message propagation in Atlanta, Georgia, I-75 Corridor 1910, 82–89.

[138] Q. Xu, T. Mak, J. Ko, and R. Sengupta, Vehicle-to-vehicle safety messaging in DSRC. In: *International Conference on Mobile Computing and Networking* (2004), pages 19–28.

[139] Q. Yang and H. N. Koutsopoulos (1996) A microscopic traffic simulator for evaluation of dynamic traffic management systems. *Transportation Research Part C: Emerging Technologies* 4(3), 113.

[140] X. Yang and W. Recker (2005) Simulation studies of information propagation in a self-organized distributed traffic information system. *Transportation Research Part C: Emerging Technologies* 13(5-6), 370–390.

[141] S. Yousif and J. Hunt (1995) Modelling lane utilization on British dual-carriageway roads: effects on lane-changing. *Traffic Engineering + Control* 36(12), 680 – 687.

Online References

[142] AIMSUN (Advanced Interactive Microscopic Simulator for Urban and Non-urban Networks). http://www.aimsun.com – Access date: May 5, 2007.

[143] Quadstone PARAMICS (Parallel microscopic traffic simulator). http://www.paramics-online.com – Access date: May 5, 2007.

[144] Standard ASTM D 3565, Standard Test Method for Tableware Pattern Removal by Mechanical Dishwasher Detergents (2003). ASTM International, http://www.astm.org – Access date: May 5, 2007.

[145] VISSIM (Verkehr In Städten). Microscopic traffic simulator of the PTV AG. http://www.english.ptv.de/cgi-bin/traffic/traf_vissim.pl – Access date: May 5, 2007.

[146] Deutsches Zentrum für Luft- und Raumfahrt (DLR). Clearing house for transport data and transport models. http://www.dlr.de/cs/ – Access date: May 5, 2007.

[147] Dutch Ministry of Transport, Public Works and Water Management (2007). Innovation programm 'Roads to the future'. http://www.roadstothefuture.nl – Access date: May 5, 2007.

[148] European Commission (2001). Energy & Transport, White Paper European Transport Policy for 2010: "Time to Decide". COM (2001) 370 final.

[149] European Commission (2003). European Road Safety Action Programme – "Saving 20,000 lives on our roads". COM (2003) 311 final.

[150] German Federal Ministry of Economics and Technology (BMWi) (2007). Research project AKTIV (Adaptive und kooperative Technologien für den intelligenten Verkehr). http://www.aktiv-online.org – Access date: May 5, 2007.

[151] German Federal Ministry of Education and Research (BMBF) (2005). Research project INVENT (Intelligent Traffic and User-Friendly Technology). http://www.invent-online.de – Access date: May 5, 2007.

[152] Ministry of Transport, Energy and Spatial Planning of Nordrhein-Westfalen (2007). Traffic state prediction for the freeway network. http://autobahn.nrw.de – Access date: May 5, 2007.

[153] Statistisches Bundesamt (2006). Verkehr in Deutschland 2006.

[154] M. Treiber (2007). The website http://www.traffic-simulation.de provides an interactive simulation of the Intelligent Driver Model. – Access date: May 5, 2007.

[155] US Department of Transportation (2006). NGSIM – Next Generation Simulation. http://www.ngsim.fhwa.dot.gov – Access date: May 5, 2007.

[156] M. Wall (1996). Galib: A C++ library of genetic algorithms components. http://lancet.mit.edu/ga/ – Access date: May 5, 2007.

[157] Wikipedia (2006). http://en.wikipedia.org/wiki/Genetic_algorithm – Access date: May 5, 2007.

Kurzfassung

Kontext und Ausgangspunkt

Leistungsfähige und effiziente Verkehrssysteme bilden die Grundlage für eine stabile wirtschaftliche Entwicklung unserer heutigen globalen Industriegesellschaften. Darüber hinaus ist die individuelle Mobilität ein wichtiger Bestandteil persönlicher Freiheit und Selbstverwirklichung. Der Hauptanteil der Verkehrsleistung wird von motorisiertem Individualverkehr erbracht. Allgegenwärtige Verkehrsstaus verdeutlichen allerdings, dass die Straßenkapazität begrenzt ist. Sie verursachen zudem beträchtliche volkswirtschaftliche Schäden.[1] Während die Verkehrsnachfrage nur indirekt beeinflusst werden kann (v.a. durch politische Steuerung), erfordert ein Ausbau des Straßennetzes langfristige Planungen sowie hohe Investitions- und Unterhaltskosten. Zudem ist in dicht besiedelten Großräumen der Ausbau des Straßennetzes oft weder möglich noch politisch erwünscht. Daher kommt einer *effizienten Nutzung der vorhandenen Straßeninfrastruktur* eine entscheidende Bedeutung zu.

Die Vision der Verkehrstelematik besteht seit langem darin, diese Effizienz durch eine automatisierte Fahrzeugsteuerung zu erreichen. Durch Fortschritte in den Bereichen der Sensor-, Steuerungs- und Kommunikationstechnologie ist automatisiertes Fahren – zumindest auf Autobahnen und innerhalb einer Spur – schon heute Realität: *Adaptive-Cruise-Control*-Systeme (ACC)[2] greifen in die Fahrzeugkontrolle ein und regeln das Beschleunigen und Bremsen. Über einen Radarsensor wird der Abstand zum Vorderfahrzeug gemessen und in Kombination mit den Fahrzeuggeschwindigkeiten die notwendige Beschleunigung berechnet, die für das Einhalten einer vom Benutzer vorgegebenen Wunschgeschwindigkeit bzw. eines zeitlichen Abstands zum Vorderfahrzeug notwendig ist. Heutige ACC-Systeme sind für ein sicheres und komfortables Fahren auf Autobahnen bei Geschwindigkeiten über 30 km/h ausgelegt. Bereits die nächste Generation wird jedoch im gesamten Geschwindigkeitsbereich (inkl. Stop-and-go-Verkehr) anwendbar sein.[3]

[1] Die Europäische Kommission hat die volkswirtschaftlichen Kosten durch Zeitverluste und Mehrverbrauch von Kraftstoff auf 0,5 % des Bruttosozialprodukts des Jahres 2001 geschätzt und prognostiziert aufgrund einer Steigerung der globalen Verkehrsnachfrage eine Verdopplung der Kosten bis zum Jahr 2010.

[2] Deutsch: „adaptiver Geschwindigkeitsregler“ oder „radargestützte Abstandsregelung“.

[3] Eine ACC-Implementierung in einem Forschungsfahrzeug wurde von der Volkswagen AG in Zusammenarbeit mit der TU Dresden im Rahmen des Forschungsprojekts INVENT („Intelligenter Verkehr und nutzergerechte Technik”) demonstriert.

Fragestellung und Beitrag

In der Arbeit wird ein neues verkehrstelematisches Konzept für ein verkehrseffizientes Fahrverhalten entwickelt und als dezentrale Strategie zur Vermeidung und Auflösung von Verkehrsstaus auf Richtungsfahrbahnen vorgestellt. Die operative Umsetzung erfolgt durch ein ACC-System, das um eine, auf Informationen über die lokale Verkehrssituation basierende, automatisierte Fahrstrategie erweitert wird. Die Herausforderung bei einem Eingriff in das individuelle Fahrverhalten besteht – unter Berücksichtigung von Sicherheits-, Akzeptanz- und rechtlichen Aspekten – im Ausgleich der Gegensätze Fahrkomfort und Verkehrseffizienz. Während sich ein komfortables Fahren durch große Abstände bei geringen Fahrzeugbeschleunigungen auszeichnet, erfordert ein verkehrsoptimierendes Verhalten kleinere Abstände und eine schnellere Anpassung an Geschwindigkeitsänderungen der umgebenden Fahrzeuge.

Als allgemeiner Lösungsansatz wird eine *verkehrsadaptive Fahrstrategie* vorgeschlagen, die ein ACC-System mittels Anpassung der das Fahrverhalten charakterisierenden Parameter umsetzt. Die Wahl der Parameter erfolgt in Abhängigkeit von der lokalen Verkehrssituation, die auf der Basis der im Fahrzeug zur Verfügung stehenden Informationen automatisch detektiert wird. Durch die Unterscheidung verschiedener Verkehrssituationen wird ein *temporärer* Wechsel in ein verkehrseffizientes Fahrregime (zum Beispiel beim Herausfahren aus einem Stau) ermöglicht.

Machbarkeit und Wirkungspotenzial der verkehrsadaptiven Fahrstrategie werden in der Dissertation im Rahmen eines mikroskopischen Modellierungsansatzes simuliert und hinsichtlich der kollektiven Verkehrsdynamik, insbesondere der Stauentstehung und Stauauflösung, auf mehrspurigen Richtungsfahrbahnen bewertet. Die durchgeführte Modellbildung, insbesondere die Formulierung eines komplexen Modells des menschlichen Fahrverhaltens, ermöglicht eine detaillierte Analyse der im Verkehr relevanten *kollektiven Stabilität* und einer von der Stabilität abhängigen *stochastischen Streckenkapazität*. Ein tieferes Verständnis der Stauentstehung und -ausbildung wird durch das allgemeine Konzept der *Engstelle* erreicht. Dieses findet auch bei der Entwicklung der Strategie für ein stauvermeidendes Fahrverhalten Anwendung.

In der Arbeit wird die stauvermeidende und stauauflösende Wirkung eines individuellen, verkehrsadaptiven Fahrverhaltens bereits für geringe Ausstattungsgrade nachgewiesen. Vor dem Hintergrund einer zu erwartenden Verbreitung von ACC-Systemen ergibt sich damit eine vielversprechende Option für die Steigerung der Verkehrsleistung durch ein teilautomatisiertes Fahren. Der entwickelte Ansatz einer verkehrsadaptiven Fahrstrategie ist unabhängig vom ACC-System. Er erweitert dessen Funktionalität im Hinblick auf zukünftige, *informationsbasierte* Fahrerassistenzsysteme um eine neue *fahrstrategische* Dimension. Die lokale Interpretation der Verkehrssituation kann neben einer verkehrsadap-

tiven ACC-Regelung auch der Entwicklung zukünftiger Fahrerinformationssysteme dienen.

Ergebnisse der Arbeit

Die Arbeit gliedert sich in zwei Hauptteile. Gegenstand des ersten Teils ist eine mikroskopische Theorie der Verkehrsdynamik. Es werden Modelle zur Beschreibung des individuellen Beschleunigungs-, Brems- und Spurwechselverhaltens formuliert und die daraus resultierende kollektive Verkehrsdynamik und Stabilität numerisch untersucht. Die entwickelten Modelle und Simulationswerkzeuge bilden die methodischen Voraussetzungen für den zweiten Teil der Arbeit, in dem ein Konzept für eine verkehrsadaptive Regelungsstrategie von ACC-Systemen vorgestellt wird und deren Auswirkungen auf die Verkehrsdynamik auf Autobahnen mittels Verkehrssimulationen untersucht und bewertet werden.

Das mikroskopische Fahrzeugfolgemodell *Intelligent Driver Model* (IDM)[4] dient als Ausgangspunkt der Arbeit. Aus der Literatur ist bekannt, dass das IDM alle wesentlichen Phänomene der Verkehrsdynamik auf Autobahnen reproduziert. Darüber hinaus ermöglichen die leicht zu interpretierenden Modellparameter des IDM eine intuitive Charakterisierung verschiedener Fahrzeugklassen (wie PKW und LKW) sowie unterschiedlichen Fahrverhaltens. Bei der Modellierung einer verkehrsadaptiven Longitudinalsteuerung mittels eines ACC-Systems erweist sich diese Eigenschaft als vorteilhaft.

Mikroskopische Modellkalibrierung und -validierung

Für ein grundsätzliches Verständnis der Eigenschaften des IDM werden die Dynamik einzelner Fahrzeuge, die Gleichgewichtseigenschaften eines Verkehrsflusses identischer Fahrzeuge sowie das Auftreten kollektiver Instabilitäten untersucht. In der Literatur ist das Verkehrsmodell IDM anhand makroskopischer Verkehrsgrößen, welche sich z.B. aus empirischen Fluss-Dichte-Beziehungen ergeben, kalibriert worden. In der vorliegenden Arbeit wird eine mikroskopische Kalibrierungs- und Validierungsmethode für Fahrzeugfolgemodelle vorgestellt, um eine simulierte Trajektorie bestmöglich an eine empirisch gemessene Trajektorie anzupassen. Für die numerische Lösung dieses nichtlinearen Optimierungsproblems wurde ein genetischer Algorithmus entwickelt und es wurden drei verschiedene Zielfunktionen formuliert, um die Sensitivität der Kalibrierungsresultate bewerten zu können. Das IDM konnte das individuelle Fahrverhalten reproduzieren. Die anhand verschiedener Trajektorien und Optimierungskriterien kalibrierten Modellparameter lagen im erwarteten Wertebereich. Die Kalibrierungsfehler betrugen zwischen 10

[4] M. Treiber, A. Hennecke, D. Helbing, *Congested traffic states in empirical observations and microscopic simulations*, Physical Review E 62, 1805 -1824 (2000).

und 30 %, wovon der größte Teil auf dynamische Anpassungsprozesse des Fahrers (sog. *intra-driver variability*) zurückgeführt werden konnte. Die Unterschiede zwischen den kalibrierten und validierten Modellparametern waren deutlich kleiner und ließen sich im wesentlichen durch die unterschiedlichen Fahrstile verschiedener Fahrer (sog. *inter-driver variability*) erklären.

Ein Modell des menschlichen Fahrverhaltens

In der Kalibrierungsstudie wurde gezeigt, dass das IDM das menschliche Fahrverhalten auch in Einzelsituationen befriedigend beschreibt. Hinsichtlich der offensichtlichen operativen Unterschiede zwischen einem autofahrenden Menschen und einem simplifizierenden Fahrzeugfolgemodell, welches instantan auf lediglich das unmittelbare Vorderfahrzeug reagiert, stellt sich die grundsätzliche Frage nach einer theoretischen Begründung, die auch für die Modellierungsannahmen im zweiten Teil der Arbeit relevant ist.

In der Arbeit wird mit dem *Human Driver Model* (HDM) ein komplexes mikroskopisches Verkehrsmodell formuliert, das menschliche Eigenschaften explizit berücksichtigen soll. An erster Stelle ist eine nicht zu vernachlässigende menschliche Reaktionszeit zu nennen, die in der mathematischen Formulierung für die Beschleunigungsfunktion zu Delay-Differenzialgleichungen führt. Aus der Literatur ist bekannt, dass menschliche Reaktionszeiten, die in der Größenordnung von einer Sekunde liegen, zu sehr instabilem Modellverhalten führen. Weiterhin wird die Stabilität durch menschliche Wahrnehmungs- und Schätzfehler reduziert, die im HDM durch Wiener-Prozesse beschrieben werden und zu stochastischen Modellelementen führen. Zur Stabilisierung des Fahrverhaltens werden zwei Antizipationsmechanismen betrachtet: Der modellierte Fahrer reagiert nicht nur auf das unmittelbare Vorderfahrzeug, sondern auch (mit abnehmender Gewichtung) auf die Fahrzeuge davor („räumliche Antizipation“), womit das HDM über die Näherung der einfachen Fahrzeugfolgemodelle hinausgeht. Zweitens wird modelliert, dass der menschliche Fahrer bei seiner Wahrnehmung des Abstandes zum nächsten Fahrzeug um seine Reaktionszeit weiß und die Verkehrssituation entsprechend extrapoliert („zeitliche Antizipation“).

Die aus dem Zusammenwirken der verschiedenen Modellelemente resultierenden Stabilitätseigenschaften des Modells wurden anhand von Fahrzeugkolonnen unter dem Einfluss endlicher Störungen numerisch untersucht. Die kollektive Stabilität wird dabei vor allem durch drei charakteristische Zeiten bestimmt, deren Einflüsse und Wechselwirkungen erstmals durch unabhängige Parameter analysiert wurden. Neben der expliziten Reaktionszeit der Fahrer, die in erster Linie eine physiologische Größe ist, wird die kollektive Stabilität durch eine endliche Adaptionszeit an Geschwindigkeitsänderungen determiniert, die sich aus der endlichen Beschleunigungsfähigkeit der Fahrzeuge und Beschle-

unigungswilligkeit der Fahrer ergibt. In Simulationen wurden beide Instabilitätsmechanismen untersucht und qualitative Unterschiede nachgewiesen. Vergleichsweise niedrige Fahrzeugbeschleunigungen verursachen eine kollektive Instabilität durch die Ausbildung *langwelliger* Störungen, während endliche Reaktionszeiten im Zusammenspiel mit höheren Beschleunigungen zunächst kurzwellige Störungen hervorrufen. Beide Instabilitätsmechanismen können aber zur Ausbildung von (langwelligen) Stop-and-go-Wellen führen.

Weiterhin konnte gezeigt werden, dass in Gegenwart einer nicht zu vernachlässigenden Reaktionszeit eine *Vergrößerung* der Geschwindigkeitsadaptionszeit durch kleinere Beschleunigungen die kollektive Stabilität erhöhen, also eine langsamere Anpassung zur Stabilisierung von zeitverzögerten Systemen beitragen kann. Eine endliche Integrationsschrittweite, die ebenfalls eine verzögerte Anpassung bewirkt, kann als dritte, unabhängige Zeit aufgefasst werden. Obwohl sie nur eine Hilfsgröße für die numerische Integration der Differenzialgleichungen ist, wird sie in einigen Modellen in der Literatur mit der Reaktionszeit identifiziert. Die Simulationen zeigen, dass der Einfluss der Integrationsschrittweite jedoch nur dem einer halben Reaktionszeit entspricht.

Weiterhin wurde die makroskopische Verkehrsdynamik unter dem Einfluss von Reaktionszeit und Antizipation in einem komplexen Szenario mit einer „flusserhaltenden Engstelle“ (z.B. einer Baustelle) in einem offenen System simuliert. Im Modell konnten verschiedene raumzeitliche Stauzustände, die aus der Literatur bekannt sind, durch eine Variation intrinsischer Modellparameter für die Reaktionszeit und räumliche Antizipation nachgewiesen werden. Die Simulationen zeigen, dass sich die menschliche Reaktionszeit in ihrer kollektiven Wirkung durch die eingeführten Antizipationsmechanismen quantitativ kompensieren lässt. Damit lässt sich im Rahmen des vorgestellten Modells erklären, warum die auf simplifizierten Annahmen beruhenden Fahrzeugfolgemodelle in der Lage sind, die empirischen Verkehrsphänomene quantitativ zu beschreiben.

Modellierung von Spurwechselentscheidungen

Die mikroskopische Simulation des Autobahnverkehrs erfordert neben der Beschreibung des spurgebundenen Brems- und Beschleunigungsverhaltens die explizite Modellierung von Spurwechseln. Erst die Möglichkeit zum Überholen von langsameren Fahrzeugen erlaubt eine realistische Berücksichtigung von Effekten, die durch heterogene Fahrertypen und Fahrzeugklassen hervorgerufen werden. Mit dem Modell MOBIL[5] wird ein allgemeines Entscheidungsmodell formuliert, das sowohl erzwungene als auch freie Spurwechsel beschreibt. Das Modell basiert auf einem Motivations- und einem Sicherheitskriterium. Die Abwägung zwischen dem zu erwartenden eigenen Vorteil in der neuen Spur und dem Risiko, das durch einen Spurwechsel hervorgerufen wird, erfolgt auf der Basis von *longitu-*

[5]Das Akronym steht für *„Minimizing Overall Braking Induced by Lane Changes“*.

dinalen Beschleunigungen, die sich wiederum mit Hilfe eines longitudinalen Verkehrsmodells berechnen lassen. Diese „Metaformulierung“ des diskreten Entscheidungsproblems ermöglicht eine einfache und konsistente Modellformulierung, bei der die Eigenschaften des Longitudinalmodells auch in die Spurwechselentscheidung einfließen.

Der Spurwechselalgorithmus MOBIL geht über Modelle aus der Literatur hinaus, indem er neben dem individuellen Vorteil auch die Auswirkungen auf die durch den Spurwechsel beeinflussten nächsten Nachbarn berücksichtigt. Dieser Abwägungsprozess wird anschaulich durch einen „Höflichkeitsparameter“ beschrieben. Der Einfluss der Modellparameter für symmetrische und asymmetrische Spurwechselregeln (letztere mit einem Rechtsfahrgebot und einem Rechtsüberholverbot) auf das Spurwechselverhalten wurde in Verkehrssimulationen untersucht. Die resultierenden Spurwechselraten als Funktion der Verkehrsdichte liegen in einer realistischen Größenordnung und stimmen semiquantitativ mit empirischen Untersuchungen überein.

Verkehrsadaptive Strategie für ACC-Systeme

Im zweiten Teil der Arbeit wird ein Konzept für zukünftige ACC-Systeme vorgestellt, das neben dem individuellen Fahrkomfort und der Verkehrssicherheit als drittes Kriterium eine positive Beeinflussung der kollektiven Verkehrsleistung berücksichtigt. Während ein komfortorientiertes Fahrverhalten mit geringen Fahrzeugbeschleunigungen bei großen Abständen umgesetzt werden kann, ist ein auf Verkehrseffizienz ausgelegtes Fahrverhalten mit kleineren Zeitlücken und höheren Beschleunigungen verbunden. Um diese gegensätzlichen Zielkriterien miteinander vereinbaren zu können, wird eine *verkehrsadaptive Regelungsstrategie* für ACC-Systeme vorgeschlagen und im Rahmen von mikroskopischen Simulationen auf ihre kollektive Wirkung untersucht. Das Konzept umfasst als Modellkomponenten eine *verkehrszustandsabhängige Fahrstrategie*, ein *autonomes Detektionsmodell* zur Bestimmung der lokalen Verkehrssituation und eine *Umsetzung der Fahrstrategie* in einem ACC-Modell.

Die entwickelte verkehrsadaptive Fahrstrategie unterscheidet fünf Verkehrszustände, deren unterschiedliche Zielsetzungen durch eine Anpassung des aktuellen Fahrverhaltens in Form der folgenden *Fahrstrategiematrix* umgesetzt werden: Im Zustand „Freier Verkehr“ ist das Zielkriterium ein komfortabler Fahrstil, der von den benutzerdefinierten Standardeinstellungen des ACC-Systems gewährleistet wird. Bei der „Annäherung an einen Stau“ soll so frühzeitig und sanft wie möglich gebremst werden, um das Risiko von Auffahrunfällen zu reduzieren. Im Zustand „Stau“ wird ebenfalls die Standardeinstellung des ACC-Systems gewählt, weil ein Fahrer im Stau die Verkehrsleistung nicht direkt beeinflussen kann. Dagegen kommt es bei der „Ausfahrt aus dem Stau“ darauf an, dass die Fahrzeuge rechtzeitig und zügig beschleunigt werden, um den Ausfluss aus dem Stau zu erhöhen. Im Hinblick

auf das Kriterium einer Steigerung der Verkehrsleistung ist darüber hinaus das Fahrverhalten beim Passieren einer „Engstelle“ von Bedeutung. Da eine lokale Kapazitätsreduktion das definierende Merkmal einer Engstelle ist, ist das Ziel in dieser Verkehrssituation eine Abschwächung des Engpasses durch ein aufmerksames Fahren bei kleineren Zeitabständen.

Die verkehrsabhängige Fahrstrategie erfordert eine autonome Bestimmung des lokalen Verkehrszustandes im Fahrzeug. Das formulierte Detektionsmodell enthält Kriterien für die eingeführten Verkehrszustände sowie eine Heuristik für das korrespondierende Entscheidungsproblem bei der Auswahl eines Verkehrszustandes. Die Kriterien basieren auf lokalen, im Fahrzeug zur Verfügung stehenden Informationen wie der Zeitreihe der Geschwindigkeit oder der georeferenzierten Fahrzeugposition in Verbindung mit einer digitalen Karte. Die digitale Karte ist um Attribute infrastruktureller Engstellen, wie z.B. Auf- und Abfahrten von Autobahnen, Steigungsstrecken oder Baustellen, ergänzt, da aus empirischen Untersuchungen von Verkehrsstaus bekannt ist, dass die meisten Verkehrszusammenbrüche an diesen stationären Engstellen lokalisiert sind.

In Abhängigkeit vom lokal detektierten Verkehrszustand wird die zugehörige Fahrstrategie von einem ACC-Modell umgesetzt. Formal entspricht dies einem Fahrzeugfolgemodell mit einer automatischen, ereignisgesteuerten Wahl der Modellparameter, die damit zeitabhängig werden. Die Anpassung der Modellparameter ist in der Fahrstrategiematrix relativ formuliert, um individuelle ACC-Einstellungen des Fahrers zu berücksichtigen.

Analyse und Bewertung in der mikroskopischen Simulation

Die Auswirkungen eines (hypothetischen) Anteils von ACC-Fahrzeugen auf die kollektive Verkehrsdynamik kann nur im Rahmen von Simulationen untersucht werden. Die Bewertung der vorgestellten verkehrsadaptiven ACC-Fahrstrategie mit ihrer fahrzeugbasierten Verkehrszustandsdetektion erfordert einen *mikroskopischen Simulationsansatz*. Mit Hilfe der entwickelten Software wurden mehrspurige Streckenabschnitte mit verschiedenen Engstellen und Randbedingungen simuliert. Für eine realistische Wahl der stromaufwärtigen Randbedingungen des offenen Systems wurden u.a. zeitabhängige Detektordaten der deutschen Autobahn 9 (München-Salzburg) für den Verkehrsfluss und einen variablen LKW-Anteil benutzt.

Im Rahmen der Simulation von Verkehrszusammenbrüchen konnte bereits ab einem ACC-Anteil von zehn Prozent eine positive Wirkung der verkehrsadaptiven Fahrstrategie beobachtet werden. Abhängig vom ACC-Ausstattungsgrad bewirkt die Fahrstrategie im Verkehrszustand „Passieren einer Engstelle“ eine Reduzierung der Engpassstärke und damit eine Verzögerung bzw. Verhinderung des Verkehrszusammenbruchs. Ein Wechsel des Fahrregimes im Zustand „Ausfahrt aus dem Stau“ bewirkt einen höheren Ausfluss bei geringeren Rückstaulängen und damit eine schnellere Stauauflösung. Zur Bewertung

wurde die *aktuelle Reisezeit* (als wichtiges Kriterium für die Verkehrsteilnehmer) sowie die *kumulierte Reisezeit* (als Indikator für die Systemleistung) herangezogen. Eine systematische Untersuchung der kumulierten Reisezeiten ergab einen monoton abnehmenden Zusammenhang bei zunehmendem Anteil von ACC-Fahrzeugen, wodurch eine graduelle Verbesserung der Verkehrseffizienz auch bei kleinen (und damit realistischen) ACC-Ausstattungsgraden nachgewiesen wurde.

Für eine systematische Untersuchung der Dynamik wurden die externen Parameter wie der ACC-Anteil, der LKW-Anteil sowie die Parametrierung der Fahrstrategiematrix variiert, wobei die *maximale freie Kapazität* im freien Verkehr und die *dynamische Kapazität*, die den Ausfluss aus dem Stau beschreibt, als relevante dynamische Größen betrachtet wurden. Die freie Kapazität bestimmt den maximal möglichen Durchsatz des Systems, bis es zum Verkehrszusammenbruch kommt. Als dynamische Größe hängt sie von der kollektiven Stabilität ab und ist damit von der statischen Streckenkapazität zu unterscheiden. Zur Verdeutlichung der stochastischen Natur des Verkehrszusammenbruchs wurde die maximale Kapazität als Zufallsvariable betrachtet, die sich in guter Näherung durch eine Gaußverteilung beschreiben ließ. Die Varianz hängt von der Heterogenität des Fahrer-Fahrzeug-Ensembles ab, wobei die Berücksichtigung unterschiedlicher Fahrzeugklassen einen größeren Einfluss hatte als die Berücksichtigung statistisch verteilter Modellparameter innerhalb der Fahrzeugklassen.

Die Grenzen der autonomen Verkehrszustandsdetektion wurden im Rahmen der Simulationen identifiziert. Auf der Basis der lokal verfügbaren Informationen können propagierende Staufronten (z.B. Stop-and-go-Wellen) nicht zuverlässig für eine rechtzeitige Anpassung der Fahrstrategie detektiert werden. Daher wird eine Erweiterung des Detektionsmodells um nichtlokale Informationen diskutiert, welche in der Zukunft z.B. durch eine Kommunikation zwischen Fahrzeugen (*inter-vehicle communication*) oder mit stationären Sendern (sog. *road-side units*) zur Verfügung gestellt werden können. In einer Machbarkeitsstudie wurde die Informationsgenerierung und eine ausreichend schnelle Informationsübermittlung, auch unter den Einschränkungen, dass nur sehr wenige Fahrzeuge mit einem Kommunikationsmodul ausgestattet sind und die Senderreichweite begrenzt ist, demonstriert, wobei die ausgestatteten Fahrzeuge in der Gegenrichtung als dynamische Relaisstationen genutzt wurden (*store-and-forward*), um eine ausreichende Konnektivität zu gewährleisten. Eine Detektion, Interpretation und Voraussage der lokalen Verkehrssituation in Verbindung mit zukünftigen Kommunikationstechnologien kann neben einer verkehrsadaptiven ACC-Regelung auch der Entwicklung zukünftiger Fahrerinformationssysteme dienen. Eine Demonstration beider Anwendungsebenen ist von der Volkswagen AG im Rahmen des Forschungsprojekts AKTIV[6] geplant.

[6]Das Akronym steht für „Adaptive und kooperative Technologien für den intelligenten Verkehr“.

List of Publications

Publications as first author:

1. A. Kesting, M. Treiber, M. Schönhof and D. Helbing, *Adaptive cruise control design for active congestion avoidance*, Transportation Research Part C: Emerging Technologies, Volume 16, Issue 6, Pages 668-683, 2008.

2. A. Kesting and M. Treiber, *How reaction time, update time and adaptation time influence the stability of traffic flow*, Computer-Aided Civil and Infrastructure Engineering, Volume 23, Issue 2, Pages 125-137, 2008.

3. A. Kesting and M. Treiber, *Calibrating car-following models by using trajectory data: Methodological study*, Transportation Research Record: Journal of the Transportation Research Board, Volume 2088, Pages 148-156, 2008.

4. A. Kesting, M. Treiber, M. Schönhof and D. Helbing, *Extending adaptive cruise control (ACC) towards adaptive driving strategies*, Transportation Research Record: Journal of the Transportation Research Board, Volume 2000, Pages 16-24, 2007.

5. A. Kesting, M. Treiber and D. Helbing, *General lane-changing model MOBIL for car-following models*, Transportation Research Record: Journal of the Transportation Research Board, Volume 1999, Pages 86-94, 2007.

6. A. Kesting, M. Treiber, M. Schönhof, F. Kranke and D. Helbing, *Jam-avoiding adaptive cruise control (ACC) and its impact on traffic dynamics*, Traffic and Granular Flow '05, Springer, Pages 633-643, 2007.

7. A. Kesting, M. Schönhof, S. Lämmer, M. Treiber and D. Helbing, *Decentralized approaches to adaptive traffic control*, Pages 179-199. Contribution to *Managing Complexity. Insights, Concepts, Applications* edited by D. Helbing, Springer, 2008.

8. A. Kesting, M. Treiber and D. Helbing, *Agents for traffic simulation*. Contribution to *Agents, Simulation and Applications* edited by A. Uhrmacher and D. Weyns, Taylor and Francis, in print, 2008.

9. A. Kesting and M. Treiber, *Calibration of car-following models using floating car data*, Traffic and Granular Flow '07, Springer, in print, 2008.

Co-authored publications:

1. C. Thiemann, M. Treiber and A. Kesting, *Estimating acceleration and lane-changing dynamics from Next Generation Simulation trajectory data*, Transportation Research Record: Journal of the Transportation Research Board, Volume 2088, Pages 90-101, 2008.

2. M. Treiber, A. Kesting and D. Helbing, *Understanding widely scattered traffic flows, the capacity drop, and platoons as effects of variance-driven time gaps*, Physical Review E 74, 016123, 2006.

3. M. Treiber, A. Kesting and D. Helbing, *Delays, inaccuracies and anticipation in microscopic traffic models*, Physica A, 360, Issue 1, Pages 71-88, 2006.

4. M. Schönhof, M. Treiber, A. Kesting and D. Helbing, *Autonomous detection and anticipation of jam-fronts from messages propagated by inter-vehicle communication*, Transportation Research Record: Journal of the Transportation Research Board, Volume 1999, Pages 3-12, 2007.

5. M. Schönhof, A. Kesting, M. Treiber and D. Helbing, *Coupled vehicle and information flows: Message transport on a dynamic vehicle network*, Physica A, Volume 363, Issue 1, Pages 73-81, 2006.

6. M. Treiber, A. Kesting and D. Helbing, *Influence of reaction times and anticipation on stability of vehicular traffic flow*, Transportation Research Record: Journal of the Transportation Research Board, Volume 1999, Pages 23-29, 2007.

7. D. Helbing, M. Treiber and A. Kesting, *Understanding arrival and departure time statistics from interactions in queuing systems*, Physica A, 363, Issue 1, 62-72, 2006.

8. M. Schönhof, A. Kesting, M. Treiber and D. Helbing, *Inter-vehicle communication on highways: Statistical properties of information propagation*, Traffic and Granular Flow '05, Pages 645-655, Springer, 2007.

9. M. Treiber, A. Kesting and D. Helbing, *Variance-driven traffic dynamics and statistical aspects of single-vehicle data*, Traffic and Granular Flow '05, Pages 551-557, Springer, 2007.

10. M. Treiber, A. Kesting and D. Helbing, *Verkehr verstehen und beherrschen.* Contribution to *Für eine neue deutsche Verkehrspolitik (Edition Internationales Verkehrswesen)* edited by U. Stopka and W. Pällmann, Deutscher Verkehrs-Verlag, 2005.

11. F. Kranke, H. Poppe, M. Treiber and A. Kesting, *Fahrerassistenzsysteme zur aktiven Stauvermeidung*, VDI-Berichte zur 22. VDI/VW Gemeinschaftstagung Integrierte Sicherheit und Fahrerassistenzsysteme, VDI-Verlag, 2006.